

**3-D FINITE ELEMENT INVESTIGATION**

**OF**

**DISCRETE DEADMAN ANCHOR**

**FOR**

**EARTH RETAINING WALL**

**CHAI KOH SIONG**

**THE UNIVERSITY OF NOTTINGHAM**

**2015**

**3-D FINITE ELEMENT INVESTIGATION**  
**OF**  
**DISCRETE DEADMAN ANCHOR**  
**FOR**  
**EARTH RETAINING WALL**

**CHAI KOH SIONG**

*(M. Eng. (Hons.), the University of Nottingham)*

**A THESIS SUBMITTED**  
**FOR THE DEGREE OF DOCTOR OF PHILOSOPHY**  
**DEPARTMENT OF CIVIL ENGINEERING**  
**THE UNIVERSITY OF NOTTINGHAM**

**2015**

*Dedicated to my mother Mdm. Tan Yoke Heong*

*for her understanding and endless love*

# ACKNOWLEDGEMENT

---

---

I would like to take this opportunity to express my sincere appreciation to my Ph.D. supervisor at the University of Nottingham, Ir. Dr. Chan Swee Huat. This thesis could not have been accomplished without his excellent guidance, useful advice and perennial encouragement.

Sincerely, I would also like to express my heartfelt gratitude to Dr. Sandy Kok Sien Ti, Dr. Song Ki Il and Dr. Mostapha Boulbibane from the Department of Civil engineering for their helpful advice and invaluable guidance during the course of my thesis.

Furthermore, grateful acknowledgement is made to the Engineering Computer Laboratory Technician, Mr. Kumaravehlo S/O Bathumalai for his effort in installing *PLAXIS 3D* on my workstation.

I must record my irreparable debt to my family and relatives for their support and encouragement. Last but not least, I would like to thank my fellow friends, colleagues and staff members for giving me priceless support throughout this thesis.

# PERFACE

---

---

The following publications were published during the term of candidature:

1. Chai, K. S. & Chan, S. H. (2014). A Study on Finite Element Modelling of Earth Retaining Wall Anchored by Deadman Anchor. *ICSMGE 2014: International Conference on Soil Mechanics and Geotechnical Engineering*, Paris, France.
2. Chai, K. S. & Chan, S. H. (2015). Evaluate on the Pull-out of Discrete Deadman Anchorage in Sand. *Geotechnical Engineering Journal of the SEAGS and AGSSEA*. (Submitted)

# ABSTRACT

---

---

In the past several years, considerable attention has been given to the ultimate horizontal pull-out resistance of vertical deadman anchors, which are usually used together with earth retaining wall. Unfortunately, no significant effort has been made to understand/study the behaviour of discrete deadman anchor in earth retaining wall (anchored wall) subjected to the deflection of earth retaining wall. Therefore, this research aims to fill up this gap.

The study on the behaviour of single-plate discrete deadman anchor in anchored wall subjected to the deflection of earth retaining wall is carried out by three-dimensional (3-D) finite element analysis adopting finite element software named *PLAXIS*. The behaviour of discrete deadman anchor is studied by investigating the effects of several key factors. These include the effects of length of tie rod, embedment depth of anchor, spacing between deadman anchors, friction angle of soil, depth of anchored wall, and stiffness of anchored wall.

Practicing geotechnical engineers are able to understand the interactions among soil-anchor-wall by studying the effects of several key factors on the behaviour of discrete deadman anchor. This allows practicing geotechnical

engineers to determine the potential failure mechanisms and hence provide the most suitable design of anchored wall in geotechnical engineering.

Furthermore, the effects of abovementioned key factors are summarised and design charts are proposed for the preliminary design of anchored wall. The design charts are developed based on limiting the wall deflection to 0.5% of excavation height. The major contribution of this research is the development of design charts for the preliminary design of anchored wall. These design charts may be implemented during early design stages, which serves the purpose for earthwork planning, cost estimation, bill of quantity and others. These design charts are set as a guideline for the preliminary design.

Last but not least, the embedment depth of deadman anchor in this research is studied up to 3.0m deep. Deadman anchorage system embedded deeper than 3.0m from ground surface is considered to be impractical due to the difficulty in installation and increase of construction cost and time.

**Keywords:** 3-D finite element analysis, discrete deadman anchor, earth retaining wall, sand.

# TABLE OF CONTENTS

---

---

ACKNOWLEDGEMENT.....	II
PERFACE .....	III
ABSTRACT .....	IV
TABLE OF CONTENTS.....	VI
LIST OF FIGURES.....	XIII
LIST OF TABLES.....	XXVI
NOMENCLATURE .....	XXIX
CHAPTER 1 INTRODUCTION.....	1
1.1 INTRODUCTION.....	1
1.2 BACKGROUND .....	3
1.2.1 <i>Earth Retaining Wall</i> .....	3
1.2.1.1 Anchored Wall.....	6
1.2.2 <i>Types of Anchorage for Anchored Wall</i> .....	7
1.2.2.1 Deadman Anchor .....	8
1.3 OBJECTIVES AND SCOPE OF WORK.....	11
1.4 THESIS OUTLINE .....	12

<b>CHAPTER 2 LITERATURE REVIEW .....</b>	<b>14</b>
2.1 INTRODUCTION.....	14
2.2 LATERAL EARTH PRESSURE THEORY .....	14
2.2.1 Rankine's Theory.....	15
2.2.2 Coulomb's Theory .....	16
2.2.3 Logarithmic Spiral Theory.....	16
2.3 FAILURE MECHANISMS OF EARTH RETAINING WALL .....	17
2.3.1 Deep Seated Failure .....	18
2.3.2 Rotational Failure .....	18
2.3.3 Flexural Failure .....	18
2.3.4 Anchorage Failures.....	20
2.3.4.1 Anchor Passive Failure.....	21
2.3.4.2 Tie Rod Failure .....	22
2.3.4.3 Bearing Plate Failure.....	22
2.4 HISTORICAL REVIEW .....	22
2.4.1 Analytical Studies .....	23
2.4.1.1 Summary of Analytical Studies .....	40
2.4.2 Experimental Studies.....	40
2.4.2.1 Summary of Experimental Studies .....	49
2.4.3 Field Test Studies .....	49
2.5 SUMMARY.....	50
<b>CHAPTER 3 METHODOLOGY.....</b>	<b>54</b>
3.1 INTRODUCTION.....	54
3.2 FINITE ELEMENT ANALYSIS (FEA) .....	54

3.3	PROTOTYPE CONFIGURATION.....	56
3.4	DESIGN CRITERIA.....	58
3.5	BEHAVIOUR OF DISCRETE DEADMAN ANCHORAGE SYSTEM.....	58
3.6	PLAXIS MODEL.....	60
3.6.1	<i>3-D Model</i> .....	60
3.6.1.1	Soil.....	60
3.6.1.2	Earth Retaining Wall and Deadman Anchor.....	61
3.6.1.3	Tie Rod.....	62
3.6.1.4	Material.....	62
3.6.1.5	Boundary Conditions.....	65
3.6.1.6	Mesh Investigation.....	66
3.6.2	<i>2-D Model</i> .....	70
3.6.2.1	Soil.....	70
3.6.2.2	Earth Retaining Wall and Deadman Anchor.....	71
3.6.2.3	Tie Rod.....	72
3.7	VERIFICATION OF FINITE ELEMENT SOFTWARE.....	72
3.8	SUMMARY.....	75
<b>CHAPTER 4 1-G SMALL SCLAE LABORATORY TEST.....</b>		<b>77</b>
4.1	INTRODUCTION.....	77
4.2	1-G SMALL-SCALE LABORATORY TEST SET UP.....	78
4.2.1	<i>Sand Box</i> .....	78
4.2.2	<i>Deadman Anchorage System</i> .....	80
4.2.3	<i>Pull-out System</i> .....	81
4.3	SOIL CHARACTERISATION.....	84

4.3.1	<i>Sieve Analysis Test</i> .....	85
4.3.2	<i>Direct Shear Box Test</i> .....	88
4.3.3	<i>Oedometer Test</i> .....	92
4.3.4	<i>Density Test with Pre-determined Sand Placement Height</i> .....	95
4.3.5	<i>Summary</i> .....	96
4.4	PROCEDURE FOR 1-G SMALL-SCALE LABORATORY TEST.....	96
4.5	1-G SMALL-SCALE LABORATORY TEST .....	100
4.5.1	<i>Result and Discussion</i> .....	103
4.6	SUMMARY.....	105
<b>CHAPTER 5 ANALYTICAL SOLUTIONS.....</b>		<b>107</b>
5.1	INTRODUCTION.....	107
5.2	DETERMINATION OF THE ULTIMATE PULL-OUT CAPACITY.....	109
5.3	COMPARISON OF ANALYTICAL SOLUTIONS WITH FEA .....	111
5.4	COMPARISON OF PUBLISHED EXPERIMENTAL WORK WITH ANALYTICAL SOLUTIONS.....	116
5.5	EFFECT OF ANCHOR SIZE .....	120
5.6	SUMMARY.....	123
<b>CHAPTER 6 2-D AND 3-D FINITE ELEMENT ANALYSES .....</b>		<b>125</b>
6.1	INTRODUCTION.....	125
6.2	COMPARISON STUDY ON 2-D AND 3-D FINITE ELEMENT ANALYSES .....	126
6.2.1	<i>Effect of Anchor Spacing</i> .....	128
6.2.2	<i>Effect of Wall Thickness</i> .....	133
6.3	BENEFITS OF 3-D FINITE ELEMENT ANALYSIS .....	140

6.3.1	<i>Study on the Presence of Deadman Anchorage System in Earth Retaining Wall</i> .....	142
6.4	SUMMARY.....	147
<b>CHAPTER 7 MODEL SIMPLIFICATION</b> .....		<b>150</b>
7.1	INTRODUCTION.....	150
7.2	MODEL SIMPLIFICATION .....	151
7.2.1	<i>Wall Deflection</i> .....	153
7.2.2	<i>Pull-out Force</i> .....	155
7.2.3	<i>Lateral Movement of Soil</i> .....	156
7.2.4	<i>Effective Stress of Soil</i> .....	158
7.2.5	<i>Results of Model Simplification</i> .....	160
7.3	MODEL SIMPLIFICATION CHART .....	160
7.3.1	<i>Verification and Validation of Model Simplification Chart</i> .....	164
7.3.1.1	<i>Effect of Friction Angle (<math>\phi</math>)</i> .....	164
7.3.1.2	<i>Effect of Wall Stiffness (<math>EI</math>)</i> .....	167
7.4	SUMMARY.....	168
<b>CHAPTER 8 BEHAVIOUR OF DISCRETE DEADMAN ANCHORAGE SYSTEM IN ANCHORED WALL</b> .....		<b>171</b>
8.1	INTRODUCTION.....	171
8.2	PARAMETRIC STUDY .....	172
8.2.1	<i>Effect of Tie Rod Length</i> .....	174
8.2.2	<i>Effect of Anchor Embedment Depth</i> .....	178
8.2.3	<i>Effect of Anchor Spacing</i> .....	181
8.2.4	<i>Effect of Soil Friction Angle</i> .....	184

8.2.5	<i>Effect of Wall Depth</i> .....	187
8.2.6	<i>Effect of Wall Stiffness</i> .....	192
8.3	SUMMARY.....	194
<b>CHAPTER 9 DESIGN CHARTS .....</b>		<b>196</b>
9.1	INTRODUCTION.....	196
9.2	RELATIONSHIP AMONG TIE ROD LENGTH, ANCHOR EMBEDMENT DEPTH AND WALL DEPTH .....	197
9.3	RELATIONSHIP OF THE LOAD CORRESPONDING TO THE OPTIMUM RESPONSE OF ANCHORED WALL.....	200
9.4	DESIGN CHARTS .....	203
9.4.1	<i>Case 1: Anchor Spacing (s) = 2.0m and Friction Angle of Soil (<math>\phi</math>) = 30°</i> .....	204
9.4.1.1	For Wall Depth (D) of 15.0m.....	204
9.4.1.2	For Wall Depth (D) of 20.0m.....	206
9.4.2	<i>Case 2: Anchor Spacing (s) = 2.0m and Friction Angle of Soil (<math>\phi</math>) = 40°</i> .....	207
9.4.2.1	For Wall Depth (D) of 10.0m.....	207
9.4.2.2	For Wall Depth (D) of 15.0m.....	209
9.4.2.3	For Wall Depth (D) of 20.0m.....	210
9.4.3	<i>Case 3: Anchor Spacing (s) = 5.0m and Friction Angle of Soil (<math>\phi</math>) = 30°</i> .....	212
9.4.3.1	For Wall Depth (D) of 10.0m.....	212
9.4.3.2	For Wall Depth (D) of 15.0m.....	213
9.4.3.3	For Wall Depth (D) of 20.0m.....	215

9.4.4 Case 4: Anchor Spacing ( $s$ ) = 5.0m and Friction Angle of Soil	
( $\phi$ ) = 40° .....	216
9.4.4.1 For Wall Depth ( $D$ ) of 10.0m.....	216
9.4.4.2 For Wall Depth ( $D$ ) of 15.0m.....	218
9.4.4.3 For Wall Depth ( $D$ ) of 20.0m.....	219
9.5 APPLICATION ON THE DESIGN CHARTS .....	221
9.6 SUMMARY.....	221
<b>CHAPTER 10 CONCLUSIONS AND RECOMMENDATIONS.....</b>	<b>223</b>
10.1 CONCLUSIONS .....	223
10.2 RECOMMENDATIONS FOR FUTURE RESEARCH.....	226
<b>REFERENCES .....</b>	<b>228</b>
<b>APPENDIX A MATERIAL PROPERTIES.....</b>	<b>239</b>
A.1 SOIL PROPERTIES.....	239
A.2 CONCRETE PROPERTIES .....	241
A.3 STEEL PROPERTIES.....	242
A.4 SHEET PILE WALL PROPERTIES.....	244
<b>APPENDIX B RESULTS OF SOIL TEST .....</b>	<b>245</b>
B.1 DIRECT SHEAR BOX TEST .....	245
B.2 OEDOMETER TEST .....	247

# LIST OF FIGURES

---

---

## **CHAPTER 1: INTRODUCTION**

Figure 1.1: Types of earth retaining wall.	5
Figure 1.2: Anchored wall with (a) single and (b) multiple anchorage system.	7
Figure 1.3: Shapes of anchorage for anchored wall. (Merifield, 2002)	9
Figure 1.4: Foundation support for transmission tower. (Merifield, 2002)	10
Figure 1.5: Submerged pipeline support subjected to vertical uplift pressure. (Merifield, 2002)	11

## **CHAPTER 2: LITERATURE REVIEW**

Figure 2.1: Deep seated failure. (Weissenbach et al., 2002)	19
Figure 2.2: Rotational failure. (Weissenbach et al., 2002)	19
Figure 2.3: Flexural failure. (Weissenbach et al., 2002)	20
Figure 2.4: Anchorage failures – (a) anchor passive failure, (b) tie rod failure and (c) bearing plate failure. (Weissenbach et al., 2002)	21
Figure 2.5: Shear pattern around shallow anchor in sand. (Terzaghi, 1943)	25

Figure 2.6: Shear resistance ( $P_s$ ) for single anchor. (Terzaghi, 1943)	26
Figure 2.7: Failure mechanism for surface anchors proposed by Hansen (1953).	27
Figure 2.8: Failure mechanism for deep anchors proposed by Biarez, Boucraut and Negre (1965).	29
Figure 2.9: Failure surface (a) surcharge analysis method and (b) equivalent free surface method. (Neely et al., 1973)	32
Figure 2.10: $k_4$ failure concept. (Rowe & Davis, 1982a)	34
Figure 2.11: Deadman anchor with acting forces. (Naser, 2006)	37
Figure 2.12: Typical nature of load-displacement diagram. (Neely et al., 1973)	44

### **CHAPTER 3: METHODOLOGY**

Figure 3.1: Prototype configuration – a. Site Elevation, b. Plan Elevation and c. 3-D View.	57
Figure 3.2: Local numbering and positioning of node (•) and integration points (x) of a ten-node tetrahedral element. ( <i>Plaxis 3D User Manual</i> , 2012)	61
Figure 3.3: Local numbering and positioning of node (•) and integration points (x) of a six-node triangular plate element. ( <i>Plaxis 3D User Manual</i> , 2012)	62
Figure 3.4: Lateral movement of the soil ( $U_x$ ).	66

Figure 3.5: Types of meshes – a) very coarse mesh, b) medium mesh and c) very fine mesh.	68
Figure 3.6: Wall deflection ( $\delta$ ) for various types of mesh.	69
Figure 3.7: Pull-out force ( $F$ ) for various types of mesh.	69
Figure 3.8: Position of stress points ( $x$ ) and nodes ( $\bullet$ ) of a fifteen- node triangular element. (Brinkgreve et al., 2006)	71
Figure 3.9: Position of stress points ( $x$ ) and nodes ( $\bullet$ ) of a five-node beam element. (Brinkgreve et al., 2006)	72
Figure 3.10: Schematic diagram of 1-g small-scale laboratory test (Plan View).	73
Figure 3.11: Schematic diagram of 1-g small-scale laboratory test (Side View).	74
Figure 3.12: Schematic diagram of 1-g small-scale laboratory test (Front View).	74

#### **CHAPTER 4: 1-G SMALL-SCALE LABORATORY TEST**

Figure 4.1: Sand box.	79
Figure 4.2: Front elevation of sand box.	80
Figure 4.3: (a) deadman anchor; (b) steel plate; and (c) steel rod.	81
Figure 4.4: Hollow plunger cylinder (Enerpac™ RCH-123).	82
Figure 4.5: Hand pumped hydraulic jack (Enerpac™ P-84).	83
Figure 4.6: Mitutoya™ dial gauge.	83
Figure 4.7: SMC™ hydraulic pressure gauge.	84

Figure 4.8: Mechanical shaker and sieve trays.	86
Figure 4.9: Grain size distribution curve.	88
Figure 4.10: ELE International digital direct shear box test apparatus.	92
Figure 4.11: ELE International oedometer test apparatus.	94
Figure 4.12: Installation of deadman anchorage system (side elevation).	98
Figure 4.13: Installation of deadman anchorage system (plan elevation).	98
Figure 4.14: Sand backfilled up to desire height, 0.8m.	99
Figure 4.15: Pull-out displacement of the hydraulic plunger.	99
Figure 4.16: Load-displacement relationship from laboratory test.	100
Figure 4.17: Finite element prototype.	101
Figure 4.18: Load-displacement relationship from finite element analysis.	102
Figure 4.19: Load-displacement relationship between 1-g small-scale laboratory test and finite element analysis.	103
Figure 4.20: Effect of Young's Modulus of sand adopted in FEA on load-displacement relationship.	105

## **CHAPTER 5: ANALYTICAL SOLUTIONS**

Figure 5.1: Geometry of problem.	108
----------------------------------	-----

Figure 5.2: Comparison of pull-out force coefficient ( $M_{\gamma q}$ ) between FEA and analytical solutions.	112
Figure 5.3: Comparison of pull-out force coefficient ( $M_{\gamma q}$ ) in ultimate limit state between FEA and analytical solutions.	114
Figure 5.4: Comparison of pull-out force coefficient ( $M_{\gamma q}$ ) between experimental work of Hoshiya and Mandal and analytical solutions.	116
Figure 5.5: Comparison of pull-out force coefficient ( $M_{\gamma q}$ ) in ultimate limit state between experimental work of Hoshiya and Mandal and analytical solutions.	117
Figure 5.6: Effect of anchor size on the pull-out force coefficient ( $M_{\gamma q}$ ).	120
Figure 5.7: Comparison on the effect of anchor size between FEA and previous experimental works.	122

## **CHAPTER 6: 2-D AND 3-D FINITE ELEMENT ANALYSES**

Figure 6.1: 2-D finite element prototype.	127
Figure 6.2: 3-D finite element prototype.	127
Figure 6.3: Numbering system for each deadman anchor.	127
Figure 6.4: Wall deflection ( $\delta$ ) between 2-D and 3-D FEA for $s/B = 2$ .	129

Figure 6.5: Wall deflection ( $\delta$ ) between 2-D and 3-D FEA for $s/B =$ 5.	130
Figure 6.6: Pull-out force ( $F$ ) between 2-D and 3-D FEA for $s/B = 2$ .	131
Figure 6.7: Pull-out force ( $F$ ) between 2-D and 3-D FEA for $s/B = 5$ .	131
Figure 6.8: Wall deflection ( $\delta$ ) for rigid wall between 2-D and 3-D FEA.	134
Figure 6.9: Wall deflection ( $\delta$ ) for flexible wall between 2-D and 3- D FEA.	134
Figure 6.10: Lateral movement of soil ( $U_x$ ) for rigid wall.	136
Figure 6.11: Lateral movement of soil ( $U_x$ ) for flexible wall	136
Figure 6.12: Effective stresses of soil ( $\sigma'_{xx}$ ) for rigid wall.	137
Figure 6.13: Effective stresses of soil ( $\sigma'_{xx}$ ) for flexible wall.	137
Figure 6.14: Pull-out force ( $F$ ) for rigid wall between 2-D and 3-D FEA.	139
Figure 6.15: Pull-out force ( $F$ ) for flexible wall between 2-D and 3- D FEA.	139
Figure 6.16: Vertical bending moment for 3-D model with $T = 0.5\text{m}$ and $s/B = 2$ .	141
Figure 6.17: Horizontal bending moment for 3-D model with $T =$ $0.5\text{m}$ and $s/B = 2$ (Plan view).	142
Figure 6.18: Effective stresses ( $\sigma'_{xx}$ ) for Models A and B at initial stage.	144
Figure 6.19: Effective stresses ( $\sigma'_{xx}$ ) for Models A and B at excavation height ( $H$ ) $4.5\text{m}$ .	144

Figure 6.20: Effective stresses ( $\sigma'_{xx}$ ) for Models A and B at $H = 6.0\text{m}$ .	145
Figure 6.21: Lateral movements of soil ( $U_x$ ) for Models A and B at $H = 6.0\text{m}$ .	145
Figure 6.22: Wall deflections ( $\delta$ ) for Models A and B at $H = 6.0\text{m}$ .	146

## **CHAPTER 7: MODEL SIMPLIFICATION**

Figure 7.1: Wall deflection ( $\delta$ ) at $H = 6.5\text{m}$ among models.	155
Figure 7.2: Pull-out force ( $F$ ) among models.	156
Figure 7.3: Colour contour for lateral movements of soil at $H = 6.5\text{m}$ among models.	157
Figure 7.4: Colour contour for effective stresses of soil at $H = 6.5\text{m}$ among models.	159
Figure 7.5: Result for anchor embedment ratio of 1.	161
Figure 7.6: Result for anchor embedment ratio of 2.	162
Figure 7.7: Result for anchor embedment ratio of 3.	162
Figure 7.8: Model simplification chart for friction angle ( $\phi$ ) of $30^\circ$ .	163
Figure 7.9: Effect of friction angle ( $\phi$ ) on model simplification chart of $d/h=2$ .	165
Figure 7.10: Model simplification chart for friction angle ( $\phi$ ) of $20^\circ$ .	166
Figure 7.11: Effect of wall stiffness ( $EI$ ) on model simplification chart of $d/h=2$ .	168

## **CHAPTER 8: BEHAVIOUR OF DISCRETE DEADMAN ANCHORAGE**

### **SYSTEM IN ANCHORED WALL**

Figure 8.1: Effect of wall deflection ( $\delta$ ) on tie rod lengths for $d = 2$ and $s = 2$ .	175
Figure 8.2: Effect of pull-out force ( $F$ ) on tie rod length for $d = 2$ and $s = 2$ .	176
Figure 8.3: Wall deflection and elongation of tie rod for $d = 2$ and $s$ $= 2$ .	177
Figure 8.4: Effect of wall deflection ( $\delta$ ) on anchor embedment depth for $L = 10\text{m}$ and $s = 2$ .	179
Figure 8.5: Effect on pull-out force ( $F$ ) on anchor embedment depth for $L = 10\text{m}$ and $s = 2$ .	180
Figure 8.6: Effect of wall deflection ( $\delta$ ) on anchor spacing for $L =$ $10\text{m}$ and $d = 2$ .	182
Figure 8.7: Effect of pull-out force ( $F$ ) on anchor spacing for $L = 10\text{m}$ and $d/h = 2$ .	184
Figure 8.8: Effect of wall deflection ( $\delta$ ) on soil friction angle for $L =$ $10\text{m}$ , $d = 2$ and $s = 2$ .	185
Figure 8.9: Effect of pull-out force ( $F$ ) on soil friction angle for $L =$ $10\text{m}$ , $d = 2$ and $s = 2$ .	187
Figure 8.10: Effect of wall deflection ( $\delta$ ) on wall depth for $L = 10\text{m}$ , $d = 2$ and $s = 2$ .	188

Figure 8.11: Effect of pull-out force ( $F$ ) on wall depth for $L = 10\text{m}$ , $d = 2$ and $s = 2$ .	190
Figure 8.12: Effect of the ultimate pull-out force on wall depth for $L$ $= 10\text{m}$ , $d = 2$ and $s = 2$ .	191
Figure 8.13: Effect of wall deflection ( $\delta$ ) on wall stiffness for $L = 10\text{m}$ , $d = 2$ and $s = 2$ .	193
Figure 8.14: Effect of pull-out force ( $F$ ) on wall stiffness for $L = 10\text{m}$ , $d = 2$ and $s = 2$ .	193

## **CHAPTER 9: DESIGN CHARTS**

Figure 9.1: Relationship for $D = 10.0\text{m}$ with anchor embedment depth of 1m.	198
Figure 9.2: Relationship for $D = 10.0\text{m}$ with anchor embedment depth of 2m.	198
Figure 9.3: Relationship for $D = 10.0\text{m}$ with anchor embedment depth of 3m.	199
Figure 9.4: Design chart for case of $D = 10.0\text{m}$ , $s = 2.0\text{m}$ and $\phi = 30^\circ$ .	199
Figure 9.5: Relationship of corresponding load to the optimum response of anchored wall ( $D=10.0\text{m}$ ) for anchor embedment depth of 1.0m.	201

Figure 9.6: Relationship of corresponding load to the optimum response of anchored wall ( $D=10.0\text{m}$ ) for anchor embedment depth of $2.0\text{m}$ .	201
Figure 9.7: Relationship of corresponding load to the optimum response of anchored wall ( $D=10.0\text{m}$ ) for anchor embedment depth of $3.0\text{m}$ .	202
Figure 9.8: Design chart of corresponding load for case of $D = 10.0\text{m}$ , $s = 2.0\text{m}$ and $\phi = 30^\circ$ .	202
Figure 9.9: Design chart for case of $D = 15.0\text{m}$ , $s = 2.0\text{m}$ and $\phi = 30^\circ$ .	205
Figure 9.10: Design chart of corresponding load for case of $D = 15.0\text{m}$ , $s = 2.0\text{m}$ and $\phi = 30^\circ$ .	205
Figure 9.11: Design chart for case of $D = 20.0\text{m}$ , $s = 2.0\text{m}$ and $\phi = 30^\circ$ .	206
Figure 9.12: Design chart of corresponding load for case of $D = 20.0\text{m}$ , $s = 2.0\text{m}$ and $\phi = 30^\circ$ .	207
Figure 9.13: Design chart for case of $D = 10.0\text{m}$ , $s = 2.0\text{m}$ and $\phi = 40^\circ$ .	208
Figure 9.14: Design chart of corresponding load for case of $D = 10.0\text{m}$ , $s = 2.0\text{m}$ and $\phi = 40^\circ$ .	208
Figure 9.15: Design chart for case of $D = 15.0\text{m}$ , $s = 2.0\text{m}$ and $\phi = 40^\circ$ .	209
Figure 9.16: Design chart of corresponding load for case of $D = 15.0\text{m}$ , $s = 2.0\text{m}$ and $\phi = 40^\circ$ .	210

Figure 9.17: Design chart for case of $D = 20.0\text{m}$ , $s = 2.0\text{m}$ and $\phi = 40^\circ$ .	211
Figure 9.18: Design chart of corresponding load for case of $D = 20.0\text{m}$ , $s = 2.0\text{m}$ and $\phi = 40^\circ$ .	211
Figure 9.19: Design chart for case of $D = 10.0\text{m}$ , $s = 5.0\text{m}$ and $\phi = 30^\circ$ .	212
Figure 9.20: Design chart of corresponding load for case of $D = 10.0\text{m}$ , $s = 5.0\text{m}$ and $\phi = 30^\circ$ .	213
Figure 9.21: Design chart for case of $D = 15.0\text{m}$ , $s = 5.0\text{m}$ and $\phi = 30^\circ$ .	214
Figure 9.22: Design chart of corresponding load for case of $D = 15.0\text{m}$ , $s = 5.0\text{m}$ and $\phi = 30^\circ$ .	214
Figure 9.23: Design chart for case of $D = 20.0\text{m}$ , $s = 5.0\text{m}$ and $\phi = 30^\circ$ .	215
Figure 9.24: Design chart of corresponding load for case of $D = 20.0\text{m}$ , $s = 5.0\text{m}$ and $\phi = 30^\circ$ .	216
Figure 9.25: Design chart for case of $D = 10.0\text{m}$ , $s = 5.0\text{m}$ and $\phi = 40^\circ$ .	217
Figure 9.26: Design chart of corresponding load for case of $D = 10.0\text{m}$ , $s = 5.0\text{m}$ and $\phi = 40^\circ$ .	217
Figure 9.27: Design chart for case of $D = 15.0\text{m}$ , $S = 5.0\text{m}$ and $\phi = 40^\circ$ .	218
Figure 9.28: Design chart of corresponding load for case of $D = 15.0\text{m}$ , $s = 5.0\text{m}$ and $\phi = 40^\circ$ .	219

Figure 9.29: Design chart for case of $D = 20.0\text{m}$ , $s = 5.0\text{m}$ and $\phi = 40^\circ$ .	220
Figure 9.30: Design chart of corresponding load for case of $D = 20.0\text{m}$ , $s = 5.0\text{m}$ and $\phi = 40^\circ$ .	220

## **APPENDIX A: MATERIAL PROPERTIES**

Figure A.1: Unified Soil Classification System (ASTM Designation D-2487). (“Standard practice for classification of soils for engineering purpose (Unified Soil Classification System),” 2006)	239
Figure A.2: Relationship between SPT ‘N’ value and $\phi$ , $N_q$ and $N_\gamma$ . (Peck, Hanson, & Thornburn, 1974)	240
Figure A.3: Relationship between SPT ‘N’ value and Young’s Modulus. (Source: unknown)	241
Figure A.4: Examples of specific room temperature shear stress-strain data and Poisson’s ratio for several plastics and other materials. (Rosato et al., 2001)	242
Figure A.5: Examples of room temperature tensile stress-strain data for several plastics and other materials. (Rosato et al., 2001)	243
Figure A.6: Examples of sheet pile properties (Sum Hup Sheet Piling Sdn Bhd)	244

## **APPENDIX B: RESULTS OF SOIL TEST**

Figure B.1: Shear stress against normal stress plot for direct shear

box test.

247

Figure B.2: Stress strain plot for oedometer test.

248

# LIST OF TABLES

---

---

## **CHAPTER 2: LITERATURE REVIEW**

Table 2.1: Analytical studies on vertical anchors in cohesion-less soils. 51

Table 2.2: Experimental studies on vertical anchors in cohesion-less soils. 52

## **CHAPTER 3: METHODOLOGY**

Table 3.1: Magnitude of key parameter for parametric study. 59

Table 3.2: The size of prototype. 66

Table 3.3: Number of elements and nodes for various types of mesh. 67

## **CHAPTER 4: 1-G SMALL-SCALE LABORATORY TEST**

Table 4.1: Sieve analysis results. 87

Table 4.2: Physical properties of sand. 96

Table 4.3: Parameters adopted for laboratory test. 100

## **CHAPTER 5: ANALYTICAL SOLUTIONS**

Table 5.1: Comparison of pull-out force coefficient ( $M_{\gamma q}$ ) between typical nature load-displacement and $k_4$ failure concept.	110
Table 5.2: Comparison of pull-out force coefficient ( $M_{\gamma q}$ ) between finite element analysis and available analytical solutions.	113
Table 5.3: Comparison of pull-out force coefficient ( $M_{\gamma q}$ ) in ultimate limit state between finite element analysis and available analytical solutions.	114
Table 5.4: Comparison of pull-out force coefficient ( $M_{\gamma q}$ ) in ultimate limit state between experimental work of Hoshiya and Mandal and the available analytical solutions.	118
Table 5.5: Comparison on the effect of anchor size between FEA and previous experimental works.	121

## **CHAPTER 7: 3-D FINITE ELEMENT ANALYSES**

Table 7.1: Parametric studies for model simplification.	152
Table 7.2: Parameters adopted in the study of model simplification.	153
Table 7.3: The variations of wall deflection between simplified and complex model.	154

**CHAPTER 8: BEHAVIOUR OF DISCRETE DEADMAN ANCHORAGE  
SYSTEM IN ANCHORED WALL**

Table 8.1: Basic set of parameter studies.	173
Table 8.2: Magnitude of key parameter for parametric study.	173

**APPENDIX A: MATERIAL PROPERTIES**

Table A.1: Typical range for the static modulus of elasticity at 28 days of normal-weight concrete. (BS 8110-2, 1985)	241
--	-----

**APPENDIX B: RESULTS OF SOIL TEST**

Table B.1: Summary of the results for direct shear box test.	245
Table B.2: Measurement input table for direct shear box test.	246
Table B.3: Measurement of the consolidation ring for oedometer test.	247
Table B.4: Summary of the results for oedometer test.	248

# NOMENCLATURE

---

---

•	node
1-D	one-dimensional
2-D	two-dimensional
3-D	three-dimensional
$A_c$	area of concrete
$A_s$	area of steel
$B$	breadth of deadman anchor
BS	British Standard
$B/h$	aspect ratio
$c$	cohesion
$c_c$	coefficient of uniformity
$c_u$	coefficient of concavity/curvature
$d$	embedment depth of deadman anchor to the base of anchor plate

$dia$	diameter of circular deadman anchor
$d/h$	anchor embedment ratio
$D$	depth of earth retaining wall
$D_{10}$	grain size of 10% passing rate
$D_{30}$	grain size of 30% passing rate
$D_{60}$	grain size of 60% passing rate
$E$	embedment factor (chapter 2)
$E$	Young's Modulus of soil
$EC$	Euro Code
$E_0$	constraint modulus of soil
$E_c$	Young's Modulus of concrete
$EI$	stiffness of wall
$E_s$	Young's Modulus of steel
$E_{50}^{ref}$	secant stiffness in standard drained triaxial test
$E_{oed}^{ref}$	tangent stiffness for primary oedometer loading
$E_{ur}^{ref}$	unloading/reloading stiffness
$f_{cu,28} / f_{ck,cube}$	concrete cube strength

$F$	shape factor (chapter 2)
$F$	pull-out force
FEA	finite element analysis
FEM	finite element method
Fos	Factor of safety
$F_b$	effective friction force at the top of deadman anchor
$F_s$	effective friction force at the bottom of deadman anchor
$F_t$	effective friction force at two sides of deadman anchor
$F_\gamma$	capacity of deadman anchor for basic case
$g$	acceleration due to gravity (gravitational force)
$h$	height of deadman anchor
$H$	height of excavation
$H_{max}$	maximum allowable excavation height
$K_0$	coefficient of lateral earth pressure at rest
$K_a$	coefficient of active lateral earth pressure

$K_b$	coefficient of lateral earth pressure (Meyerhof)
$K_p$	coefficient of passive lateral earth pressure
$L$	length of tie rod
$L_o$	original length of tie rod
$m$	degree of mobilisation (chapter 2)
$m$	power for stress-level dependency of stiffness (chapter 3)
$M$	3-D correction factor (chapter 2)
$M$	mass of soil (chapter 4)
$M_{\gamma q}$	coefficient of pull-out force
$N$	normal force
$N_{\gamma}$	break-out factor
$P_a$	active resistance
$P_p$	passive resistance
$P_s$	shear resistance
$R_K$	correction factor for effect of initial stress state
$R_{ov}$	reduction factor

$R_R$	correction factor for effect of deadman anchor roughness
$R_\psi$	correction factor for effect of soil dilatancy
$s$	centre-to-centre spacing between two deadman anchors
$s/B$	separation ratio
$S$	shape factor
SLS	service limit state
$t$	thickness of deadman anchor
$T$	thickness of earth retaining wall
$T_0$	pull-out capacity for basic case
$T_s$	pull-out capacity for buried case
$T_u$	ultimate pull-out capacity of deadman anchor
$T_{u(B)}$	ultimate pull-out capacity for basic case
ULS	ultimate limit state
USCS	Unified Soil Classification System
$U_x$	Horizontal displacement in X-direction

$U_x, U_y$ and $U_z$	translational degrees of freedom in X-, Y- and Z- directions, respectively
$\nu$	Poisson's ratio
$\nu_{ur}$	Poisson's ratio for unloading-reloading
$V$	volume of soil
$W_b$	weight of deadman anchor
$W_s$	weight of soil above the deadman anchor
$x$	Integration point
$\delta$	interface between soil and deadman anchor (chapter 2)
$\delta$	deflection of earth retaining wall
$\delta_b$	angle of friction between soil and bottom surface of the deadman anchor
$\delta_t$	angle of friction between soil and bottom surface of the deadman anchor
$\phi$	angle of friction
$\phi_x, \phi_y$ and $\phi_z$	rotational degrees of freedom in X-, Y- and Z- directions, respectively

$\gamma$	unit weight of soil
$\gamma'$	effective unit weight of soil
$\gamma_c$	unit weight of concrete
$\gamma_s$	unit weight of steel
$\eta$	factor of efficiency
$\rho$	density of soil
$\tau$	shear strength of soil
$\sigma$	normal stress of soil
$\sigma'$	effective normal stress of soil
$\varepsilon$	strain of soil
$\psi$	angle of dilatancy
$\xi, \eta$ and $\zeta$	local coordinates

# CHAPTER 1

---

## INTRODUCTION

### 1.1 Introduction

Throughout the world, the development of infrastructure in urban areas is growing rapidly (Abdi & Arjomand, 2011). This may be potentially due to the growth of population and economy in countries such as Hong Kong, China, Malaysia and others. However, due to the limited urban spaces, the construction of proposed railways, highways, roads, bridges, tunnels and buildings are therefore more closer to the existing structures (Chan, 2002). The construction could become very critical when these existing structures are sensitive to the surrounding ground movement (Gue & Tan, 1998).

To study and minimise the effects of surrounding ground movement for new developments, geotechnical engineering applications and designs

have been introduced. The geotechnical engineering design is aimed to find a better solution which is more cost efficient.

Anchored wall, which also is known as tieback wall, is one of the solutions. It is formed by an earth retaining wall with a proper combination of deadman anchorage system.

Anchored wall provides significant construction advantages as it allows larger working spaces (Muntohar & Liao, 2013). Besides that, anchored wall is able to increase the resistance capacity of the earth retaining wall and reduces the ground movement during construction.

The current geotechnical design solution is no longer concerned on the stability issues only; it also focuses on the restriction of ground movement. For example in countries such as Taiwan (Ou, Hsien, & Chiou, 1993), Singapore (Wong, Poh, & Chuah, 1997), United Kingdom (Carder, 1995; Fernie & Suckling, 1996) and others are very concerned on the restriction of ground movement. This is because ground movement is a sensitive parameter of measurement particularly for those constraint areas where only limited ground movement is permitted.

Finite element techniques offer efficient and effective estimation of deformation and stability on the study of anchored wall. This is because finite element analysis takes into account the construction sequence (David & Lidija, 2001) of anchored wall, such as installation of anchored wall and excavation processes, which acts as a whole system.

The purpose of this chapter is to provide a brief introduction on anchored wall, which consists of earth retaining wall and deadman anchorage system. This chapter draws to the end by an overview of the thesis.

## **1.2 Background**

Literally, soil retention is one of the earliest issues in geotechnical engineering. Some developed fundamental principles during the early days of soil mechanics are meant for soil retention design (Terzaghi, 1943). Earth retaining wall is one of the soil retention designs.

### **1.2.1 Earth Retaining Wall**

Earth retaining wall is a rigid structure, which can be used to resist thrust of a bank of earth. It can also be used to accommodate and redistribute lateral earth pressure due to sloping effects.

Furthermore, earth retaining wall provides lateral support to vertical slope that would otherwise collapse into a more natural shape. It substitutes the steep face of the wall creating a gentle natural slope (Abdullahi, 2009), and subsequently providing useful platforms at different elevations (e.g. railways, highways and road cut, buildings, substructures, etc.).

In general, the earth retaining wall used in civil engineering practice can be divided into four common types, as shown in Figure 1.1:

- a. Gravity wall
- b. Cantilever wall
- c. Sheet piles wall
- d. Anchored wall/ Tieback wall

A more comprehensive review on these walls is presented by Visone (2008) and Coduto (2011). Gravity wall is the oldest and simplest earth retaining wall. It is a rigid body, which is thick and stiff in nature. Thus, it can support itself based on its own weight without any additional supports to resist the lateral earth pressure.

Cantilever wall is a type of flexible retaining walls, which depends on its flexural strength to resist the lateral earth pressure. It transmits earth pressures to a large structural footing, which converts the lateral earth pressure from behind the retaining wall to the vertical earth pressure to the ground.

Sheet pile wall is another type of flexible retaining wall. It is usually implemented in unfavourable soils conditions (e.g. soft soils) and in limited working spaces. In addition, sheet pile wall is usually driven directly into the ground.

Anchored wall can be constructed from either gravity wall, cantilever wall or sheet pile wall. It is constrained against lateral movements by the

presence of additional anchors supports which are embedded in the soil behind the retaining wall.

Lastly, for an appropriate earth retaining wall design, the hydrostatic pressure and the seepage force due to the presence of water must be included. Thus, the provision of drainage system (seepage holes) is an important factor for retaining wall design. This allows ground water to escape and hence release excessive pore water pressure and keep the earth retaining wall in a stable condition.

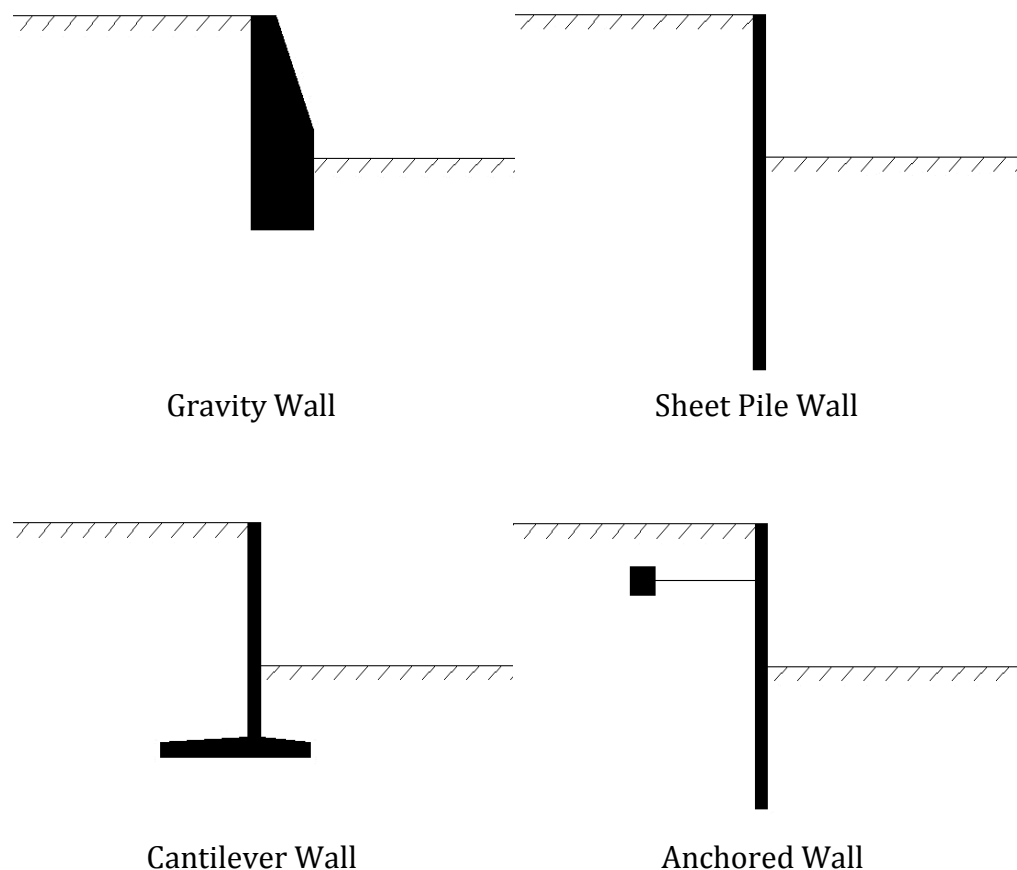


Figure 1.1: Types of earth retaining wall.

### 1.2.1.1 Anchored Wall

Initially, anchored wall was used as temporary support for vertical excavation. Subsequently, the application of anchored wall was extended and used as permanent retention system for vertical excavation. The use of anchored wall has become increasingly common as a support for vertical excavation, especially when only limited ground movement is allowed.

The first classification of the embedded earth retaining wall was based on the constraints scheme (Visone, 2008). The embedded earth retaining wall can be categorised as:-

- a. Conventional retaining wall, with no constraint, is used to sustain excavation height ( $H$ ) of less than 5 to 6m.
- b. Anchored wall with single constraint (see Figure 1.2a) is used to sustain excavation height ( $H$ ) up to 10m.
- c. Anchored wall with multiple constraints (see Figure 1.2b) is used to sustain excavation height ( $H$ ) beyond 10m.

The selection of the above classification is dependent on the material of embedded earth retaining wall (e.g. timber, steel or reinforced concrete retaining wall) and the embedded depth of earth retaining wall.

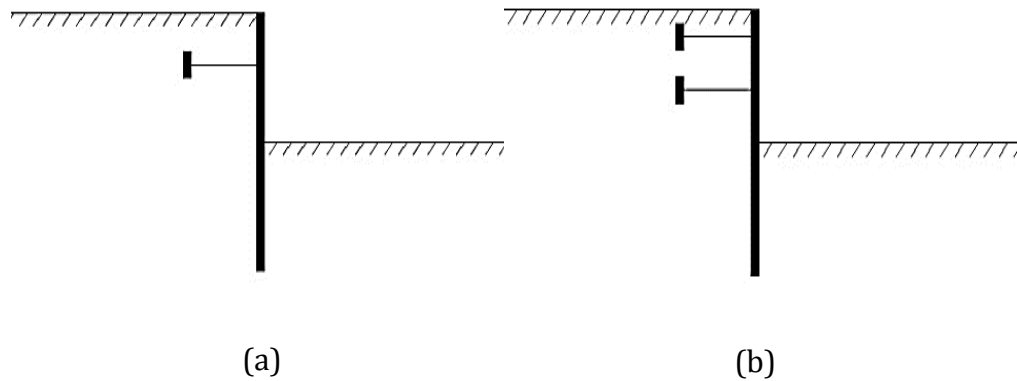


Figure 1.2: Anchored wall with (a) single and (b) multiple anchorage system.

The role of anchored wall is generally essential when dealing with the following circumstances (Visone, 2008):

- a. The required excavation height ( $H$ ) is greater than 5m.
- b. The allowable ground movement is limited.
- c. The penetration depth of earth retaining wall is limited due to the presence of bedrock or boulders.

When conventional retaining wall (e.g. gravity wall, sheet pile wall and cantilever wall) faces these constraints, it is necessarily to introduce additional support for the wall system (e.g. anchorages) to minimise the ground movement.

### 1.2.2 Types of Anchorage for Anchored Wall

Anchorage is a light-weighted structure and is typically attached to earth retaining wall in common civil engineering practice. It is embedded

sufficiently to a certain depth in the ground to resist vertical uplift and horizontal forces.

In general, the types of anchorage for anchored wall can be divided into four basic categories (Merifield, 2002):-

- a. “Deadman” anchor/ plate anchor
- b. Screw anchor
- c. Grout injected anchor
- d. Anchor pile

All of these anchors are usually made of steel or concrete. Anchor is used to transmit tensile forces from retaining structure to the surrounding soil. The tensile forces can be transmitted to the surrounding soil by different approaches between various types of anchorages.

Deadman anchor and screw anchors transfer tensile force through direct bearing, whereas grout injected anchors transfer tensile force through shaft friction. Anchor piles transfer tensile force through a combination of both direct bearing and shaft friction approaches (Merifield, 2002). Deadman anchorage system is the subject of interest in this research.

### **1.2.2.1 Deadman Anchor**

Deadman anchor is a structure buried in ground and is placed behind an earth retaining wall. It is used as tieback support for retaining structure from excessive lateral movements. Deadman anchor can be continuous

(e.g. steel sheet piles, strip beams, etc.) or discrete/ individual (e.g. driven piles, concrete blocks, etc.).

The construction sequence of deadman anchorage system is as follows:

- a. An open trench is excavated behind earth retaining wall up to a desired location.
- b. Deadman anchor block/plate is buried in the excavated trench.
- c. A tie rod is placed between deadman anchor and the earth retaining wall.
- d. The excavated trench is then backfilled with soil.

In general, deadman anchor can be formed in various shapes, for example, circular, square and rectangle shapes, as illustrated in Figure 1.3. It can also be positioned horizontally or inclined depending on the requirement.

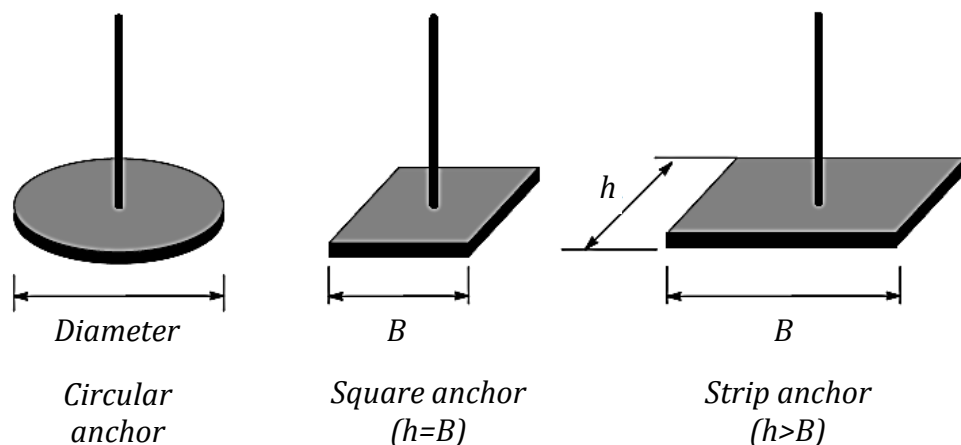


Figure 1.3: Shapes of anchorage for anchored wall. (Merifield, 2002)

Das (1990) detailed these anchorages system in term of their applications, such as:

- a. Tieback support for retaining structure
- b. Foundation support for transmission towers, marine moorings and utility poles (see Figure 1.4)
- c. Break-out support for submerged pipelines and other structures, which is subjected to vertical uplift pressures (see Figure 1.5)

Therefore, it can be concluded that apart from civil engineering practice, the application of deadman anchors has been widely used in marine engineering, oil and gas engineering practices etc.

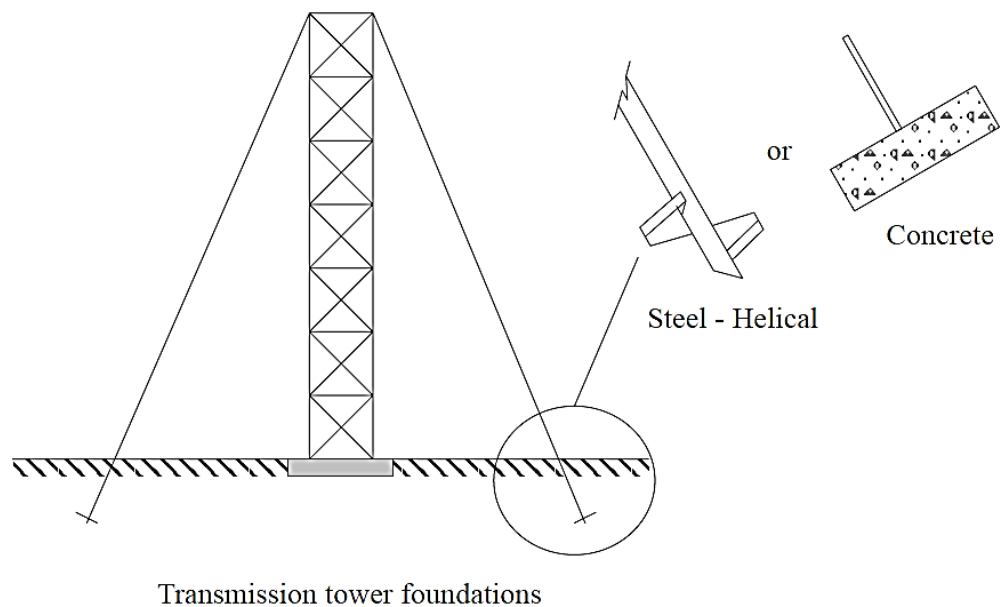


Figure 1.4: Foundation support for transmission tower. (Merifield, 2002)

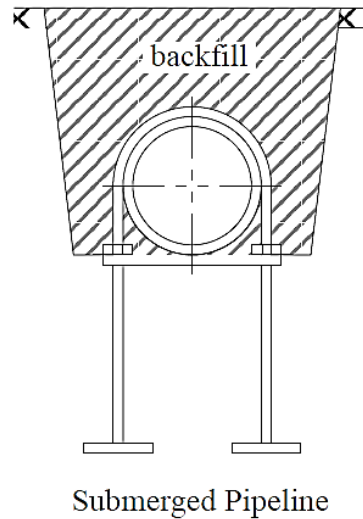


Figure 1.5: Submerged pipeline support subjected to vertical uplift pressure. (Merifield, 2002)

### 1.3 Objectives and Scope of Work

The main objective of this research is to develop design charts for the application of anchored wall. These design charts are performed by using finite element approach. The specific objectives of this research are listed as follows:

1. To emphasize the finite element prototype for numerical studies.
2. To verify the finite element prediction with 1-g small-scale laboratory test and compare the finite element prediction with existing analytical solutions in literature.
3. To assess two-dimensional (2-D) finite element analysis (FEA) and compare with three-dimensional (3-D) finite element analyses.

4. To study the behaviour of discrete deadman anchorage system by investigating the effects of the following key parameters:-
  - a. Length of tie-rod
  - b. Embedment depth of anchor
  - c. Spacing of anchor
  - d. Friction angle of soil
  - e. Depth of anchored wall
  - f. Stiffness of anchored wall
5. To develop design charts for earth retaining wall with discrete deadman anchorage system.

## **1.4 Thesis Outline**

Following the Introduction in Chapter 1, this thesis is divided into nine additional chapters.

- Chapter 2 reviews the relevant literature and analytical studies. A thorough review on the pull-out of deadman anchor has been conducted.
- Chapter 3 introduces the methodology used in this research.
- Chapter 4 presents the 1-g small-scale laboratory test to examine the accuracy of finite element estimation.
- Chapter 5 presents the comparison between existing analytical solutions in literature and finite element analysis.

- Chapter 6 assesses the 2-D finite element analyses and compares with 3-D finite element analyses.
- Chapter 7 investigates the simplification of finite element prototype.
- Chapter 8 presents the parametric studies of several effects on the mechanisms of the entire anchored wall system.
- Chapter 9 develops the design charts for the preliminary and/or early stage design of anchored wall.
- Chapter 10 draws the thesis to the end by summarising all the main findings of the research. Recommendations for future research are also included.

# CHAPTER 2

---

## LITERATURE REVIEW

### 2.1 Introduction

This chapter introduces the theory of lateral earth pressure and potential failure modes of earth retaining wall. Subsequently, it presents the relevant literature.

### 2.2 Lateral Earth Pressure Theory

A comprehensive review of lateral earth pressure theory is given by Visone (2008). In general, there are two types of lateral earth pressure, namely active and passive earth pressures.

Active earth pressure is the pressure that causes the retaining wall to move away from the soil in active zone, which is located behind the wall, thereby

causing extensional lateral strain in the soil. Passive earth pressure is the pressure that occurs when the retaining wall moves towards the soil in active zone, thereby causing compressive lateral strain in the soil.

There are three well-known theories to determine lateral earth pressure, namely Rankine's theory, Coulomb's theory and Logarithmic Spiral theory. Nevertheless, the result of lateral earth pressure depends on the theories applied. Different theories may have different assumptions on the nature of structure (smooth or rough structure), soil type and soil-structure interface.

### **2.2.1 Rankine's Theory**

In 1857, Rankine developed the simplest approach to compute active and passive earth pressures (Rankine, 1857). The assumptions made in this approach were the soil is cohesion-less, the wall is frictionless, the soil-wall interface is vertical, and the planar failure surface and the resultant force are angled parallel to the backfill surface. This theory is satisfied for brittle materials, but is not applicable to ductile materials. Furthermore, Rankine's theory is also known as Maximum Stress Theory.

### **2.2.2 Coulomb's Theory**

In 1776, Coulomb was the first person who studied the problems of lateral earth pressure acting on retaining structures (Coulomb, 1776). Coulomb's theory applied limit equilibrium theory and assumed the failing soil block as a free body in order to determine the magnitude of earth resultant pressures acting on the wall for both active and passive conditions. Since the problem is indeterminate, a number of potential failure surfaces must be analysed to identify the critical failure surface. In addition, Coulomb's theory does not precisely predict the distribution of active earth pressure for dry homogeneous cohesion-less soil.

### **2.2.3 Logarithmic Spiral Theory**

Logarithmic spiral theory is another well-known theory to determine the lateral earth pressure, which assumes that the critical failure surface consists of a curve and linear portion for both active and passive earth pressure conditions.

Log-spiral approach provides slightly more accurate result on both active and passive earth pressure coefficients compared to Rankine's or Coulomb's theory (Caquot & Kerisel, 1948). This is because Rankine's and Coulomb's theories underestimate and overestimate, respectively, the maximum passive earth pressure. However, the Coulomb's theory is

usually adopted to determine the active earth pressure coefficient, as it is more convenient and the difference is significantly small.

Apart from these three well-known theories, Slip-line Field Theory (Sokolovskii, 1965) is another theory which is used to determine lateral earth pressures.

### **2.3 Failure Mechanisms of Earth Retaining Wall**

The earth retaining wall may fail when the lateral earth pressure exceeds the resistance capacity of the retaining structure. There are variety of potential failure models which lead to soil body collapse or otherwise, structural failure.

A detailed study on the failure mechanisms is given by Weissenbach and co-workers (2002). The potential failure modes are as follows:-

- a. Deep seated failure (see Figure 2.1)
- b. Rotational failure (see Figure 2.2)
- c. Flexural failure (see Figure 2.3)
- d. Anchorage failures (see Figure 2.4)

### **2.3.1 Deep Seated Failure**

Deep seated failure is a potential rotational failure due to the weight of the soil itself. It is independent on the structural characteristics of the wall and/or anchor. Hence, it cannot be resolved by increasing the wall penetration depth or by repositioning the anchor. However, it can be minimized by improving the soil strength or by changing the geometry of the retained material.

### **2.3.2 Rotational Failure**

Rotational failure is due to insufficient pile penetration depth, which causes excessive lateral earth pressure acting on the wall system. It can be remedied by providing sufficient sheet pile penetration depth in the wall system and/or by a proper combination of anchor position.

### **2.3.3 Flexural Failure**

Flexural failure is due to overstressing of the sheet pile in the wall system. Overstressing the sheet pile tends to the change the property of sheet pile from elastic to plastic form. Nevertheless, it can be prevented by increasing the stiffness of sheet pile.

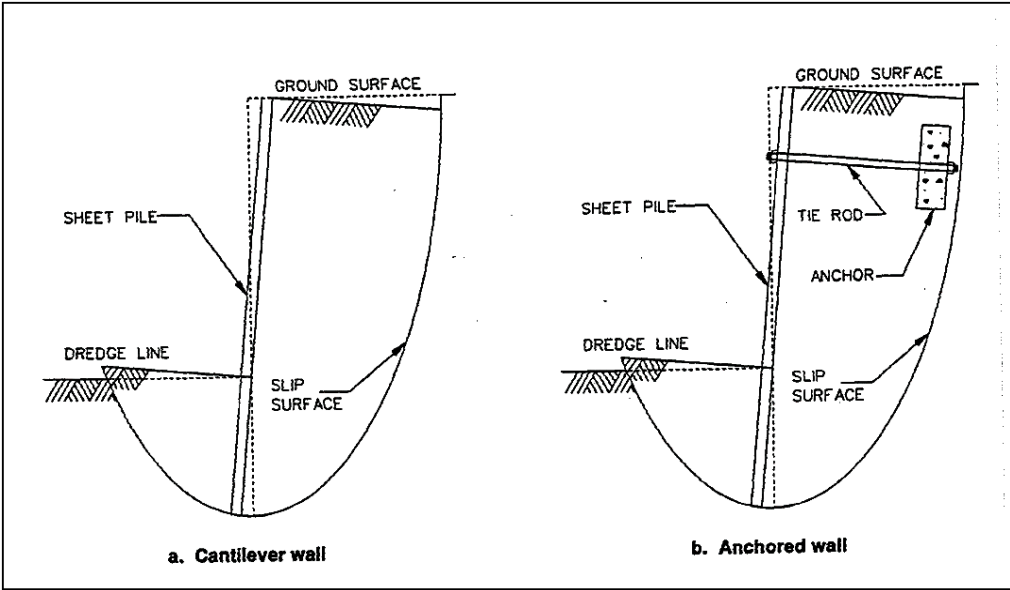


Figure 2.1: Deep seated failure. (Weissenbach et al., 2002)

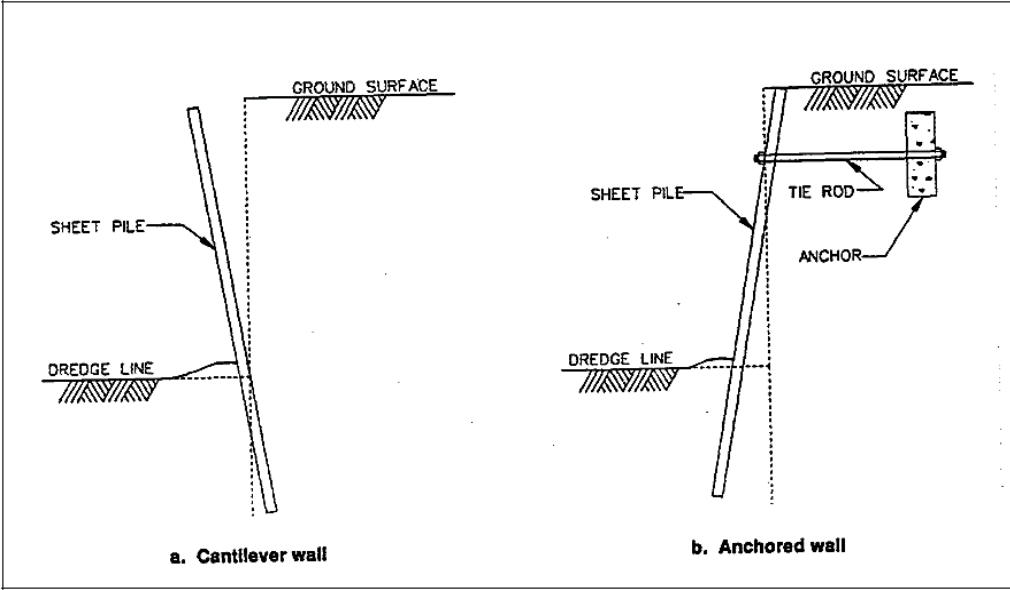


Figure 2.2: Rotational failure. (Weissenbach et al., 2002)

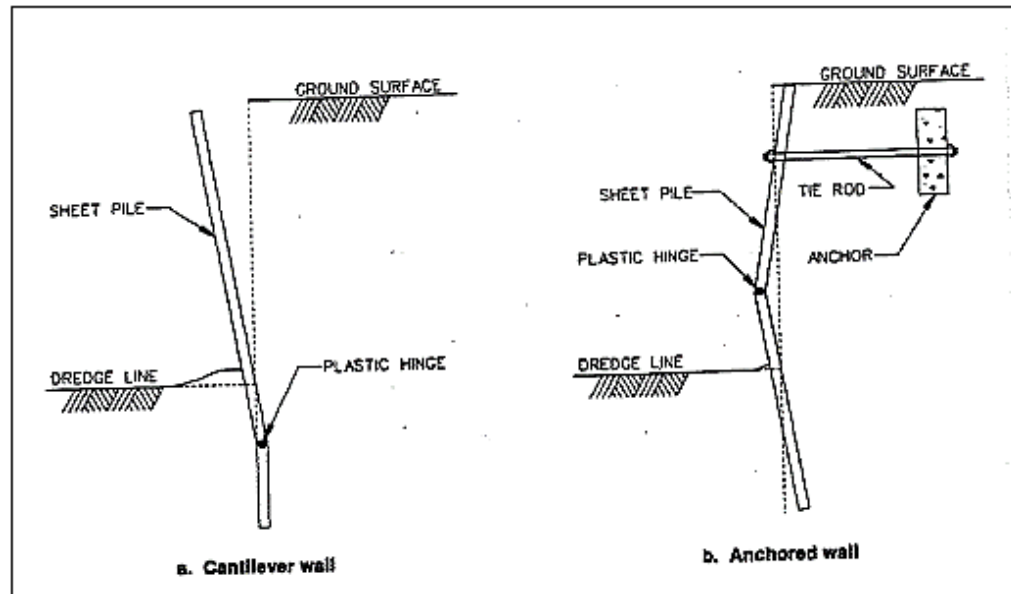


Figure 2.3: Flexural failure. (Weissenbach et al., 2002)

### 2.3.4 Anchorage Failures

In general, anchor provides additional support to the retaining structure in order to resist larger lateral earth pressure. Nevertheless, anchorage itself may have some weaknesses, which may lead to earth retaining wall failure.

These anchorage failures include:

- a. Anchor passive failure (see Figure 2.4a)
- b. Tie rod failure (see Figure 2.4b)
- c. Bearing plate failure (see Figure 2.4c)

### 2.3.4.1 Anchor Passive Failure

Anchor passive failure is due to lateral earth pressure acting on the wall system, leading to the deadman anchor being pulled outwards.

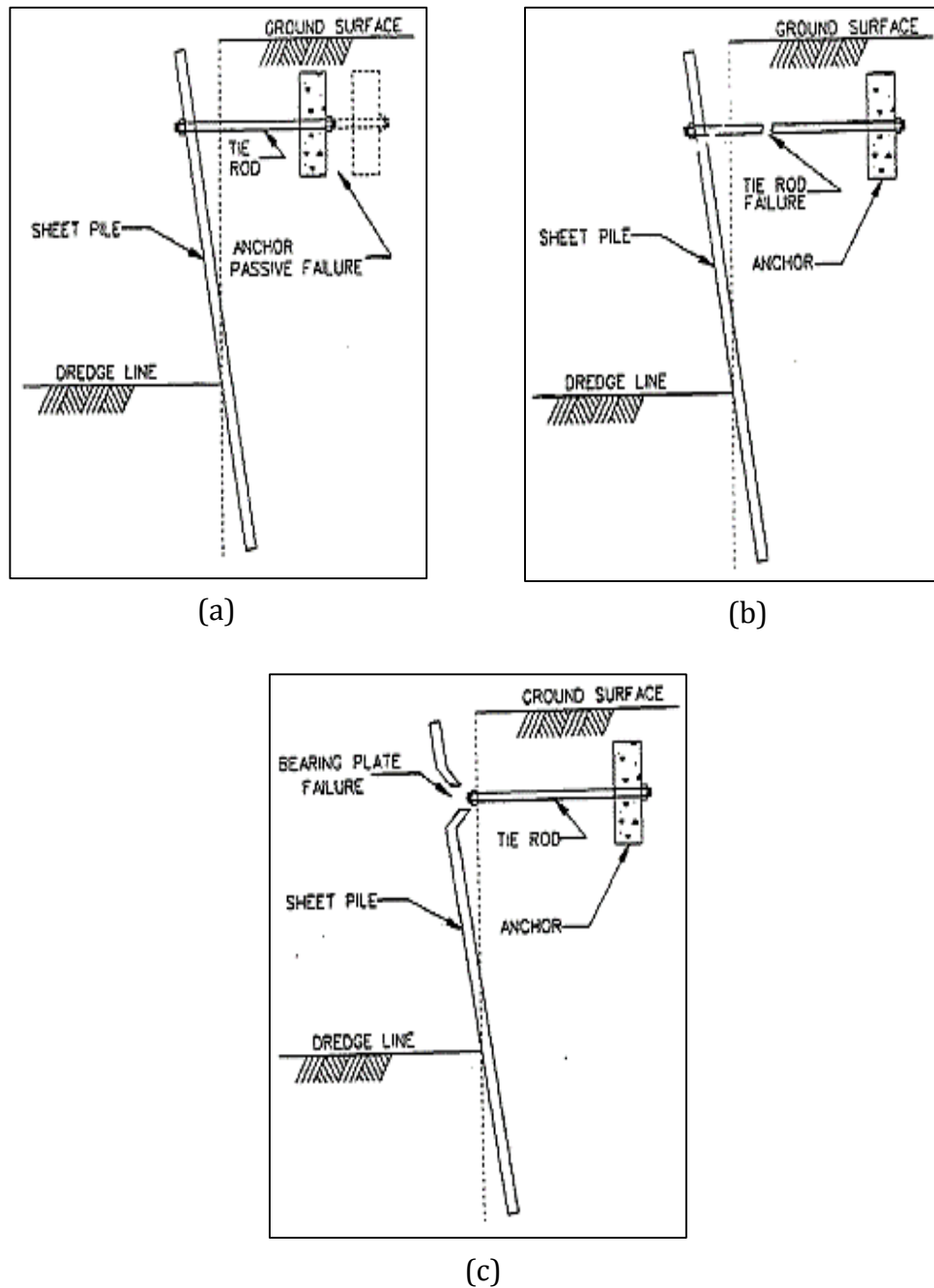


Figure 2.4: Anchorage failures – (a) anchor passive failure, (b) tie rod failure and (c) bearing plate failure. (Weissenbach et al., 2002)

### **2.3.4.2 Tie Rod Failure**

Tie rod failure is due to the pull-out capacity of deadman anchor exceeding the resistance capacity of the tie rod and hence, failure of the tie rod.

### **2.3.4.3 Bearing Plate Failure**

Bearing plate failure is also named as wale system failure. This potential failure occurs at the connection between sheet pile and tie rod. It is due to the resistance capacity of sheet pile that is weaker than the tie rod. Thus, the sheet pile will fail before the tie rod fails.

## **2.4 Historical Review**

In the past several decades, considerable attention has been given to the behaviour of deadman anchor in terms of the ultimate pull-out resistance. One of the earliest research was presented by Balla (1961). Initially, the application of deadman anchor is focused on resisting vertical uplift force. As the range of application for anchor expanded to date, the application of anchor is now extended to restraining vertical structure from lateral pressure.

Research into the behaviour of deadman anchor can be based on analytical and/or experimental studies. A brief review on the existing research has been separated based on this division. In addition, the behaviour of

deadman anchor subjected to the deflection of anchored wall has not been reviewed.

Many researchers have proposed similar approaches to determine the pull-out capacity of deadman anchor in numerical studies. Most of the approaches involve the concept of limit equilibrium, cavity expansion, limit analysis (upper bound and lower bound limit analysis), and finite element approaches. On the other hand, conventional approach under “normal gravity” conditions or centrifuge system was implemented in experimental studies.

This part categorises the studies of deadman anchor into three principle divisions, namely analytical studies, experimental studies and field test studies.

### **2.4.1 Analytical Studies**

In analytical studies, the behaviour of deadman anchor can be divided into shallow anchor and deep anchor behaviours (Rowe & Davis, 1982a, 1982b). For shallow anchor, the ultimate pull-out capacity ( $T_u$ ) is determined based on earth pressure theory whereas for deep anchor, the ultimate pull-out capacity is determined based on the modified bearing capacity theory.

In numerical studies, the behaviour of deadman anchor is simulated by adopting two-dimensional (2-D) numerical analysis, which assumed plane strain condition and/or by adopting three-dimensional (3-D) numerical

analysis. Unfortunately, very few 2-D numerical studies can be considered rigorous in determining the ultimate pull-out capacity of deadman anchor.

Nevertheless, very few researchers take into account the 3-D effect on deadman anchor. Therefore, the literature contribution in determining the ultimate pull-out capacity of deadman anchor by adopting 3-D numerical analysis is still very lacking.

Numerical results are essential to be verified with experimental results as experimental results are typically problem-specific, which is good for comparison purpose. But, not every case can be proven experimentally due to cost constraint. Therefore, numerical analysis can provide reasonable solution for design purposes. Numerical simulation is highly recommended when dealing with highly non-linear material and scale effects.

The existing numerical studies can be found in the works of Meyerhof and Adams (1968), Meyerhof (1973), Neely, Stuart, and Graham (1973), Rowe and Davis (1982a, 1982b), Murray and Geddes (1987, 1989a), Basudhar and Singh (1994), Dickin and King (1997), Merifield and Sloan (2006), Premalatha (2009), Kumar and Sahoo (2012), and Bhattacharya and Kumar (2012). Several research papers were referred as benchmark for future research.

In 1943, Terzaghi reported that the application of conventional Rankine's theory has been widely adopted to determine the ultimate pull-out

capacity for shallow vertical continuous anchor. The failure zone of a shallow anchor is extended to the soil surface (Terzaghi, 1943).

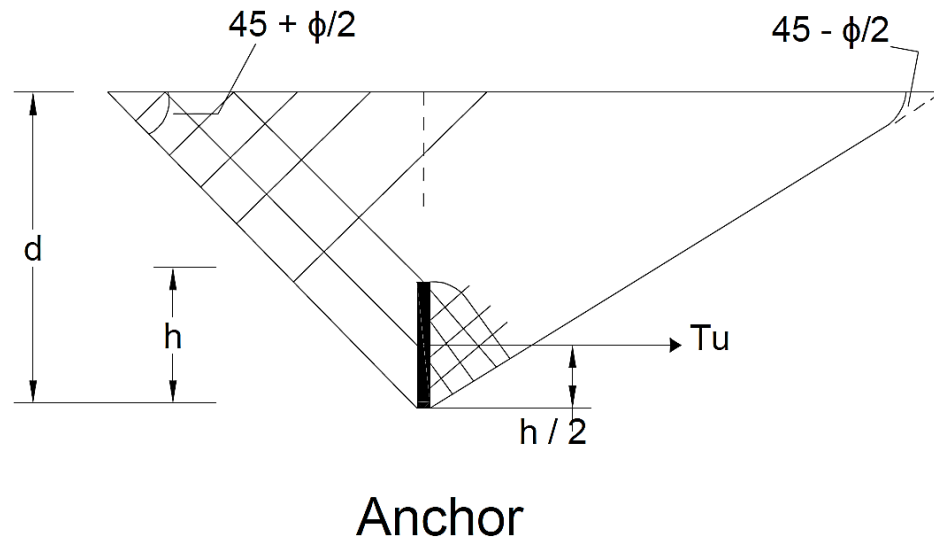


Figure 2.5: Shear pattern around shallow anchor in sand. (Terzaghi, 1943)

The conventional Rankine theory assumed that active and passive pressures are fully developed in front and behind the anchor, which is illustrated in Figure 2.5.

Thus, the ultimate pull-out capacity can be expressed as:

$$T_u = P_p - P_a \quad \text{Eq. 2.1}$$

Nevertheless, Terzaghi also reported that this equation is only valid for anchor embedment ratio (ratio of anchor embedded depth over height of anchor,  $d/h$ ) of less than 2 as it failed to address the friction resistance on the anchor. For single anchor plate, Terzaghi allowed additional shear

resistance ( $P_s$ ) on both sides of the wedge of anchor. The sides of the wedge are assumed to be parallel with the tie rod, as shown in Figure 2.6.

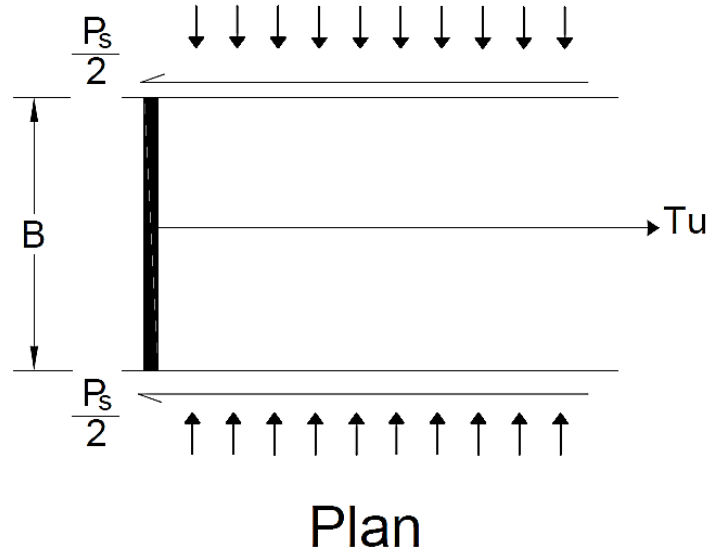


Figure 2.6: Shear resistance ( $P_s$ ) for single anchor. (Terzaghi, 1943)

Therefore, the ultimate pull-out capacity for single anchor can be further expressed as:

$$T_u = (P_p + P_s) - P_a \quad \text{Eq. 2.2}$$

This equation is adopted in British Code of Practice. The shear resistance for cohesion-less soil is given by:

$$P_s = K_a \frac{\gamma d^3}{3} \tan \left( 45 + \frac{\phi}{2} \right) \tan \phi \quad \text{Eq. 2.3}$$



In 1964, Ovesen (Ovesen, 1964) adopted the failure mechanism that was proposed by Hansen (1953). For the basic case, the assumed failure zone combines both Rankine and Logarithmic Spiral Prandtl zones as illustrated in Figure 2.7.

Ovesen derived a formula with empirical reduction applied to the basic case. The ultimate pull-out capacity is expressed as:

$$T_u = T_{u(B)} R_{ov} \quad \text{Eq. 2.5}$$

where the reduction factor ( $R_{ov}$ ) can be expressed as:

$$R_{ov} = \frac{T_s}{T_o} = \frac{C_{ov} + 1}{C_{ov} + d/h} \quad \text{Eq. 2.6}$$

where,

$T_s$  = pull-out capacity for the buried case.

$T_o$  = pull-out capacity for the basic case.

$C_{ov}$  = 19 and 14 for dense and loose sands, respectively.

In addition, Ovesen also derived a formula for ultimate pull-out capacity of deep continuous anchor, which is based on deep strip foundation, as follows:

$$T_u = \gamma d h K_0 e^{\pi \tan \phi} \tan^2 \left( 45 + \frac{\phi}{2} \right) d_c \quad \text{Eq. 2.7}$$

where,

$$d_c = 1 + 0.35 / [h/H + 0.6 / (1 + 7 \tan^4 \phi)]$$

$$d_c = 1.6 + 4.1 \tan^4 \phi \quad (\text{for very deep anchors})$$

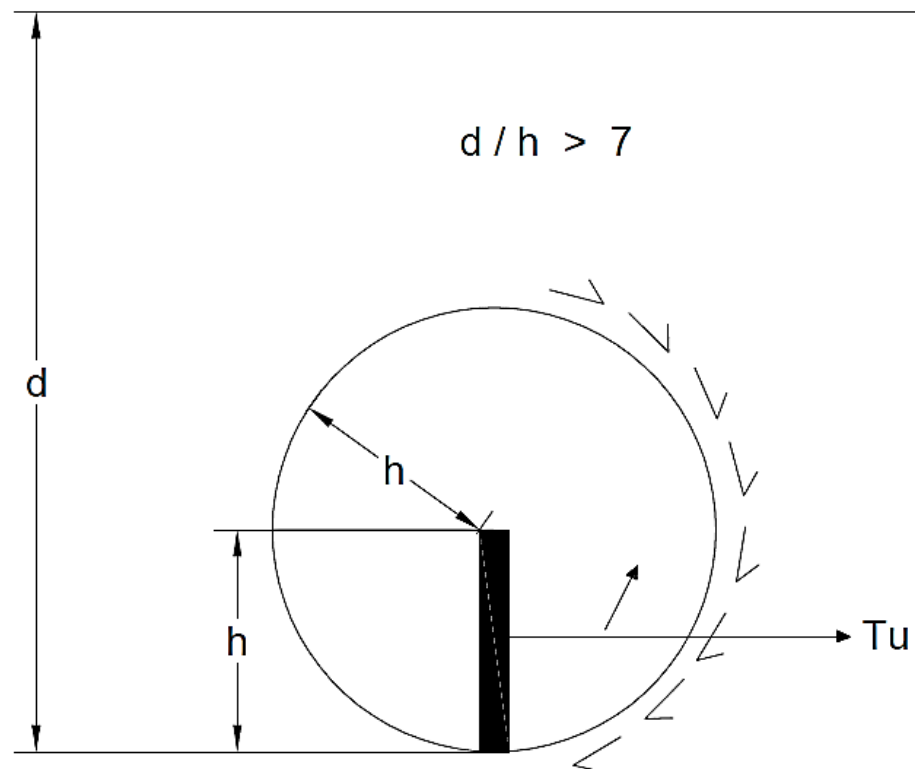


Figure 2.8: Failure mechanism for deep anchors proposed by Biarez, Boucraut and Negre (1965).

In 1965, Biarez and co-workers presented mathematical approaches for vertical deadman anchor that is subjected to translation or rotation. Earth pressure coefficient was derived from limit analysis and summarised into design charts (Biarez et al., 1965).

Biarez and co-workers also reported that the pull-out capacity for shallow anchor ( $d/h < 4$ ) depended on the roughness and weight of anchor. The dimensionless pull-out force coefficient ( $M_{\gamma q} = T_u/\gamma Bh^2$ ) for shallow anchor ( $d/h < 4$ ) and intermediate anchor ( $4 < d/h < 7$ ) can be expressed in a simplified form as:

$$M_{\gamma q} = (K_p - K_a) \left( \frac{d}{h} - \frac{1}{2} \right) + \frac{K_p \sin 2\phi}{2 \tan \left( 45 + \frac{\phi}{2} \right)} \left( \frac{d}{h} - 1 \right)^2 \quad \text{Eq. 2.8}$$

For continuous case,  $B$  in the pull-out force coefficient is found to be 1.

In addition, the pull-out force coefficient for single shallow anchor ( $M_{\gamma qs}$ ) can be further expressed as:

$$M_{\gamma qs} = M_{\gamma q} + \phi \frac{h}{B} (\sqrt{K_p} - \sqrt{K_a}) \left( \frac{d}{h} - \frac{2}{3} \right) + \frac{1}{2} (1 + \phi) \frac{h}{B} K_p \sin 2\phi \left( \frac{d}{h} - 1 \right) \quad \text{Eq. 2.9}$$

Furthermore, the pull-out force coefficient for deep continuous anchor, which is subjected to rotational mechanism (see Figure 2.8) can be expressed as:

$$M_{\gamma q} = 4\pi \left( \frac{d}{h} - 1 \right) \tan \phi \quad \text{Eq. 2.10}$$

In 1973, Meyerhof extended his previous uplift theory (Meyerhof & Adams, 1968), which was used to determine the pull-out capacity of inclined anchors for both shallow and deep continuous anchor. The earth pressure

coefficients that were used in Meyerhof's theory were proposed by Caquot and Kerisel (1948) and Sokolovskii (1965).

The ultimate pull-out capacity of anchor can be expressed as:

$$T_u = \frac{1}{2} \gamma d^2 K_b \quad \text{Eq. 2.11}$$

where  $K_b$  is the pull-out coefficient that can be obtained from a graph using soil friction angle (Kame, Dewaikar, & Choudhury, 2012).

In the same year, Neely and co-workers (Neely et al., 1973) used the theory of plasticity to determine the ultimate pull-out capacity of continuous deadman anchor. Two approaches adopted in their research, namely surcharge approach and equivalent free surface approach. The failure zones are bound by the combination of straight lines and Logarithmic Spirals failure surface, which is illustrated in Figure 2.9.

Furthermore, Neely and co-workers developed design charts for ultimate pull-out capacity in terms of the dimensionless pull-out force coefficient ( $M_{\gamma q}$ ). They also reported that the surcharge approach provides more conservative solution in predicting the pull-out force coefficient. This is because surcharge approach does not take into consideration the shear strength of soil above deadman anchor.

The second approach, equivalent free surface approach, which was adopted from Meyerhof (1951) by manipulating the degree of mobilisation ( $m$ ) of the shear strength of soil above deadman anchor. Neely and co-workers also stated that the value of pull-out force coefficient for  $m=1$  is

10% higher than those for  $m=0$ . It should be noted that the active pressure behind deadman anchor and the kinematic behaviour of material were not considered in their research.

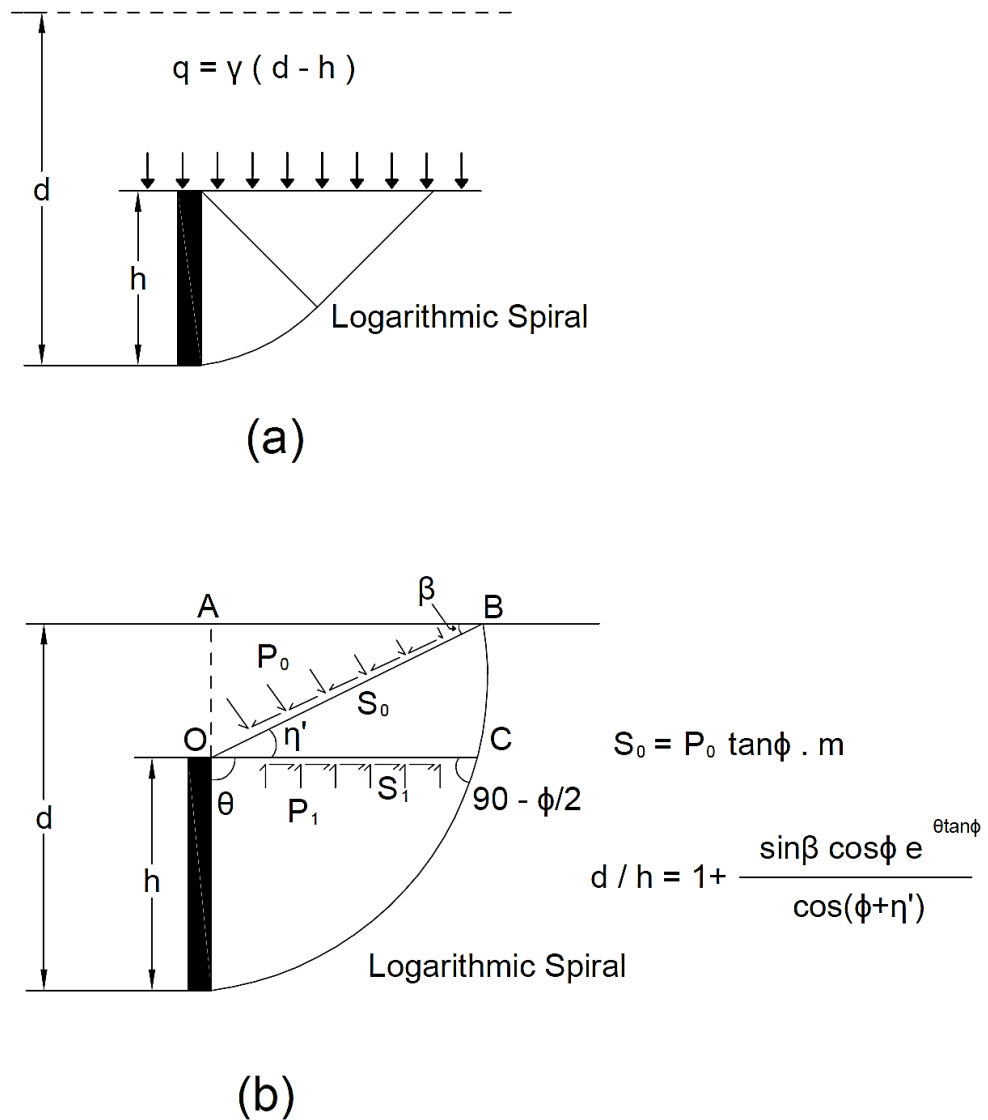


Figure 2.9: Failure surface (a) surcharge analysis method and (b) equivalent free surface method. (Neely et al., 1973)

In 1982, the most rigorous numerical study on the behaviour of deadman anchor up to date was presented by Rowe and Davis (1982a, 1982b). A two dimensional finite element approach with elasto-plastic soil model was used to study the behaviour of deadman anchor. The behaviour of deadman anchor was determined based on soil-structure interaction theory. The soil-structure interaction theory is described in the work of Rowe, Booker and Balaam (1978).

In addition, the effects of anchor embedment depth, friction and dilation angle, initial stress state, anchor roughness, associated and non-associated flow rule were evaluated (Rowe & Davis, 1982b). The non-dimensional pull-out force coefficient for continuous deadman anchor can be expressed as:

$$M_{\gamma q} = F_{\gamma} R_{\psi} R_R R_K \quad \text{Eq. 2.12}$$

where the anchor is assumed to be thin and perfectly rigid.

Furthermore, the ultimate pull-out capacity used in Eq. 2.12 was determined based on  $k_4$  failure concept (see Figure 2.10), which was proposed by Rowe and Davis (1982a). The  $k_4$  failure load corresponds to an apparent stiffness of one quarter of the elastic stiffness.

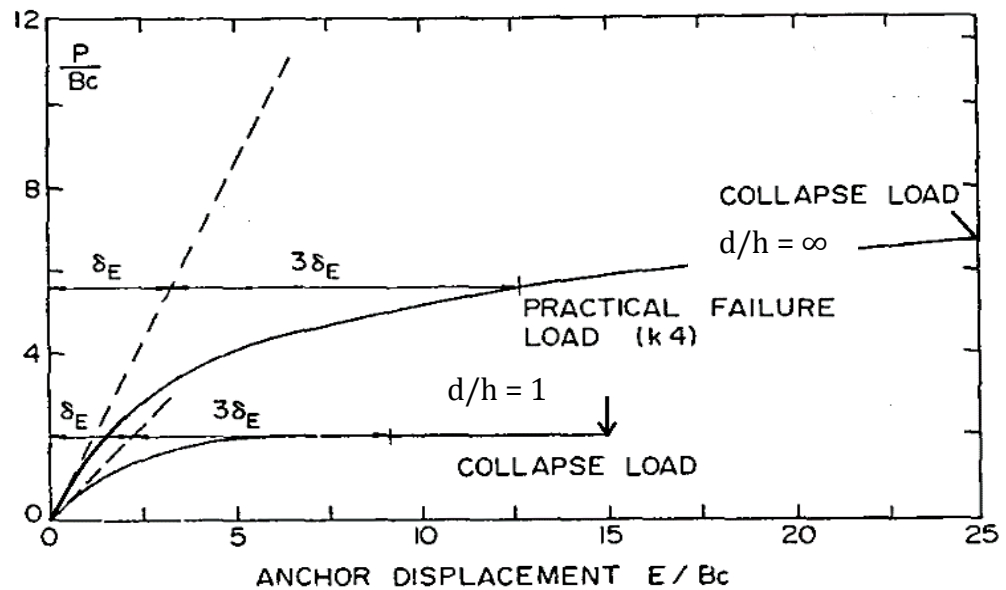


Figure 2.10:  $k_4$  failure concept. (Rowe & Davis, 1982a)

The multiple of 4 was chosen because it provides a typical safety factor of 2.5 to 3 in order to ensure that the working load was close to the linear range. Hence, the displacement of anchor can be predicted by elastic solution (Rowe & Davis, 1982a).

In addition, the  $k_4$  failure load was adopted in order to minimize the contained plasticity and creep effect at working loads. This is because increasing plasticity within soil increases the creep effect.

In 1987, Murray and Geddes adopted limit analysis and limit equilibrium approaches to predict the ultimate pull-out capacity of horizontal deadman anchors pulled vertically in cohesion-less soil. Subsequently, in 1989, Murray and Geddes used the similar approaches to estimate the ultimate pull-out capacity of vertical deadman anchor pulled horizontally. The

ultimate pull-out capacity of a strip anchor based on lower bound solution can be expressed as:

$$T_u = K_p \left(1 - 0.5 \frac{B}{d}\right) \gamma B d \quad \text{Eq. 2.13}$$

In 1994, a generalised lower bound procedure based on finite element and non-linear programming was proposed by Basudhar and Singh. This technique is used to predict the ultimate pull-out capacity of strip deadman anchor (Basudhar & Singh, 1994). Furthermore, the non-linear programming is similar to that used by Sloan (1988).

In 1997, Dickin and King studied the behaviour of deadman anchor by using finite element approach. Two constitutive soil models: (1) the well-established variable-elastic hyperbolic model (Duncan & Chang, 1970) and (2) elasto-plastic model as proposed by Lade and Duncan (1975) were used in the plane strain program named *SOSTV* (Chandrasekaran & King, 1974).

In 2006, another rigorous numerical study on the behaviour of deadman anchor was presented by Merifield and Sloan. They adopted the numerical approaches, such as linear finite element coupled with upper and lower limit analyses, nonlinear finite element coupled with lower bound limit analyses, and displacement finite element using Solid Nonlinear Analysis Code (*SNAC*) to estimate the ultimate pull-out capacity of deadman anchor. *SNAC* is an algorithm developed by Abbo (1997), Abbo and Sloan (1998)

(as cited in Merifield & Sloan, 2006). The ultimate pull-out capacity for strip anchor can be expressed as

$$T_u = \gamma dhN_\gamma \quad \text{Eq. 2.14}$$

In addition, Merifield observed that the soil retained behind deadman anchor can significantly affect the ultimate pull-out capacity of shallow anchor. Furthermore, the effect of interface roughness that changed from perfectly rough ( $\delta = \phi$ ) to perfectly smooth ( $\delta = 0$ ) led to a reduction as much as 65% of the anchor capacity.

In the same year, Naser (2006) analysed the ultimate pull-out capacity of deadman anchor by using limit equilibrium approach. Naser was the only researcher who took into account the effect of three dimensions. Naser derived a three-dimensional (3-D) correction factor ( $M$ ), which can be expressed as:

$$M = 1 + (K_p - K_a)^{0.67} \left[ 1.1E^4 + \frac{1.6F}{1 + 5(B/h)} + \frac{0.4(K_p - K_a)E^3 F^2}{1 + 0.05(B/h)} \right] \quad \text{Eq. 2.15}$$

where,

$E$  = embedment factor =  $1 - h / (d+h)$

$F$  = shape factor =  $1 - (B/s)^2$

$s$  = centre-to-centre spacing between two anchors

The correction factor formula takes into account the shape factor ( $F$ ) and the embedment factor ( $E$ ). For continuous anchor, the value of  $F$  is 0.0; for discrete anchor, the value of  $F$  is 1.0.

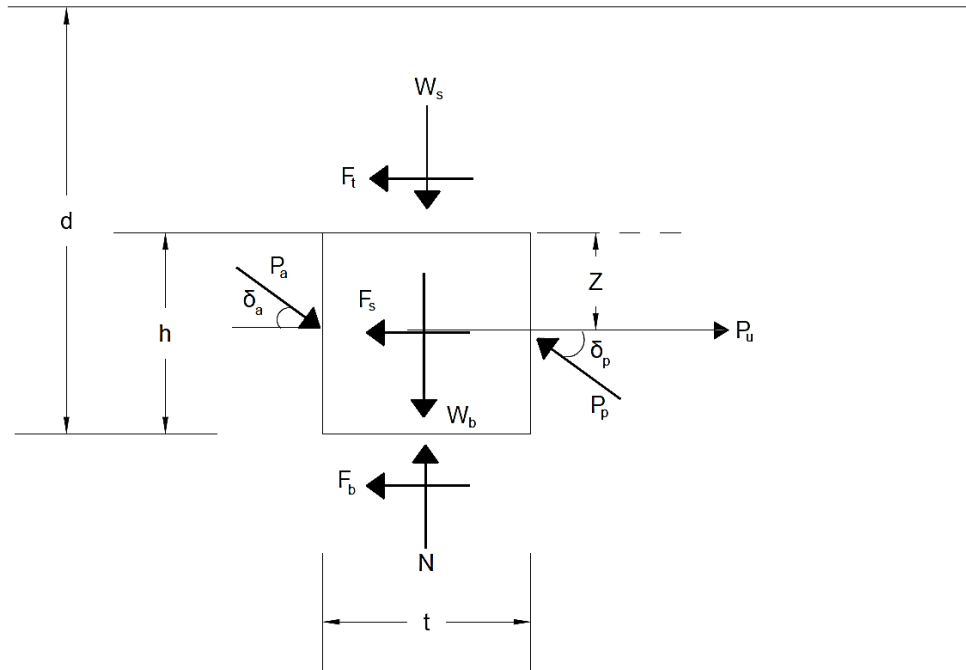


Figure 2.11: Deadman anchor with acting forces. (Naser, 2006)

Thus, the ultimate pull-out capacity with 3-D correction factor can be further expressed as (see Figure 2.11):

$$P_u = M (P_p - P_a) + F_t + F_s + F_b \quad \text{Eq. 2.16}$$

where,

$F_t$  = effective friction force at the top of deadman anchor

$$= W_s * \tan \delta_b$$

$F_s$  = effective friction force at the bottom of deadman anchor

$$= N * \tan \delta_b$$

$F_b$  = effective friction force at two sides of deadman anchor

$$= 2 * K_o * \gamma * d \tan \delta_b * h * t$$

In 2009, Premalatha investigated the effect of tie rod with deadman anchorage system in berthing structure numerically. The soil model follows Mohr-Coulomb failure criterion in finite element software named *PLAXIS*. Premalatha observed that the increase of tie rod length leads to reduction in wall deflection. Nevertheless, beyond certain length of tie rod, the tie rod force and wall deflection have no significant difference and remain constant thereafter.

In 2012, Kumar and Sahoo studied the behaviour of deadman anchor using upper bound theorem of the limit analysis in combination with finite elements. Furthermore, the effect of anchor embedment ratio ( $d/h$ ), friction angle ( $\phi$ ) and soil anchor interface ( $\delta$ ) in influencing the ultimate pull-out capacity of deadman anchor were evaluated. In this research, Kumar and Sahoo concluded that the pull-out capacity increased with the increase in anchor embedment ratio, friction angle and soil anchor interface.

In year 2012, the behaviour of a group of two strip anchor plates embedded in sand along the same vertical plane was presented by Bhattacharya and Kumar. The effect of anchor embedded ratio, friction angle, vertical

spacing between anchors, and the group efficiency factor ( $\eta$ ) were evaluated by using finite element approach with lower bound limit analysis.

Furthermore, Bhattacharya and Kumar concluded that the ultimate pull-out capacity of a group of two anchors increased up to a maximum of 43% compared to a single anchor. In addition, they also reported that deadman anchor is usually placed in a group. Unfortunately, there is hardly any literature reviewing on the horizontal pull-out capacity of a group of deadman anchor.

In the same year, Kame and co-workers (2012) proposed an analytical solution based on limit analysis and limit equilibrium approaches. This proposed analytical solution was used to estimate the ultimate pull-out capacity for strip deadman anchor in terms of dimensionless pull-out force coefficient ( $M_{\gamma q}$ ). The proposed failure mechanism consists of the combination of Logarithmic Spiral and straight lines inclined at  $45^\circ - \phi/2$  to the horizontal in the passive zone, whilst a plane failure surface based on Coulomb failure mechanism in the active zone.

The results from proposed solution are compared with some available experimental and analytical results. The proposed solution can make reasonably good prediction for certain experimental tests (Dickin & Leung, 1985) up to anchor embedment ratio ( $d/h$ ) of 3.0. In addition, Kame and co-workers also reported that there is no unique analytical solution in predicting the ultimate pull-out capacity of deadman anchor in cohesionless soil.

### **2.4.1.1 Summary of Analytical Studies**

The summary of analytical studies is as follows:

1. Most of the numerical studies are focused on the behaviour of direct pull-out for vertical strip deadman anchor.
2. Majority of the existing numerical studies are carried by using 2-D finite element analysis.
3. The most rigorous numerical paper on the behaviour of deadman anchor was delivered by Rowe and Davis (1982b). The soil-structure interaction is discussed.
4. In the real scenario, discrete deadman anchor can only be modelled in 3-D. The behaviour of deadman anchor between 2-D and 3-D may be different. Unfortunately, very few researchers take into account the 3-D effect of deadman anchor.
5. No attempt has been made to determine the behaviour of discrete deadman anchor together with the retaining wall system.

### **2.4.2 Experimental Studies**

In experimental studies, small-scale laboratory model tests on deadman anchor can be performed by either conventional approach under “normal gravity” condition, or centrifuge system, or simultaneously. In conventional approach, the apparatus required is easy to set up and the equipment used can be easily obtained. Therefore, the cost for laboratory

model test under conventional approach is relatively cheaper compared to the centrifuge test. However, the application of small-scale laboratory test is limited unless suitable 'modelling law' is established and is correctly applied.

In centrifuge test, the physical scaling law is implemented to meet the actual field condition. By controlling the gravitational acceleration ( $g$ -value) in centrifuge test, the stress level for centrifuge test can model the actual field condition accurately.

For centrifuge test, the set-up is set to a static gravitational acceleration, which is equal to 1- $g$  at rest. In order to simulate the field stresses for various burial depths, the model is rotated in a centrifugal motion, under gravitational acceleration greater than 1- $g$  to generate the desired stress field. For example, a 1m soil model undergoes acceleration of 40- $g$ . This makes the vertical stress equivalent to that of a depth of 40m below the ground surface. Nevertheless, the centrifuge machine and the set-up cost are very costly; therefore, only a few research institutions possess such equipment.

The main advantage of small-scale laboratory tests over centrifuge tests is that it is able to provide closed, controlled conditions during the laboratory tests. Furthermore, it allows the behavioural trends to be established economically to develop a better understanding on the performance for larger scales (Dickin & Leung, 1983). The observations from laboratory tests can be employed in conjunction with mathematical analysis to

develop semi-empirical theory, which may solve a wide range of geotechnical engineering issues.

The main concern associated with the small-scale conventional test is the presence of scale effects. The stress intensity that arises from the self-weight of soil body may be lower than the actual field prototype. Therefore, it may fail to reflect the actual field condition accurately (Dickin & Leung, 1983). In comparison with small-scale laboratory test, full-scale field test produces the most adequate results. Nevertheless, full-scale test incurs high cost and is time consuming and unfeasible for most of the cases (Merifield, 2002). This is due to the difficulties in obtaining reliable field data under closed, controlled condition, which greatly reduces its viability for research purposes. Therefore, very few researchers conducted full-scale field test to investigate the behaviour of deadman anchor. Consequently, small scale laboratory test is recommended as it is cost effective and convenient in nature.

The existing experimental studies can be found in the works of Balla (1961), Neely and co-workers (1973), Akinmusuru (1978), Rowe (1978), Dickin and Leung (1983, 1985), Murray and Geddes (1987, 1989), Hoshiya and Mandal (1984), Geddes and Murray (1996), Naser (2006), and El Sawwaf and Nazir (2006). Several research papers were used as touchstone for further references.

In 1961, Balla, one of the earliest researchers, investigated the behaviour of deadman anchor. As mentioned earlier, the application of deadman anchor in the early stage was used to resist vertical uplift forces, which

acted as support for transmission towers. Preliminarily, these towers were supported by large mass concrete blocks (deadman) which provided sufficient uplift resistance capacity to overcome the vertical uplift force. Nevertheless, this design was not encouraged as it is very costly and unpractical. Thereby, Balla carried out a research in order to discover a more economical solution. The solution developed by Balla is known as belled piers or mushroom foundation.

In 1973, Neely and co-workers, few of the earliest researchers, who investigated the behaviour of vertical deadman anchors in sand using small-scale laboratory test. The laboratory tests were conducted using anchor, with aspect ratios ( $B/h$ ) 1 (square), 2 and 5 (both rectangular), embedded in sand with friction angle of  $38.5^\circ$ . In their experiment, the anchors were investigated up to anchor embedment ratio ( $d/h$ ) of 5. The observations obtained in the experiment were:

- i. The load-displacement relationships were correlated positively until the end of the tests.
- ii. Square anchors with  $d/h > 2$  had very large movement.

In conclusion, Neely and co-workers were unable to determine the ultimate pull-out capacity and the critical embedment depth for deadman anchors. Therefore, an alternative criterion is introduced to determine the ultimate pull-out capacity, namely typical nature of load-displacement approach (see Figure 2.12).

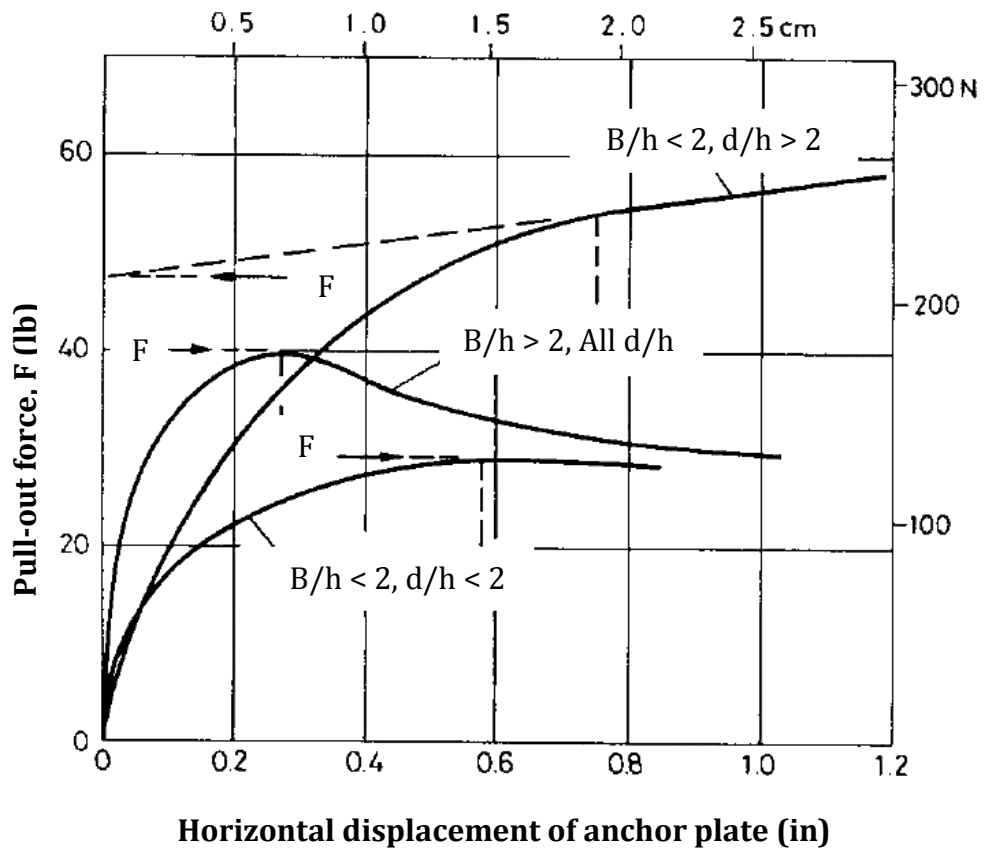


Figure 2.12: Typical nature of load-displacement diagram. (Neely et al., 1973)

In 1975, Das and Seeley were the first researchers who were concerned on the allowable pull-out displacement that imposed restrictions on the design load. In their experiment, deadman anchors with aspect ratio ( $B/h$ ) of 1, 3 and 5 with thickness of 50mm were embedded in sand with friction angle of  $34^\circ$ . The anchor embedment ratios investigated in this pull-out test were up to  $d/h = 4$ .

Das and Seeley also proposed a simple semi-empirical relation to estimate the ultimate pull-out capacity of anchor. The semi-empirical relation is derived from the laboratory model tests. For single anchor, the

dimensionless pull-out force coefficient from semi-empirical relation can be expressed as:

$$M_{\gamma q} = (4.59 \times 10^{-5}) S \phi^{3.22} \left(\frac{d}{h}\right)^n \quad \text{Eq. 2.17}$$

where,

$S$  = shape factor (which is a function of  $d/h$  and  $\phi$ )

The  $n$  value varies linearly from 1.8 to 1.65 for  $B/h = 1$  to 5. The load-displacement relationship developed is used to assist the design of structures where total displacement is the controlling criteria.

In 1978, Akinmusuru studied the behaviour of deeper deadman anchors in sand. Anchor with various shapes, such as square ( $B/h = 1$ ), rectangular ( $B/h = 2, 10$ ) and circular with embedment ratio of up to 10 were examined in the small-scale laboratory test. The novelty of this research was that the soil was simulated using 76mm steel pins in order to provide better observation on the failure mechanism for deadman anchors, especially for the case with  $B/h = 10$ . The soil also produced friction angles of  $24^\circ$  and  $35^\circ$ . In addition, the movement of steel pins was photographed for each test.

The observations made from this experiment were:

- i. The behaviour of deadman anchor changed from shallow to deep at  $d/h = 6.5$ .
- ii. A circular failure shape formed immediately above the deadman anchor (see Figure 2.8) for  $d/h > 6.5$ .

- iii. Pull-out capacity continuously increased and no peak load was observed until the end of the test.
- iv. Circular anchor had the largest pull-out force compared to others.

Consequently, Akinmusuru was unable to determine the ultimate pull-out capacity for deadman anchors even though the critical embedment ratio was clearly defined at 6.5.

In 1983, the most rigorous experimental study into the behaviour of deadman anchor in dense sand was presented by Dickin and Leung. Square and rectangular deadman anchors were used in both conventional and centrifuge tests in their research. They found that the results obtained were significantly different between conventional and centrifugal tests. For a square deadman anchor, the predicted ultimate pull-out capacity varied as much as 80% for the most extreme case.

Furthermore, they concluded that:

- i. Centrifuge test could successfully predict the field scale behaviour of deadman anchor, which was better than conventional test.
- ii. The errors between these tests arised mainly due to the characteristic stress-dependent behaviour of dense sand.
- iii. The critical embedment ratio decreased with anchor size.

In 1984, investigation on the behaviour of square and rectangular aluminium anchors in loose sand was presented by Hoshiya and Mandal.

They adopted the smallest sand box with dimension of 0.3m x 0.4m x 0.4m for their laboratory test. The purpose of this smallest testing chamber was to introduce the edge effects into the experimental results. The conclusion from their research was that the critical embedment ratio for rectangular anchors is approximately 5.

In 1985, Dickin and Leung extended their previous research in 1983 to evaluate the existing available analytical solutions and compared them with their conventional and centrifuge model tests for single and continuous anchors embedded in dense sand. The observations made by Dickin and Leung were:

- i. For 50mm anchor, the results were significantly dissimilar with the existing analytical solutions.
- ii. For 1m anchor, the results were in a good agreement with the analytical solutions developed by Ovesen and Stromann (1972) and Meyerhof (1973) provided that the mobilised friction angle is in the mass rather than in the peak.
- iii. The design charts developed based on finite element analysis by Rowe and Davis (1982b) gave slightly overoptimistic prediction.

In 1989, Murray and Geddes extended their early research in 1987 into investigation on the pull-out tests of vertical and inclined deadman anchors in dense sand. In contrast to the outcomes of Hoshiya and Mandal (1984), there was no critical anchor embedment ratio observed in their research.

In 1996, Geddes and Murray conducted laboratory tests to study the behaviour of anchor groups pulled vertically in sand. It is worth mentioning this literature as they studied the effects of anchor groups and the spacing between anchors ( $s$ ). These tests were carried out in groups of two, four and five discrete deadman anchors embedded at a constant depth.

The efficiency of a two-plate group increased from approximately 59% to approximately 90% for separation ratio ( $s/B$ ) = 0 to 2. For a four-plate group in square configuration, the efficiency is less than two-plate group for specific  $s/B$  ratio. For a five-plate group in row configuration, the efficiency increased from 35% to 100% for  $s/B = 0$  to 2.

The conclusion from this research were:

- i. The efficiency of a group of anchors increases from a relatively low value as the spacing between anchors is increased.
- ii. The maximum efficiency (100%) is reachable at a critical spacing ratio ( $s/B$ ) at 2.9 for all configurations and number of anchors. The maximum efficiency of anchor groups remain at 100% even when  $s/B > 2.9$ .
- iii. The individual load at both ends of the anchors in a five-plate group with row configuration carried the greatest load, whereas the central anchor carried the least load.

In 2006, Naser conducted small-scale laboratory tests to investigate the effect of degree of saturation (wet, dry and saturated conditions) on the

pull-out capacity of 0.15m<sup>3</sup> deadman anchor block. In the experiment, sand pluviation technique was used to ensure uniform and reproducible density of soil. Naser derived the 3-D correction factor ( $M$ ) for the analytical solution in determining the pull-out capacity of deadman anchor (see Eq. 2.15 and Eq. 2.16). The results with the 3-D effects were in a good agreement with Rankine's theory.

### **2.4.2.1 Summary of Experimental Studies**

The summary of experimental studies is as follows:

- a. Vertical deadman anchors are usually used as tieback support for retaining structures, however, the experimental studies on vertical deadman anchors are still limited compared to horizontal deadman anchors.
- b. Results obtained from experimental studies are limited to specific cases, however, these results are difficult to extend to solve similar problems that involve different material and/or geometry variables.

### **2.4.3 Field Test Studies**

Full scale field test produces the most adequate results. However, full-scale field test is very expensive and is difficult to obtain reliable field data under closed, controlled test condition that greatly reduces its viability for

research purposes. Therefore, researchers rarely conducted full scale field test to investigate the behaviour of deadman anchor.

Geddes and Murray (1996) reported that the horizontal translation of rows of three square anchor plates pulled vertically in sand, which was presented by Hueckel (1957), who found that below a particular spacing between anchor plates, the efficiency of the group of anchor plates decreased as the spacing was further reduced.

The results reported by Hueckel (1957) under laboratory test were agreed by Smith (1962), who also carried out experiment on horizontal translation of groups of three anchor plates pulled vertically in sand under full-scale field test. (Geddes & Murray, 1996)

Therefore, full-scale field condition can be reasonably simulated by numerical analysis provided that the numerical analysis has been verified by laboratory test.

## **2.5 Summary**

A summary on previous analytical and experimental studies is presented in Table 2.1 and Table 2.2, respectively.

Table 2.1: Analytical studies on vertical anchors in cohesion-less soils.

Sources	Analysis method	Anchor shape	Friction angle (°)	d/h
<b>(Biarez et al., 1965)</b>	Limit equilibrium	Strip	All	All
<b>(Meyerhof, 1973)</b>	Limit equilibrium – semi analytical	Strip	All	All
<b>(Neely et al., 1973)</b>	Limit equilibrium and method of characteristics	Strip	30-45	1-5.5
<b>(Rowe &amp; Davis, 1982a, 1982b)</b>	Elasto-plastic finite element	Strip	0-45	1-8
<b>(Hanna, Das, &amp; Foriero, 1988)</b>	Limit equilibrium	Strip; inclined	All	All
<b>(Murray &amp; Geddes, 1989)</b>	Limit analysis – upper bound	Strip; inclined	43.6	1-8
<b>(Basudhar &amp; Singh, 1994)</b>	Limit analysis – lower bound	Strip	32; 35; 38	1-5
<b>(Dickin &amp; King, 1997)</b>	Finite element analyses	Strip	All	3,5,7, 9,12
<b>(Merifield &amp; Sloan, 2006)</b>	Finite element upper and lower bound, displacement finite element	Square; rectangular; circular; Inclined	20; 30; 40	All
<b>(Bhattacharya &amp; Kumar, 2012)</b>	Lower bound finite element limit analysis	Strip	25-40	5;7
<b>(Kumar &amp; Sahoo, 2012)</b>	Upper bound finite limit analysis	Strip	20-45	1-7

Table 2.2: Experimental studies on vertical anchors in cohesion-less soils.

Sources	Type of testing	Anchor shape	Anchor size (mm)	Friction angle (°)	d/h or d/Dia
(Neely et al., 1973)	Chamber	Square; rectangular	50.8	38.5	1-5
(Das, 1975)	Chamber	Square, circular	38-76	34	1-5
(Das & Seeley, 1975)	Chamber	Square, rectangular	50	34	1-4
(Akinmusuru, 1978)	Chamber	Square; rectangular; strip; circular	50	24;35	1-10
(Ovesen, 1981)	Centrifuge; field	Square	20	29.5-37.7	1-3.39
(Dickin & Leung, 1983, 1985)	Centrifuge chamber	Square, rectangular strip	25; 50	52	1-8; 1-13
(Hoshiya & Mandal, 1984)	Sand chamber	Square; rectangular	25.4	29.5	1-6
(Murray & Geddes, 1989)	Sand chamber	Square; rectangular	50.8	43.6	1-8
(Geddes & Murray, 1996)	Sand chamber	Square	50.8	43.6	4
(Naser, 2006)	Sand chamber	Square	150	44.9	0.5
(El Sawwaf & Nazir, 2006)	Sand chamber	Strip; square	75	37;41	1.5-2.5

The existing analytical studies presented in Table 2.1 are mostly focused on the ultimate pull-out capacity of strip deadman anchor (2-D condition). Whereas, the existing experimental studies presented in Table 2.2 are focused on the ultimate pull-out capacity of discrete deadman anchor (3-D condition) in both square and rectangular shapes. In fact, deadman anchor is 3-D in nature. The effect of three-dimensional (3-D) on the behaviour of discrete deadman anchor is of considerable importance. However, the literature contribution in determining the ultimate pull-out capacity of deadman anchor by adopting 3-D numerical analysis is still very lacking.

In addition, none of the literature contribution takes into consideration of the presence of anchored wall during the study on the behaviour of discrete deadman anchor. The following chapter presents the methodology of finite element analysis for the study on the behaviour of discrete deadman anchor with the presence of anchored wall.

# CHAPTER 3

---

## METHODOLOGY

### 3.1 Introduction

This chapter discusses the methodology of finite element analysis (FEA) for both two-dimensional (2-D) and three-dimensional (3-D) models that were used in this research study. The chapter, furthermore, discusses the 1-g small-scale laboratory test that was used for verification of finite element prediction. The finite element analysis is carried out by using finite element software named *PLAXIS*.

### 3.2 Finite Element Analysis (FEA)

The previous chapter reported that most of the rigorous numerical research studies (Merifield & Sloan, 2006; Rowe & Davis, 1982b) were

carried out using Finite Element Method (FEM). This is because the main advantage of FEM is that the FEM is capable to simulate complicated geotechnical problems. The non-linear solver in FEM can solve problem that involves various types of geometric and material properties (e.g. rock, soil, concrete, steel, etc.).

FEM solves governing differential equation of a system through discretisation process. It discretises the whole structure (system) into finite elements. The computational techniques based on FEM have become more popular and are used widely to solve the complicated geotechnical engineering problems, which are unable to be solved by the traditional analytical analysis methods.

In geotechnical engineering practice, the important phenomena include behaviour/mechanism, construction sequence and time-dependent consolidation that can be predicted reasonably well by FEM, provided that the input parameters are set appropriately. Thus, the complexity of interactions between soil-anchor-wall in this research can be predicted reasonably well by FEM. In addition, three dimensional (3-D) finite element analyses can predict a more realistic scenario on geotechnical problems.

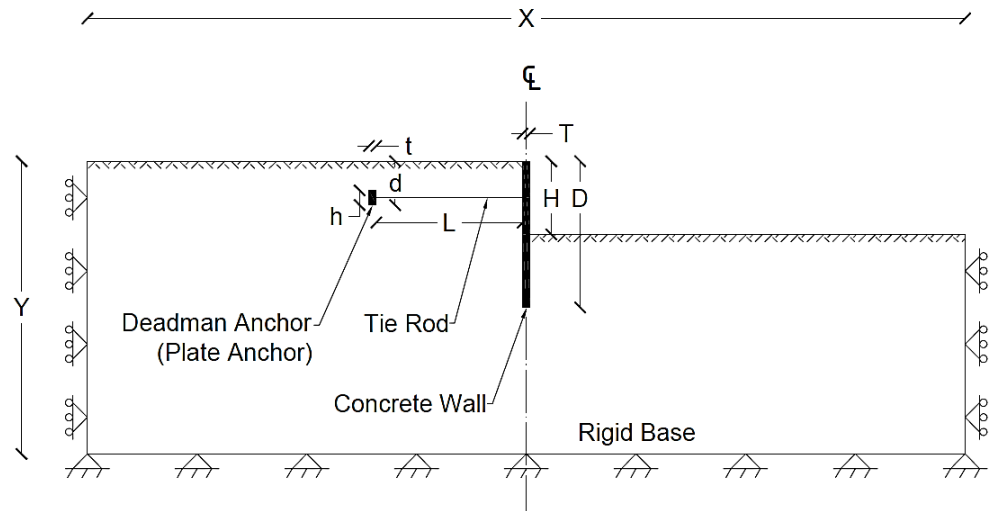
Therefore, finite element approach was chosen to carry out numerical simulations in this research. The finite element software named *PLAXIS* was adopted. *PLAXIS* was developed based on a set of complex numerical formulations. The computational algorithm evaluates the problems by using an elastic stiffness matrix (Brinkgreve, Broere, & Waterman, 2006).

The following sub-chapters discuss the finite element model, element, material property, boundary condition and finite element mesh used in *PLAXIS* in this research.

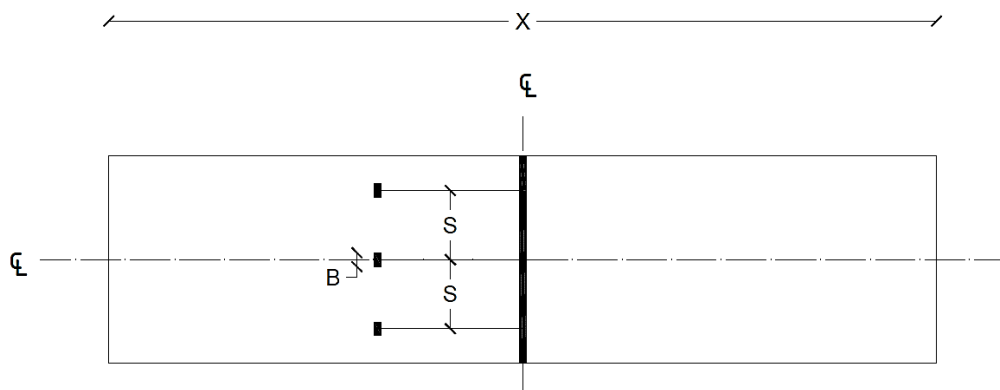
### **3.3 Prototype Configuration**

The prototype adopted in finite element analysis comprises of four types of elements, which are soil, deadman anchor, earth retaining wall and tie rod. The configuration of the prototype is that the earth retaining wall is installed prior to the installation of deadman anchor. Subsequently, deadman anchor is embedded into an excavated trench behind the earth retaining wall. The earth retaining wall and deadman anchor are connected by tie rod, which known as anchored wall and it is illustrated in Figure 3.1.

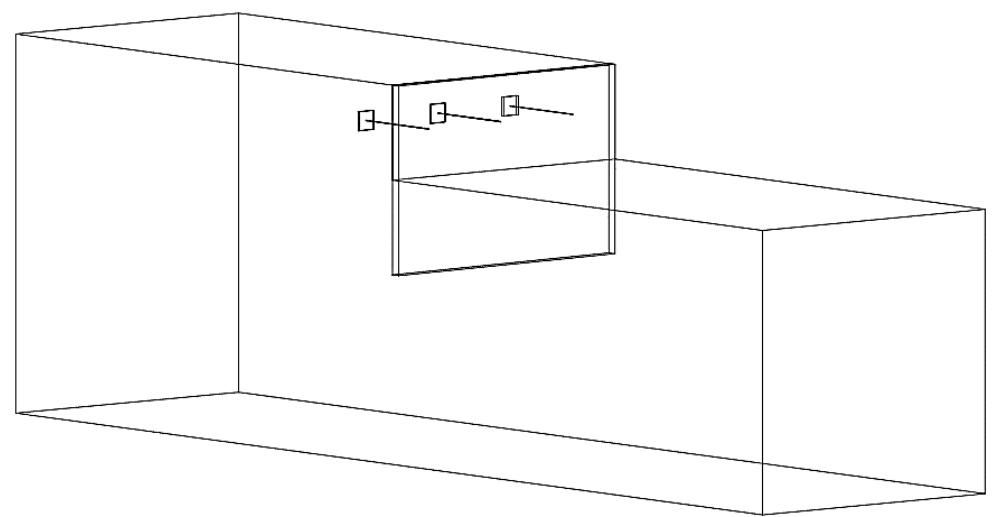
Once the installation process is accomplished, the excavation to every 0.5m interval begins until it reaches the maximum allowable excavation height ( $H_{max}$ ). The excavation to each 0.5m interval reflects actual scenario on the construction site. The excavation height for each layer is limited to 0.5m, which aims to avoid the collapse of soil body due to excavation.



a. Side Elevation



b. Plan Elevation



c. 3-D View

Figure 3.1: Prototype configuration – a. Site Elevation, b. Plan Elevation and c. 3-D View.

### **3.4 Design Criteria**

In this research, the study of behaviour of discrete deadman anchorage system is subjected to the deflection of earth retaining wall. The maximum allowable excavation height ( $H_{max}$ ) is determined based on the constraint of wall deflection that is limited to 0.5% of the excavation height ( $H$ ). This is recommended in British Standard BS-8002 (1994): Clause 3.2.2.4, which is also applied for “unplanned” excavation in front of retaining wall, minimum surcharge loading and water pressure regime.

Furthermore, Long summarised 300 cases of worldwide histories on retaining walls and ground movements in deep excavation, 226 cases on stiff soil and 74 cases on soft soil (Long, 2001). Long observed that there were approximately 92.5% out of 226 cases of stiff soil in which the wall deflection did not exceed 0.5%  $H$ . This complied with the design criteria that stated in BS-8002.

### **3.5 Behaviour of Discrete Deadman Anchorage System**

The behaviour of discrete deadman anchorage system in anchored wall are carried out using parametric studies. The key parameters used to study the behaviour of discrete deadman anchorage system in anchored wall are as follows:-

- a. Length of tie-rod
- b. Embedment depth of anchor

- c. Spacing of anchor
- d. Friction angle of soil
- e. Depth of anchored wall
- f. Stiffness of anchored wall

The behaviour of discrete deadman anchorage system in anchored wall are studied by investigating the effect of these parameters. During the study on the effect of these parameters, only a single parameter is investigated, while the remaining parameters are kept constant. The magnitude used to study the effect of each parameter is tabulated in Table 3.1.

Table 3.1: Magnitude of key parameter for parametric study.

<b>Influence Factors</b>		
<b>Tie rod length, <math>L</math> (m)</b>	:	5, 10, 15
<b>Anchor embedment depth, <math>d</math> (m)</b>	:	1, 2, 3
<b>Anchor spacing, <math>s</math> (m)</b>	:	2, 3, 5
<b>Friction angle of soil, <math>\phi</math> (°)</b>	:	20, 25, 30, 35, 40
<b>Wall depth, <math>D</math> (m)</b>	:	10, 15, 20
<b>Wall stiffness, <math>EI</math> (kNm<sup>2</sup>)</b>	:	2.708E+05 (Diaphragm wall) 4.560E+04 (FSP IIIA) 1.445E+05 (PU 32)

For this research, the general geometries of deadman anchorage system comprise of 25mm diameter of tie rod and 1.0m x 1.0m x 0.5m of concrete deadman anchor.

## 3.6 PLAXIS Model

In *PLAXIS*, a set of pre-processing input is required before the simulation commences. The pre-processing input comprises of model, element, material properties, boundary conditions and finite element mesh. The pre-processing input process determines the accuracy of finite element analysis (FEA). The pre-processing input for both 2-D and 3-D models is discussed below.

### 3.6.1 3-D Model

#### 3.6.1.1 Soil

The soil was modelled using the Hardening Soil (HS) model with ten-node tetrahedral elements. The HS model was chosen as it takes into account the variation of stiffness between virgin-loading and unloading-reloading (Kok, 2010). The ten-node tetrahedral elements allow a second order interpolation of displacements. It contained three local coordinates ( $\xi$ ,  $\eta$  and  $\zeta$ ) and was numerically integrated using four-point Gaussian integration (see Figure 3.2).

In general, HS model requires some basic soil parameters in *PLAXIS*, such as:

- a. Stress dependent stiffness according to a power law ( $m$ )
- b. Secant stiffness for triaxial test ( $E_{50}^{ref}$ )

- c. Tangent oedometer stiffness ( $E_{oed}^{ref}$ )
- d. Elastic unloading/reloading ( $E_{ur}^{ref}, \nu_{ur}$ )
- e. Mohr-Coulomb failure criterion:
  - i. Friction angle ( $\phi$ )
  - ii. Dilatancy angle ( $\psi$ )
  - iii. Cohesion ( $c$ ).

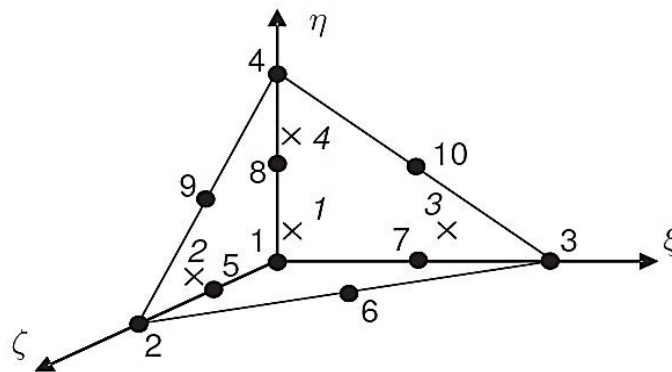


Figure 3.2: Local numbering and positioning of node (•) and integration points (x) of a ten-node tetrahedral element. (*Plaxis 3D User Manual, 2012*)

### 3.6.1.2 Earth Retaining Wall and Deadman Anchor

The earth retaining wall and deadman anchor were modelled using linear elastic model with six-node triangular plate elements (structural area elements). The six-node triangular plate elements have six degrees of freedom per node, three translational degrees of freedom ( $U_x$ ,  $U_y$  and  $U_z$ ) and three rotational degrees of freedom ( $\phi_x$ ,  $\phi_y$  and  $\phi_z$ ). They are directly integrated over their cross section and are numerically integrated using three-point Gaussian integration (see Figure 3.3).

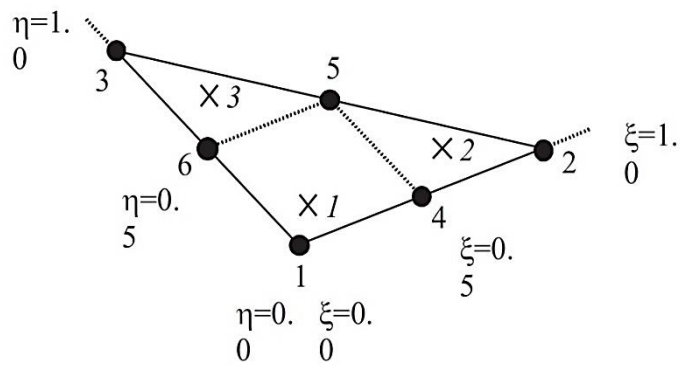


Figure 3.3: Local numbering and positioning of node ( $\bullet$ ) and integration points (x) of a six-node triangular plate element. (*Plaxis 3D User Manual*, 2012)

### 3.6.1.3 Tie Rod

The tie rod was modelled using linear elastic model with structural line elements (node-to-node anchor). The structural line elements consist of a two-node element with one degree of freedom per node in the rotated coordinate system.

### 3.6.1.4 Material

The general material properties that were assigned to these structural models are as follows:

**a. Soil Properties:**

Unit weight of soil, $\gamma$ (kN/m <sup>3</sup> )	=	20.00
Secant stiffness for triaxial test, $E_{50}^{ref}$ (kN/m <sup>2</sup> )	=	30.00E+03
Tangent oedometer stiffness, $E_{oed}^{ref}$ (kN/m <sup>2</sup> )	=	30.00E+03
Unloading/reloading stiffness, $E_{ur}^{ref}$ (kN/m <sup>2</sup> )	=	90.00E+03
Friction angle, $\phi$ (°)	=	30.00
Dilatancy angle, $\psi$ (°)	=	0.00
Cohesion, $c_{ref}$ (kN/m <sup>2</sup> )	=	0.00
Effective Poisson's ratio, $\nu_{ur}'$	=	0.30

**b. Concrete properties:**

Unit weight of concrete, $\gamma_c$ (kN/m <sup>3</sup> )	=	24.00
Concrete cube strength, $f_{cu,28} / f_{ck,cube}$ (kN/m <sup>2</sup> )	=	30.00E+03
Young's Modulus of concrete, $E_c$ (kN/m <sup>2</sup> )	=	26.00E+06
Effective Poisson's ratio, $\nu'$	=	0.18

BS 8110 part 2

pg. 52

$$E_{c,28} = K_0 + 0.2 f_{cu,28}$$

$$K_0 = 20 \text{ kN/mm}^2$$

Eq. 3.1

$$E_{cd} = \frac{E_{cm}}{\gamma_{ce}} \quad \text{Eq. 3.2}$$

$$\gamma_{ce} = 1.2$$

BS,EN 1992-1-1: Clause 5.8.6

The Young's Modulus of concrete based on the concrete cube strength ( $f_{cu,28}$ ) of 30.0MPa for both British Standard (BS 8110-2, 1985) and Euro Code (BS EN 1992-1-2, 2004) were determined to be 26.0GPa and 25.8GPa, respectively (See Eqs. 3.1 and 3.2). The results from BS and EC were similarly close, thus the Young's Modulus of concrete was adopted to be 26.0GPa.

**c. Steel properties:**

Unit weight of steel, $\gamma_s$ (kN/m <sup>3</sup> )	=	78.50
Elastic modulus of steel, $E_s$ (kN/m <sup>2</sup> )	=	20.00e+07
Poisson's ratio, $\nu$	=	0.27

The basic physical properties of steel (structural ASTM A7-61T) were obtained from Rosato and co-workers (2001).

### 3.6.1.5 Boundary Conditions

The boundary condition is one of the factors that may influence the accuracy of finite element analysis (FEA). The boundary condition for the finite element prototype is illustrated in Figure 3.1. The vertical boundaries of the prototype were set as roller, which means that it was restrained from horizontal movement, whilst the bottom boundary was pinned, which means that it was completely restrained from any movement. However, this restriction was automatically generated by the finite element software, *PLAXIS 3D*.

If the size of prototype was inadequate, the boundary effect might occur and influence the accuracy of FEA. Insufficient prototype size might restrict the soil movement, and might not simulate the actual behaviour of the problem. Therefore, the boundary effect was necessary to be avoided.

An investigation into the boundary effect was carried out in order to determine the adequate size for finite element prototype. The longest tie rod was used for this investigative study. Figure 3.4 shows that the maximum lateral soil movement did not occur proximate to the boundaries. This provides sufficient evidence to conclude that the size of prototype was sufficient for FEA, which is able to eliminate the boundary effect.

The result of prototype size for various depths of retaining wall ( $D$ ) is presented in Table 3.2.

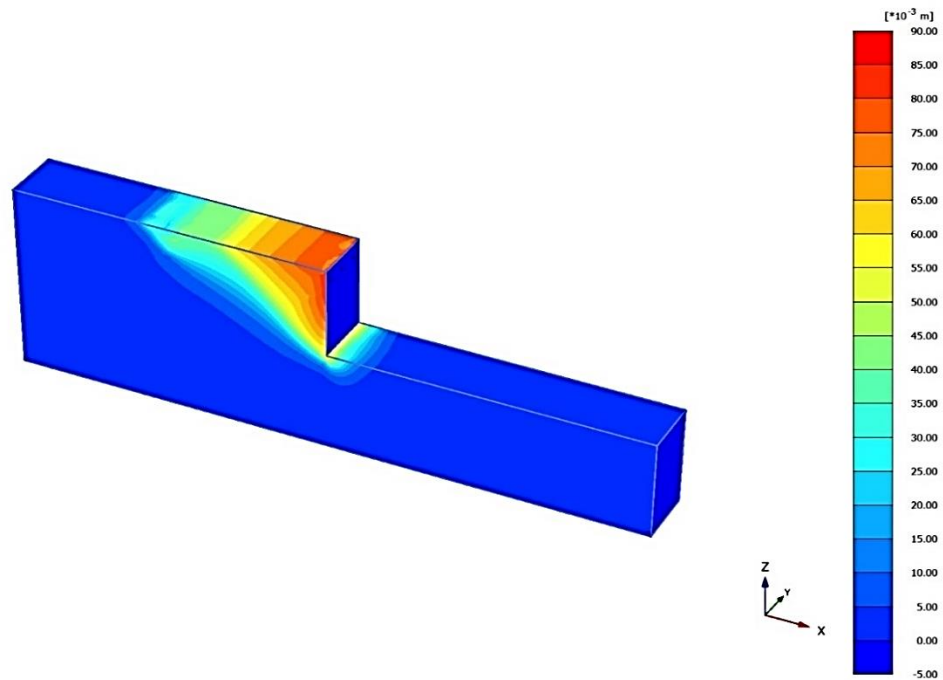


Figure 3.4: Lateral movement of the soil ( $U_x$ ).

Table 3.2: The size of prototype.

D (m)	X (m)	Y (m)
10	60	20
15	60	20
20	100	40
25	100	40

### 3.6.1.6 Mesh Investigation

The accuracy of FEA is not only depending on the type of elements and boundary condition, but it also depends on the size and arrangement of the elements (Merifield, 2002). The arrangement of elements is automatically

distributed by *PLAXIS*. An investigation into the size of elements (mesh studies) was carried out to study the effect of mesh size. The main aim of this study was to emphasize the mesh adopted in FEA.

Five types of mesh (i.e. very coarse, coarse, medium, fine and very fine mesh) were used in this investigative study (see Figure 3.5). The number of elements and nodes for each mesh is given in Table 3.3. The result of this study was determined based on the wall deflection and the pull-out force.

The very fine mesh has the most amount of elements and nodes compared to other meshes as shown in Table 3.3. The very fine mesh has greatest number of elements and nodes aggregated around deadman anchor and tie rod as shown in Figure 3.5. This allows smoothest deformation, and hence provides better estimation. In addition, Merifield reported that more number of elements and nodes could provide better solution (Merifield, 2002).

Table 3.3: Number of elements and nodes for various types of mesh.

<b>Mesh</b>	<b>Elements</b>	<b>Nodes</b>
<b>Very coarse</b>	3226	5498
<b>Coarse</b>	7120	11349
<b>Medium</b>	15112	23188
<b>Fine</b>	23679	36021
<b>Very fine</b>	48294	71507

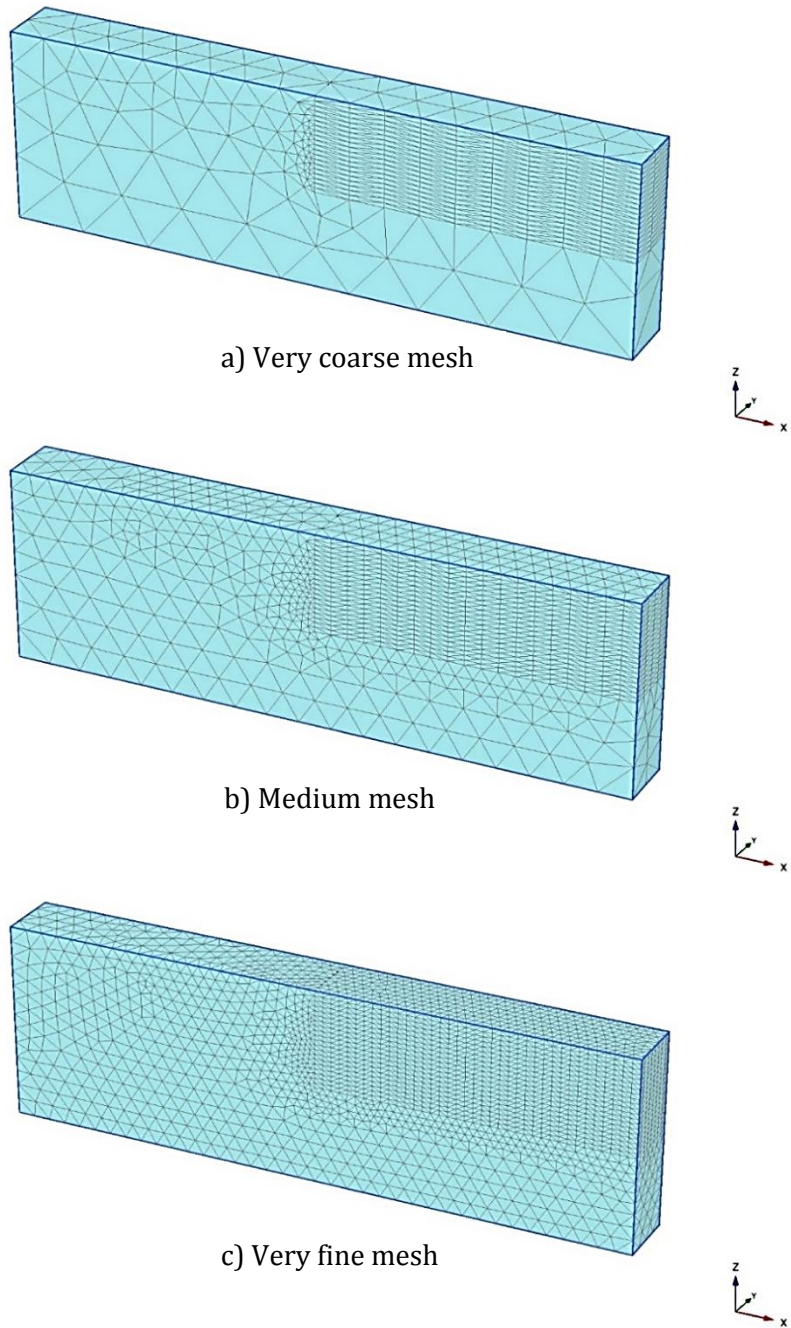


Figure 3.5: Types of meshes – a) very coarse mesh, b) medium mesh and c) very fine mesh.

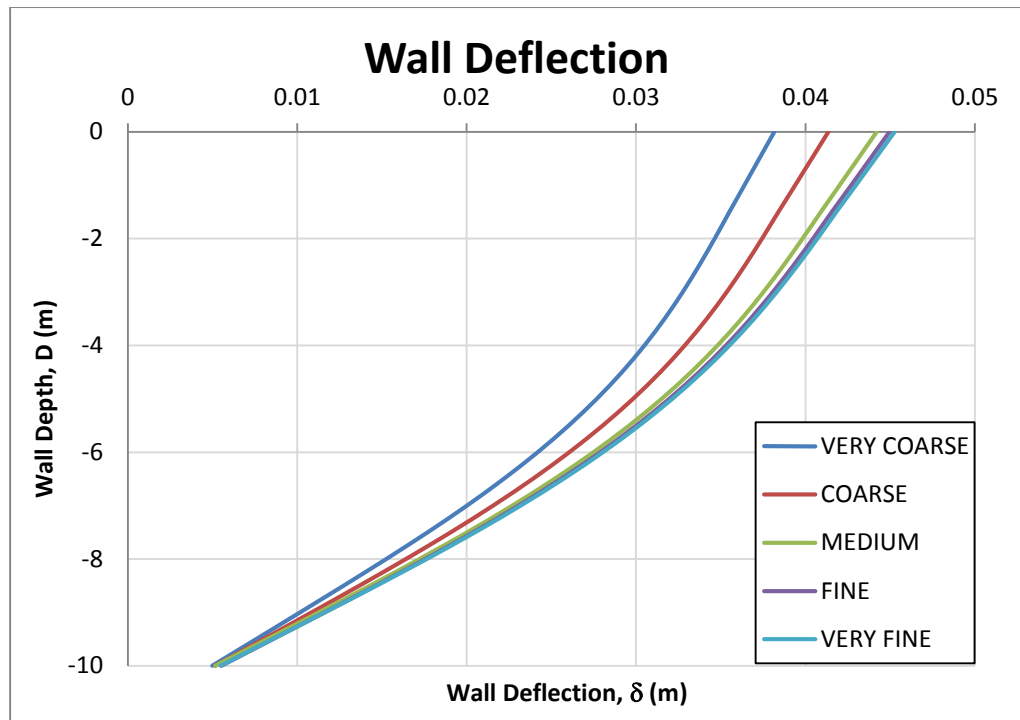


Figure 3.6: Wall deflection ( $\delta$ ) for various types of mesh.

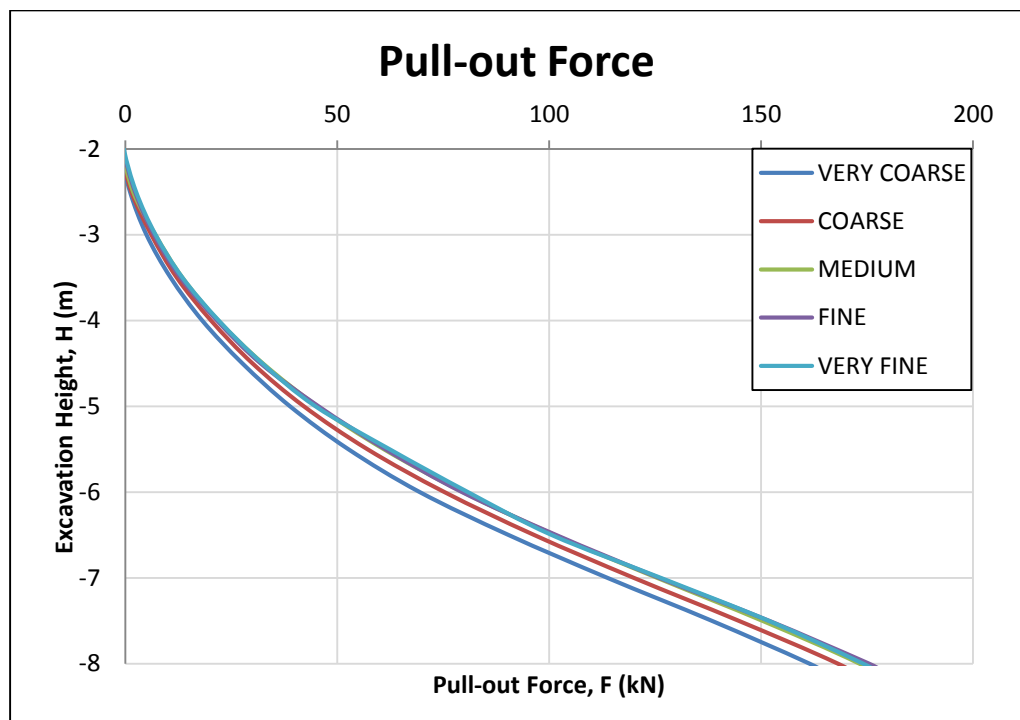


Figure 3.7: Pull-out force ( $F$ ) for various types of mesh.

Figure 3.6 and Figure 3.7 show wall deflection and pull-out force converging from very coarse mesh to very fine mesh. The percentage of variation from fine to very fine is relatively small compared to other meshes.

Therefore, it is believed that if the very fine mesh refine to extremely fine mesh, the percentage of variation may reduce with similar rate as the refinement from fine mesh to very fine mesh. Thus, the very fine mesh is considered to be the most suitable mesh for FEA.

### **3.6.2 2-D Model**

In 2-D model, the model elements implemented in modelling are completely different from 3-D model. However, the size of prototype, materials, boundary conditions and mesh adopted in 2-D model were exactly identical with 3-D model.

#### **3.6.2.1 Soil**

The soil was modelled using HS model with fifteen-node triangular elements. Although fifteen-node triangular elements have the same total number of nodes and stress points as four six-node triangular elements (see Figure 3.8), however, the fifteen-node triangular elements are more powerful than four six-node triangular elements. This is because fifteen-

node triangular elements produce high quality stress results for complicated problems, which able to provide more accurate estimation on deformation and stability.

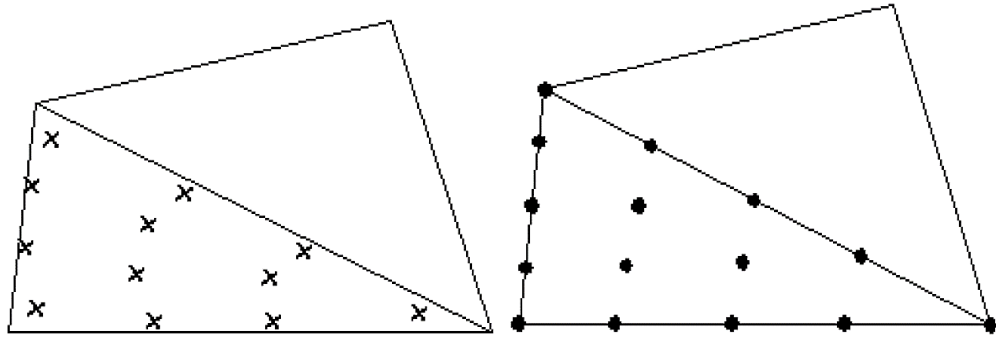


Figure 3.8: Position of stress points (x) and nodes (•) of a fifteen-node triangular element. (Brinkgreve et al., 2006)

### 3.6.2.2 Earth Retaining Wall and Deadman Anchor

The earth retaining wall and deadman anchor were modelled using linear elastic model with five-node beam elements. Beam elements have three degrees of freedom per node, two translational degrees of freedom ( $U_x$  and  $U_y$ ) and a rotational degree of freedom ( $\phi_z$ ). Five-node beam elements contain four pair of stress points as shown in Figure 3.9.

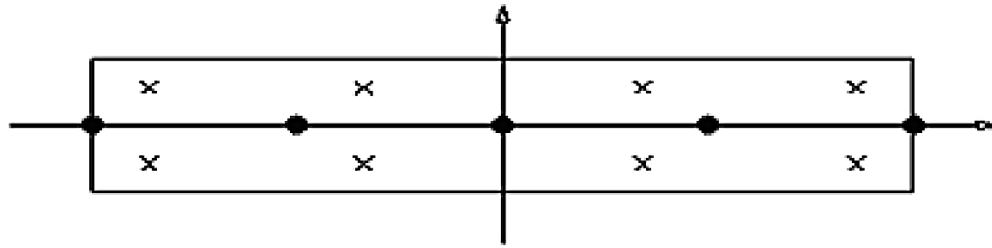


Figure 3.9: Position of stress points (x) and nodes (•) of a five-node beam element. (Brinkgreve et al., 2006)

### 3.6.2.3 Tie Rod

The tie rod was modelled using linear elastic model with node-to-node anchor element. The node-to-node anchor is a two-node elastic spring element with constant spring stiffness.

## 3.7 Verification of Finite Element Software

This section presents the methodology on the verification of finite element analysis adopting 1-g small-scale laboratory test. Partial verification on the finite element analysis was carried out with pull-out test of discrete deadman anchor.

A random test verification was chosen to examine the accuracy of finite element estimation on the pull-out test of discrete deadman anchor. Prior to 1-g small-scale laboratory test, the characteristic of soil has to be

determined as the physical properties of soil may have significant effect on the accuracy of finite element estimation.

The physical properties of soil were identified by a series of laboratory tests, which are:-

- a. Sieve analysis test,
- b. Direct shear box test,
- c. Oedometer test, and
- d. Density test with pre-determined sand placement height.

The schematic diagram of 1-g small-scale laboratory test set up is illustrated in Figure 3.10 to Figure 3.12. The set-up and procedure of laboratory test will be detail discussed in Chapter 4.

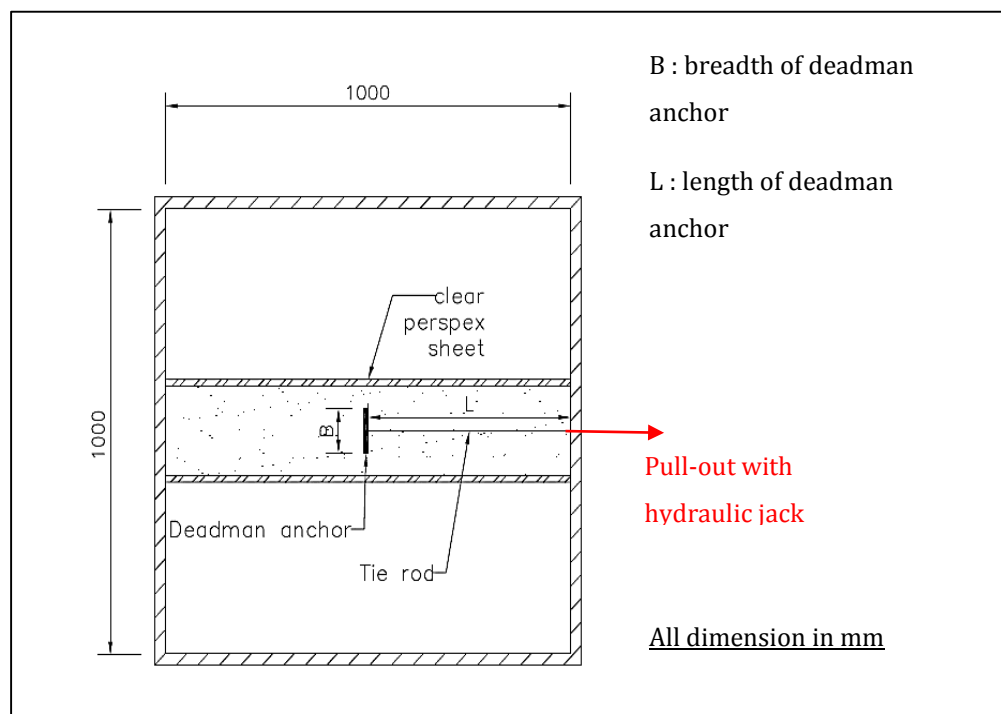


Figure 3.10: Schematic diagram of 1-g small-scale laboratory test (Plan View).

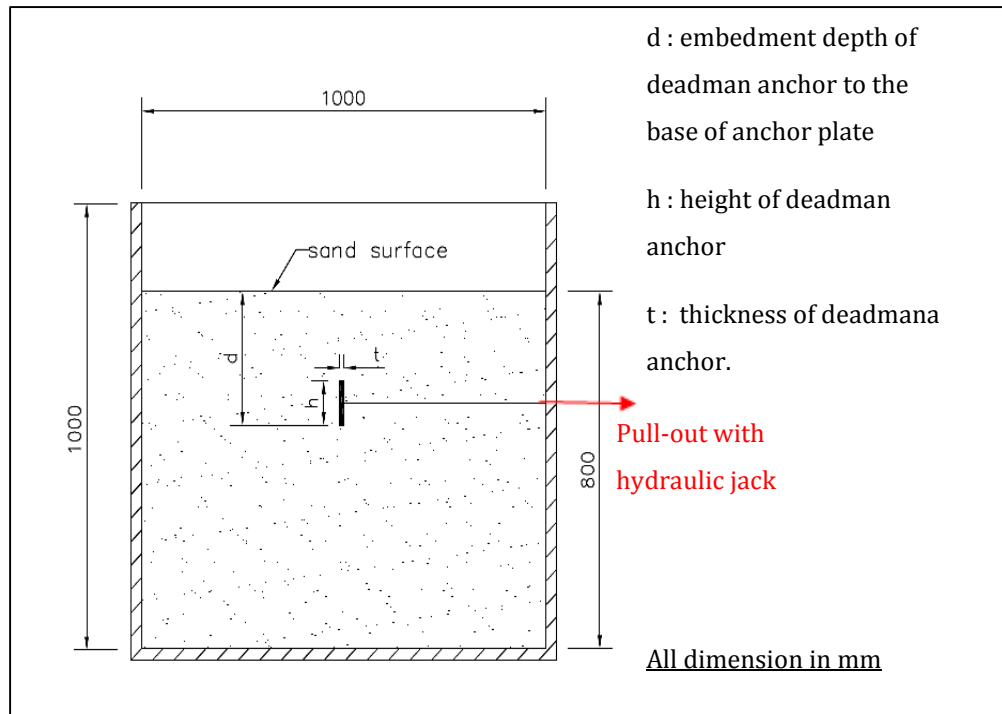


Figure 3.11: Schematic diagram of 1-g small-scale laboratory test (Side View).

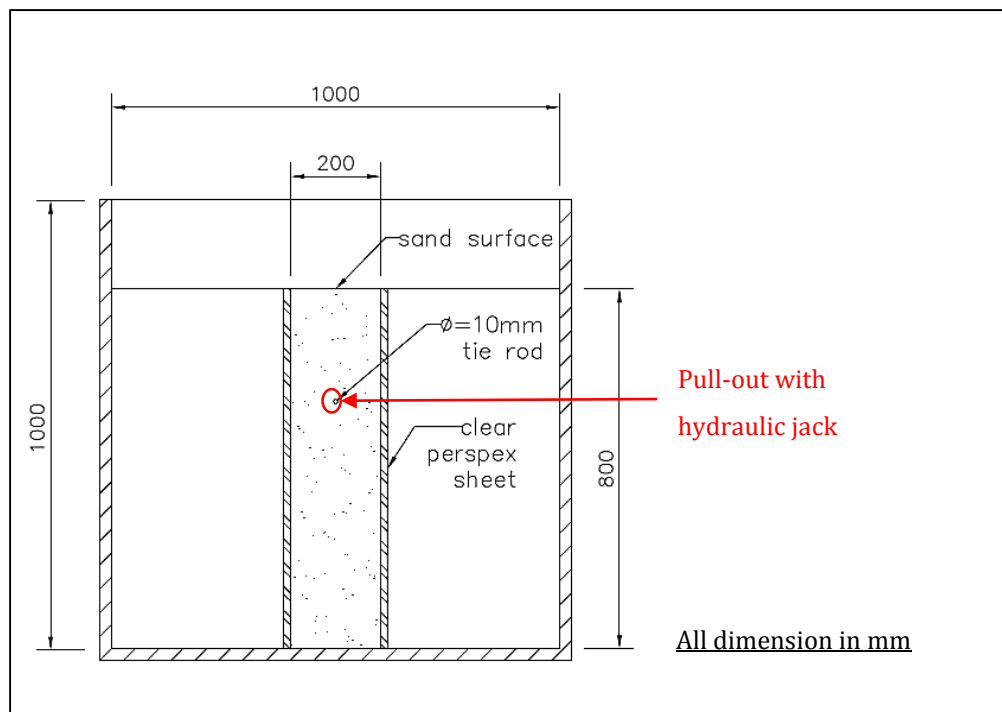


Figure 3.12: Schematic diagram of 1-g small-scale laboratory test (Front View).

### 3.8 Summary

This chapter presents the methodology of finite element analysis that was implemented in this research. The finite element analysis was concluded utilising the finite element software named *PLAXIS*. The configuration prototype used in finite element analysis was discussed. The parameters used to study the behaviour of deadman anchorage system were introduced.

In *PLAXIS*, the boundary condition of prototype was examined to ensure that the size of prototype was adequate in order to eliminate the boundary effect. Furthermore, the 'very fine' mesh was nominated as the most suitable mesh for the finite element prototype. This is because the results from mesh investigation converged from very coarse mesh to very fine mesh.

Moreover, the types of model element and material that were assigned to the finite element prototype for 2-D and 3-D models in *PLAXIS* were discussed. The model elements adopted in 2-D and 3-D models in *PLAXIS* were completely different as the 2-D model was in plane strain assumption whereas the latter reflects more realistic conditions.

In addition, methodology on the verification of finite element analysis using 1-g small-scale laboratory test was presented. Partial verification on the finite element analysis was carried out with pull-out test of discrete deadman anchor. A random test verification was chosen to examine the accuracy of finite element estimation on the pull-out test of discrete

deadman anchor. The set-up and procedure of 1-g small-scale laboratory test will be in detail discussed in Chapter 4.

# CHAPTER 4

---

## 1-G SMALL-SCALE LABORATORY TEST

### 4.1 Introduction

This chapter presents the comprehensive methodology and procedure of 1-g small-scale laboratory test, which includes laboratory test set-up and all the preparation work prior to laboratory test. The small-scale laboratory test set-up consisted of a sand box, deadman anchorage system and a pull-out system. Prior to the small-scale laboratory test, the characteristics of soil were identified.

Even though *PLAXIS* is a well-established commercial software with sufficient verification and validation, a simple verification on the pull-out test of discrete deadman anchor had been carried out for modelling

verification purpose. Therefore, the main aim of 1-g small-scale laboratory test was to examine the capability of finite element prediction on the pull-out of discrete deadman anchor.

Random test verification, one of the verification approaches, was chosen to examine the accuracy of finite element estimation on the pull-out model of discrete deadman anchor. Furthermore, the determination of the characteristic of soil was very important as the physical properties of soil may have significant effect on the accuracy of finite element estimation.

## **4.2 1-G Small-scale Laboratory Test Set Up**

### **4.2.1 Sand Box**

A sand box with dimensions of 1.0m x 1.0m x 1.0m was used in the small-scale laboratory test. The front and back walls of the sand box were made of plywood with thickness of 25mm. Both sides of the walls were made of clear perspex sheet (transparent sheet) with thickness of 15mm. The sand box was stiffened by steel frame, which consisted of four vertical steel columns and eight horizontal steel beams to sustain the soil pressure, as shown in Figure 4.1.

The front wall was drilled with 45 holes, orientated with 5 holes in a row with 0.2m interval spacing and 9 holes in a column with 0.1m interval spacing (see Figure 4.2). These holes were meant for tie rod installation purposes. Besides that, the clear perspex sheets for side walls allowed a

clear visualisation during the preparation and the observation of soil deformations during the laboratory test. The clear perspex sheets were adjustable with spacing of every 0.2m increment up to 1.0m.

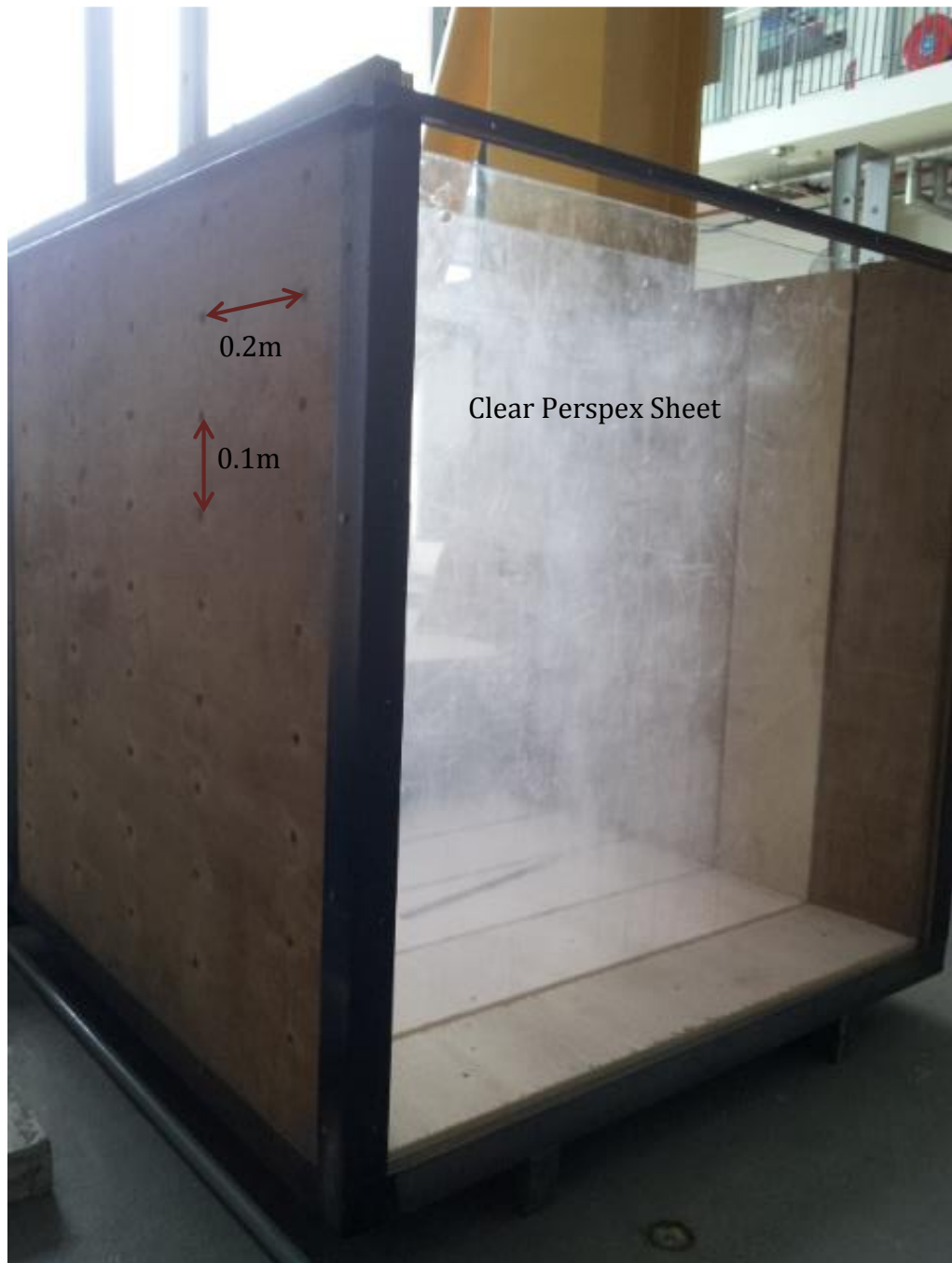
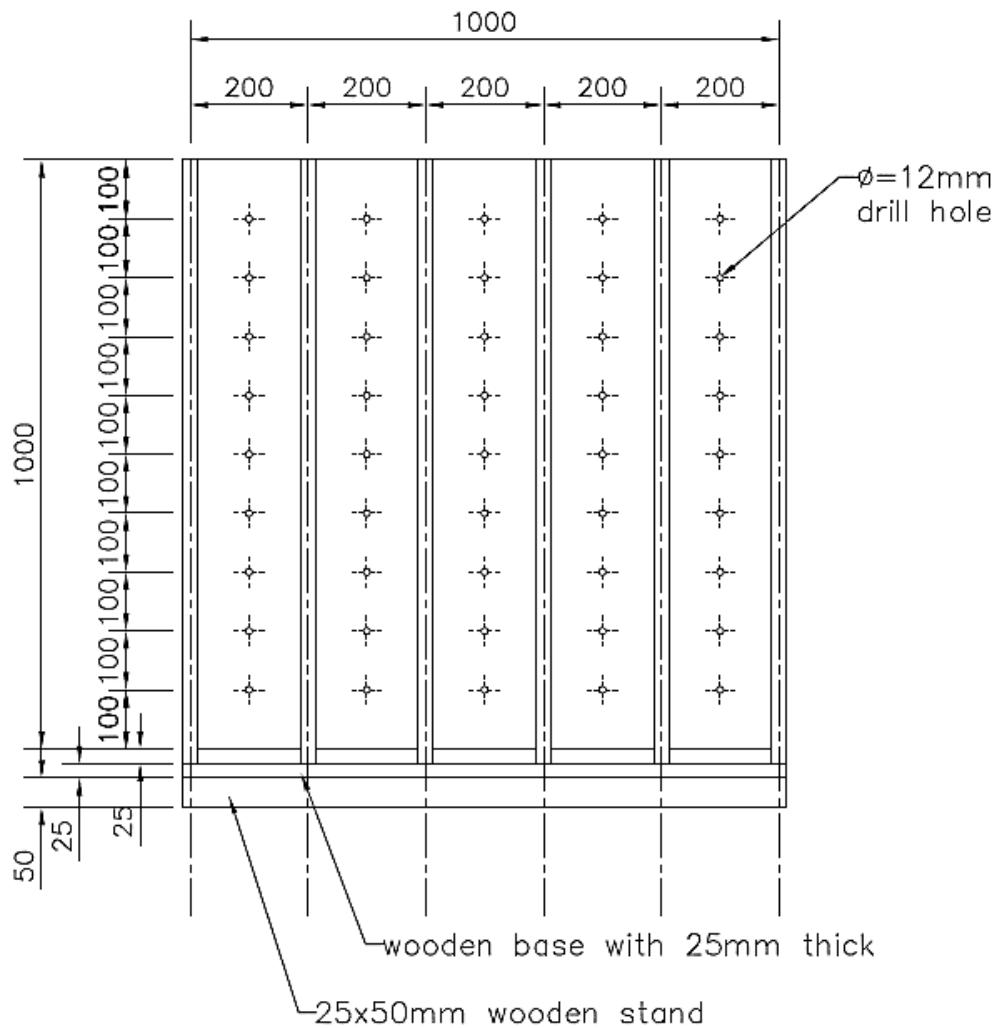


Figure 4.1: Sand box.



All dimension in mm

Figure 4.2: Front elevation of sand box.

### 4.2.2 Deadman Anchorage System

Deadman anchorage system (see Figure 4.3a) consisted of a steel rod with diameter of 10mm (see Figure 4.3c) connected to the deadman anchor (steel plate) with dimension of 0.1m x 0.1m x 0.01m (see Figure 4.3b). Deadman anchor system was installed to the desired embedment depth

through the sand passing hole during the model preparation. In addition, part of the steel rod length is remained at the outside of the sand box for pull-out purpose.

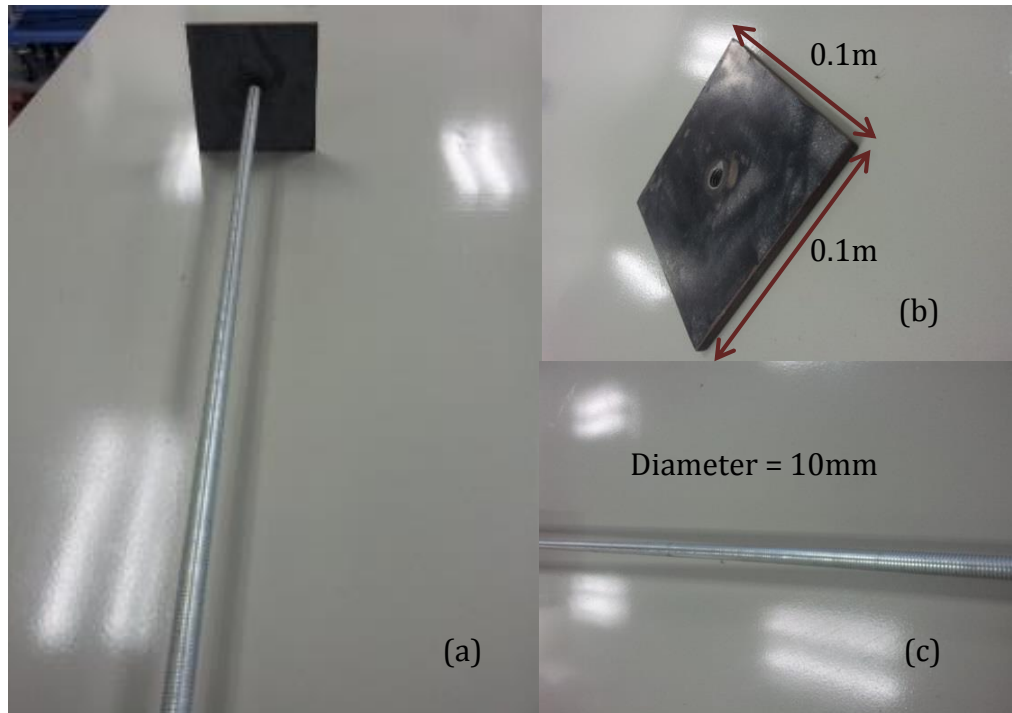


Figure 4.3: (a) deadman anchor; (b) steel plate; and (c) steel rod.

### 4.2.3 Pull-out System

The pull-out system consisted of a hydraulic hollow plunger cylinder (see Figure 4.4) attached to the remained steel rod. The hydraulic hollow plunger cylinder was connected to hydraulic pump (see Figure 4.5) in order to apply the pull-out pressure on the plunger. The back face of the hollow plunger was attached closely to the sand box whereas the front face

was restrained by a steel plate. A dial gauge (see Figure 4.6) was placed in front of the steel plate.

The installation of steel plate is very important for the entire pull-out system as it functions as follows:-

1. To ensure that no movement is allowed before the experiment starts.
2. To allow the inner cylinder of hydraulic plunger to push against the steel plate when the pull-out pressure is applied. This indirectly pulls the deadman anchor outward.
3. To allow the measurement of pull-out displacement to take place during the laboratory test. The distance of steel plate movement indicates the pull-out displacement of deadman anchor.



Figure 4.4: Hollow plunger cylinder (Enerpac™ RCH-123).



Figure 4.5: Hand pumped hydraulic jack (Enerpac™ P-84).



Figure 4.6: Mitutoya™ dial gauge.



Figure 4.7: SMC™ hydraulic pressure gauge.

In addition, the hydraulic pressure gauge (see Figure 4.7) with a capacity of 11 bars was used in the small-scale laboratory test. This was because the pull-out pressure of deadman anchor in this experiment was not more than 11 bars.

### 4.3 Soil Characterisation

Prior to the small-scale laboratory test on the pull-out of discrete deadman anchor, the physical properties of the sand had to be determined. The basic physical properties of sand were sand grade, grain size distribution, friction angle, Young's Modulus and unit weight of sand.

The sand used in the small-scale laboratory test was selected from local quarry. The physical properties of this soil sample were identified by a series of laboratory tests, which included:-

- a. Sieve analysis test,
- b. Direct shear box test,
- c. Oedometer test, and
- d. Density test with pre-determined sand placement height.

#### **4.3.1 Sieve Analysis Test**

The sieve analysis test was conducted to determine the grade and grain size distribution of the soil sample in the small-scale laboratory test. This test was conducted based on the Unified Soil Classification System.

A dry soil sample (dried in an electric oven at 110 °C for 24 hours) with mass of 1500grams was used to carry out the sieve analysis test. The arrangement of the test sieve aperture sizes as required by British Standard (BS 1377-2, 1990) from top to bottom, i.e. 6.3mm , 5.0mm, 3.35mm, 2.00mm, 1.18mm, 0.6mm, 0.425mm, 0.3mm, 0.212mm, 0.15mm and 0.063mm. The apparatus of sieve analysis test is shown in Figure 4.8.

The detailed procedure for sieve analysis was described in BS 1377-2: 1990, Clause 9.

1. The 1500g dry soil sample was placed on the most top sieve tray with sieve size of 6.3mm.

2. The sieve trays were placed on the mechanical shaker machine; subsequently, they were covered with a lid and secured tightly to the mechanical shaker machine.
3. The test was carried out for a duration of 30 minutes.
4. Once the test was completed, the weight of retained soil on each sieve tray was recorded.
5. The grain size distribution curve were plotted based on the percentage of retained soil on each sieve tray.



Figure 4.8: Mechanical shaker and sieve trays.

The relative grain size distribution of the soil sample from sieve analysis test is presented in Table 4.1 and the grain size distribution curve of soil sample is illustrated in Figure 4.9.

Table 4.1: Sieve analysis results.

Test sieve aperture size (mm)	Mass of Passing (g)	Mass of Retained (g)	Percentage of Passing (%)	Percentage of Retained (%)
6.300	1500.0	0.0	100.000	0.000
5.000	1498.0	2.0	99.867	0.133
3.350	1492.0	6.0	99.467	0.400
2.000	1438.0	54.0	95.867	3.600
1.180	1328.0	110.0	88.533	7.333
0.600	1078.0	250.0	71.867	16.667
0.425	655.0	423.0	43.667	28.200
0.300	552.0	103.0	36.800	6.867
0.212	276.0	276.0	18.400	18.400
0.150	183.0	93.0	12.200	6.200
0.063	39.0	144.0	2.600	9.600
PAN	0.0	39.0	0.000	2.600
		<b><u>1500.0</u></b>		<b><u>100.000</u></b>

From the grain size distribution curve, the values of  $D_{10}$ ,  $D_{30}$  and  $D_{60}$  were found to be 0.13mm, 0.28mm and 0.52mm, respectively (see Figure 4.9). By applying Eq. 4.1 and Eq. 4.2, the coefficient of uniformity ( $c_u$ ) was determined to be 4.00, and the coefficient of concavity/curvature ( $c_c$ ) was calculated to be 1.16. Based on the USCS ASTM Designation D-2487, the soil was categorised as poorly-graded (*SP*) clean sand.



grid and bearing were used in the test. The apparatus of direct shear box test is shown in Figure 4.10.

The procedure of direct shear box test was conducted based on BS 1377-7 Test 4 (BS 1377-7, 1990).

1. The mass of shear box (both halves), bottom plate, bottom grid and two joining screws were recorded as  $M_1$ .
2. The mass of top half of shear box, top grid, screws and bearing were recorded as  $M_2$ .
3. The two halves of shear box were assembled by adapting the two joining screws and the bottom plate was placed in the shear box.
4. The effective thicknesses of the top and bottom grids were recorded as  $t_t$  and  $t_b$ , respectively. The depth to the bottom plate ( $d_1$ ) was measured from the top edge of the sand box. (\*\*Note: Average reading was obtained from the four corners)
5. The soil was filled in three layers (approximately 11mm each) evenly into the sand box using a measuring tin. Each layer of soil was compacted five blows using a wooden tamper. The wooden tamper fell under its self-weight. (\*\*Note: No compaction is applied in this research.)
6. The mass of sand box with soil sample was weighed and recorded as  $M_3$ . The mass of the soil sample was recorded as  $M_s$  ( $M_s = M_3 - M_1$ ). (\*\*Note: There was no issue if some soil has lost before obtaining  $M_3$ ).

7. The upper grid was placed on the soil sample. The depth to the top grid ( $d_2$ ) was measured from the top edge of the sand box. (\*\*Note: Average reading was obtained from the four corners)
8. The thickness of soil sample was recorded as  $t_s$ . The density of the sand was calculated adapting Eq. 4.3. The bearing was placed on top of the top grid.

$$\rho = \frac{M}{V} \quad \text{Eq. 4.3}$$

9. The prepared shear box was placed in the digital shear machine and the load ( $M_5$ ) was placed on the hanger.
10. The jack screw was contacted with the outer box. The joining screws were removed and the lifting screws were screwed into other corners. (\*\*Note: these lifting screws were slightly raised on the top half of the box, which allowed the soil to shear through)
11. All the dial gauges were set to zero and the test was begun using the digital shear machine with a shearing constant rate of 1mm/min.
12. The values from the vertical dial gauge and proving ring were recorded as the horizontal displacement dial gauge reached the given values.
13. Once the experiments for various loads were completed, the results were recorded.

Four different loads (0, 20, 40 and 60kg) were applied on the sand sample. It is important to note that the load on hanger was equivalent to ten times

of the weight acting on the sand sample. For example, a mass of 2kg hanging on the hanger was equivalent to 20kg acting on the soil sample). The direct shear box test was repeated three times in order to obtain an average result.

The shear strength of soil can be expressed as,

$$\tau = c' + \sigma' \tan \phi' \quad \text{Eq. 4.4}$$

For cohesion-less soil ( $c' = 0$ ), Eq. 4.4 can be simplified as,

$$\tau = \sigma' \tan \phi' \quad \text{Eq. 4.5}$$

where,

$\tau$  = shear strength of soil (kN/m<sup>2</sup>)

$\sigma'$  = effective normal stress of soil (kN/m<sup>2</sup>)

$\phi'$  = effective friction angle of the soil (°)

The unit weight of the soil sample can be determined from,

$$\gamma = \rho g \quad \text{Eq. 4.6}$$

where,

$\gamma$  = unit weight of soil (kN/m<sup>3</sup>)

$\rho$  = density of soil (mass per unit volume, kg/m<sup>3</sup>)

$g$  = acceleration due to gravity (on earth usually given as 9.81, m/s<sup>2</sup>)



Figure 4.10: ELE International digital direct shear box test apparatus.

The average friction angle and unit weight of sand were determined to be  $28.5^\circ$  and  $15.1\text{kN/m}^3$ , respectively.

### 4.3.3 Oedometer Test

The objective of carrying out oedometer test was to determine the Young's Modulus of sand. The oedometer test is also known as one-dimensional (1-D) consolidation test. In oedometer, a cell, cutting ring, locking ring, three thumb-nuts, cap, top and bottom porous stones were used in the test. The oedometer test apparatus is shown in Figure 4.11.

The full procedure of oedometer test is detailed in BS 1377-5 Test 3 (BS 1377-5, 1990) and is briefly described as follows:

1. The cutting ring was placed on the rough surface of porous stone at the bottom. The saturated soil was filled into the cutting ring.
2. Once the saturated soil was filled, the top porous stone was positioned gently on top of the saturated soil.
3. Then, assembled specimen was placed on the cell base and centered inside the three studs.
4. The locking ring was fitted onto the cutting ring and hence tightening the three thumb-nuts onto the three studs.
5. The cap was located on the upper porous stone and the entire cell was placed onto the consolidation frame.
6. The jack screw was adjusted until there was an approximately 6mm gap between the upper surface of the beam and the underside slot of the consolidation frame.
7. The cell was filled up with distilled water to ensure that the specimen was in fully saturated condition.
8. The load was placed on the hanger and the vertical dial gauge reading was set to zero.
9. Once the experiments for various loads were completed, the results were recorded.



Figure 4.11: ELE International oedometer test apparatus.

Five different loads (0.5, 1.0, 1.5, 2.0, and 2.5kg) were applied on the sand sample for this test. It is important to note that a mass of 1.0kg weight hanging on the hanger corresponds to 50kPa acting on the sand sample. The 1-D consolidation test was repeated three times in order to obtain an average result.

The constraint modulus of the soil ( $E_0$ ) sample can be expressed as,

$$E_0 = \frac{\sigma}{\varepsilon} \quad \text{Eq. 4.7}$$

where,

$\sigma$  = stress applied on the soil sample (kN/m<sup>2</sup>)

$\varepsilon$  = normalised measurement of deformation representing the elongation of the sample relative to the reference/origin length

The Young's Modulus of soil ( $E$ ) of the soil can be determined from,

$$E = \frac{(1 + \nu)(1 - 2\nu)E_0}{(1 - \nu)} \quad \text{Eq. 4.8}$$

where,

$E_0$  = constraint modulus of soil (kN/m<sup>2</sup>)

$\nu$  = Poisson's ratio of soil

The average constraint modulus of sand obtained was found to be 3971.2 kN/m<sup>2</sup>. By applying Eq. 4.8 and assuming the effective Poisson's ratio to be 0.3, the average Young's Modulus of the sand was calculated to be 2950 kN/m<sup>2</sup>.

#### **4.3.4 Density Test with Pre-determined Sand Placement Height**

The purpose of conducting the density test was to determine the unit weight of sand. During the preparation for 1-g small-scale laboratory test, a tin container (with known weight and volume) was embedded at pre-determine heights (0.3m, 0.5m and 0.8m below the sand surface).

After the sand was filled by pluviation approach, the tin was removed and the mass was measured and recorded. By using the Eq. 4.3 and Eq. 4.6, the average unit weight of the sand sample was found to be  $15.1\text{kN/m}^3$ , which has similar observation with direct shear box test.

### 4.3.5 Summary

The physical properties of sand obtained from a series of laboratory tests is summarised in Table 4.2.

Table 4.2: Physical properties of sand.

Laboratory test	Result
Sieve Analysis Test	Poorly-graded ( <i>SP</i> ) clean sand
Direct Shear Box Test	Average friction angle = $28.5^\circ$
Oedometer Test	Average Young's Modulus = $2950\text{ kN/m}^2$
Density Test	Average unit weight = $15.1\text{kN/m}^3$

## 4.4 Procedure for 1-G Small-scale Laboratory Test

The procedures for 1-g small-scale laboratory test are as follows:-

1. First of all, unnecessary holes were sealed by masking tape in order to avoid the sand leakage.

2. The sand box was filled with sand by pluviation (rain fall) method to produce uniform, sand at approximately every 0.1m from bottom of the sand box.
3. The sand was rained in layers up to the desired embedment height.
4. Deadman anchor was placed to the desired distance away from the front wall of the sand box.
5. The steel rod was inserted through the front wall and connected to the deadman anchor (see Figure 4.12 and Figure 4.13).
6. The sand was backfilled up to the desired height (see Figure 4.14).
7. Once the sand was completely set up, the steel rod was clamped to a hollow plunger cylinder. The hollow plunger cylinder was connected to the hydraulic jack.
8. A steel plate was screwed and fixed at the front face of the hollow plunger cylinder in order to restrain the steel rod movement.
9. A dial gauge was attached to the front face of steel plate in order to monitor and record the pull-out displacement.
10. Once the experiment set up was completed, the steel rod was pulled using the hand pumped hydraulic jack (see Figure 4.15). The pressure reading was recorded for every 1mm pull-out displacement.
11. The small-scale laboratory test was repeated three times in order to obtain an average result on the load-displacement relationship.



Figure 4.12: Installation of deadman anchorage system (side elevation).



Figure 4.13: Installation of deadman anchorage system (plan elevation).



Figure 4.14: Sand backfilled up to desire height, 0.8m.

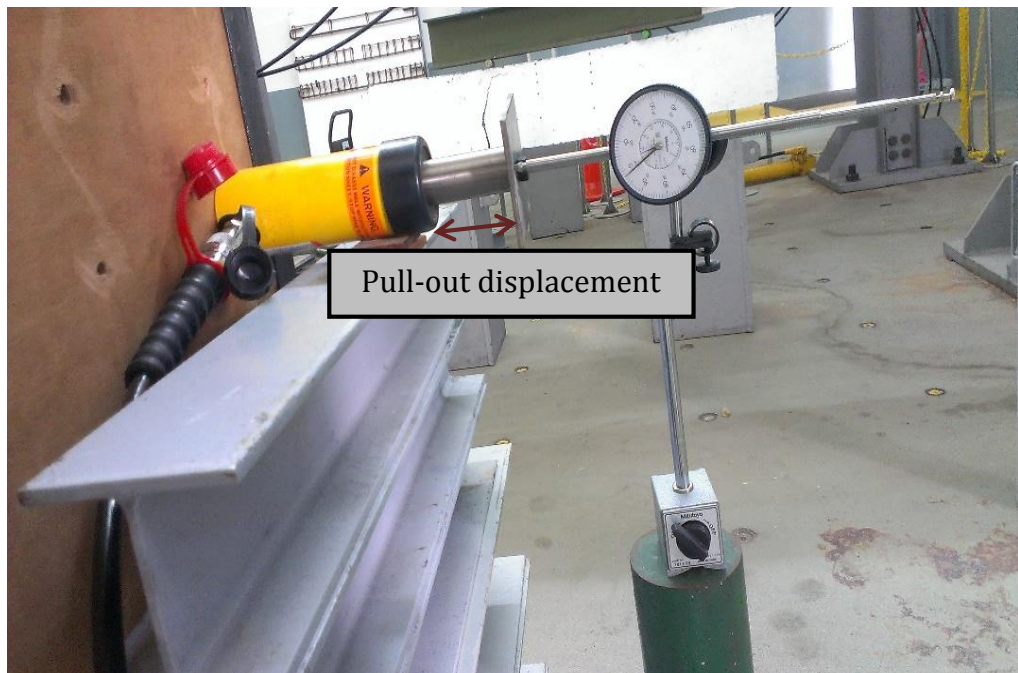


Figure 4.15: Pull-out displacement of the hydraulic plunger.

## 4.5 1-G Small-scale Laboratory Test

One of the verification approaches, random test verification, was chosen to be carried out in 1-g small-scale laboratory test on the pull-out of discrete deadman anchor, which aimed to examine the accuracy of finite element estimation. A random set of parameter was nominated for the 1-g small-scale laboratory test and is tabulated in Table 4.3. Moreover, the schematic diagram of 1-g small-scale laboratory test is illustrated in Figure 3.10 to Figure 3.12.

Table 4.3: Parameters adopted for laboratory test.

Parameters	
Tie rod length, $L$ (m)	: 0.5
Anchor spacing, $s$ (m)	: 0.2
Anchor embedment depth, $d$ (m)	: 0.3

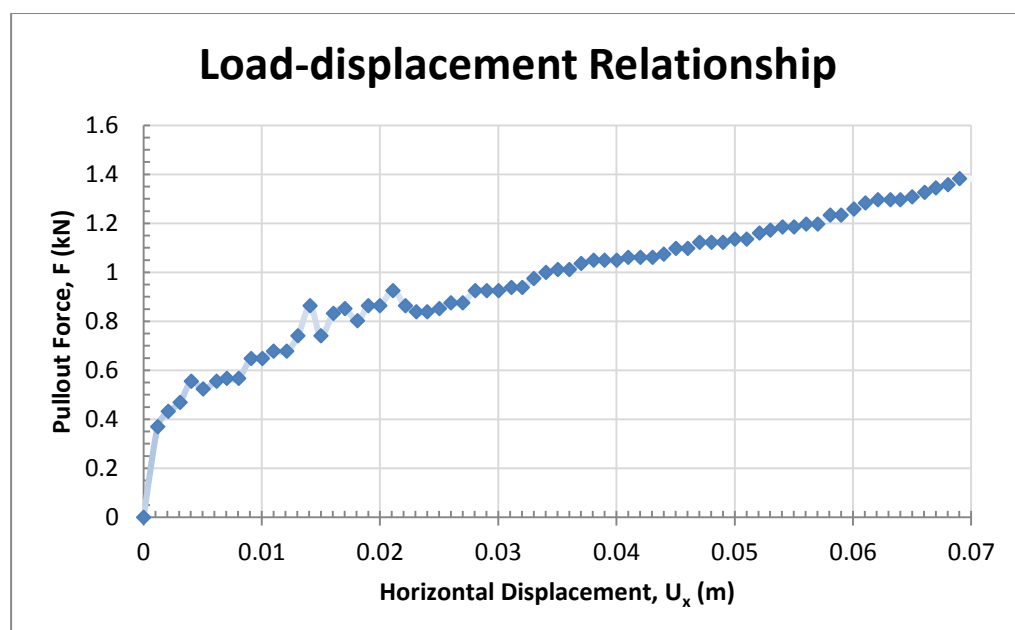


Figure 4.16: Load-displacement relationship from laboratory test.

The results on the pull-out of discrete deadman anchor, load-displacement relationship, obtained from 1-g laboratory test is presented in Figure 4.16. A three-dimensional (3-D) finite element analysis (FEA) on the pull-out test was carried out. The dimension of finite element prototype was modelled identically to the dimension implemented in the 1-g small-scale laboratory test (see Figure 4.17).

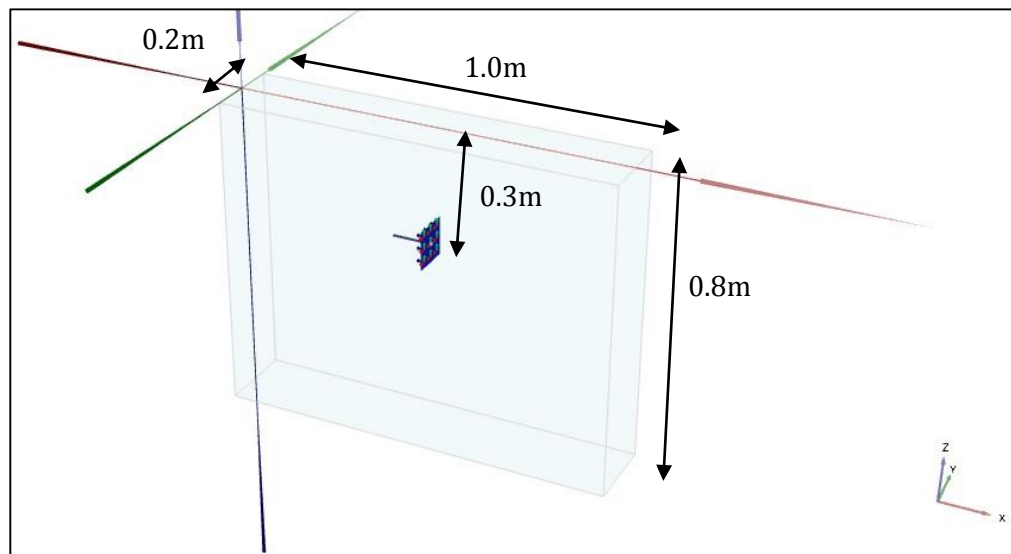


Figure 4.17: Finite element prototype.

The material properties adopted in FEA were exactly same as determined from a series of laboratory tests. The material properties are as follows:-

**a. Soil Properties**

Unit weight of soil, $\gamma$ (kN/m <sup>3</sup> )	=	15.10
Secant stiffness for triaxial test, $E_{50}^{ref}$ (kN/m <sup>2</sup> )	=	2950.00
Tangent oedometer stiffness, $E_{oed}^{ref}$ (kN/m <sup>2</sup> )	=	2950.00
Unloading/reloading stiffness, $E_{ur}^{ref}$ (kN/m <sup>2</sup> )	=	8850.00

Friction angle, $\phi$ ( $^{\circ}$ )	=	28.50
Dilatancy angle, $\psi$ ( $^{\circ}$ )	=	0.00
Cohesion, $c_{ref}$ ( $\text{N}/\text{m}^2$ )	=	0.00
Effective Poisson's ratio, $\nu_{ur}'$	=	0.30

### b. Steel Properties

Unit weight of steel, $\gamma_s$ ( $\text{kN}/\text{m}^3$ )	=	78.50
Elastic modulus of steel, $E_s$ ( $\text{kN}/\text{m}^2$ )	=	20.00e+07
Effective Poisson's ratio, $\nu'$		0.27

The results on the pull-out of discrete deadman anchor, load-displacement relationship, obtained from finite element analysis is presented in Figure 4.18.

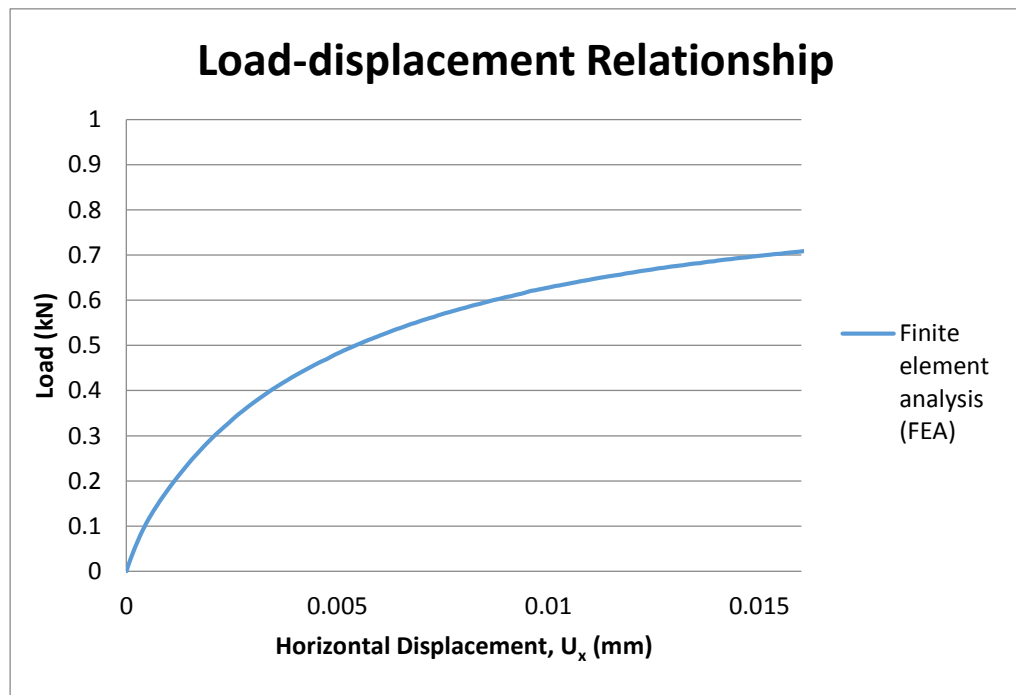


Figure 4.18: Load-displacement relationship from finite element analysis.

### 4.5.1 Result and Discussion

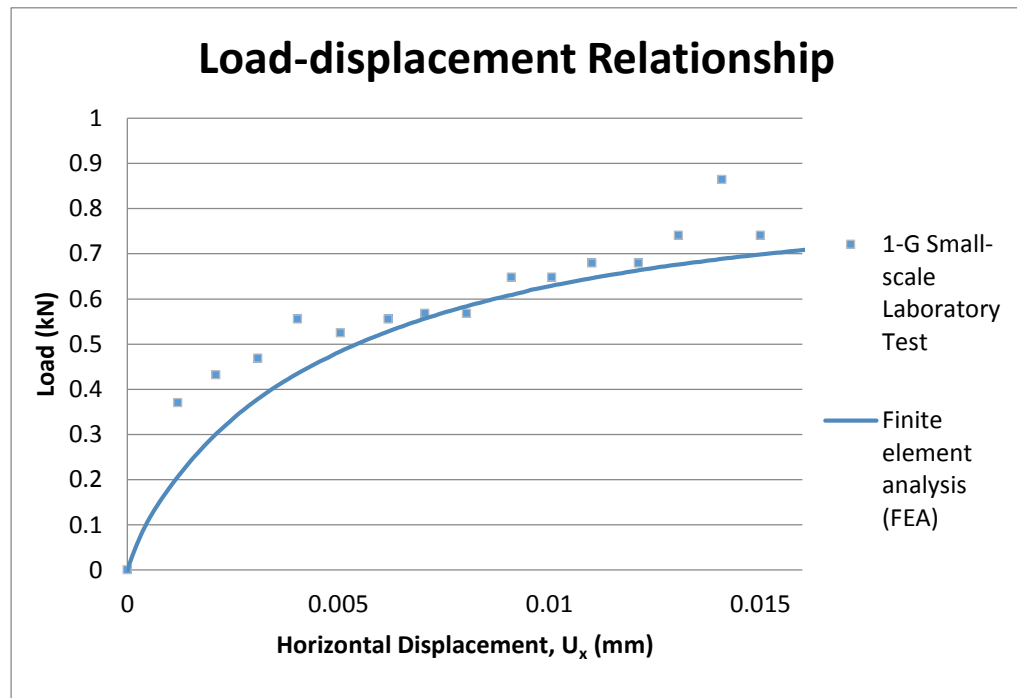


Figure 4.19: Load-displacement relationship between 1-g small-scale laboratory test and finite element analysis.

Figure 4.19 shows the load-displacement relationship on the pull-out of discrete deadman anchor between 1-g small-scale laboratory test and finite element analysis. In Figure 4.19, the prediction on load-displacement relationship of deadman anchorage system from finite element analysis prediction was found to be in a good agreement with the small-scale laboratory test.

Nevertheless, the accuracy of finite element prediction on 1-g small-scale laboratory test is very dependent on the input physical parameters, which determined from a series of laboratory tests.

The Young's Modulus of sand adopted in finite element analysis were obtained indirectly from oedometer test. The Young's Modulus of sand were found to have a wide range of variation during laboratory test, which are from 2700kPa to 3200kPa. This may be due to errors occurring during the sample preparation stage. The degree of moisture content of the soil sample may be varied during the initial stage of oedometer test.

Furthermore, the assumption on the effective Poisson's ratio adopted in the conversion equation from constraint modulus to Young's Modulus of sand may have affected the load-displacement result in comparison with 1-g small-scale laboratory test.

Since the Young's Modulus of sand had inconsistent values, hence an investigation on the effect of Young's Modulus of sand on the pull-out of discrete deadman anchor was carried out. The investigation was carried out using Young's Modulus of sand with 3200kPa and 4000kPa and the results were compared against those presented in Figure 4.19.

Figure 4.20 shows the effect of Young's Modulus of sand adopted in FEA on load-displacement relationship for the pull-out of discrete deadman anchor. From Figure 4.20, the maximum Young's Modulus of sand obtained from laboratory test ( $E = 3200\text{kPa}$ ) have better estimation on the 1-g small-scale laboratory test for the pull-out of discrete deadman anchor. Whereas, the Young's Modulus with 4000kPa gives slight overestimation on the 1-g small-scale laboratory test for the pull-out of discrete deadman anchor. Nevertheless, both of these Young's Modulus results are considered in good

agreement on the 1-g small-scale laboratory test for the pull-out of discrete deadman anchor.

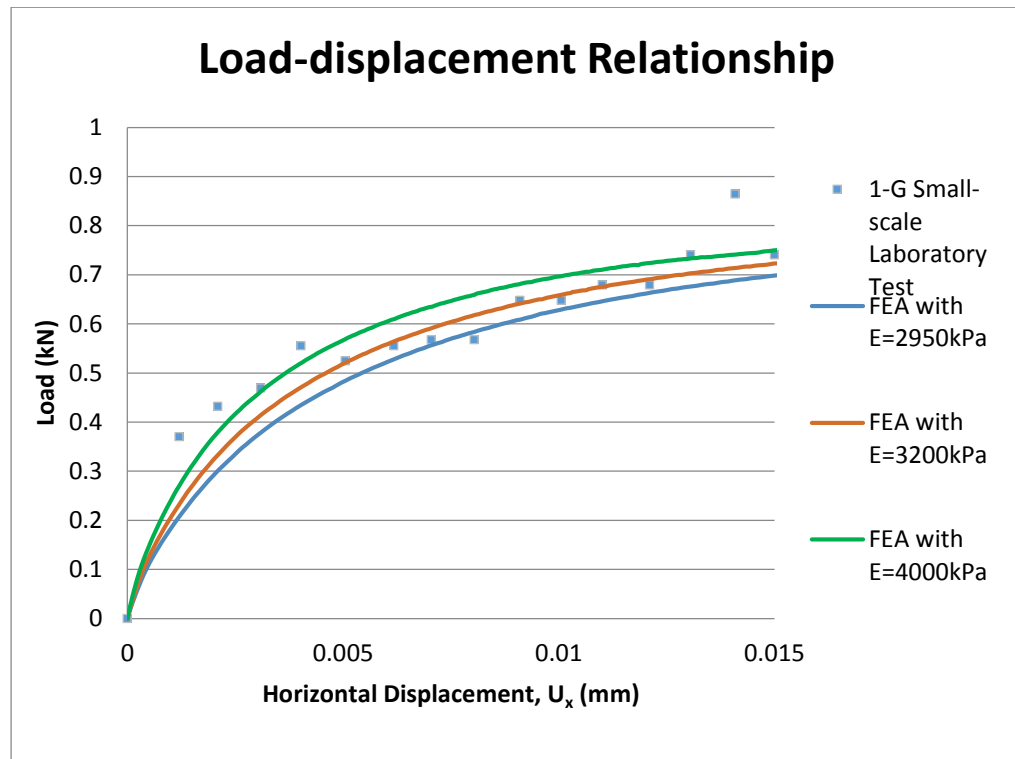


Figure 4.20: Effect of Young's Modulus of sand adopted in FEA on load-displacement relationship.

In conclusion, 1-g small-scale laboratory test on the pull-out of discrete deadman anchor can be predicted reasonably well by finite element analysis.

## 4.6 Summary

This chapter examines the capability of *PLAXIS 3D* in modelling the pull-out test of discrete deadman anchor. The accuracy of finite element prediction is very dependent on material properties.

The soil characterisation, which determines the physical properties of soil from laboratory tests, is very important in order to ensure the accuracy of finite element prediction.

Nevertheless, the Young's Modulus determined from oedometer test have variation from 2700kPa to 3200kPa. An average Young's Modulus with 2950kPa is adopted in FEA to predict the 1-g small-scale laboratory test on pull-out of discrete deadman anchor. The result from FEA is found to be in good agreement with the 1-g small-scale laboratory test.

In conclusion, 1-g small-scale laboratory test on the pull-out of discrete deadman anchor can be simulated by FEA. The result of laboratory test can be predicted reasonably well by FEA provided that the input parameters are set appropriately

# CHAPTER 5

---

## ANALYTICAL SOLUTIONS

### 5.1 Introduction

Previous chapter shows that the finite element software, *PLAXIS 3D*, can predict the pull-out test of discrete deadman anchor in 1-g small-scale laboratory test reasonably well. Subsequently, this chapter further assesses the pull-out analysis of deadman anchor between the existing available analytical solutions in literature and finite element prediction. The strength and weakness of these analytical solutions are discussed.

There are a number of rigorous analytical solutions in determining the pull-out capacity of deadman anchor that is pulled horizontally. However, most of the mathematical solutions are based on two-dimensional (2-D) plane strain assumption. In addition, the breadth of deadman anchor must be taken into consideration for a more accurate prediction. By considering

the breadth of deadman anchor, the problems must be treated as three-dimensional (3-D).

The rigours available analytical solutions were presented by Terzaghi (1943), Ovesen (1964), Biarez and co-workers (1965), Rowe and Davis (1982b), Ghaly (1997), Merifield and Sloan (2006) and Naser (2006). The result from FEA is compared with these available analytical solutions. The geometry of problem is illustrated in Figure 5.1.

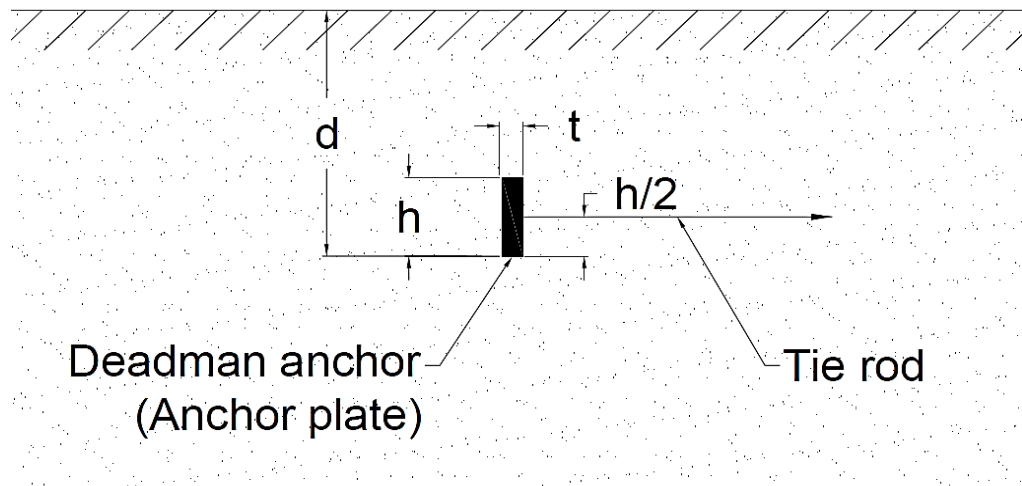


Figure 5.1: Geometry of problem.

The comparison were performed using the non-dimensional pull-out force coefficient,  $M_{\gamma q}$ , which is defined as:

$$M_{\gamma q} = \frac{T_u}{\gamma B h^2} \quad \text{Eq. 5.1}$$

where,

$M_{\gamma q}$  = pull-out force coefficient

$T_u$  = ultimate pull-out force of deadman anchor (kN)

$\gamma$  = unit weight of soil (kN/m<sup>3</sup>)

$B$  = breadth of deadman anchor (m)

$h$  = height of deadman anchor (m)

For square discrete deadman anchor, Eq. 5.1 can be further simplified as:

$$M_{\gamma q} = \frac{T_u}{\gamma h^3} \quad \text{Eq. 5.2}$$

where,

$M_{\gamma q}$  = pull-out force coefficient

$T_u$  = ultimate pull-out force of deadman anchor (kN)

$\gamma$  = unit weight of soil (kN/m<sup>3</sup>)

$h$  = height of deadman anchor (m)

## 5.2 Determination of the Ultimate Pull-out Capacity

There are two alternative approaches that used to determine the ultimate pull-out capacity of deadman anchor, as mentioned in Chapter 2, namely  $k_4$

failure concept (see Figure 2.10) and typical nature of load-displacement approach (see Figure 2.12).

A comparison on the pull-out force coefficient, for current small-scale laboratory test and finite element analyses (FEA), by adopting these approaches is tabulated in Table 5.1. It was observed that the numerical error in determining elastic stiffness can be very significant, and hence leading to a huge variation, especially on the  $k_4$  failure approach, which is three times the value of elastic stiffness. Whereas, the typical nature of load-displacement approach had less numerical error compared to  $k_4$  failure approach.

Therefore, the pull-out force coefficient ( $M_{\gamma q}$ ) used in this research was determined by adopting the typical nature load displacement diagram from the laboratory model tests by Neely and co-workers (1973).

Table 5.1: Comparison of pull-out force coefficient ( $M_{\gamma q}$ ) between typical nature load-displacement and  $k_4$  failure concept.

	$M_{\gamma q}$ ( $k_4$ failure)		$M_{\gamma q}$ (Typical)	
	$d/h = 2$	$d/h = 3$	$d/h = 2$	$d/h = 3$
<b>Current Small-scale Laboratory Test</b>	36.00	52.00	26.00	42.00
<b>FEA with <math>E=2950\text{kPa}</math></b>	32.00	50.00	26.00	41.00

### 5.3 Comparison of Analytical Solutions with FEA

Figure 5.2 presents the comparison of pull-out force coefficient ( $M_{\gamma q}$ ) between FEA and existing analytical solutions in literature for a similar set of unit weight ( $\gamma$ ), soil friction angle ( $\phi$ ) and size of deadman anchor ( $h$ ). The existing analytical solutions, which were developed based on limit equilibrium approaches, are over predicted the pull-out force coefficient compared to those obtained from FEA.

In limit equilibrium approach, a failure surface is assumed along with a distribution of stress along the failure surface. Equilibrium conditions are then considered for the failing soil mass, and an estimate of the collapse load is obtained (Merifield & Sloan, 2006). In addition, limit equilibrium concept is based on total failure mechanism regardless of large deflection are developed. These solutions may predict the 2-D plane strain and continuous deadman anchor problems in ultimate limit state (ULS) reasonably well.

The closest analytical solution in comparison with FEA is proposed by Ghaly (1997), which developed from 104 laboratory tests, 15 centrifugal model tests and 9 field tests. The pull-out force coefficient of FEA was computed to be 26 and 41 for  $d/h = 2$  and 3, respectively. Whereas the pull-out force coefficient calculated from the closest analytical solution (Ghaly's solution) was determined to be 20.87 and 42.96 for  $d/h = 2$  and 3, respectively.

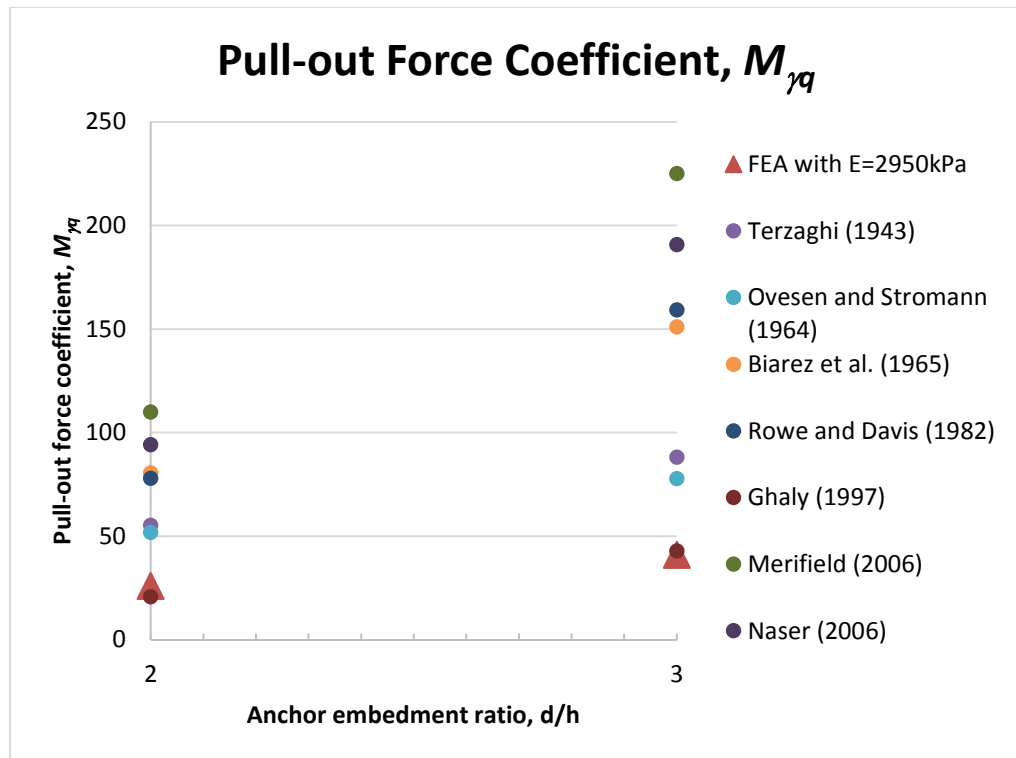


Figure 5.2: Comparison of pull-out force coefficient ( $M_{\gamma q}$ ) between FEA and analytical solutions.

The failure displacement of deadman anchor in Ghaly's analytical solution that was found to be 7.2% of  $h$ , which was close to the failure displacement of deadman anchor determined in FEA (6.5% and 8.0% of  $h$  for  $d/h = 2$  and 3, respectively). Whereas, the rest of the analytical solutions did not discuss the failure displacement of deadman anchor.

Table 5.2 shows the principle of development of these analytical solutions.

The pull-out force coefficient calculated from these analytical solutions for embedment ratio ( $d/h$ ) of 2 and 3 is also shown in Table 5.2.

Table 5.2: Comparison of pull-out force coefficient ( $M_{\gamma q}$ ) between finite element analysis and available analytical solutions.

Sources	Parameters			$M_{\gamma q}$		Remarks
	$\gamma$ (kN/m <sup>3</sup> )	$\phi$ (°)	$h$ (mm)	$d/h = 2$	$d/h = 3$	
<b>Finite Element Analysis (FEA)</b>	15.1	28.50	100	26.00	41.00	Failure displacement of deadman anchor for $d/h = 2$ is 6.5% of $h$ and for $d/h = 3$ is 8.0% of $h$ .
<b>Terzaghi (1943)</b>				55.23	88.17	The earth pressure coefficient is adopting the conventional Rankine Theory. For single anchors, additional shear resistance on the side faces of the wedge of anchor is included.
<b>Ovesen (1964)</b>				51.78	77.79	Adopt failure mechanism proposed by Hansen (1953). Furthermore, empirical reductions were applied to the basic equation.
<b>Biarez et al. (1965)</b>				80.63	151.10	Use equation developed from limit equilibrium approach.
<b>Rowe and Davis (1982)</b>				78.00	159.30	Use design charts which developed from 2-D finite element analysis adopting elasto-plastic soil model.
<b>Ghaly (1997)</b>				20.87	42.96	Use equation which developed from 104 laboratory tests, 15 centrifugal model tests and 9 field tests.
<b>Merifield (2006)</b>				110.00	225.00	Use design charts which developed from finite element analysis adopting Solid Nonlinear Analysis Code (SNAC).
<b>Naser (2006)</b>				94.14	190.77	Using equation which developed from limit equilibrium approach. Furthermore, 3-D correction factor (M) was applied to the equation.

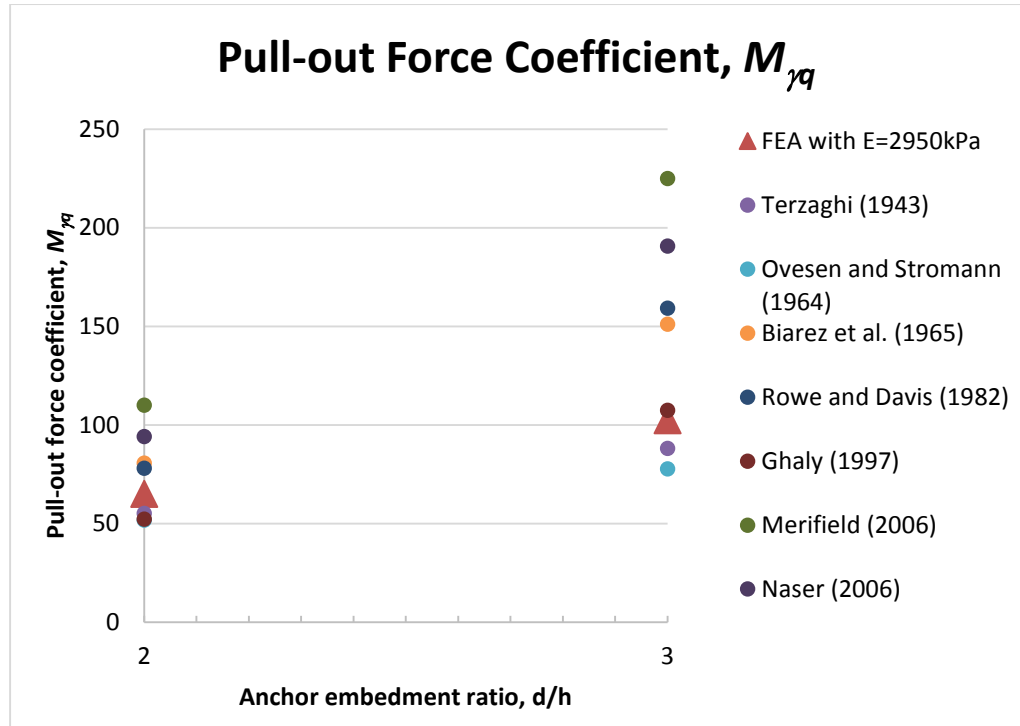


Figure 5.3: Comparison of pull-out force coefficient ( $M_{\gamma q}$ ) in ultimate limit state between FEA and analytical solutions.

Table 5.3: Comparison of pull-out force coefficient ( $M_{\gamma q}$ ) in ultimate limit state between finite element analysis and available analytical solutions.

Sources	Parameters			$M_{\gamma q}$	
	$\gamma$ ( $\text{kN/m}^3$ )	$\phi$ ( $^\circ$ )	$h$ (mm)	$d/h = 2$	$d/h = 3$
Finite Element Analysis (FEA)	15.1	28.50	100	65.00	102.50
Terzaghi (1943)				55.23	88.17
Ovesen (1964)				51.78	77.79
Biarez et al. (1965)				80.63	151.10
Rowe and Davis (1982)				78.00	159.30
Ghaly (1997)				52.18	107.40
Merifield (2006)				110.00	225.00
Naser (2006)				94.14	190.77

Ghaly proposed solution is believed to be in service limit state (SLS) whereas for those analytical solutions that did not consider the failure displacement of deadman anchor are believed to be in ultimate limit state (ULS). Hence, an assumed factor of safety (FoS) of 2.5 is applied for SLS proposed solution in order for the comparison of pull-out force coefficient in ultimate limit state condition.

Furthermore, a factor of safety (FoS) of 2.5 is applied for finite element analysis for the comparison of pull-out force coefficient in ultimate limit state condition. The results are presented in Figure 5.3 and Table 5.3. The results show that most of the analytical solutions predict the FEA with a factor of safety more than 2.5. However, the analytical solutions proposed by Terzaghi (1943) and Oversen (1964) predict the FEA's results with factor of safety more than 1.0 but less than 2.5 (see Figure 5.2 and Figure 5.3).

Similar observations were made in Kame's work (Kame et al., 2012), who studies strip anchor (with  $B/h=5$ ) with the previous experimental works and analytical solutions. Kame reported that there was no unique analytical solution for analysis of strip anchor in cohesion-less soil. In addition, Table 5.2 shows that the capability of current available analytical solutions are not good enough for the analysis of square discrete deadman anchor in cohesion-less soil.

## 5.4 Comparison of Published Experimental Work with Analytical Solutions

The published experimental work used for the comparison with analytical solution is chosen from the work of Hoshiya and Mandal (1984). The results are presented in Figure 5.4. Figure 5.4 shows there is significant variation on the pull-out force coefficient ( $M_{\gamma q}$ ) between Hoshiya and Mandal's experimental results and the available analytical solutions for a similar set of unit weight ( $\gamma$ ), soil friction angle ( $\phi$ ) and size of deadman anchor ( $h$ ).

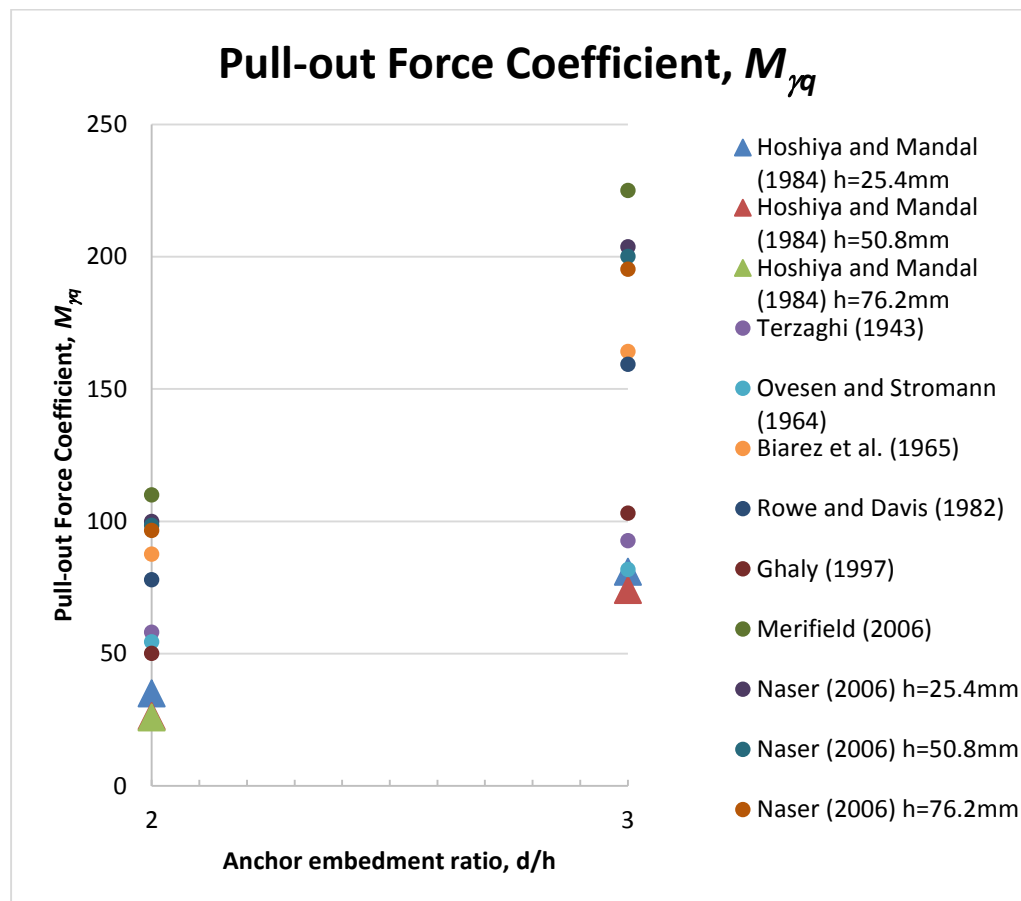


Figure 5.4: Comparison of pull-out force coefficient ( $M_{\gamma q}$ ) between experimental work of Hoshiya and Mandal and analytical solutions.

The pull-out force coefficients of Hoshiya and Mandal's experimental work were found to be lower compared to the available analytical solutions. All the available analytical solutions are over predicted the value of  $M_{\gamma q}$ . This may be potentially due to the pull-out force coefficient determined from Hoshiya and Mandal's experimental work is in service limit state. Thus, an assumed factor of safety (FoS) of 2.0 is adopted in Hoshiya and Mandal's experimental work for the comparison of pull-out force coefficient in ultimate limit state condition.

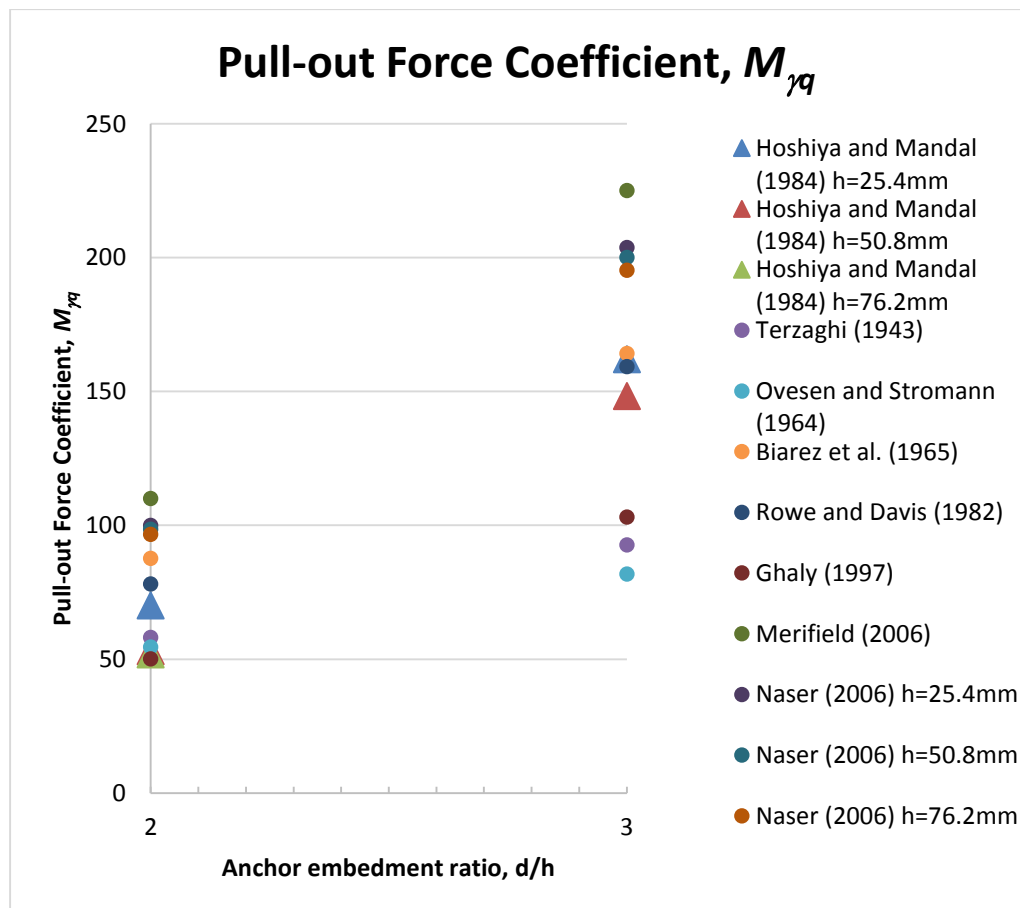


Figure 5.5: Comparison of pull-out force coefficient ( $M_{\gamma q}$ ) in ultimate limit state between experimental work of Hoshiya and Mandal and analytical solutions.

Table 5.4: Comparison of pull-out force coefficient ( $M_{\gamma q}$ ) in ultimate limit state between experimental work of Hoshiya and Mandal and the available analytical solutions.

Sources	Parameters			$M_{\gamma q}$	
	$\gamma$ (kN/m <sup>3</sup> )	$\phi$ (°)	$h$ (mm)	$d/h = 2$	$d/h = 3$
<b>Hoshiya and Mandal (1984)</b>	14.12	29.5	25.4	70.00	162.00
			50.8	52.94	148.24
			76.2	51.76	-
<b>Terzaghi (1943)</b>			25.4/ 50.8/ 76.2	58.08	92.68
<b>Ovesen (1964)</b>				54.45	81.77
<b>Biarez et al. (1965)</b>				87.58	164.20
<b>Rowe and Davis (1982)</b>				78.00	159.30
<b>Ghaly (1997)</b>				50.08	103.05
<b>Merifield (2006)</b>				110.00	225.00
<b>Naser (2006)</b>			25.4	99.92	203.70
	50.8	98.48	200.08		
	76.2	96.56	195.29		

The comparison of pull-out force coefficient ( $M_{\gamma q}$ ) in ultimate limit state between experimental work of Hoshiya and Mandal and analytical solutions is presented in Figure 5.5. The results show that most of the analytical solutions predict the experimental work of Hoshiya and Mandal more than a factor of safety of 2.0. Unlike the analytical solutions proposed by Terzaghi (1943) and Oversen (1964) predict the experimental work of Hoshiya and Mandal with factor of safety less than 2.0 (see Figure 5.4 and Figure 5.5).

Furthermore, it can be observed that various sizes of anchor gave various pull-out force coefficient in Hoshiya's experimental work, which is illustrated in Figure 5.5 and is tabulated in Table 5.4. Increasing the size of deadman anchor reduces the value of  $M_{\gamma q}$ . This shows that the size of deadman anchor is one of the factors in influencing the value of  $M_{\gamma q}$ .

In Table 5.4, it can be clearly observed that the value of  $M_{\gamma q}$  calculated from most of the available analytical solutions gave identical results regardless of the size of deadman anchor. This explains that most of the available analytical solutions does not take into account the effect of anchor size.

In contrast with these solutions, Naser's analytical solution (Naser, 2006) gave different results for different sizes of deadman anchor (see Table 3). This is because the dimension of sand box used in Hoshiya's experiment is remained constant at 0.4m x 0.3m x H+0.0762m.

Increasing the size of deadman anchor reduces the spacing of anchor. Hence, there were slight variations that occurred in Naser's analytical solution for different sizes of deadman anchor due to variation in the spacing of deadman anchor. In conclusion, Naser was the only researcher who proposed the analytical solution that took into consideration the spacing of deadman anchor.

## 5.5 Effect of Anchor Size

Table 5.4 shows that anchor size affects the pull-out force coefficient in Hoshiya's experimental work. Therefore, an investigation on anchor size was carried out in order to examine the effect of anchor size in influencing the value of pull-out force coefficient. Anchor size of 25mm, 50mm, 100mm, 500mm and 1000mm were adopted in finite element analysis. Figure 5.6 shows that increasing the anchor size reduces the pull-out force coefficient. However, the rate of reduction reduces and remain stationary as the anchor spacing increases.

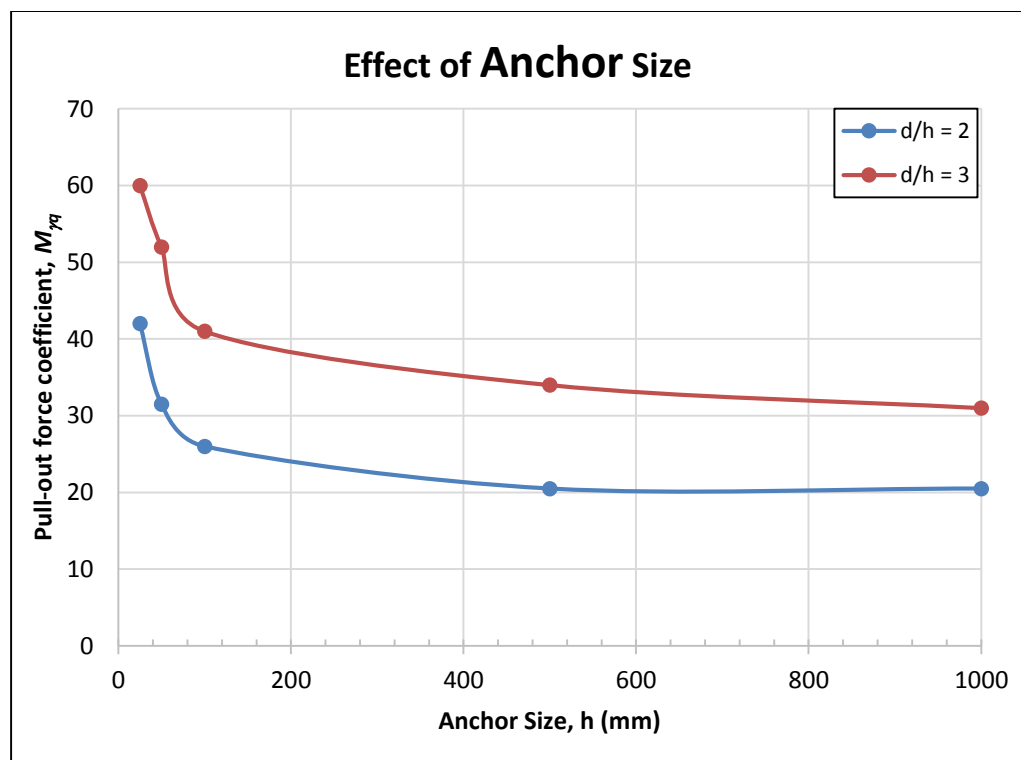


Figure 5.6: Effect of anchor size on the pull-out force coefficient ( $M_{\gamma q}$ ).

Moreover, two experimental studies investigated various size of deadman anchor in influencing the pull-out force coefficient among the rigours published experimental works, namely by Dickin and Leung (1983, 1985) and Hoshiya and Mandal (1984).

Dickin and Leung studied larger anchor size, such as 25mm, 50mm, 500mm, and 1000mm, whereas, Hoshiya and Mandal studied on smaller anchor size, for instance 25.4mm, 50.8mm and 76.2mm. The results of these experimental studies and FEA are tabulated in Table 5.5.

Table 5.5: Comparison on the effect of anchor size between FEA and previous experimental works.

Researcher	Anchor Size (mm)	$M_{\gamma q}$	
		$d/h = 2$	$d/h = 3$
FEA	25	42.00	60.00
	50	31.50	52.00
	100	26.00	41.00
	500	20.50	34.00
	1000	20.50	31.00
Dickin and Leung (1983, 1985)	25	50.00	110.00
	50	37.00	90.00
	500	35.00	75.00
	1000	32.00	65.00
Hoshiya and Mandal (1984)	25.4	35.00	81.00
	50.8	26.47	74.12
	76.2	25.88	-

Figure 5.7 shows that the prediction from FEA has the similar observation with Dickin's and Hoshiya's experimental works, whereby increasing the anchor size reduces the pull-out force coefficient. Nevertheless, the value of pull-out force coefficient ( $M_{\gamma q}$ ) is varies among these research. This is potentially due to the material and experimental set-up that were used in each research is various. Furthermore, the approaches that were used to determine the ultimate pull-out capacity of deadman anchor is different. Nevertheless, these research concluded that increasing the anchor size reduces the pull-out force coefficient.

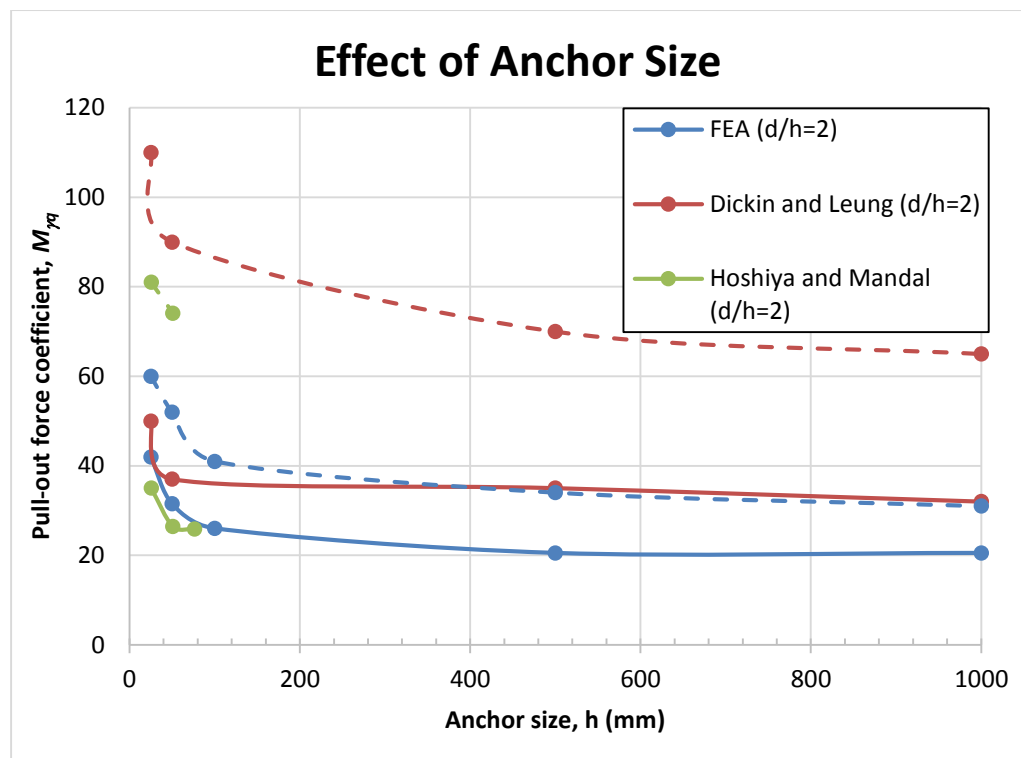


Figure 5.7: Comparison on the effect of anchor size between FEA and previous experimental works.

## 5.6 Summary

This chapter examines the capability of the existing analytical solutions in literature for pull-out analysis. All the available analytical solutions were found to over-predict the results of finite element analysis. Most of the analytical solutions predict the FEA result with a factor of safety more than 2.5.

Similar observation was found in Hoshiya's and Dickin's experimental work when compared with these available analytical solution. Most of the analytical solutions predict the Hoshiya's and Dickin's experimental work with a factor of safety more than 2.0.

Thus, it can be concluded that most of the existing analytical solutions in literature over-predict the results of finite element analysis and experimental works with a factor of safety greater than 2.0 except the analytical solutions proposed by Terzaghi (1943) and Oversen (1964).

Furthermore, Kame (2012), who evaluated strip anchor with previous experimental works and analytical solutions, also reported that there was no unique analytical solution for the analysis of strip anchor in cohesion-less soil.

An investigative study on the effect of anchor size that was carried out by adopting FEA shows that increasing anchor size decreases the pull-out force coefficient. This observation agrees with the results of Hoshiya's and Dickin's experimental works. However, most of the analytical solutions does not consider the dimension of deadman anchor in predicting the pull-

out force coefficient of deadman anchor as the result was found to be identical regardless of the size of deadman anchor.

# CHAPTER 6

---

## 2-D AND 3-D FINITE ELEMENT ANALYSES

### 6.1 Introduction

The model elements implemented in two-dimensional (2-D) and three-dimensional (3-D) models in *PLAXIS* are completely different. This is mainly because the model in two-dimension is assuming plane strain condition whereas the latter reflects more realistic condition. Therefore, a comparison study on 2-D and 3-D finite element analysis (FEA) has been carried out to investigate the variation between 2-D plane strain assumption and 3-D realistic condition. The strength and weakness of these finite element analyses are discussed. Furthermore, the benefits of 3-D FEA are illustrated.

## 6.2 Comparison Study on 2-D and 3-D Finite Element Analyses

The comparison study on 2-D and 3-D FEA was conducted by adopting the methodology discussed in Chapter 3. The potential variables that may cause variation between 2-D and 3-D FEA are spacing of discrete deadman anchorage system and wall thickness (wall stiffness).

This is mainly due to 2-D FEA with plane strain assumption is unable to model the 3-D nature of discrete deadman anchorage system, especially on the spacing effect of deadman anchor. In 2-D model, the actual properties of deadman anchorage system in the out-of plane direction are obtaining the 'equivalent' properties per meter width (Kok, 2010). Therefore, the nature of deadman anchorage system is then represented by an equivalent plane element in 2-D FEA.

Furthermore, retaining wall was modelled as a beam element in 2-D FEA. Hence, only one limited set of wall deflection was observed. This may be valid for a very rigid wall in real scenario. However, for a very thin wall, the wall deflection may be vary for different locations.

The prototype used in this comparison study is illustrated in Figure 6.1 and Figure 6.2, respectively. Five numbers of discrete deadman anchorage system are modelled in 3-D model. The numbering system for each deadman anchor used in 3-D model is presented in Figure 6.3.

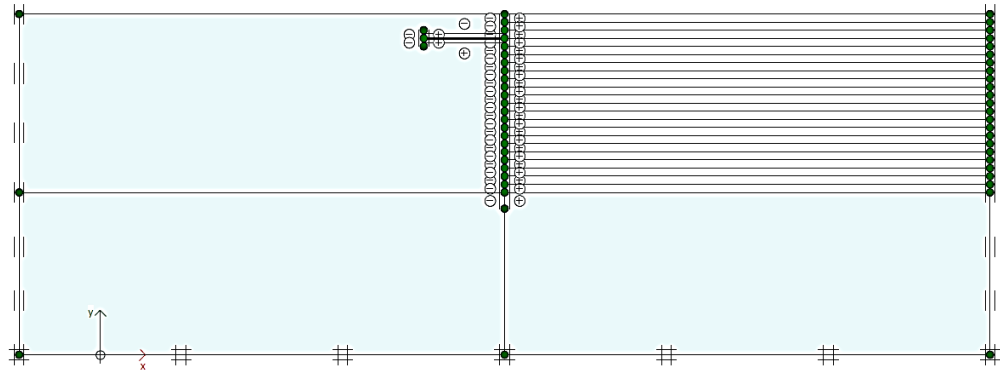


Figure 6.1: 2-D finite element prototype.

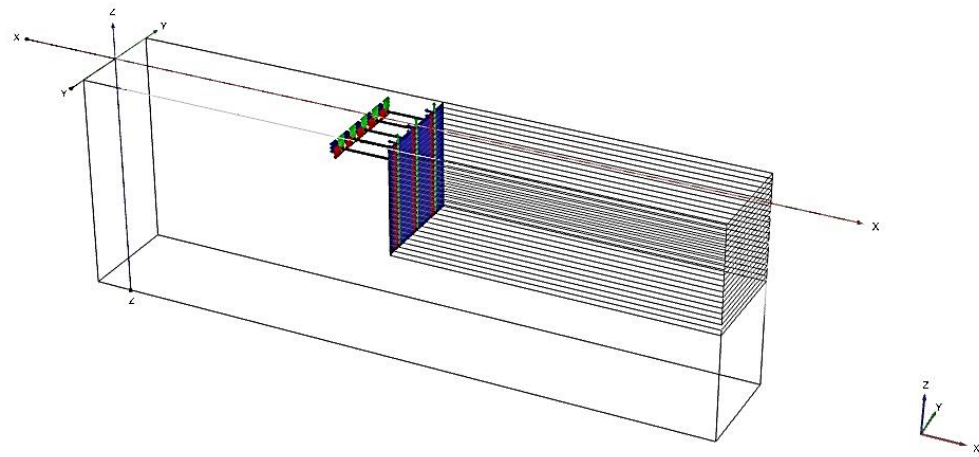


Figure 6.2: 3-D finite element prototype.

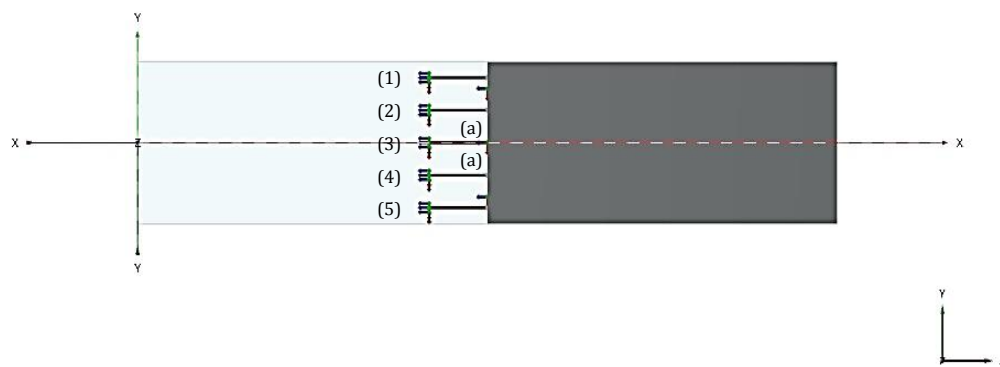


Figure 6.3: Numbering system for each deadman anchor.

A set of basic parameters that used in this comparison study is presented in Table 6.1. Diaphragm wall was adopted in this investigative study. Thus, the wall thickness is then represented the wall stiffness.

Table 6.1: Basic set of parameter for 2-D and 3-D finite element analyses.

Parameter		
<b>Tie rod length, <math>L</math> (m)</b>	:	5
<b>Anchor embedment depth, <math>d</math> (m)</b>	:	2
<b>Anchor spacing, <math>s</math> (m)</b>	:	5
<b>Friction angle of soil, <math>\phi</math> (°)</b>	:	30
<b>Wall depth, <math>D</math> (m)</b>	:	10
<b>Wall thickness, <math>T</math> (m)</b>	:	0.5

The comparison study on 2-D and 3-D finite element analysis (FEA) is studied by investigating the effects of anchor spacing and of wall thickness. The results presented are determined based on the maximum allowable excavation height ( $H_{max}$ ).

### 6.2.1 Effect of Anchor Spacing

The comparison study on the effect of anchor spacing between 2-D and 3-D FEA was conducted by comparing two different anchor spacing ( $s$ ), which are 2.0m and 5.0m. This gave separation ratio ( $s/B$ ) of 2 and 5, respectively, while the remaining parameters are kept constant as tabulated in Table 6.1. The breadth of anchor ( $B$ ) was adopted as 1.0m, which had been mentioned in Section 3.4.

The maximum allowable excavation height ( $H_{max}$ ) reached 6.0m and 5.5m for anchor separation ratio ( $s/B$ ) of 2 and 5, respectively. Nevertheless, for the ease of comparison purpose, all the results presented in this comparison study were based on  $H_{max} = 5.5\text{m}$ .

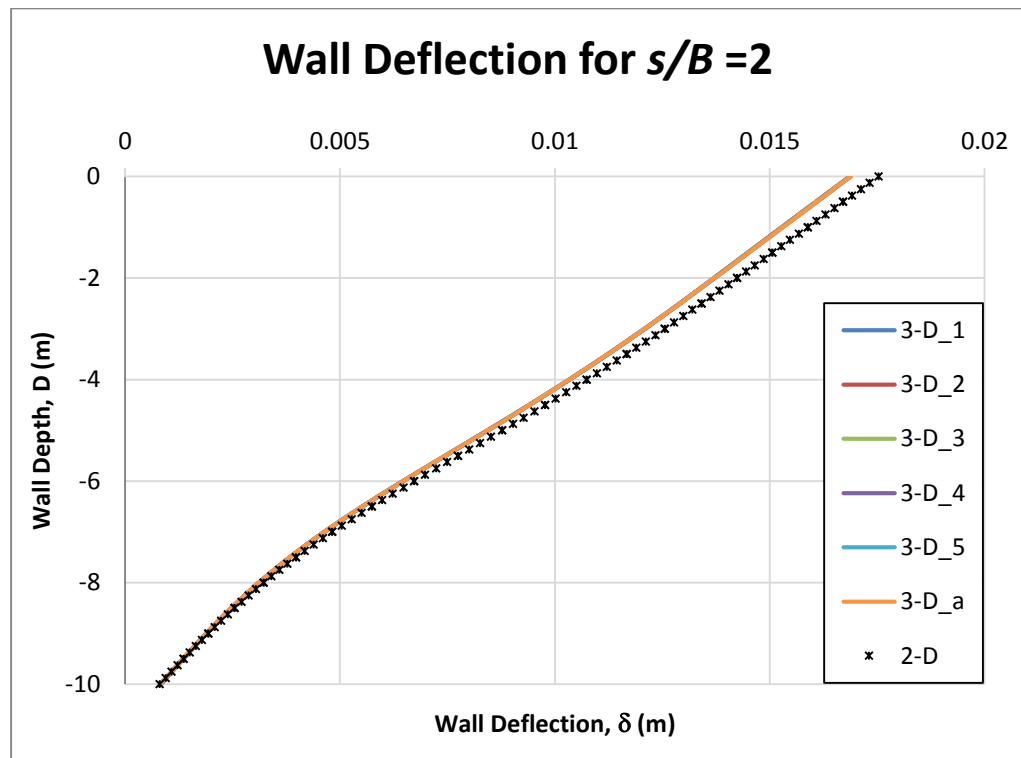


Figure 6.4: Wall deflection ( $\delta$ ) between 2-D and 3-D FEA for  $s/B = 2$ .

Figure 6.4 shows the comparison on wall deflection between 2-D and 3-D FEA for anchor separation ratio ( $s/B$ ) of 2. The percentage of variation on wall deflection between 2-D and 3-D FEA was up to 4.0%. In addition, the wall deflection restrained by discrete deadman anchor at various locations ( $3D_1$  to  $3D_5$ ) and those between anchors ( $3-D_a$ ) in 3-D model gave almost identical results.

In contrast to  $s = 2$ , the comparison on wall deflection between 2-D and 3-D FEA for  $s = 5\text{m}$  is presented in Figure 6.5. The percentage of variation on

wall deflection between 2-D and 3-D FEA was up to 8.0%. Furthermore, the wall deflections of  $s/B = 5$  in 3-D FEA ( $3D_1$  to  $3D_5$  and  $3-D_a$ ) gave almost identical results, which had similar observation with  $s/B = 2$ .

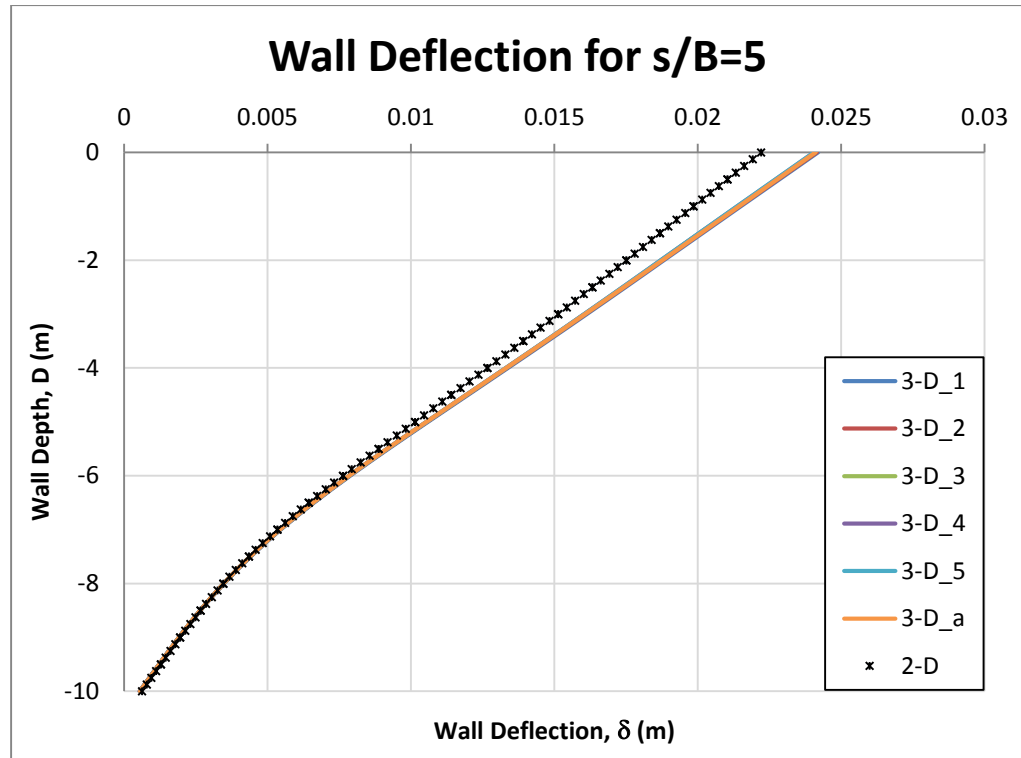


Figure 6.5: Wall deflection ( $\delta$ ) between 2-D and 3-D FEA for  $s/B = 5$ .

Figure 6.6 and Figure 6.7 show the pull-out force corresponding to the excavation level between 2-D and 3-D FEA for  $s/B = 2$  and 5, respectively. For  $s/B = 2$ , the percentage of variation on the pull-out force between 2-D and 3-D FEA was up to 6%, which was still within the acceptable range. On the other hand, the percentage of variation on the pull-out force between 2-D and 3-D FEA was up to 25% for  $s/B = 5$ .

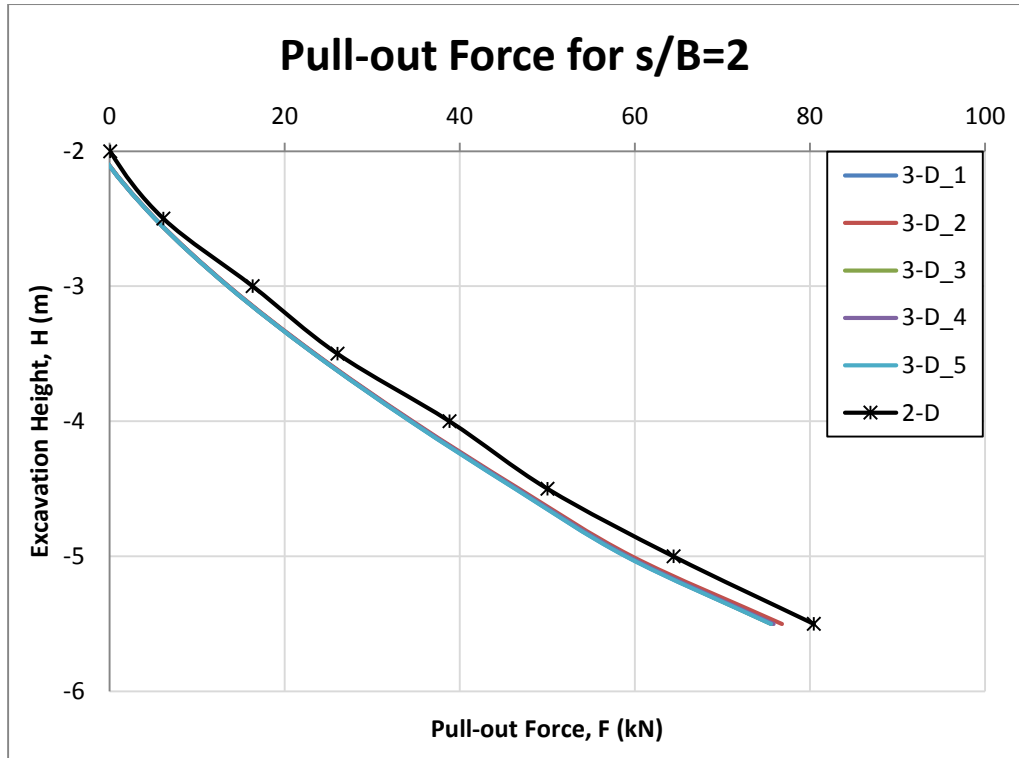


Figure 6.6: Pull-out force ( $F$ ) between 2-D and 3-D FEA for  $s/B = 2$ .

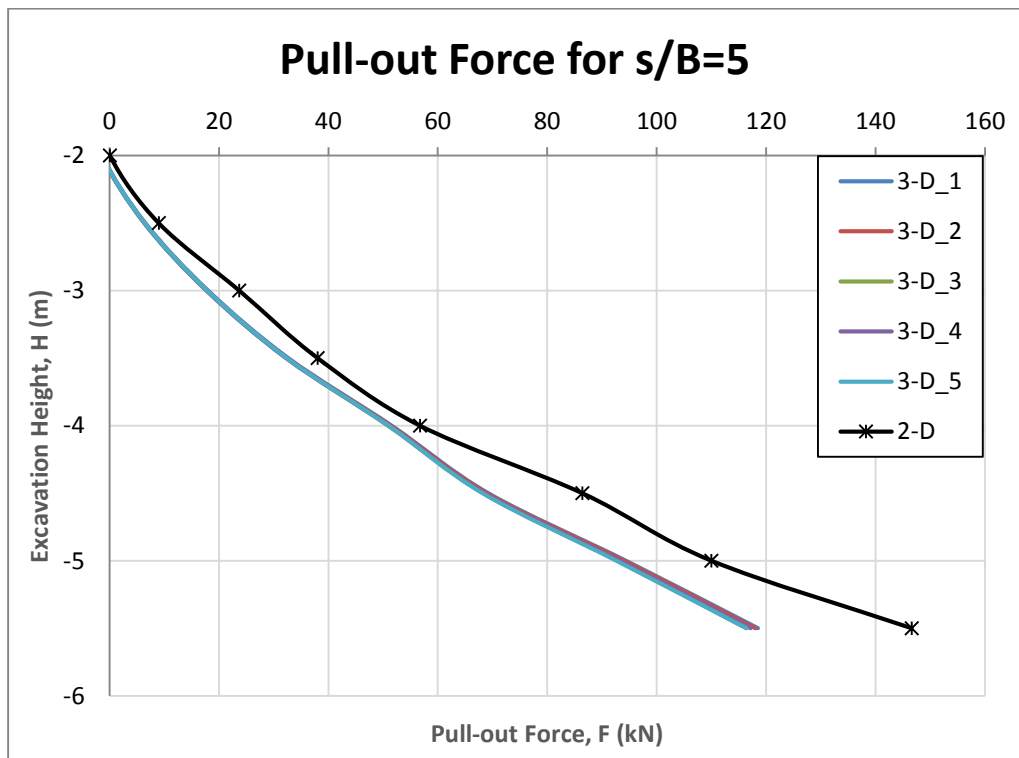


Figure 6.7: Pull-out force ( $F$ ) between 2-D and 3-D FEA for  $s/B = 5$ .

Furthermore, the percentage variation in 3-D FEA was not more than 1.5% regardless of the wall deflection restrained by each discrete deadman anchor or the pull-out force of each tie rod. This may be due to the automatic feature of meshes in *PLAXIS* as the meshes may not be distributed evenly or symmetrically.

From Figure 6.4 and Figure 6.6, it can be clearly observed that there was slight difference on the wall deflection and pull-out force for the case with  $s/B = 2$ . The percentage of variation on wall deflection and pull-out force was found to be 4% and 6%, respectively.

Moreover, the wall deflection at various locations (*3D\_1* to *3D\_5* and *3-D\_a*) in 3-D FEA gave almost identical result regardless of the anchor separation ratio ( $s/B$ ). This may be due to rigid retaining wall was implemented in this comparison study. Therefore, there is sufficient evidence to conclude that for a rigid wall ( $T = 0.5\text{m}$ ) with small anchor separation ratio ( $s/B$ ), 3-D problems can be simplified as 2-D problems.

In conclusion, as separation ratio ( $s/B$ ) of discrete deadman anchor increases from 2 to 5, the wall deflection at  $H_{max} = 5.5\text{m}$  increases by approximately 43%. Whereas, pull-out force increases to 55% at  $H_{max} = 5.5\text{m}$  as  $s/B$  increases from 2 to 5.

## 6.2.2 Effect of Wall Thickness

To compare the effect of wall stiffness between 2-D and 3-D FEA, two diaphragm walls with different thickness ( $T$ ) were adopted. Wall thicknesses with 0.1m (Flexible wall) and 0.5m (Rigid wall) were used in this comparison study while the remaining parameters are kept constant as tabulated in Table 6.1.

The maximum allowable excavation height ( $H_{max}$ ) achieved 4.5m and 5.5m for flexible and rigid wall, respectively. Nevertheless, for the ease of comparison purpose, all the results presented in this comparison study were based on  $H_{max} = 4.5\text{m}$ .

For rigid wall, the comparison on wall deflection between 2-D and 3-D FEA is illustrated in Figure 6.8. The results between 2-D and 3-D FEA were coincidentally in a good agreement with percentage of variation less than 1.0%.

Figure 6.9 shows the comparison on wall deflection between 2-D and 3-D FEA for flexible wall. The percentage of variation on wall deflection between 2-D and 3-D FEA was up to 31.20%. In addition, the wall deflection restrained by discrete deadman anchor at various locations ( $3D_1$  to  $3D_5$ ) had similar observation with rigid wall.

The main variation between rigid and flexible wall was the wall deflection between discrete deadman anchors ( $3D_a$ ). For rigid wall, the wall deflection between discrete deadman anchors ( $3D_a$ ) and those restrained by discrete deadman anchor ( $3D_1$  to  $3D_5$ ) gave almost identical results.

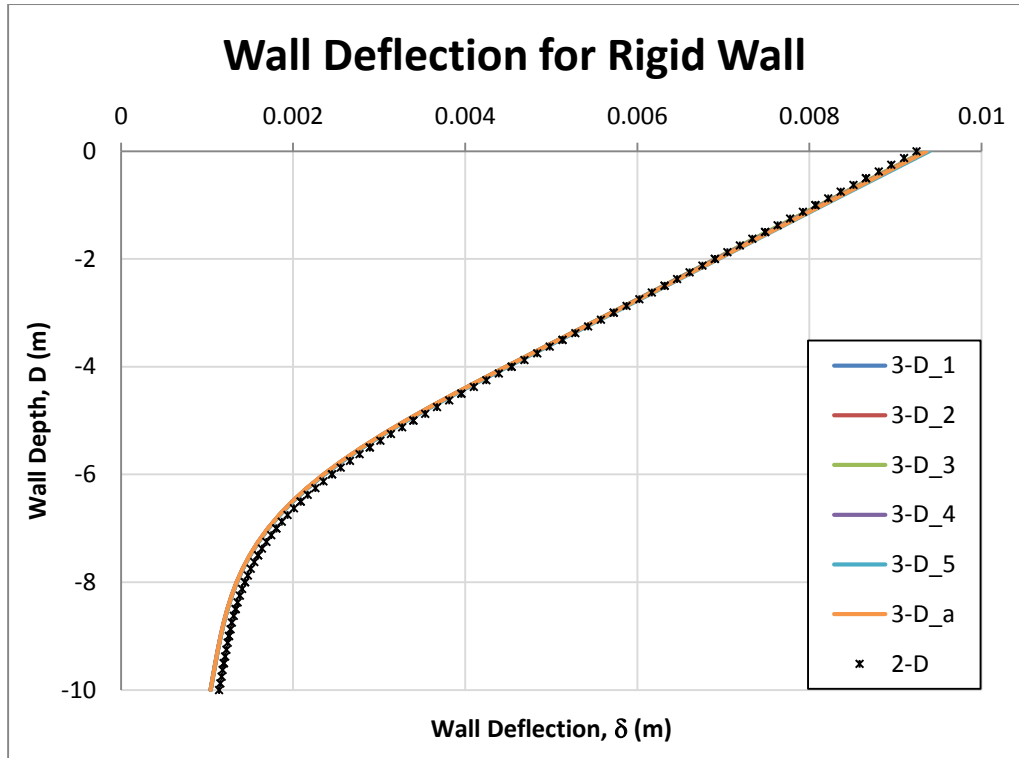


Figure 6.8: Wall deflection ( $\delta$ ) for rigid wall between 2-D and 3-D FEA.

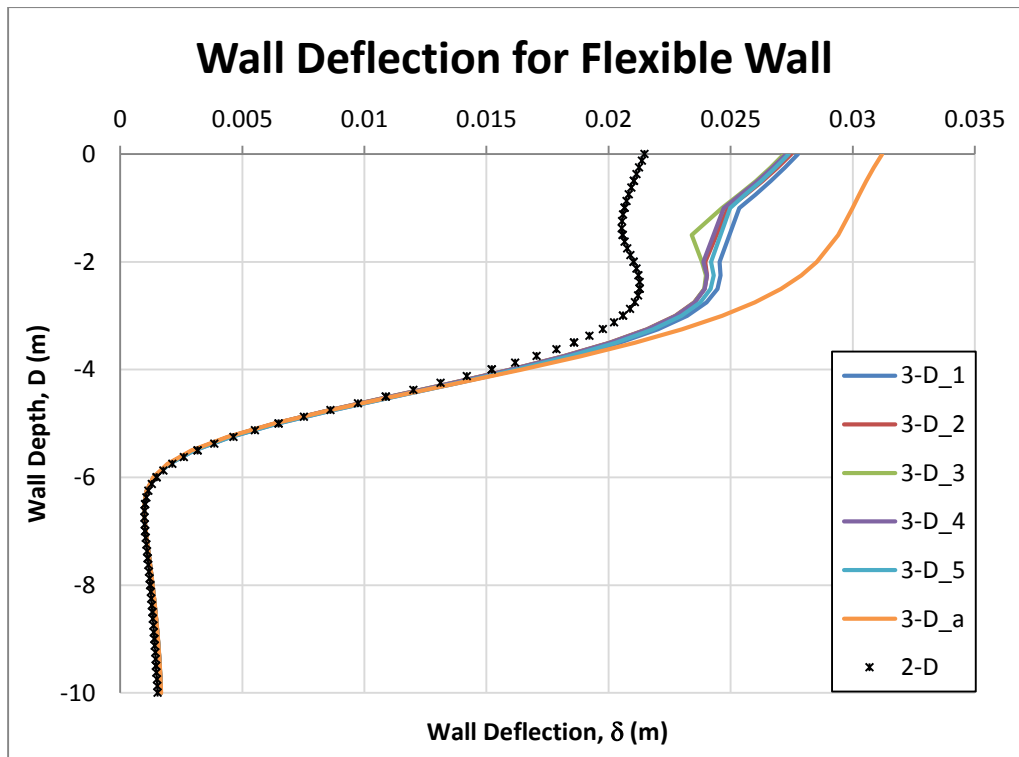


Figure 6.9: Wall deflection ( $\delta$ ) for flexible wall between 2-D and 3-D FEA.

In contrast to rigid wall, the wall deflection between deadman anchors (*3D\_a*) for flexible wall had significant variation as shown in Figure 6.9.

The percentage of variation between wall deflection restrained by each discrete deadman anchor and those between discrete deadman anchors in 3-D FEA was up to 14.0%. In conclusion, the wall deflection between deadman anchor had larger deflection compared to those restrained by discrete deadman anchors in 3-D FEA, which is illustrated in Figure 6.9.

Furthermore, the colour contour of lateral movements on the surrounding soil mass can provide a better understanding on the changes of soil movement in 3-D models. By observing the colour contour of lateral movement changes on the surrounding soil for rigid wall (see Figure 6.10), it is found that the lateral movement of soil for rigid wall follows the plane strain assumption.

This can be further explained with that the wall is relatively rigid. When a rigid wall falls, it tends to pull the discrete deadman anchor towards the passive zone (excavation side), which can cause an equivalent movement. This equivalent movement acts similar to the plane strain condition in 2-D model. Therefore, the wall deflections in 2-D and 3-D FEA for rigid wall have the same trend and results, which are illustrated in Figure 6.8.

Figure 6.11 shows the lateral movement of soil for flexible wall. It can be clearly observed that the movement of soil completely contradicted with the plane strain assumption. Hence, if the flexible wall is modelled using 2-D FEA, which only a limited set of wall deflection result is observed. This

does not show the variation of wall deflections between deadman anchors and those restrained between deadman anchors. Thus, 3-D FEA fared better than 2-D FEA as 3-D FEA can predict the actual scenario more realistically.

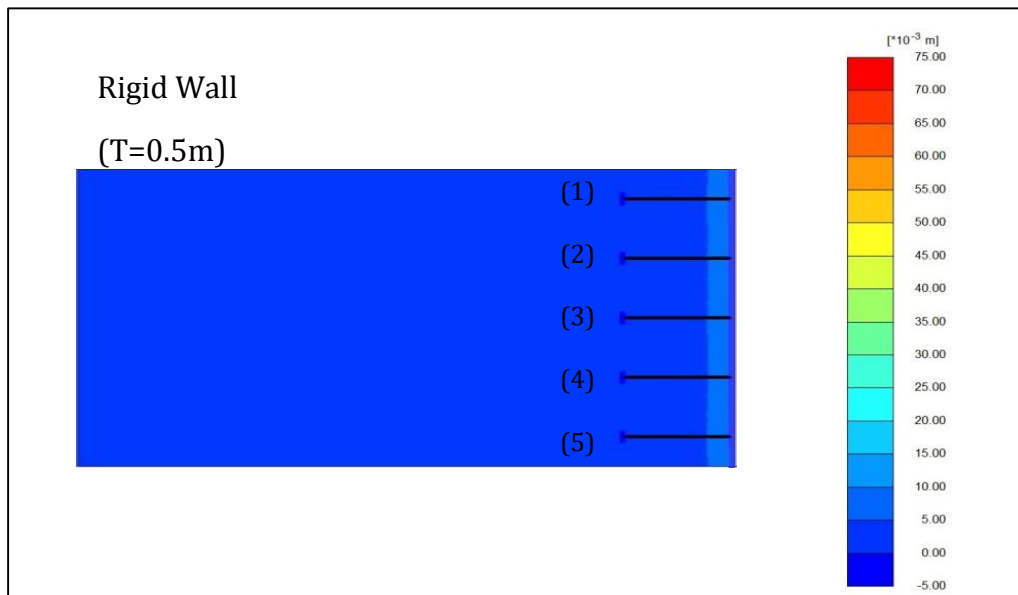


Figure 6.10: Lateral movement of soil ( $U_x$ ) for rigid wall.

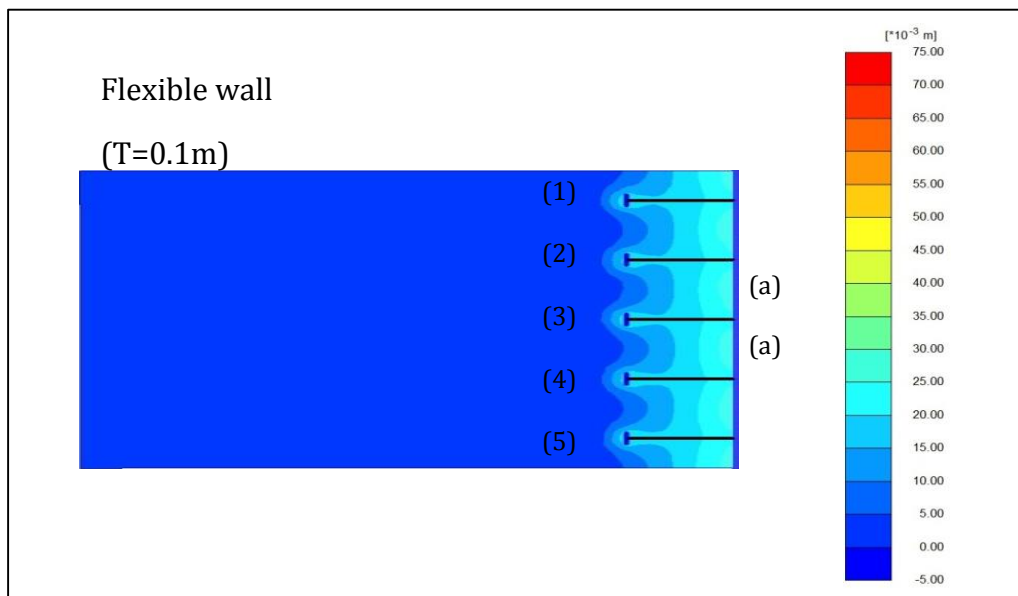


Figure 6.11: Lateral movement of soil ( $U_x$ ) for flexible wall

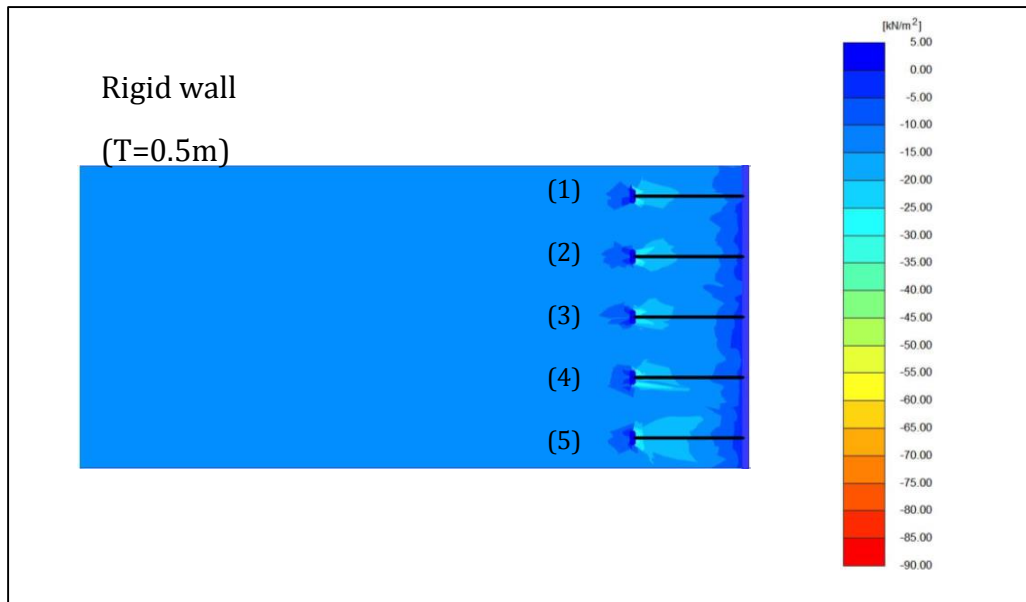


Figure 6.12: Effective stresses of soil ( $\sigma'_{xx}$ ) for rigid wall.

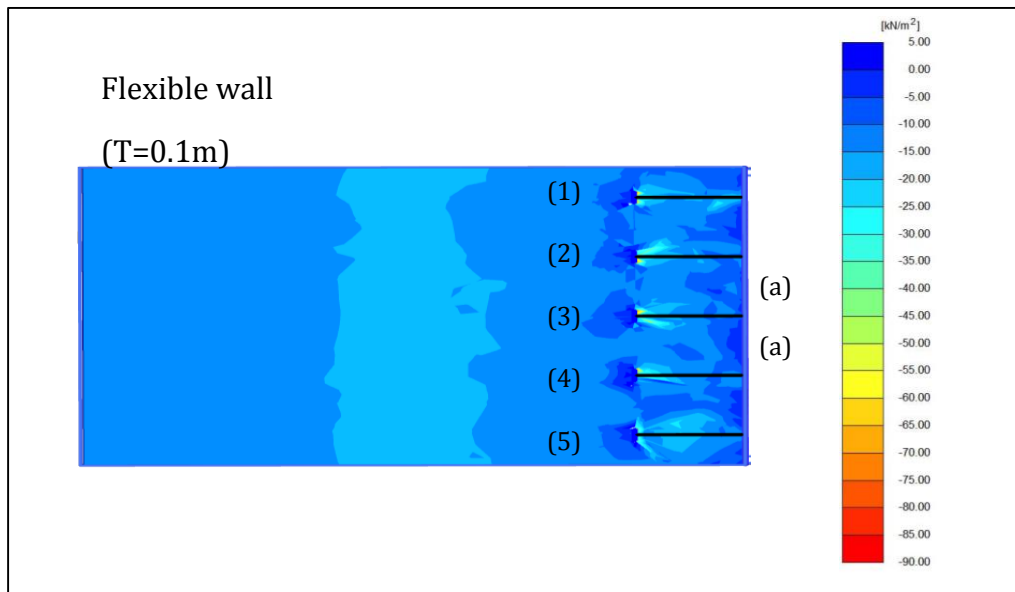


Figure 6.13: Effective stresses of soil ( $\sigma'_{xx}$ ) for flexible wall.

In addition, Figure 6.12 and Figure 6.13 show the colour contour of effective stresses of soil in x-direction for rigid wall and flexible wall, respectively. Figure 6.12 shows that the stresses of soil behind rigid wall

follow the plane strain assumption, as the magnitude of stresses of soil in plane direction are found to be similar. However, the stresses of soil surrounding deadman anchor with anchor spacing of 5.0m do not obey the plane strain assumption as the magnitude of stresses of soil are found to be discontinued from one deadman anchor to another.

In contrast to rigid wall, the stresses of soil do not obey the plane strain assumption. The stresses of soil behind earth retaining and surrounding deadman anchors are found to be discontinued as illustrated in Figure 6.13. Hence, 2-D FEA prediction on flexible wall may not be accurate.

Moreover, Figure 6.14 and Figure 6.15 show the pull-out force for rigid and flexible wall, respectively. For rigid wall, the percentage variation of the pull-out force between 2-D and 3-D FEA was up to 26.0%. However, for flexible wall, the percentage variation of the pull-out force between 2-D and 3-D FEA was up to 30%.

Therefore, these findings provide sufficient evidence to conclude that the 3-D nature effects are more superior as compared to 2-D FEA, hence 2-D results may not be reliable for certain case. This observation was agreed by Leung and co-workers (2011), who investigated the performance of deep soil mix columns between 2-D and 3-D FEA by using *PLAXIS*.

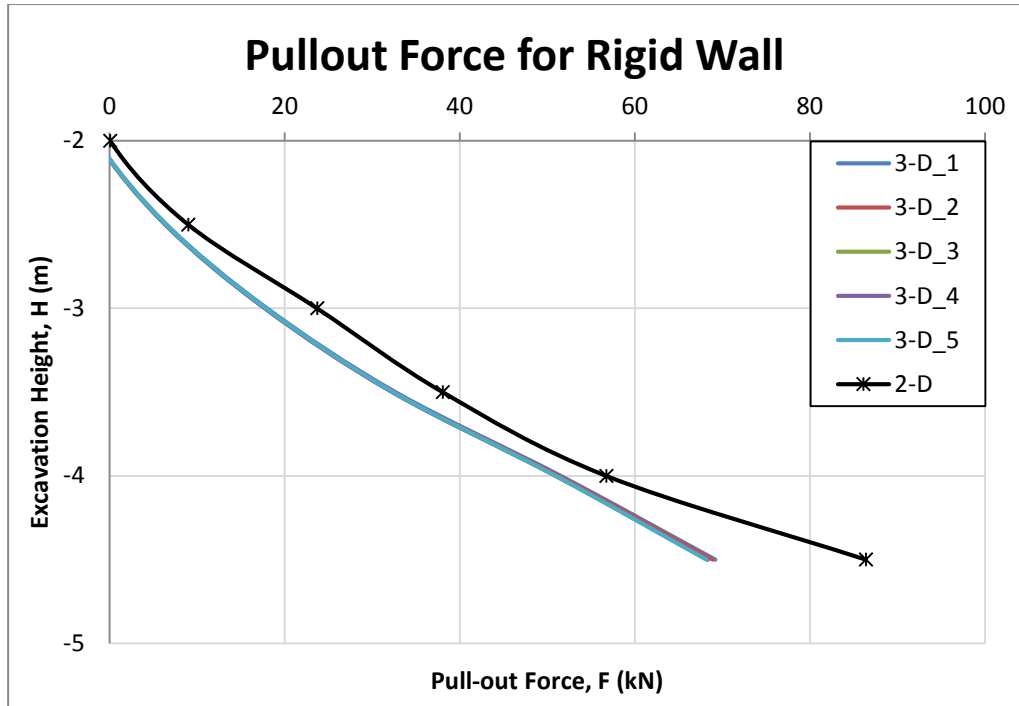


Figure 6.14: Pull-out force ( $F$ ) for rigid wall between 2-D and 3-D FEA.

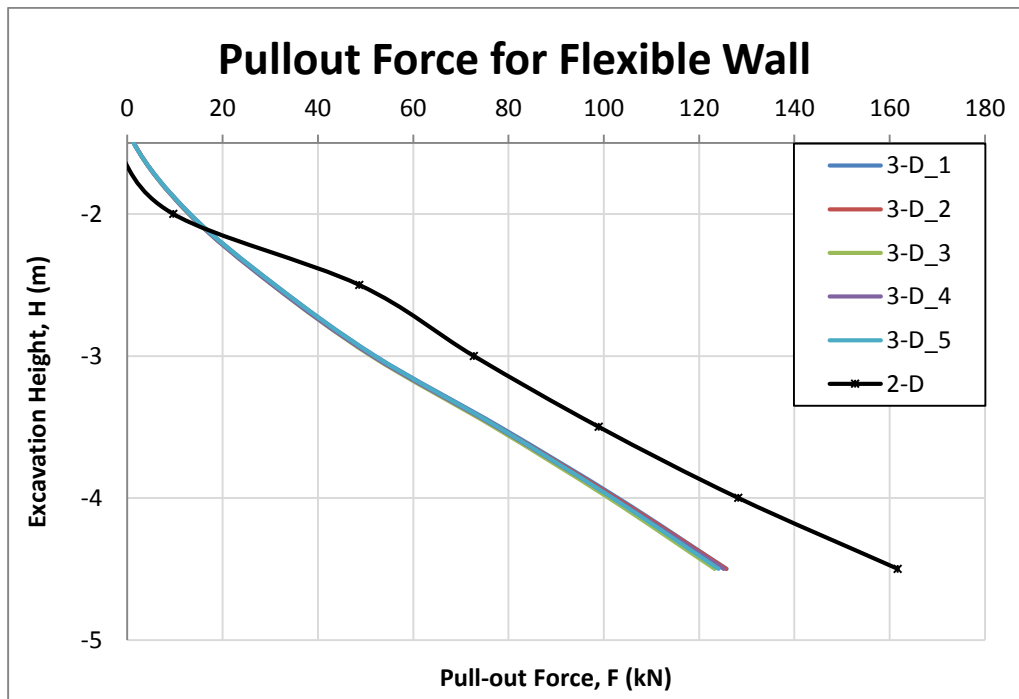


Figure 6.15: Pull-out force ( $F$ ) for flexible wall between 2-D and 3-D FEA.

### 6.3 Benefits of 3-D Finite Element Analysis

The numerical analysis for continuous deadman anchor can be simulated as 2-D plane strain assumption and the results can be predicted reasonably well with 2-D FEA. However, as discussed above, the results for discrete deadman anchors cannot be realistically simplified as 2-D problems. Thus 3-D FEA is opted to provide high accuracy results.

In addition, 3-D FEA allows a better understanding/study on the plan view interactions of deadman anchorage system with the surrounding soil mass. 3-D FEA is an excellent technique to study deadman anchorage system more accurately since it is a more realistic representation of discrete deadman anchorage system. The colour contour for lateral movements and effective stresses on the surrounding soil mass clearly indicated the soil-structure interactions. Moreover, 3-D FEA is able to provide bending moment profiles in both the vertical and horizontal directions for structural design on earth retaining wall (see Figure 6.16 and Figure 6.17, respectively), but 2-D model is not possible.

Conventionally, the design of longitudinal bars in retaining wall depends on the vertical bars, which is not based on bending moment. The longitudinal bars are designed based on the minimum percentage of reinforcement needed (BS 8110-1, 1997), which is expressed as:

$$\text{minimum percentage of reinforcement needed} = 100A_s/A_c$$

where,

$A_s$  = Area of steel.

$A_c$  = Area of concrete.

\*\*Note that in BS 8110-1 (1997): Clause 3.12.7.4 suggested that the minimum percentage of longitudinal reinforcement for rectangular wall is:-

- a. 0.30% of concrete area for mild steel ( $f_y = 250\text{N/mm}^2$ ) and
- b. 0.25% for high tensile steel ( $f_y = 500\text{N/mm}^2$ ).

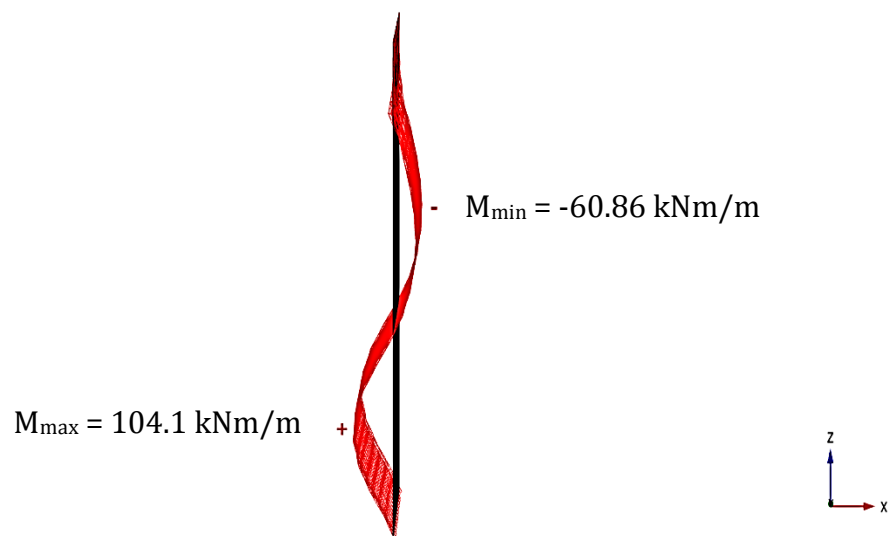


Figure 6.16: Vertical bending moment for 3-D model with  $T = 0.5\text{m}$  and  $s/B = 2$ .

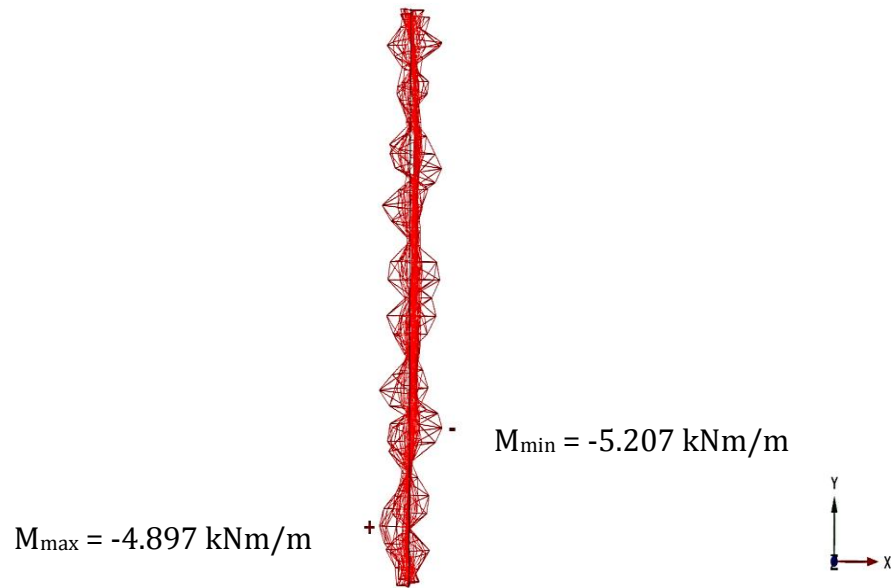


Figure 6.17: Horizontal bending moment for 3-D model with  $T = 0.5\text{m}$  and  $s/B = 2$  (Plan view).

### 6.3.1 Study on the Presence of Deadman Anchorage System in Earth Retaining Wall

This study aims to demonstrate some of the benefits in 3-D FEA by investigating the presence of deadman anchorages system. In this study, two models, namely Model A and Model B, were adopted. Furthermore, the parameters used in this study are presented in Table 6.2.

The models used in this study are:-

- a. Model A – Earth retaining wall (without deadman anchorage system);
- b. Model B – Earth retaining wall (with deadman anchorage system).

Table 6.2: Parameters for the study of the presence of deadman anchorages system in 3-D FEA.

Parameter		
<b>Tie rod length, <math>L</math> (m)</b>	:	5
<b>Anchor embedment depth, <math>d</math> (m)</b>	:	2
<b>Anchor spacing, <math>s</math> (m)</b>	:	5
<b>Friction angle of soil, <math>\phi</math> (°)</b>	:	30
<b>Wall depth, <math>D</math> (m)</b>	:	10
<b>Wall thickness, <math>T</math> (m)</b>	:	0.5

Figure 6.18 through Figure 6.20 show the effective stress of soil in X-direction ( $\sigma'_{xx}$ ) at different construction stages. At initial stage, before excavation commenced, both models had equivalent stresses of soil as shown in Figure 6.18. However, when the excavation commenced, the change of effective stresses occurred at various excavation heights (i.e.  $H = 4.5\text{m}$  and  $6.0\text{m}$ ), as illustrated in Figure 6.19 and Figure 6.20, respectively.

With the presence of deadman anchorage system, the effective stress of soil was no longer accumulated behind the retaining wall. The effective stress was partially diverted to the rear face of deadman anchors. The soil at the front face of deadman anchors experienced compression effect (passive resistance) and hence leading to stress decrease, which is clearly illustrated in Figure 6.19 and Figure 6.20.

The passive resistance induced in front of deadman anchors attempted to hold back the earth retaining wall from moving towards the excavated side. Moreover, the passive resistance reduced the lateral movements of soil and

hence, reducing the wall deflection, which is illustrated in Figure 6.21 and Figure 6.22.

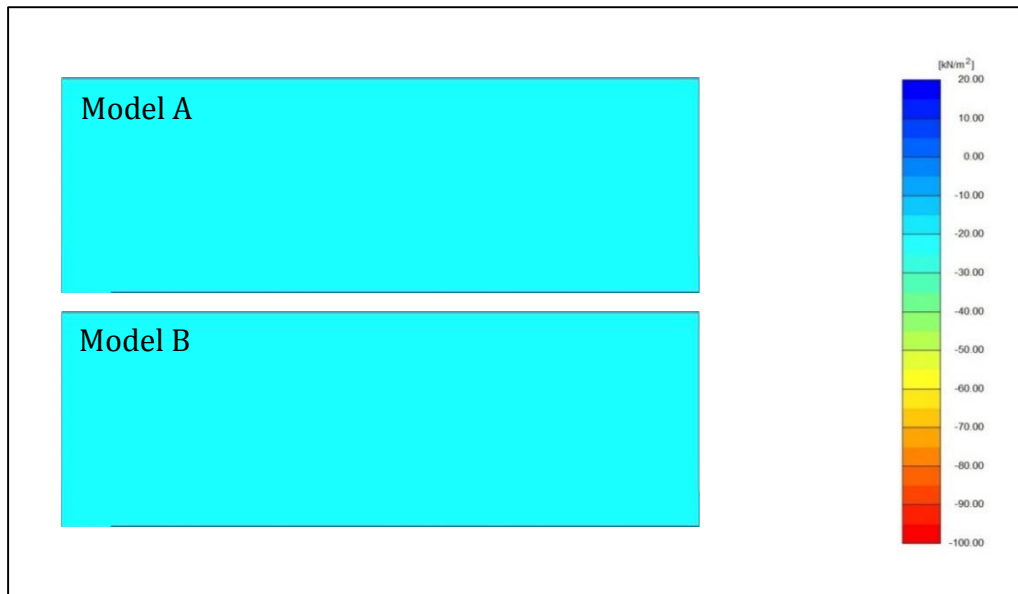


Figure 6.18: Effective stresses ( $\sigma'_{xx}$ ) for Models A and B at initial stage.

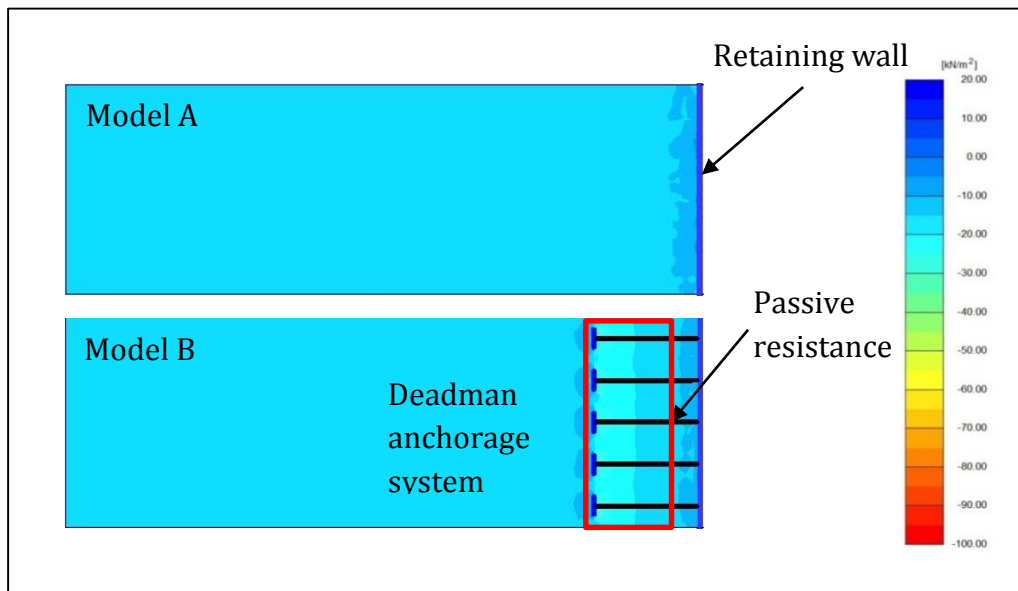


Figure 6.19: Effective stresses ( $\sigma'_{xx}$ ) for Models A and B at excavation height ( $H$ ) 4.5m.

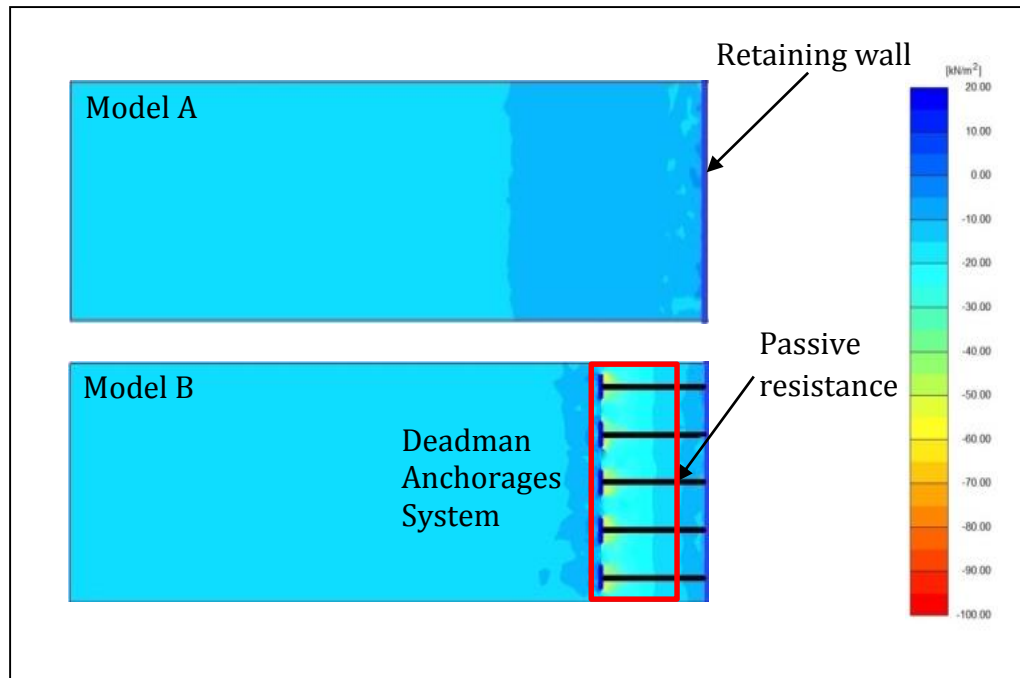


Figure 6.20: Effective stresses ( $\sigma'_{xx}$ ) for Models A and B at  $H = 6.0\text{m}$ .

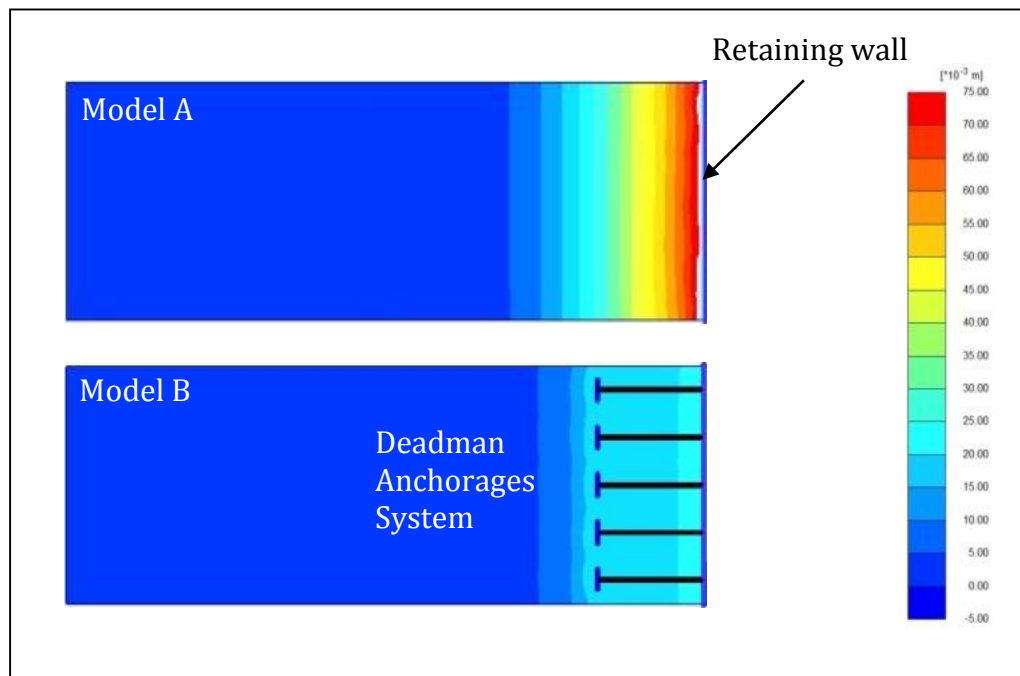


Figure 6.21: Lateral movements of soil ( $U_x$ ) for Models A and B at  $H = 6.0\text{m}$ .

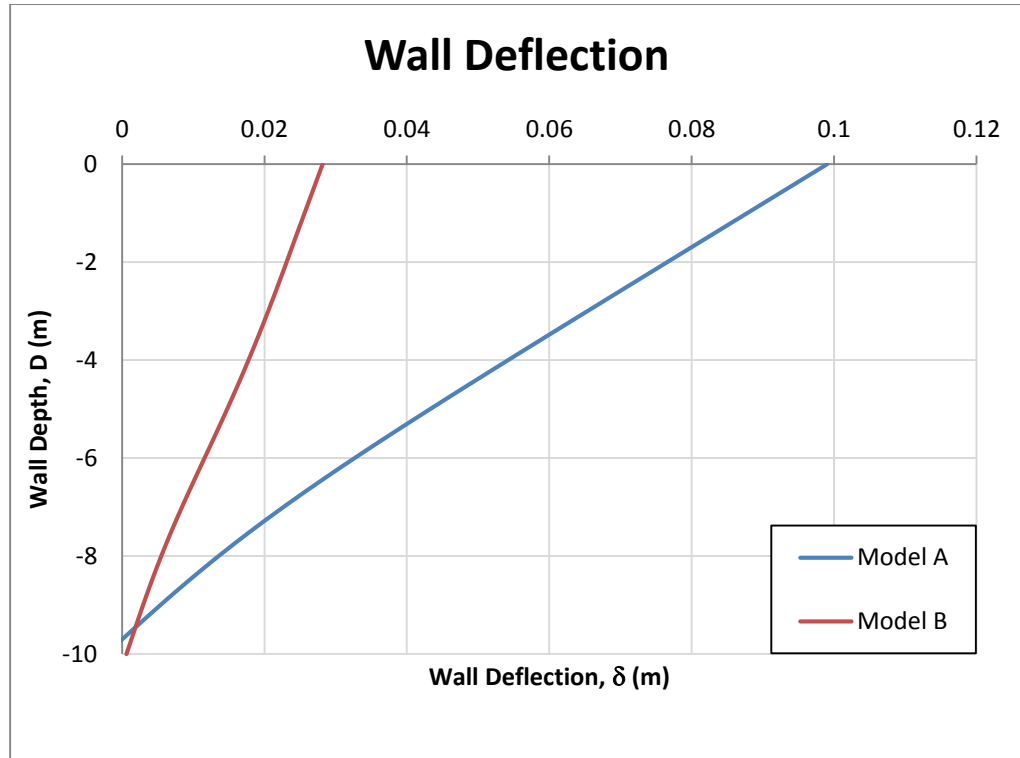


Figure 6.22: Wall deflections ( $\delta$ ) for Models A and B at  $H = 6.0\text{m}$ .

Table 6.3: Percentage of variation on wall deflection between Models A and B.

Excavation height, H (m)	Wall deflection, $\delta$ (m)		Percentage of variation (%)
	Model A	Model B	
2	2.96E-04	2.41E-04	22.74
2.5	1.16E-03	8.63E-04	33.94
3	2.64E-03	1.73E-03	52.92
3.5	5.01E-03	2.91E-03	71.85
4	9.44E-03	4.54E-03	108.01
4.5	1.41E-02	6.88E-03	105.24
5	2.53E-02	1.03E-02	146.52
5.5	4.45E-02	1.69E-02	163.53
6	9.91E-02	2.82E-02	251.63

In Table 6.3, the wall deflection with the presence of deadman anchorage system at excavation height ( $H = 6.0\text{m}$ ) was reduced as much as 252% compared to that without deadman anchorage system. This shows that the earth retaining wall with deadman anchorage system had significant reduction in terms of wall deflection. At various excavation height, the rate of reduction in wall deflection with the presence of deadman anchorage system is tabulated in Table 6.3. Therefore, deadman anchorage system plays an important role in reducing the wall deflection.

## 6.4 Summary

This chapter presents a comparison study between 2-D FEA (plane strain assumption) and 3-D FEA (realistic condition). Two potential variables, which are anchor spacing and wall stiffness, were studied in both 2-D and 3-D FEA. Results from the discussed variables showed that there are variations occurred between 2-D and 3-D FEA in terms of wall deflection and pull-out force.

In 2-D FEA with plane strain assumption, the deadman anchorages system was modelled as an “infinitely” long plane with thickness. For the effect of anchor spacing in rigid wall, the percentage of variation for wall deflection between 2-D and 3-D FEA was up to 4% and 8% for  $s/B$  of 2 and 5, respectively. On the other hand, the percentage of variation for the pull-out force between 2-D and 3-D FEA was found to be 6% and 25% for  $s/B$  of 2 and 5, respectively. In addition, the percentage of variation among

deadman anchorage system in 3-D FEA was found to be not more than 1.5% regardless of wall deflection or pull-out force.

Furthermore, the earth retaining wall was modelled as a beam element in 2-D FEA. Thus, only a limited set of wall deflection and pull-out was observed. The results may be valid for very rigid wall in real case. This is because 3-D FEA also provided similar sets of wall deflection and pull-out force. However, for the pull-out force in rigid wall, the percentage of variation between 2-D and 3-D FEA was up to 26%. On the other hand, for flexible wall, the percentage of variation in terms of wall deflection and pull-out force between 2-D and 3-D FEA were determined to be 31.2% and 30.0%, respectively.

For closer separation ratio of discrete deadman anchor, 2-D FEA can provide reasonable estimation. Nevertheless, the limitation of 2-D plane strain condition should be acknowledged and considered separately for each condition in order to ensure proper finite element modelling. This is to ensure that reliable estimation is obtained for further assessment.

Last but not least, this chapter also highlights the benefit of adopting 3-D FEA. 3-D FEA allows a better understanding/study on the plan view interactions of deadman anchorage system with the surrounding soil mass. The colour contour for lateral movements and effective stresses on the surrounding soil mass clearly indicated the soil-structure interactions.

A study on the presence of deadman anchorage system in earth retaining wall demonstrates the benefits of 3-D FEA. The changes of effective stress

on plan view for each construction stages clearly demonstrate the interactions of earth retaining wall with and without deadman anchorage system with surrounding soil mass for different construction stages. Furthermore, the colour contour of lateral movement shows movements of surrounding soil mass caused by the heights of excavation.

# CHAPTER 7

---

## MODEL SIMPLIFICATION

### 7.1 Introduction

Previous chapter highlights that three-dimensional (3-D) finite element analysis (FEA) on discrete deadman anchorage system in rigid earth retaining wall gave almost identical results for wall deflection and pull-out force regardless of anchor spacing at locations restrained by discrete deadman anchor (*3D\_1* to *3D\_5*). The percentage of variation among deadman anchorage system in 3-D FEA was found to be not more than 1.5% regardless of wall deflection or pull-out force.

Hence, it is interesting to know whether the model with more number of discrete deadman anchors (complex model) can be further simplified to a model with single discrete deadman anchor (simplified model). This technique is known as model simplification.

Model simplification aims to reduce the computational effort and duration. Besides that, model simplification aims to avoid argument on the number of discrete deadman anchors implemented to study the behaviour of discrete deadman anchorage system. The performance of model simplification is evaluated based on the computed pull-out force, wall deflection, effective stress and lateral movement of soil.

## 7.2 Model Simplification

A series of finite element analysis (FEA) was carried out to evaluate the degree of agreement of simplified model with singular discrete deadman anchor in comparison with complex models with multiple deadman anchors. Parametric studies with different manipulation of anchor spacing ( $s$ ), anchor embedment depth ( $d$ ), tie rod length ( $L$ ) and number of discrete deadman anchors used for constant friction angle ( $\phi$ ) and wall stiffness ( $EI$ ) were carried out to evaluate the degree of agreement of model simplification and to develop the model simplification chart.

For each anchor spacing ( $s = 2\text{m}, 3\text{m}$  and  $5\text{m}$ ) and each anchor embedment depth ( $d = 1\text{m}, 2\text{m}$  and  $3\text{m}$ ), length of tie rod and number of discrete deadman anchors used in the parametric studies for friction angle ( $\phi$ ) of  $30^\circ$  and wall stiffness ( $EI$ ) of  $2.708\text{E}+05\text{kNm}^2$  is presented in Table 7.1. A total number of 108 finite element analyses were conducted to evaluate the degree of agreement of simplified model in predicting the complex models and to develop the model simplification chart.

Table 7.1: Parametric studies for model simplification.

Tie rod length (L) Number of Anchor(s)	5	10	15
1	✓	✓	✓
3	✓	✓	✓
5	✓	✓	✓
7	✓	✓	✓

Literally, it is believed that the complex models with more discrete deadman anchors can provide more accurate prediction compared to fewer discrete deadman anchors as they can simulate the interaction between soil and their surrounding structure in a more realistic form. For instance, the variation between models with single and seven discrete deadman anchors should be larger compare to the variation between models with five and seven discrete deadman anchors.

Nevertheless, certain cases did not obey the statement above. Hence, the model simplification is aimed to simplify complex model with multiple discrete deadman anchors (complex model) into model with singular discrete deadman anchors (simplified model), and to avoid argument on the number of discrete deadman anchors used in FEA.

The performances of simplified model are assessed based on the computed, wall deflection, pull-out force, effective stress and lateral movement of soil. In addition, the performances of simplified model are also determined based on the maximum excavation height ( $H_{max}$ ) is limited to the deflection

of anchored wall not more than 0.5% of the excavation height ( $H$ ). The model simplification assessment are made by comparing simplified model and complex models with percentage of variation not more than 5% of complex model with seven discrete deadman anchors.

A set of parameter adopted in the study of model simplification is chosen for detailed discussion. The parameters is presented in Table 7.2. The maximum allowable excavation height ( $H_{max}$ ) for this set of parameter is up to 6.5m.

Table 7.2: Parameters adopted in the study of model simplification.

<b>Parameter</b>		
<b>Tie rod length, <math>L</math> (m)</b>	:	10.0
<b>Anchor embedment depth, <math>d</math> (m)</b>	:	2
<b>Anchor spacing, <math>s</math> (m)</b>	:	3
<b>Friction angle of soil, <math>\phi</math> (°)</b>	:	30
<b>Wall depth, <math>D</math> (m)</b>	:	10
<b>Wall stiffness, <math>EI</math> (kNm<sup>2</sup>)</b>	:	2.708E+05

### 7.2.1 Wall Deflection

Figure 7.1 shows that the results of computed wall deflection for various models are found to be similarly close. Furthermore, the result from simplified model is found to be almost identical with that from complex model with seven discrete deadman anchors.

The results of wall deflection between models with singular and seven discrete deadman anchors are presented in Table 7.3. The maximum percentage of variation is found to be 4.70%, which occurred at  $H = 4.5$ . Moreover, the maximum variation in terms of magnitude of wall deflection between models with singular and seven discrete deadman anchors is determined to be 0.517mm.

The overall variation on the wall deflection is relatively small, which is less than 5.00% and the magnitude is less than 1.0mm. This showed that the performance in terms of wall deflection from simplified model is almost in a perfectly agreement with that from complex models.

Table 7.3: The variations of wall deflection between simplified and complex model.

Excavation height, H (m)	Wall deflection, $\delta$ (m)		Variation (mm)	Percentage of variation (%)
	Simplified model	Complex model		
2	2.80E-04	2.74E-04	0.0057	2.09
2.5	9.89E-04	9.72E-04	0.0172	1.77
3	2.10E-03	2.07E-03	0.0363	1.76
3.5	3.57E-03	3.50E-03	0.0713	2.04
4	5.46E-03	5.35E-03	0.1192	2.23
4.5	8.41E-03	8.03E-03	0.3772	4.70
5	1.17E-02	1.12E-02	0.5172	4.63
5.5	1.57E-02	1.56E-02	0.1144	0.73
6	2.15E-02	2.11E-02	0.3946	1.87
6.5	2.97E-02	2.92E-02	0.4885	1.67

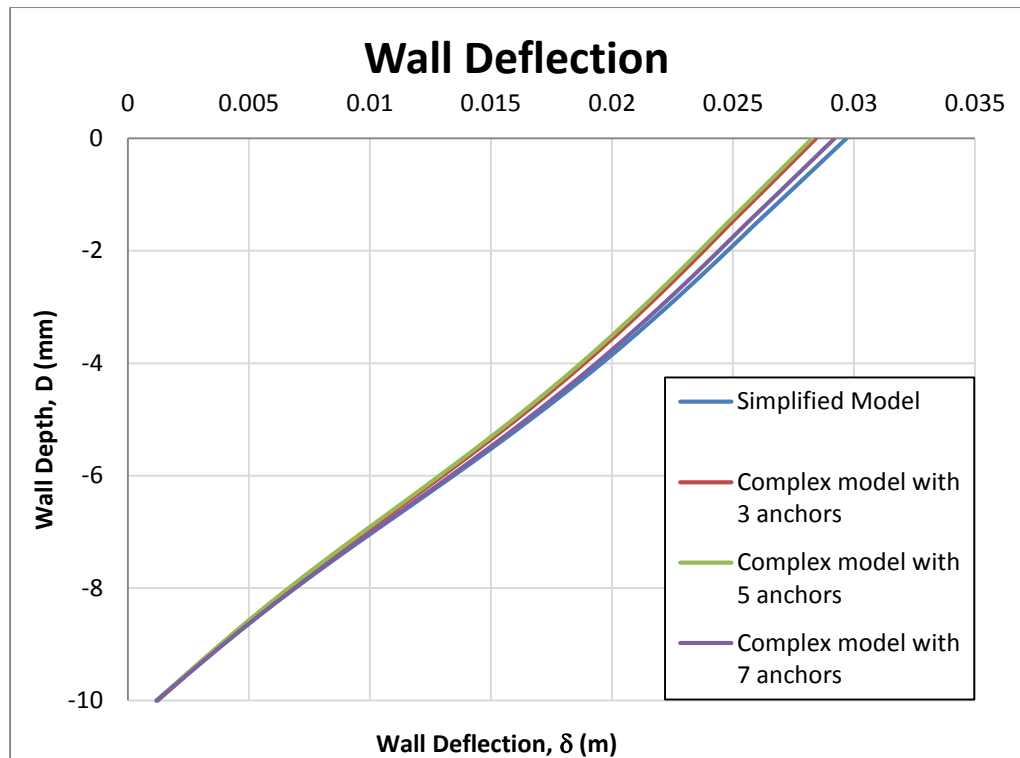


Figure 7.1: Wall deflection ( $\delta$ ) at  $H = 6.5\text{m}$  among models.

## 7.2.2 Pull-out Force

Figure 7.2 shows that the pull-out force for each model gave almost identical results up to  $H_{max} = 6.5\text{m}$ . By comparing the maximum and minimum values on the pull-out force among the models, the largest variation occur at  $H = 4.5\text{m}$ . This variation occurred between models with singular and five discrete deadman anchors, and the percentage of variation was up to 6.08%.

In addition, by comparing the simplified model with the complex model with seven discrete deadman anchors, the maximum variation also occurred at  $H = 4.5\text{m}$  with a percentage of variation of 3.79%.

Since the pull-out force were almost identical among models and the simplified model was of 3.79% difference from the complex model with seven discrete deadman anchor, which was less than 5.00%. Therefore, it is believed that the performance of simplified model is in a good agreement with complex model in terms of pull-out force.

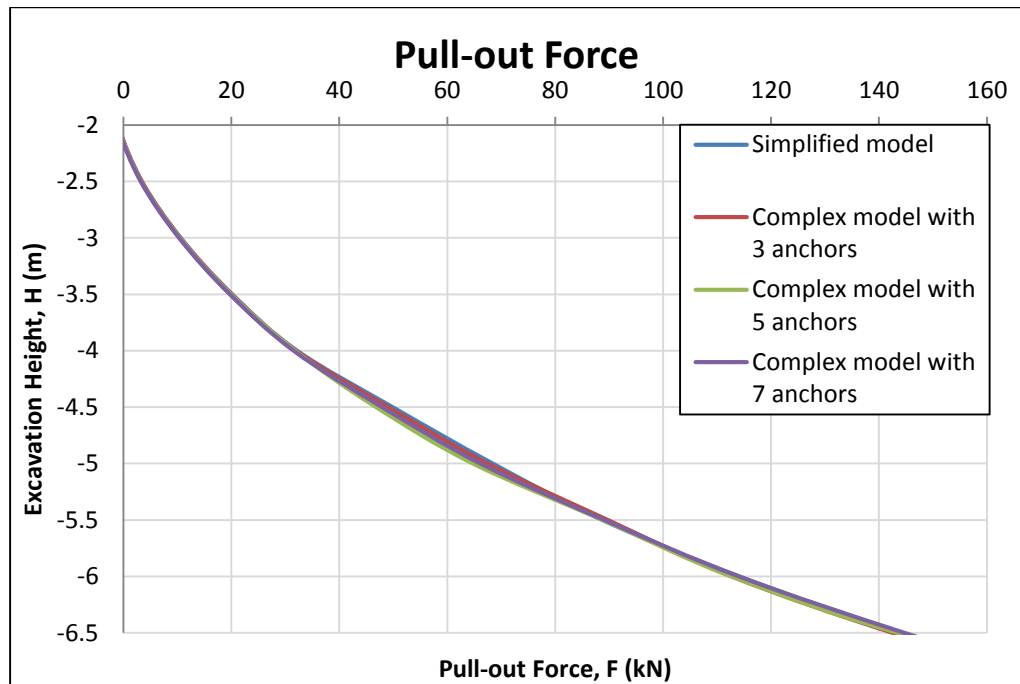


Figure 7.2: Pull-out force ( $F$ ) among models.

### 7.2.3 Lateral Movement of Soil

Figure 7.3 shows the colour contour of lateral movement of soil for each model at the maximum allowable excavation height ( $H_{max} = 6.5\text{m}$ ) and the results are observed to be of similar patterns. This explains that the movement of soil is almost identical regardless of the number of anchors modelled in FEA. This provided sufficient evidence to conclude that the

simplified model can produce a good estimation on the behaviour of soil movement in comparison with complex models.

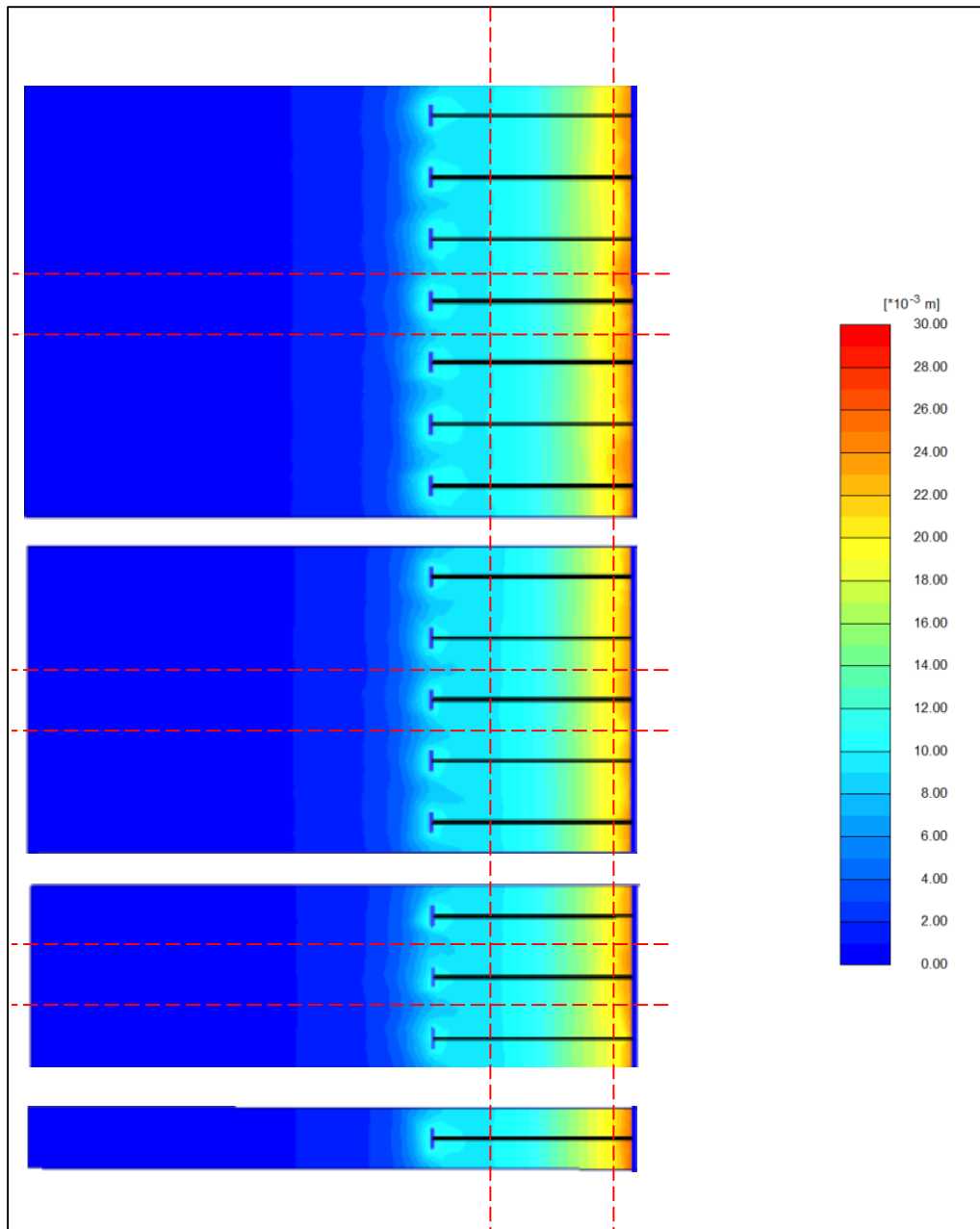


Figure 7.3: Colour contour for lateral movements of soil at  $H = 6.5\text{m}$  among models.

### 7.2.4 Effective Stress of Soil

Figure 7.4 shows the colour contour of effective stress for each model at the maximum allowable excavation height ( $H_{max} = 6.5\text{m}$ ) and the results are found to be of almost identical pattern. This explains that the effective stress for each discrete deadman anchor do not have significant interaction with one another regardless of the number of discrete deadman anchors modelled in FEA. Similar observations were obtained from a closer spacing ( $s = 2$ ). Hence, this provides additional evidence to conclude that the complex model with multiple discrete deadman anchors can be further simplified into model with singular discrete anchor as the predicted stress are found to be of almost identical pattern among models.

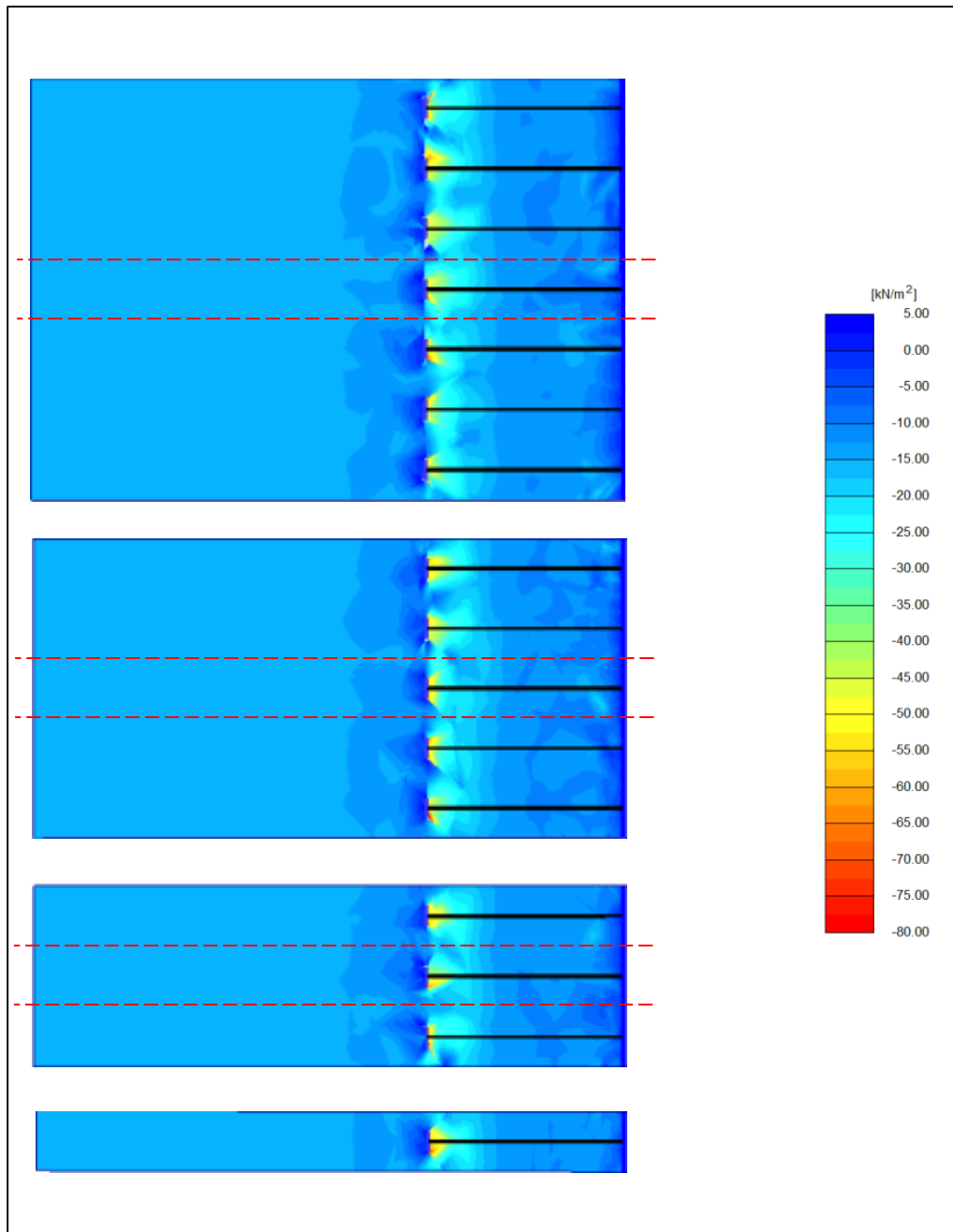


Figure 7.4: Colour contour for effective stresses of soil at  $H = 6.5\text{m}$  among models.

### 7.2.5 Results of Model Simplification

The degree of agreement of model simplification were determined based on different manipulation of anchor spacing ( $s$ ), anchor embedment depth ( $d$ ), tie rod length ( $L$ ) and number of discrete deadman anchors used in FEA model.

In section 7.2.1 to 7.2.4, it demonstrated that the simplified model can predict the behaviour of complex models with multiple discrete deadman anchors reasonably well regardless of the wall deflection, pull-out force, lateral movement of soil and effective stress of soil.

Similar observations were made for the case of the manipulation of each anchor spacing ( $s = 2\text{m}$ ,  $3\text{m}$  and  $5\text{m}$ ), anchor embedment depth ( $d = 1\text{m}$ ,  $2\text{m}$  and  $3\text{m}$ ), length of tie rod ( $L = 5\text{m}$ ,  $10\text{m}$  and  $15\text{m}$ ) and number of discrete deadman anchors modelled in FEA (1 no, 3nos, 5nos and 7nos) with friction angle ( $\phi$ ) of  $30^\circ$  and wall stiffness ( $EI$ ) of  $2.708\text{E}+05\text{kNm}^2$ .

Therefore, it provides sufficient evidence to conclude that the complex models can be simplified into model with singular discrete deadman anchor.

### 7.3 Model Simplification Chart

Follows to the evaluation on the degree of model simplification, the results of model simplification can be presented in a normalised form for each anchor embedment ratio ( $d/h$ ).

Figure 7.5 presents the result of model simplification for anchor embedment ratio ( $d/h$ ) of 1.

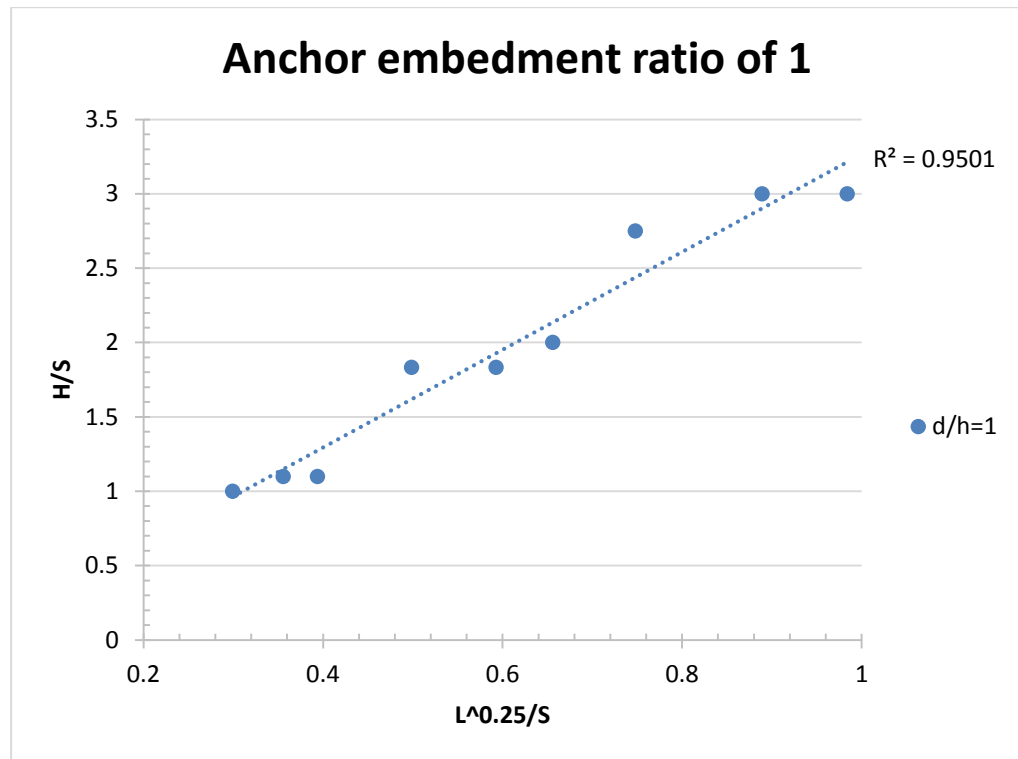


Figure 7.5: Result for anchor embedment ratio of 1.

In Figure 7.5, the  $R^2$  value for the linear best fit line of  $d/h = 1$  is found to be 0.9501. The value of  $R^2$  is a measurement of the goodness-of fit of linear regression. When  $R^2$  value is equal to 1.0, it means that all the data points rest exactly positioned on the best fit line. The X- and Y-variables can be predicted perfectly if the  $R^2$  value is 1.0. Otherwise,  $R^2$  value of 0.0 means that although the X-variable is known, the Y-variable still cannot be determined. This is because none of the data points are close to the linear best fit line. In addition, the value of  $R^2$  above 0.9 can predict the X- and Y-variables reasonably well.

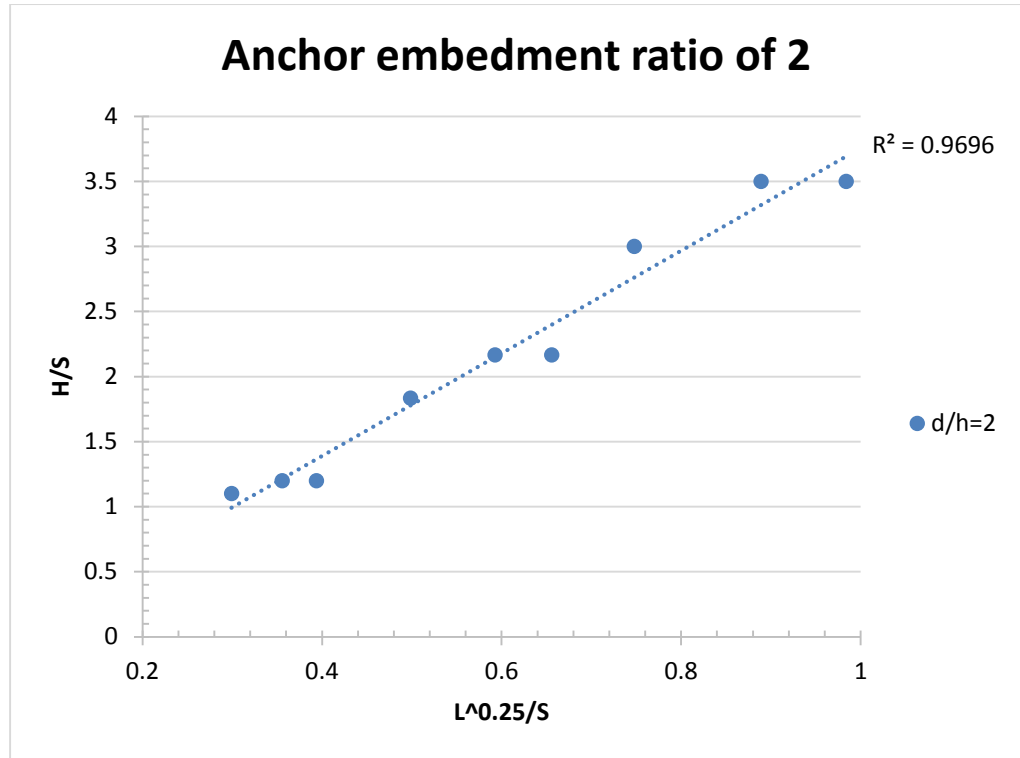


Figure 7.6: Result for anchor embedment ratio of 2.

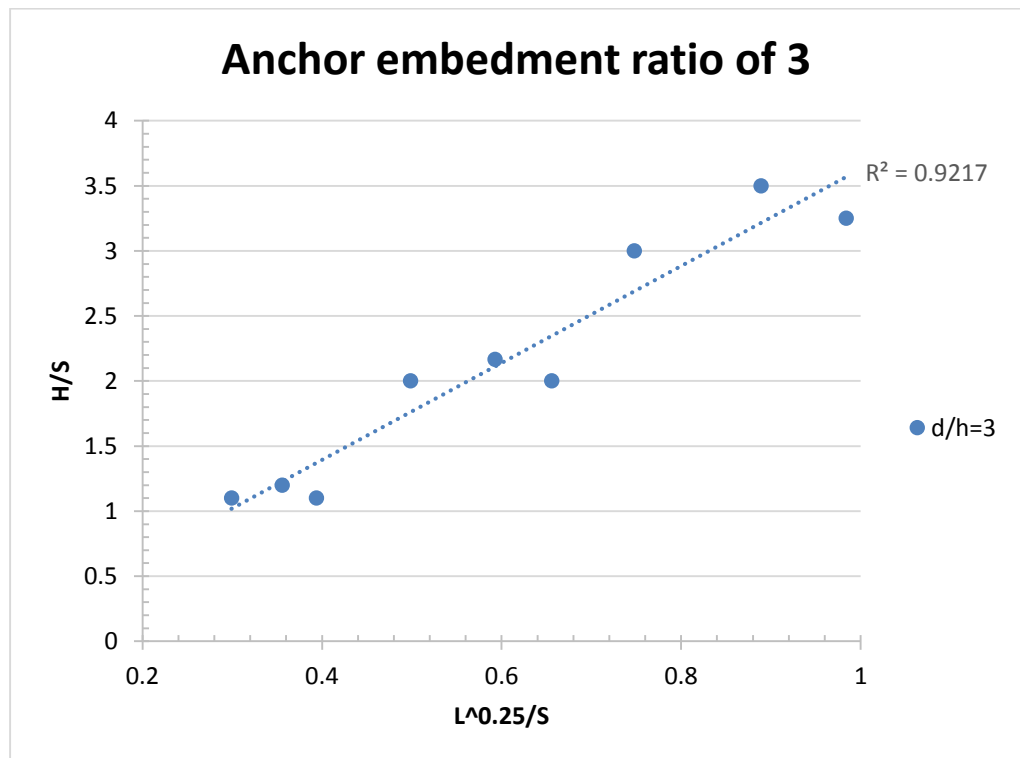


Figure 7.7: Result for anchor embedment ratio of 3.

The results of model simplification for  $d/h = 2$  and  $3$  are presented in Figure 7.6 and Figure 7.7, respectively. The  $R^2$  values for the linear best fit line of  $d/h = 2$  and  $3$  are  $0.9696$  and  $0.9217$ , respectively. The linear best fit line for each anchor embedment ratio is considered good in predicting the data points as the  $R^2$  values are beyond  $0.9$ .

By conjoining the results from each anchor embedment ratio, the model simplification chart, Figure 7.8, which is used to simplify model with multiple discrete deadman anchors into model with singular discrete deadman anchor is developed.

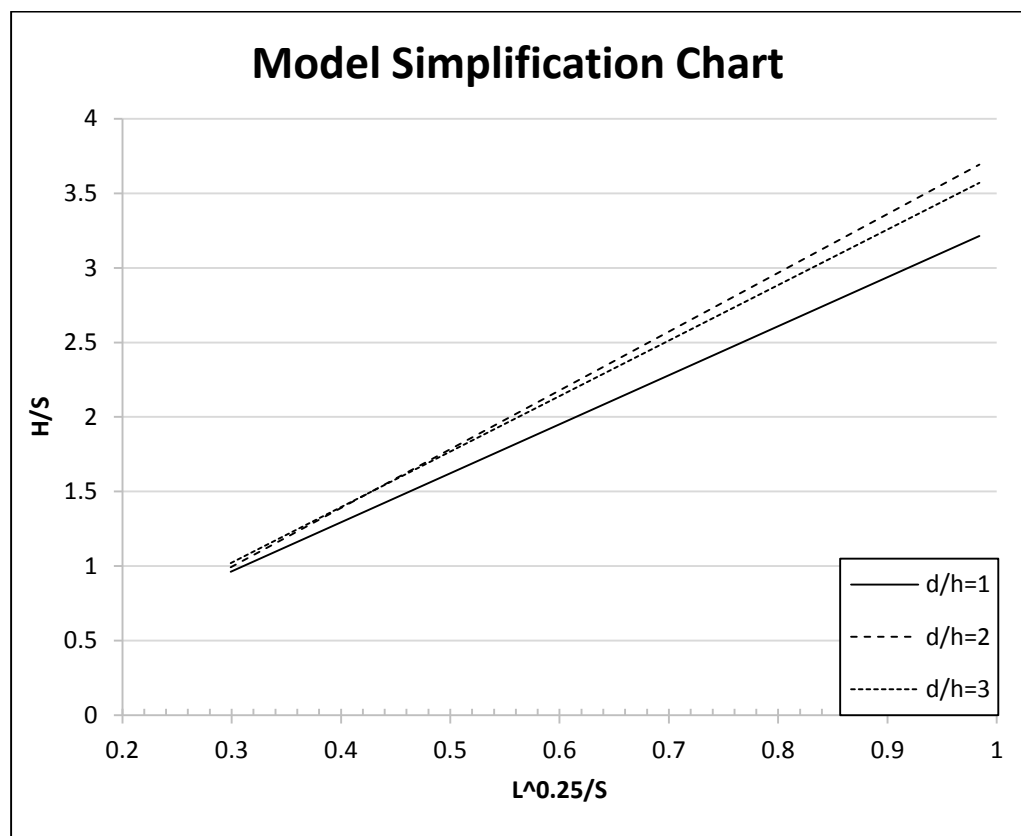


Figure 7.8: Model simplification chart for friction angle ( $\phi$ ) of  $30^\circ$ .

The best fit lines shown in Figure 7.8 represent the critical lines for the simplified model with singular discrete deadman anchor in predicting the complex models with multiple discrete deadman anchors up to anchor embedment ratio of 3. The model simplification chart is plotted up to anchor embedment ratio of 3. The anchor embedment ratio of more than 3 is beyond the research scope.

### **7.3.1 Verification and Validation of Model Simplification Chart**

The critical lines show that the complex model with multiple discrete deadman anchor can be simplified to model with singular discrete deadman anchor. Hence, it is interested to distinguish the zoning of model simplification chart for variable that is positioned either beyond or below the critical lines can adopts the model simplification technique in finite element analysis. Since the model simplification chart is developed based on friction angle ( $\phi$ ) of  $30^\circ$  and wall stiffness ( $EI$ ) of  $2.708E+05\text{kNm}^2$ . Therefore, the effect of friction angle and wall stiffness were carried out to distinguish the zoning of the model simplification chart.

#### **7.3.1.1 Effect of Friction Angle ( $\phi$ )**

In general, friction angle of soil can be varied from  $20^\circ$  to  $40^\circ$ . Since the model simplification was developed based on friction angle of  $30^\circ$ . Hence,

friction angle with  $20^\circ$  and  $40^\circ$  were carried out for anchor embedment ratio ( $d/h$ ) of 2.0 in order to distinguish the zoning and capability of model simplification chart. Moreover, it is believed that the capability of model simplification chart is capable for denser soil. This is because denser soil results in less deflection of anchored wall.

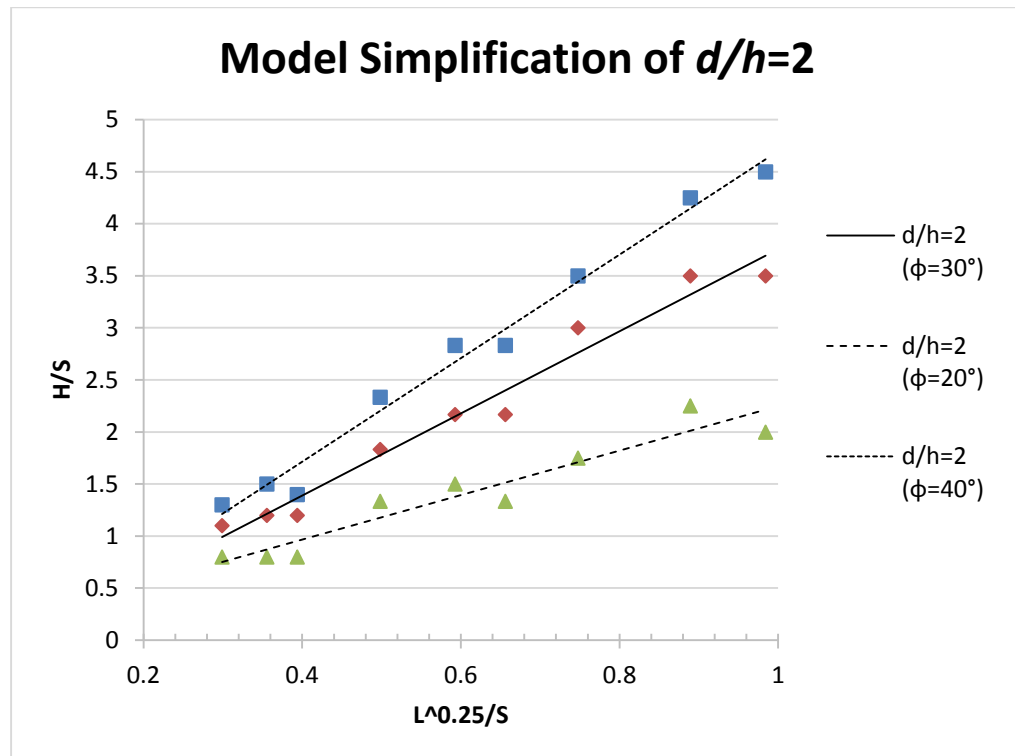


Figure 7.9: Effect of friction angle ( $\phi$ ) on model simplification chart of  $d/h=2$ .

The results of the effect of friction angle on model simplification chart for anchor embedment ratio ( $d/h$ ) of 2 is presented in Figure 7.9. It can be clearly observed that the variable is positioned beyond the critical line when friction angle greater than  $30^\circ$ . Hence, the model simplification chart is valid for complex model to adopt the model simplification technique in finite element analysis with friction angle greater than  $30^\circ$ . Whereas, the

variable is positioned below the critical line when friction angle less than  $30^\circ$ . The model simplification chart is no longer valid, hence, full finite element analysis is required.

The model simplification chart presented in Figure 7.8 is only valid for friction angle greater than  $30^\circ$ . Hence, an additional model simplification chart for loose soil with friction angle of  $20^\circ$  is developed and is illustrated in Figure 7.10. Figure 7.10 shows that the critical lines in model simplification chart of friction angle  $20^\circ$  for anchor embedment ratio ( $d/h$ ) of 2 and 3 are almost identical. This potentially means that anchor embedment ratio greater than 2 may adopts the critical line of  $d/h = 2$  for model simplification technique in finite element analysis. However, the anchor embedment ratio investigated in this research is only up to 3.0.

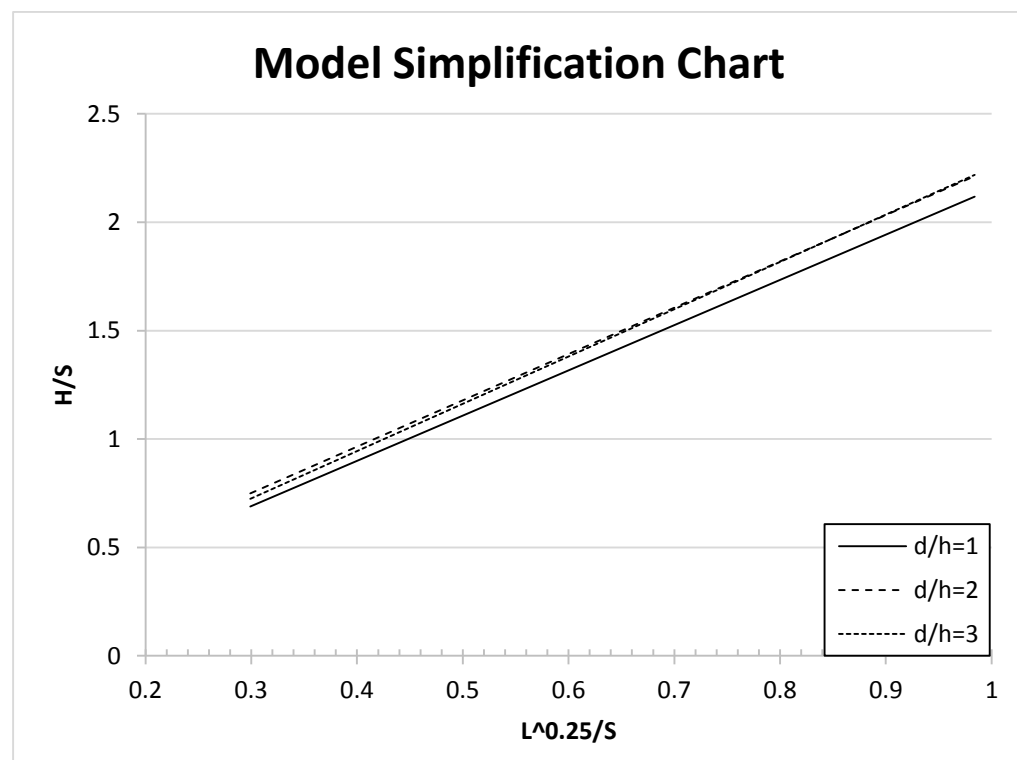


Figure 7.10: Model simplification chart for friction angle ( $\phi$ ) of  $20^\circ$ .

### 7.3.1.2 Effect of Wall Stiffness ( $EI$ )

Since the zoning of model simplification chart has been distinguished by the effect of friction angle. Thus, it is interested to further investigate the degree of capability of model simplification chart for anchored wall with less stiffness. Moreover, it is believed that the model simplification chart is valid for stiffer anchored wall, which results in less deflection of the anchored wall.

The anchored wall with Young's Modulus of concrete ( $E_c$ ) of  $26.0E+06\text{kN/m}^2$  was adopted in this investigation study. Since the Young's Modulus of concrete is kept constant, thus the variables are dependent on the wall thickness ( $T$ ). The wall thickness less than 0.25m ( $EI=3.385E+04\text{kNm}^2$ ) is no longer behaved like rigid wall. Thus, wall thickness with 0.25m, 0.30m, 0.40m, and 0.75m, which give wall stiffness of  $3.385E+04\text{kNm}^2$ ,  $5.850E+04\text{kNm}^2$ ,  $1.387E+05\text{kNm}^2$ , and  $9.141E+05\text{kNm}^2$ , respectively, was carried out in this investigation study.

The results for the effect of wall stiffness on model simplification chart for anchor embedment ratio ( $d/h$ ) of 2 is presented in Figure 7.11. It can be clearly observed that the variable is positioned beyond the critical line when the wall thickness greater than 0.50m. Hence, the model simplification chart is valid for complex model to adopt the model simplification technique in finite element analysis for wall thickness greater than 0.50m. Whereas, the variable is positioned below the critical line when the wall thickness less than 0.50m. Thus, the model

simplification chart is no longer valid, however, it is slightly under-predicted the results. Hence, full finite element analysis is required.

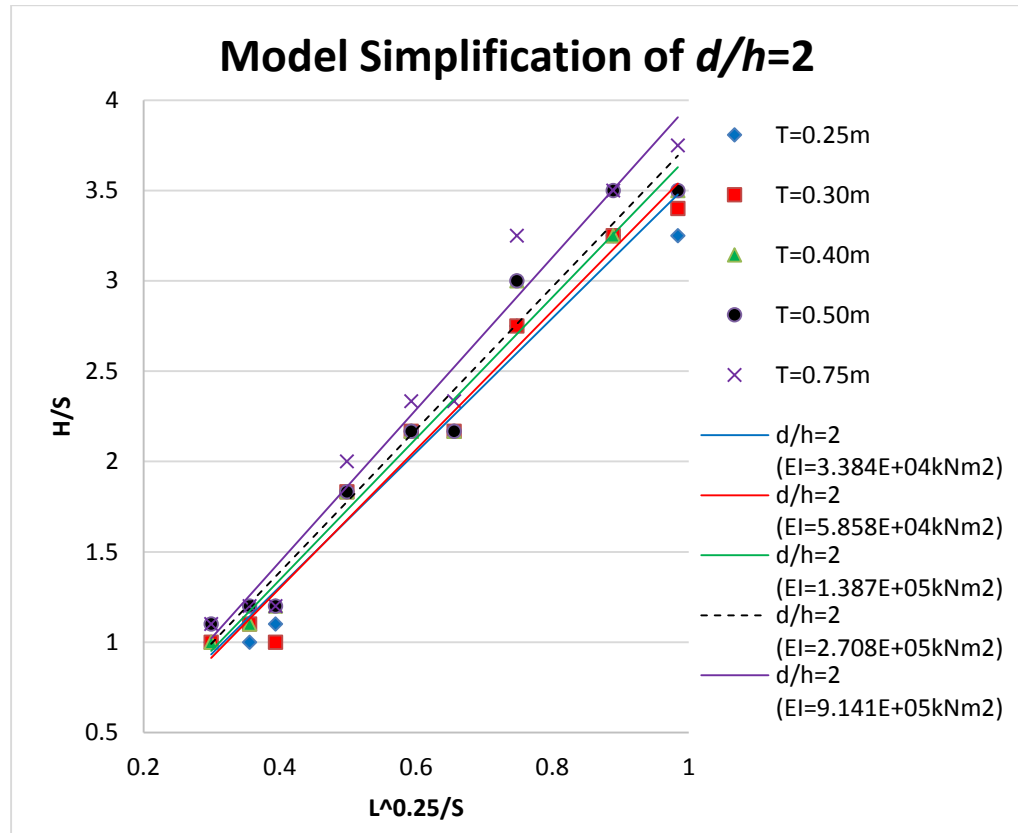


Figure 7.11: Effect of wall stiffness ( $EI$ ) on model simplification chart of  $d/h=2$ .

## 7.4 Summary

This chapter evaluates the degree of agreement of simplified model in comparison with complex models for anchor embedment ratio up to 3. The degree of agreement are assessed by comparing simplified model and complex models with percentage of variation not more than 5% of complex model with seven discrete deadman anchors.

The performances of simplified model is illustrated in the model simplification chart (see Figure 7.8). Several observations are obtained from the model simplification chart, such as:

1. The critical lines are developed to distinguish the extent to which complex model with multiple discrete deadman anchors can be simplified to model with single discrete deadman anchor.
2. The performances of simplified model are in good agreement with complex models when the variable is positioned beyond the critical lines. This means that the complex model with multiple discrete deadman anchors can be simplified as model with singular discrete deadman anchor (simplified model).
3. If the variable is positioned below the critical line, the full finite element analysis is recommended.
4. The advantage of simplified model is that only a set of computed wall deflection and pull-out force will be obtained. This eliminates the small variation in computed wall deflection and pull-out force between deadman anchors in complex models.
5. The model simplification chart are slightly under-predicted the results for wall stiffness between  $3.385\text{E}+04\text{kNm}^2$  ( $T=0.25\text{m}$ ) and  $2.708\text{E}+05\text{kNm}^2$  ( $T=0.50\text{m}$ ).
6. The model simplification chart is valid for the parameters mentioned in section 7.2 with anchored wall thickness at least 0.5m thick (wall stiffness,  $EI=2.708\text{E}+05\text{kNm}^2$ ) and friction angle of soil

not less than 30°. For parameters that beyond the scope of research, case-by-case assessment shall be carried out.

# CHAPTER 8

---

## BEHAVIOUR OF DISCRETE DEADMAN ANCHORAGE SYSTEM IN ANCHORED WALL

### 8.1 Introduction

By understanding the behaviour of discrete deadman anchorage system, geotechnical engineers can easily interpret the interaction between soil-structures, determine the potential failure mechanisms and provide the best design solution in geotechnical practice.

Study on the behaviour of deadman anchorage system was carried out by adopting the simplified model, which is presented in the previous chapter. The performances of simplified model in terms of wall deflection, pull-out

force, lateral movement of soil, and effective stress of soil were in good agreement with complex models.

## 8.2 Parametric Study

The key parameters used to study the behaviour of discrete deadman anchorage system in anchored wall are as follows:-

- a. Length of tie-rod
- b. Embedment depth of anchor
- c. Spacing of anchor
- d. Friction angle of soil
- e. Depth of anchored wall
- f. Stiffness of anchored wall

The prototype used to study the behaviour of discrete deadman anchorage system in anchored wall are illustrated in Figure 3.1. Moreover, a set of basic parameters that implements in this research is presented in Table 8.1. The behaviour of discrete deadman anchorage system in anchored wall are studied by investigating the effect of these parameters. During the study on the effect of these parameters, only a single parameter is investigated, while the remaining parameters are kept constant. The magnitude used to study the effect of each parameter is tabulated in Table 8.2.

The effect of these parameters in studying the behaviour of discrete deadman anchorage system subjected to the deflection of earth retaining wall is discussed in the following sections.

Table 8.1: Basic set of parameter studies.

Parameter		
<b>Tie rod length, <math>L</math> (m)</b>	:	10
<b>Anchor embedment depth, <math>d</math> (m)</b>	:	2
<b>Anchor spacing, <math>s</math> (m)</b>	:	2
<b>Friction angle of soil, <math>\phi</math> (°)</b>	:	30
<b>Wall depth, <math>D</math> (m)</b>	:	10
<b>Wall stiffness, <math>EI</math> (kNm<sup>2</sup>)</b>	:	2.708E+05 (Diaphragm wall)

Table 8.2: Magnitude of key parameter for parametric study.

Influence Factors		
<b>Tie rod length, <math>L</math> (m)</b>	:	5, 10, 15
<b>Anchor embedment depth, <math>d</math> (m)</b>	:	1, 2, 3
<b>Anchor spacing, <math>s</math> (m)</b>	:	2, 3, 5
<b>Friction angle of soil, <math>\phi</math> (°)</b>	:	20, 25, 30, 35, 40
<b>Wall depth, <math>D</math> (m)</b>	:	10, 15, 20
<b>Wall stiffness, <math>EI</math> (kNm<sup>2</sup>)</b>	:	2.708E+05 (Diaphragm wall) 4.560E+04 (FSP IIIA) 1.445E+05 (PU 32)

The general geometries of deadman anchorage system implemented in this research are comprised of 25mm diameter of tie rod and 1.0m x 1.0m x 0.5m of concrete deadman anchor.

### 8.2.1 Effect of Tie Rod Length

Tie rod length ( $L$ ) of 5.0m, 10.0m and 15.0m were modelled in evaluating the effect of tie rod length on the response of anchored wall. Figure 8.1 and Figure 8.2 show the wall deflection and pull-out force at  $d = 2$  and  $s = 2$ , respectively.

From Figure 8.1, the anchored wall with  $L = 5.0\text{m}$  was able to retain excavation heights ( $H$ ) up to 6.0m. The wall deflection for earth retaining wall without anchorage supports at  $H = 4.5\text{m}$  was determined to be 15.4mm, whereas the wall deflection for anchored wall with  $L = 5.0\text{m}$  at  $H = 4.5\text{m}$  was found to be 6.92mm. With anchorage supports, the wall deflection was reduced by 55.06%.

When  $L$  increased from 5.0m to 10.0m, the maximum allowable excavation height ( $H_{max}$ ) increased by 1.0m. At  $H = 6.0\text{m}$ , the wall deflection for  $L = 5.0\text{m}$  and 10.0m was found to be 29.9mm and 17.4mm, respectively. Increasing  $L$  from 5.0m to 10.0m, the wall deflection at  $H = 6.0\text{m}$  reduced by 41.98%.

Moreover, there was no significant reduction on the wall deflection when  $L$  further increases from 10.0m to 15.0m. At  $H = 7.0\text{m}$ , the wall deflection for  $L = 10.0\text{m}$  and 15.0m was determined to be 35.3mm to 31.9mm, respectively. Increasing  $L$  from 10.0m to 15.0m, the wall deflection at  $H = 7.0\text{m}$  reduced by 9.59%.

Furthermore, Figure 8.1 shows that there was no significant response on wall deflection when the length of tie rod was beyond 10.0m. This means that longer tie rod does not necessarily produce significant improvement on the response of anchored wall. This may be due to the elastic shortening effect of tie rod and the degree of mobilisation of deadman anchor. For this case, the best performance of tie rod length in influencing the anchored wall was determined to be  $1.43 H$ .

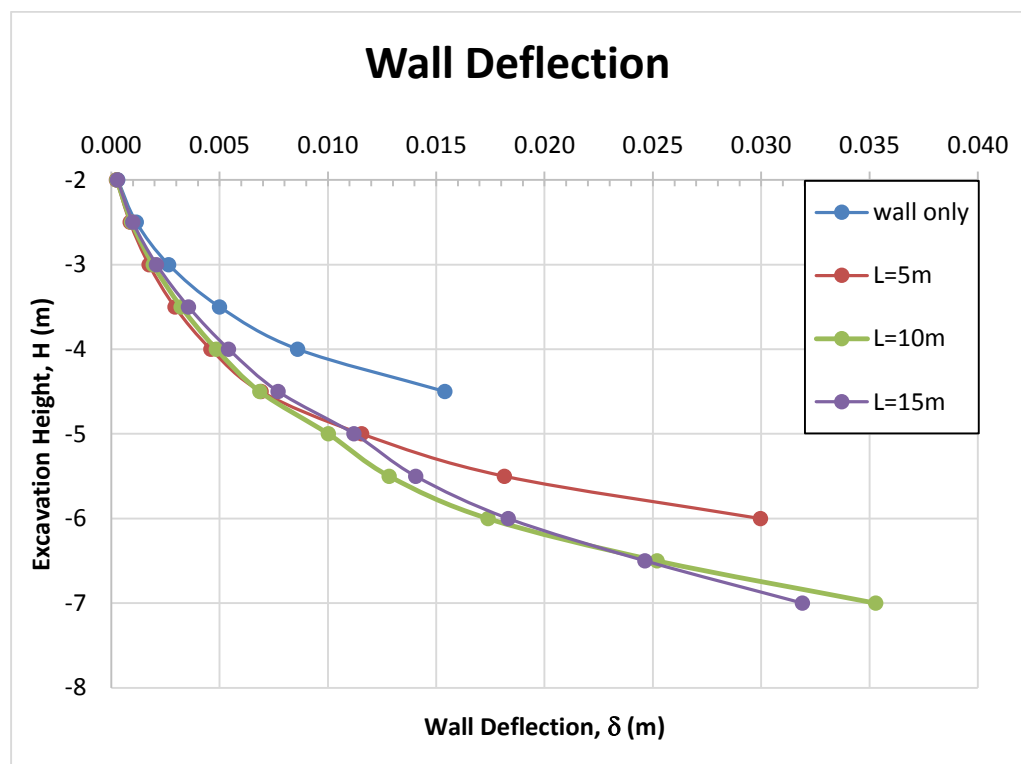


Figure 8.1: Effect of wall deflection ( $\delta$ ) on tie rod lengths for  $d = 2$  and  $s = 2$ .

Figure 8.2 shows that longer tie rod length had larger ultimate pull-out capacity, whereas, shorter tie rod length had the lower ultimate pull-out capacity. This explains that at shallow excavation heights ( $H$ ), deadman anchor with longer tie rod length had less mobilisation, which may be due to the elastic shortening effect of tie rod. As  $H$  increased, deadman anchor

with longer tie rod length started to mobilise, whilst, with shorter tie rod length, the performance stopped at  $H = 6.0\text{m}$ , as it reaches the ultimate pull-out capacity.

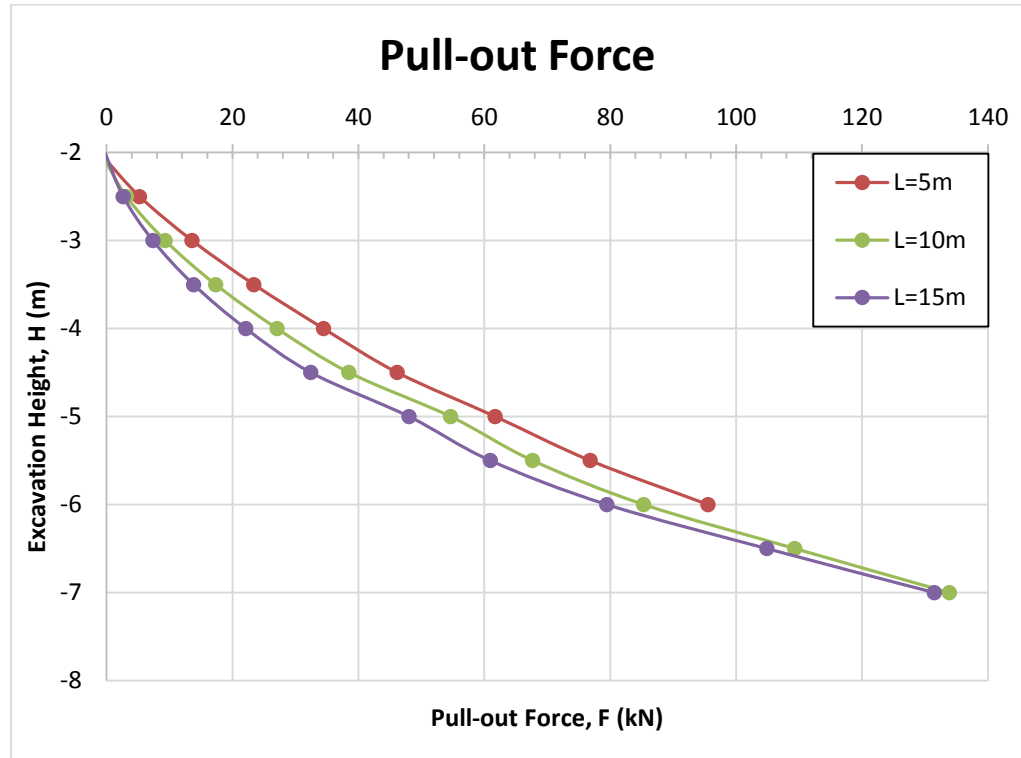


Figure 8.2: Effect of pull-out force ( $F$ ) on tie rod length for  $d = 2$  and  $s = 2$ .

The elastic shortening effect of tie rod is determined based on:

$$E = \sigma / \varepsilon \quad \text{Eq. 8.1}$$

This equation can be further expressed as:

$$\Delta L = \frac{F / A_s}{E_s} L_0 \quad \text{Eq. 8.2}$$

where,

$A_s$  = cross section area of tie rod

$E_s$  = Young's Modulus of tie rod

$L_0$  = original length of tie rod

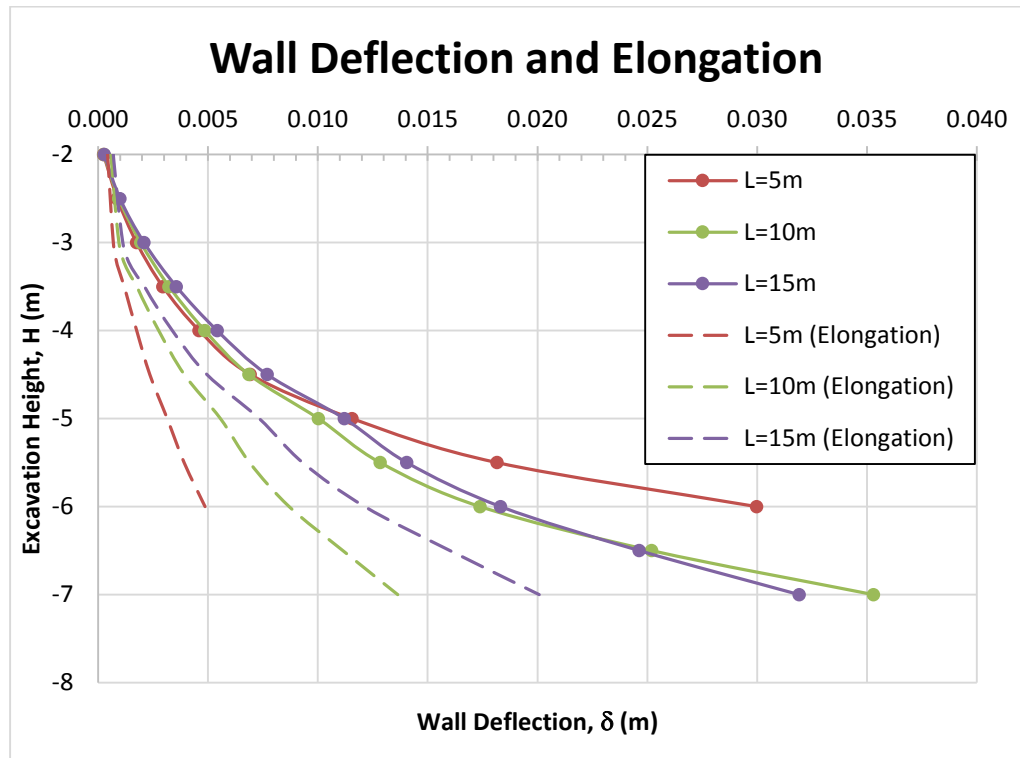


Figure 8.3: Wall deflection and elongation of tie rod for  $d = 2$  and  $s = 2$ .

The elastic shortening effect of various tie rods is presented in Figure 8.3. Figure 8.3 shows the longer tie rod has the larger elongation of tie rod. The elastic shortening effect affected the degree of mobilisation of deadman anchor.

This may be due to the load, which developed from the deformation of surrounding soil and led to wall deflection being partially transferred to tie rod and caused the elastic shortening effect. The remaining load was governed by deadman anchor.

The more the load governed by tie rod (more elongation), the less the contribution from the deadman anchor. For example, in the case of  $L = 10\text{m}$  at  $H = 5.0\text{m}$ , the elongation of tie rod governed 55.52% of the wall deflection, whereas the deadman anchor governed 44.48% of the wall deflection.

### **8.2.2 Effect of Anchor Embedment Depth**

Anchor embedment depth ( $d$ ) is one of the main concern factors. The anchor embedment depths were studied up to 3.0m in influencing the response of anchored wall. The anchor embedment depth beyond 3m was beyond our scope of studies due to the difficulty in installation, which could indirectly increase the construction time and cost. The wall deflection and pull-out force on the effect of anchor embedment depth are illustrated in Figure 8.4 and Figure 8.5, respectively.

Figure 8.4 shows that deadman anchorage system with anchor embedment depth of 1.0m could retain excavation heights ( $H$ ) up to 6.0m. The wall deflection at the maximum allowable excavation height ( $H_{max}$ ) was determined to be 27.6mm. When  $d$  increased from 1.0m to 2.0m, the maximum allowable excavation height increased by 1.0m. At  $H = 6.0\text{m}$ , the wall deflection for  $d = 1.0\text{m}$  and 2.0m was found to be 27.6mm and 17.4mm, respectively. Increasing  $d$  from 1.0m to 2.0m, the wall deflection at  $H = 6.0\text{m}$  reduced by 37.06%.

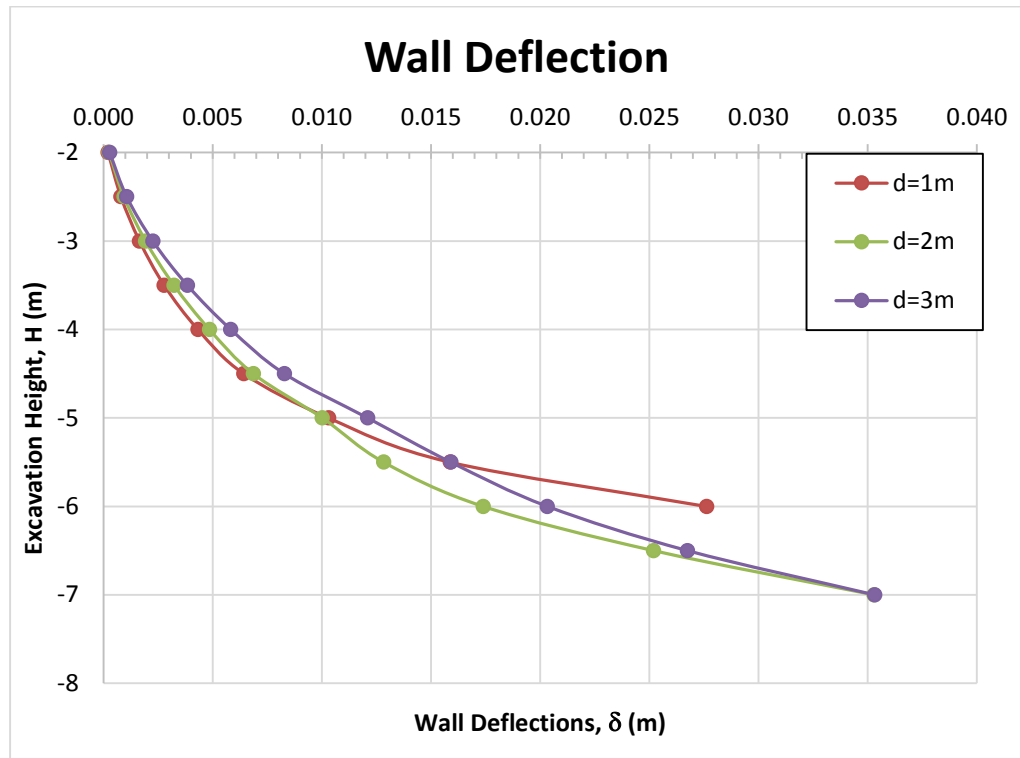


Figure 8.4: Effect of wall deflection ( $\delta$ ) on anchor embedment depth for  $L = 10\text{m}$  and  $s = 2$ .

On the other hand, deadman anchorage system with anchor embedment depth of  $3.0\text{m}$  had the similar response on the wall deflection with  $d = 2.0\text{m}$ . The maximum allowable excavation height for both  $d = 2.0\text{m}$  and  $3.0$  was found to be  $7.0\text{m}$ . The wall deflection for both  $d = 2.0\text{m}$  and  $3.0\text{m}$  was found to be  $35.3\text{mm}$  coincidentally. This shows that there was no significant improvement on wall deflection when  $d$  was beyond  $2.0\text{m}$ .

Figure 8.5 shows that deeper anchor embedment depth gave larger pull-out capacity, whilst, shallow anchor embedment depth gave lower pull-out capacity. The ultimate pull-out capacity of  $d = 1.0\text{m}$  was found to be  $60.52\text{kN}$ , which is less than  $50\%$  of the ultimate pull-out capacity of  $d =$

2.0m and 3.0m. The ultimate pull-out capacity for  $d = 2.0\text{m}$  and  $3.0$  was determined to be  $133.85\text{kN}$  and  $154.87\text{kN}$ , respectively.

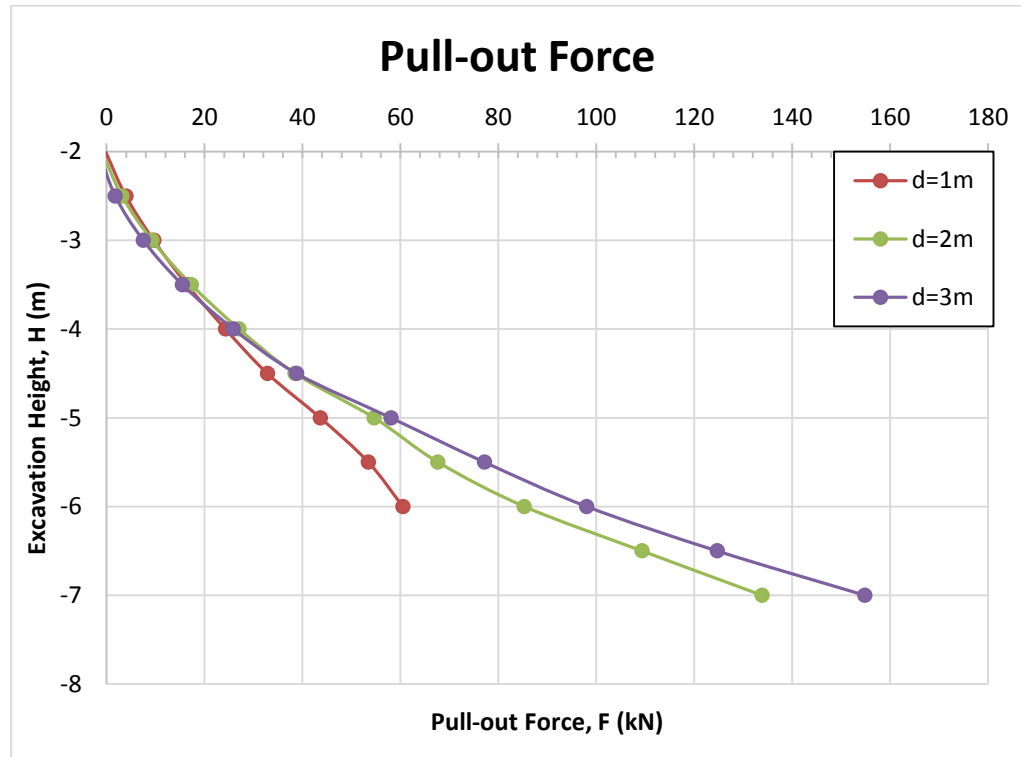


Figure 8.5: Effect on pull-out force ( $F$ ) on anchor embedment depth for  $L = 10\text{m}$  and  $s = 2$ .

The percentage of variation on the ultimate pull-out capacity between  $d = 2.0$  and  $3.0\text{m}$  was calculated to be  $15.70\%$ . Even though the ultimate pull-out capacity for  $d = 3.0\text{m}$  increased by  $15.70\%$ , however, the wall deflection did not have any improvement compared to  $d = 2.0\text{m}$ .

This can be explained by the anchor embedment depth was affected by passive resistance, which was generated by the vertical stress of soil. The deeper the anchor is embedded, the larger the passive resistance is generated. However, the deeper the anchor is embedded, it may not necessarily provide better response on the wall deflection of anchored wall.

The best performance of anchor embedment depth for this case was determined to be  $d = 2.0 h$ .

As the anchor is embedded deeper, the pull-out force increases to overcome larger passive resistance. Therefore, it has the larger ultimate pull-out capacity. Nevertheless, the maximum wall deflection occurs at the tip of the wall. Hence, while the deeper the anchor is embedded, it may not be beneficial to reduce the wall deflection although it has larger pull-out capacity.

When deadman anchor with larger pull-out capacity occurs at the same level as the anchor embedment depth, it may most likely produce significant improvement to the anchored wall in term of reducing the maximum wall deflection.

### **8.2.3 Effect of Anchor Spacing**

In general, continuous deadman anchorage system results good in minimising the deflection of anchored wall. Nevertheless, continuous deadman anchorage system has lower pull-out force coefficient compare to discrete deadman anchorage system (Dickin & Leung, 1983, 1985). Hence, this investigation explains how the anchor spacing affects the deflection of anchored wall and the contribution of deadman anchorage system. Therefore, anchor spacing ( $s$ ) of 2.0m, 3.0m and 5.0m were modelled to carry out this investigation.

Figure 8.6 shows that deadman anchorage system with anchor spacing ( $s$ ) of 2.0m could retain the maximum excavation height ( $H_{max}$ ) up to 7.0m. When  $s$  increased from 2.0m to 3.0m, the maximum allowable excavation reduced by 0.5m, which is 6.5m. Moreover, when  $s$  further increased from 3.0m to 5.0m, the maximum allowable excavation heights further reduced by 0.5m, which is 6.0m. The wall deflection for  $s = 2.0\text{m}$ ,  $3.0\text{m}$  and  $5.0\text{m}$  at the maximum allowable excavation height was found to be 35.3mm, 29.7mm and 27.8mm, respectively.

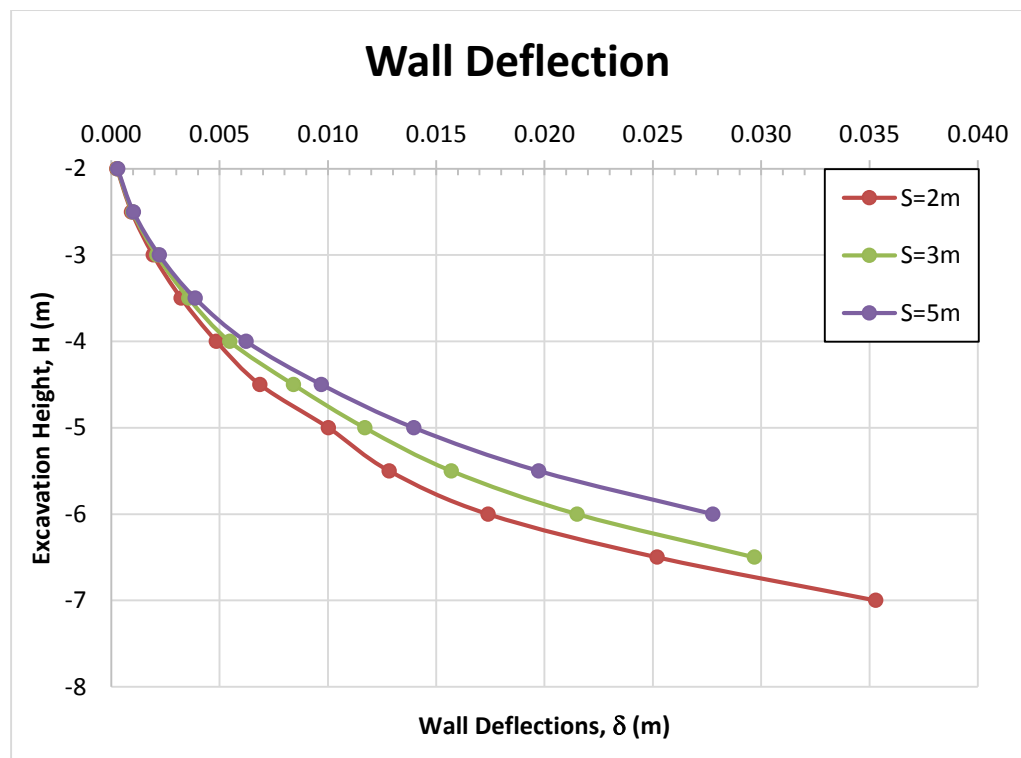


Figure 8.6: Effect of wall deflection ( $\delta$ ) on anchor spacing for  $L = 10\text{m}$  and  $d = 2$ .

At  $H = 6.0$ , the wall deflection for  $s = 2.0\text{m}$ ,  $3.0\text{m}$  and  $5.0\text{m}$  was found to be 17.4mm, 21.5mm and 27.8mm, respectively. Increasing anchor spacing from 2.0m to 3.0m, the wall deflection increased from 17.4mm to 21.5mm,

an increment of 23.65%. When anchor spacing further increased from 3.0m to 5.0m, the wall deflection increased from 21.5mm to 27.8mm, an increment of 29.10%.

Fundamentally, the minimum wall deflection is given by deadman anchorage system which generates huge passive resistance. Deadman anchorage system with spacing of 2.0m results minimum wall deflection compared to other anchor spacing as it generates the largest passive resistance. However, these passive resistance do not fully mobilise the ultimate capacity of the deadman anchor.

Figure 8.7 shows that the pull-out force (mobilised force) for deadman anchorage system with anchor spacing ( $s$ ) of 2.0m was lower compared to other anchor spacing. This shows that the mobilised force did not reach the ultimate capacity of deadman anchor, which had similar observation to the behaviour of deadman anchor pulled vertically in sand (Geddes & Murray, 1996).

Furthermore, the pull-out force increased as the anchor spacing between deadman anchorage system increased, as shown in Figure 8.7. This explains that deadman anchorage system increasing the degree of mobilisation with increases of anchor spacing in order to retain the excavation height. Hence, increasing the anchor spacing increases the efficiency of deadman anchorage system in terms of degree of mobilisation of deadman anchor.

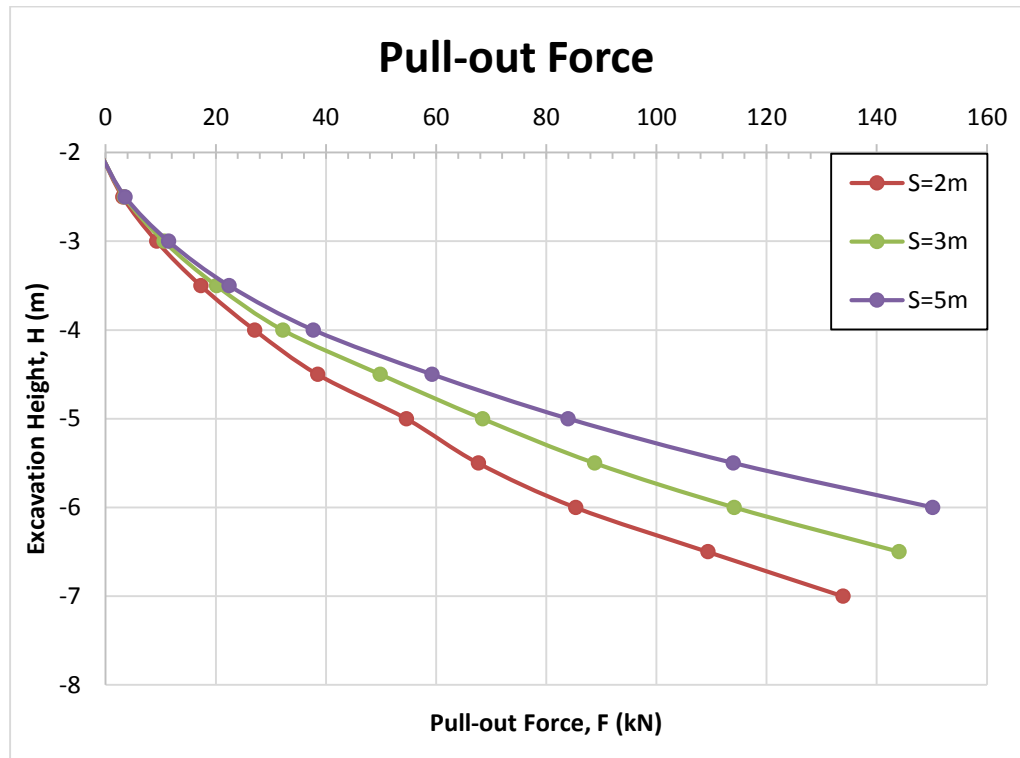


Figure 8.7: Effect of pull-out force ( $F$ ) on anchor spacing for  $L = 10\text{m}$  and  $d/h = 2$ .

### 8.2.4 Effect of Soil Friction Angle

Generally, the friction angle of soil ( $\phi$ ) varies from  $20^\circ$  to  $40^\circ$ . Therefore, the soil friction angle between  $20^\circ$  to  $40^\circ$  with an interval of  $5^\circ$  was carried out to investigate the effect of soil friction angle in influencing the response of anchored wall. The wall deflection and pull-out force on the effect of soil friction angle are illustrated in Figure 8.8 and Figure 8.9, respectively.

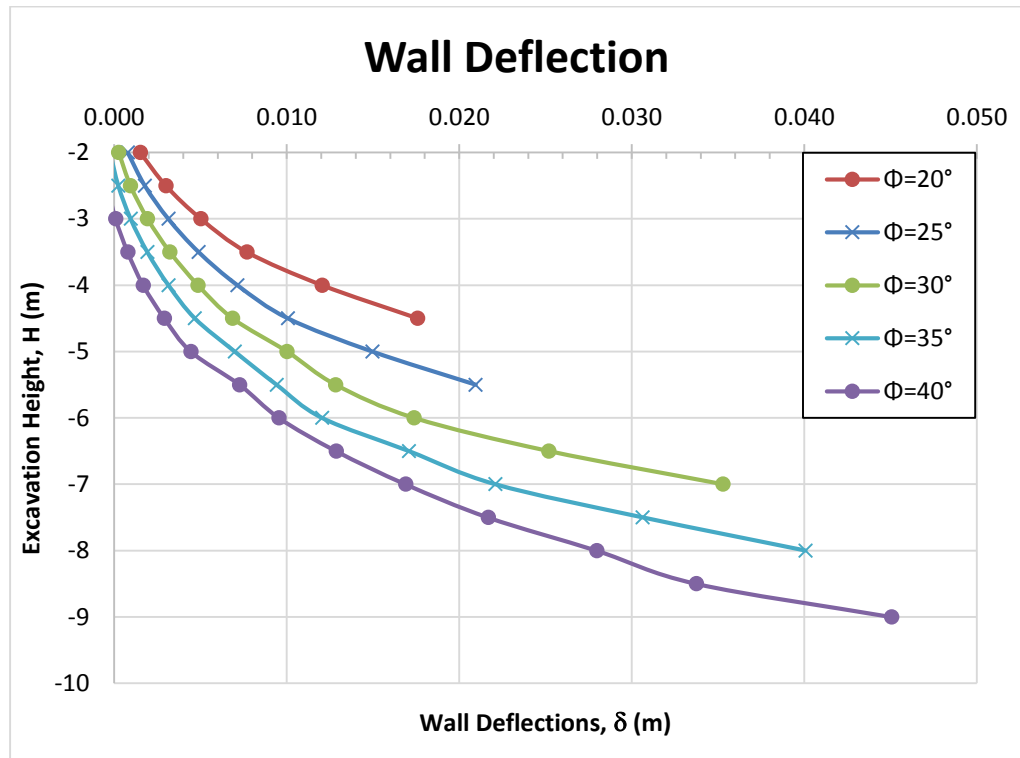


Figure 8.8: Effect of wall deflection ( $\delta$ ) on soil friction angle for  $L = 10\text{m}$ ,  $d = 2$  and  $s = 2$ .

Figure 8.8 shows that the maximum allowable excavation height ( $H_{max}$ ) for soil friction angle between  $20^\circ$  to  $40^\circ$  with an interval of  $5^\circ$  was 4.5m, 5.5m, 6.5m, 8.0m, and 9.0m. At  $H = 4.5\text{m}$ , the wall deflection for soil friction angle from  $20^\circ$  to  $40^\circ$  with  $5^\circ$  of increment was found to be 17.60mm, 10.10mm, 6.86mm, 4.68mm, and 2.92mm, respectively. It is clearly shown that the wall deflection reduces with the increases of friction angle.

The maximum allowable excavation height for ground condition with very dense sand ( $\phi = 40^\circ$ ) was found to be twice the maximum allowable excavation height with very loose sand ( $\phi = 20^\circ$ ). When  $H = 4.5\text{m}$ , the wall deflection for  $\phi = 20^\circ$  and  $40^\circ$  was found to be 17.6mm and 2.92mm, respectively. By increasing  $\phi = 20^\circ$  and  $40^\circ$ , the wall deflection was

determined to be reduced by 83.41%. In conclusion, soil friction angle has significant effect on the wall deflection response of anchored wall.

Figure 8.9 shows that the ultimate capacity of deadman anchorage system with  $L = 10\text{m}$ ,  $d = 2$  and  $s = 2$  was found to be approximately 144.44kN. The capacity of 144.44kN for this deadman anchor was considered ultimate capacity even the actual ultimate capacity of this deadman anchor was much higher. Beyond this capacity, the wall deflection may exceed 0.5% of excavation height ( $H$ ).

For very loose sand condition ( $\phi = 20^\circ$ ), the pull-out capacity did not reach the ultimate capacity of deadman anchor (144.44kN). The pull-out capacity in very loose sand condition mobilised 56.74% of its ultimate capacity. This is mainly due to the wall deflection has reached the maximum allowable excavation height before deadman anchor mobilised to the ultimate pull-out capacity.

The pull-out capacity of deadman anchorage system for soil friction angle from  $20^\circ$  to  $40^\circ$  with  $5^\circ$  of interval was found to be 81.96kN, 95.50kN, 133.85kN, 144.35kN, and 144.44kN, respectively. The pull-out capacity of deadman anchor for  $\phi = 25^\circ$ ,  $30^\circ$  and  $35^\circ$  governed 66.11%, 92.67% and 99.94%, respectively, of the ultimate pull-out capacity of deadman anchor.

Increasing the magnitude of soil friction angle increases the pull-out capacity of deadman anchor, which is clearly illustrated in Figure 8.9. In addition, similar observation was obtained from the previous research (Bhattacharya & Kumar, 2012; Merifield & Sloan, 2006).

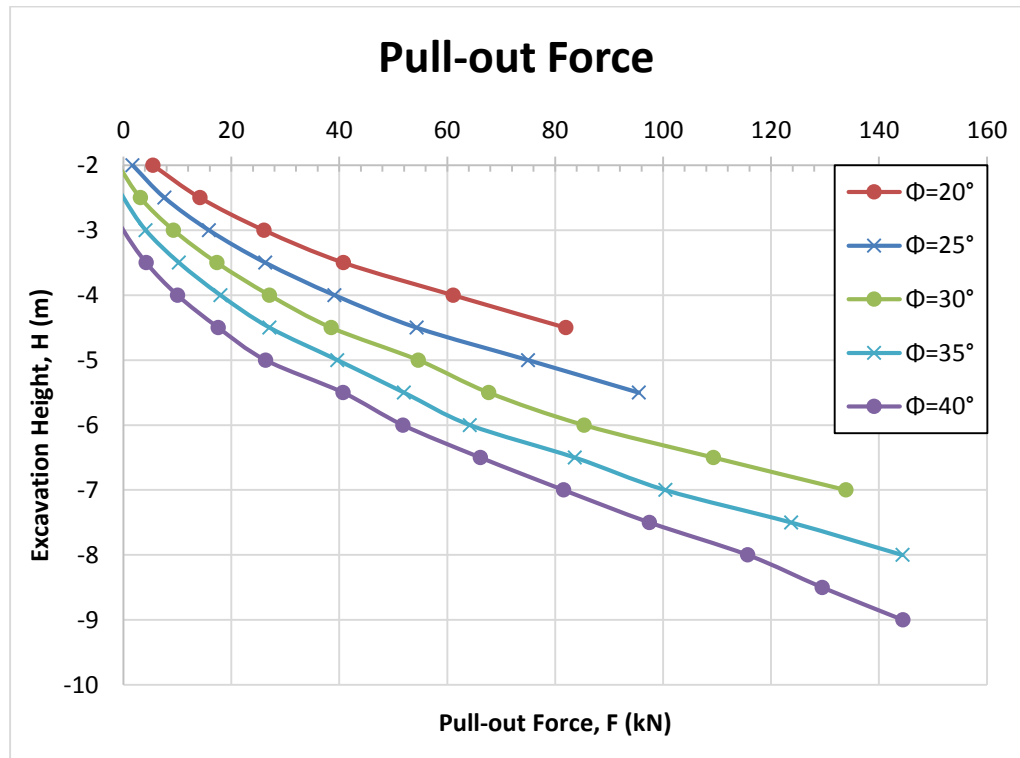


Figure 8.9: Effect of pull-out force ( $F$ ) on soil friction angle for  $L = 10\text{m}$ ,  $d = 2$  and  $s = 2$ .

### 8.2.5 Effect of Wall Depth

In geotechnical engineering practice, the range of wall depth ( $D$ ) is usually between 6m and 24m. The investigation on the effect of wall depth was carried out by adopting wall depth between 5m and 25m with intervals of 5m. The effects of wall deflection and pull-out force for various wall depth are illustrated in Figure 8.10 and Figure 8.11, respectively.

Figure 8.10 shows that the maximum allowable excavation height ( $H_{max}$ ) for wall depth from 5m to 25m with intervals of 5m was found to be 4.5m, 7.0m and 8.0m for the remaining wall depths. The results show that as wall

depth increases, excavation height ( $H$ ) increases, but remains constant at  $H = 8.0\text{m}$ .

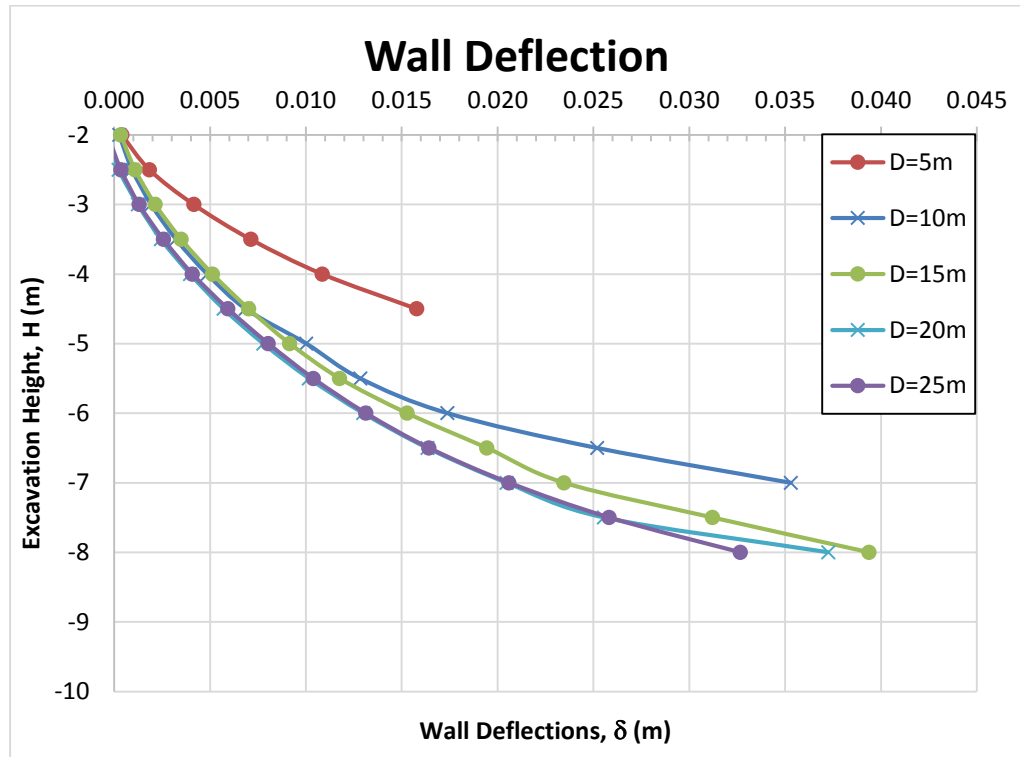


Figure 8.10: Effect of wall deflection ( $\delta$ ) on wall depth for  $L = 10\text{m}$ ,  $d = 2$  and  $s = 2$ .

At  $H = 4.5\text{m}$ , the wall deflection for wall depth from 5m to 25m with intervals of 5m was determined to be 15.78mm, 6.86mm, 7.01mm, 5.70mm, and 5.93mm, respectively. The results showed that increasing wall depth was able to reduce the wall deflection of anchored wall.

In Figure 8.10, it is clearly observed that when  $D$  increased from 5m to 10m, the maximum allowable excavation height increased from 4.5m to 7.0m. When  $D$  further increased from 10m to 15m, the maximum allowable excavation height increased by 1.0m.

Nevertheless, when  $D$  further increased from 15m to 20m or 25m, the maximum allowable excavation height did not increase further. It is believed that the wall depth beyond 15m does not have further improvement on the response of anchored wall in terms of allowable excavation height.

Furthermore, the maximum allowable excavation height for wall depth beyond 15m was found to be 8.0m. When  $D$  increased from 15m to 20m, the wall deflection for  $D = 15\text{m}$  and 20m was found to be 39.37mm and 37.25mm, which was 5.40% reduction. In addition, when  $D$  increased from 20m to 25m, the wall deflection for  $D = 20\text{m}$  and 25m was found to be 37.25mm and 32.65mm, which was 12.32% reduction. However, the design approach for wall depth beyond 15m was considered unpractical for this case. As the wall depth increased by 5m, the wall deflection did not have significant reduction.

Figure 8.11 shows that the pull-out force increases with depth of wall ( $D$ ) up to 15m. Subsequently, the pull-out force decreases with further increase of wall depth beyond  $D = 15\text{m}$ . The depth of wall with  $D = 5\text{m}$  to 15m have significant improvement on the response of anchored wall. There is less significant improvement when the depth of wall is beyond 15m.

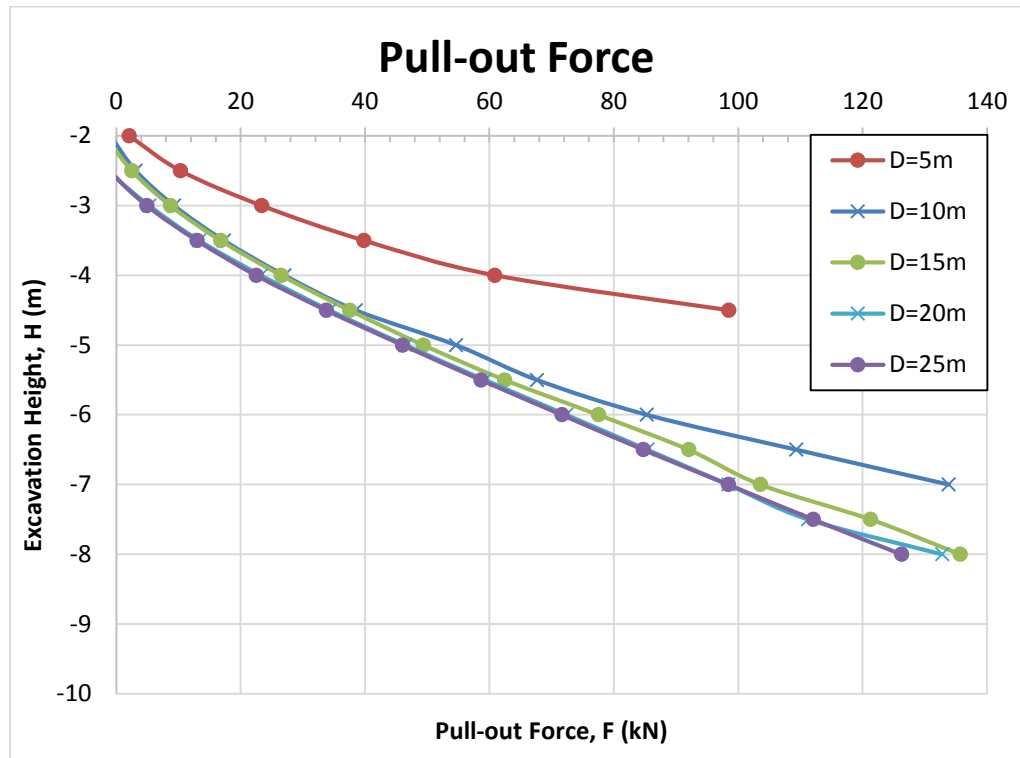


Figure 8.11: Effect of pull-out force ( $F$ ) on wall depth for  $L = 10\text{m}$ ,  $d = 2$  and  $s = 2$ .

The pull-out force at  $D = 5\text{m}$  caused the tie rod to yield and reach the plastic region, which is illustrated in Figure 8.11. Furthermore, the tie rod was entering the yield region for the pull-out force at  $D = 10\text{m}$ . On the other hand, the tie rod was just about to yield at  $D = 15\text{m}$  and  $20\text{m}$ . At  $D = 25\text{m}$ , the pull-out force showed linear relationship, which is in elastic region.

This explains that the pull-out force is transformed from plastic region to yield and elastic region while the depth of anchor wall increases. In addition,  $D = 15\text{m}$  provides the most significant impact on the response of anchored wall in term of pull-out force. Moreover, the ultimate pull-out force for various wall depths for this particular case is illustrated in Figure 8.12.

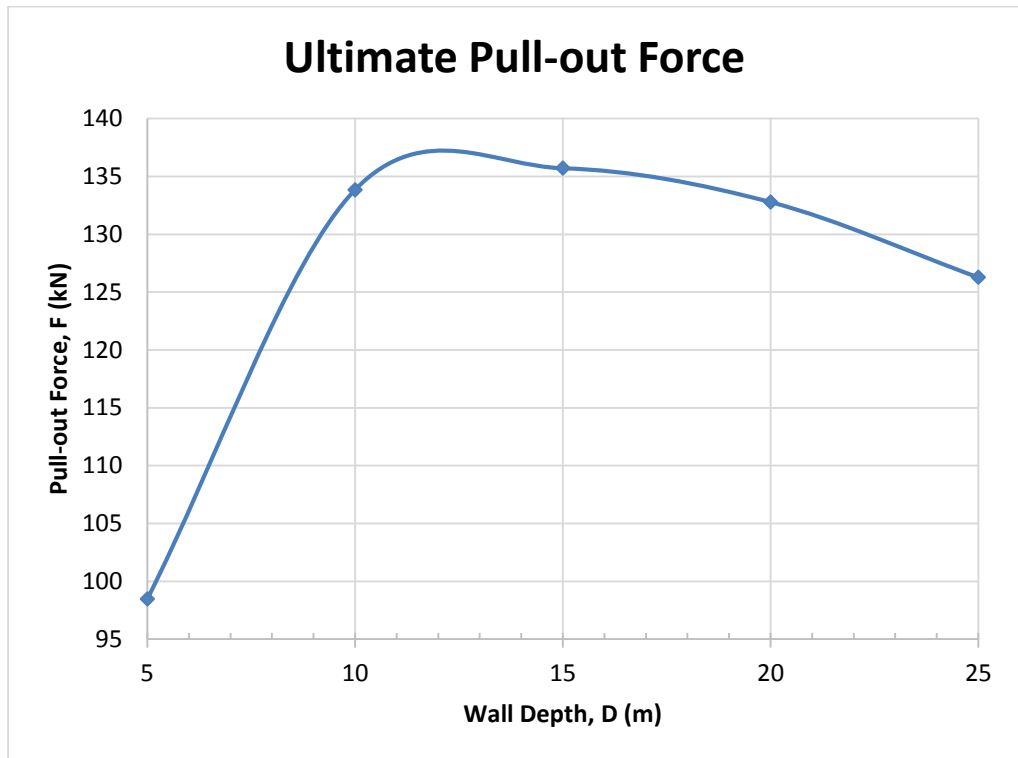


Figure 8.12: Effect of the ultimate pull-out force on wall depth for  $L = 10\text{m}$ ,  $d = 2$  and  $s = 2$ .

In Figure 8.12, it is clearly observed that the wall depth between 10m and 15m produced the largest ultimate pull-out force, which means that it can produce the best performance on the response to anchored wall.

Nevertheless, if the boundary of the site does not have enough distance for longer tie rod, the wall depth may be increased up to 20m or 25m in order to retain the desired excavation height and achieve the maximum allowable wall deflection even though it is not encouraged.

### 8.2.6 Effect of Wall Stiffness

To investigate the effect of wall stiffness ( $EI$ ) on the response of anchored wall, sheet pile wall and concrete wall were adopted in this investigation. Earth retaining wall with stiffness of  $4.560E+04\text{kNm}^2$  (FSP IIIA),  $1.445E+05\text{kNm}^2$  (PU 32) and  $2.708E+05\text{kNm}^2$  (Diaphragm wall), which commonly used in industry were modelled in investigating the effect of wall stiffness. Full finite element prototype was adopted for wall stiffness less than  $2.708E+05\text{kNm}^2$  used in this investigative study. The results of wall deflection and pull-out force on the effect of wall stiffness are illustrated in Figure 8.13 and Figure 8.14, respectively.

Figure 8.13 shows that anchored wall with these wall stiffness was able to retain the maximum allowable excavation heights ( $H_{max}$ ) up to 7.0m. Increasing the stiffness of anchored wall was able to reduce the wall deflection. However, the effect of wall stiffness in influencing the deflection of anchored wall was not significant in this study. This is because the wall stiffness (FSP IIIA) varies up to 7 times of Diaphragm wall, the deflection of anchored wall only differs up to 5%. This may be due to the wall stiffness adopted in this study is considered rigid wall.

Similar observations were made in terms of pull-out force, which shown in Figure 8.14. This shows that the behaviour of deadman anchorage system for these wall stiffness give similar results in terms of wall deflection and pull-out force.

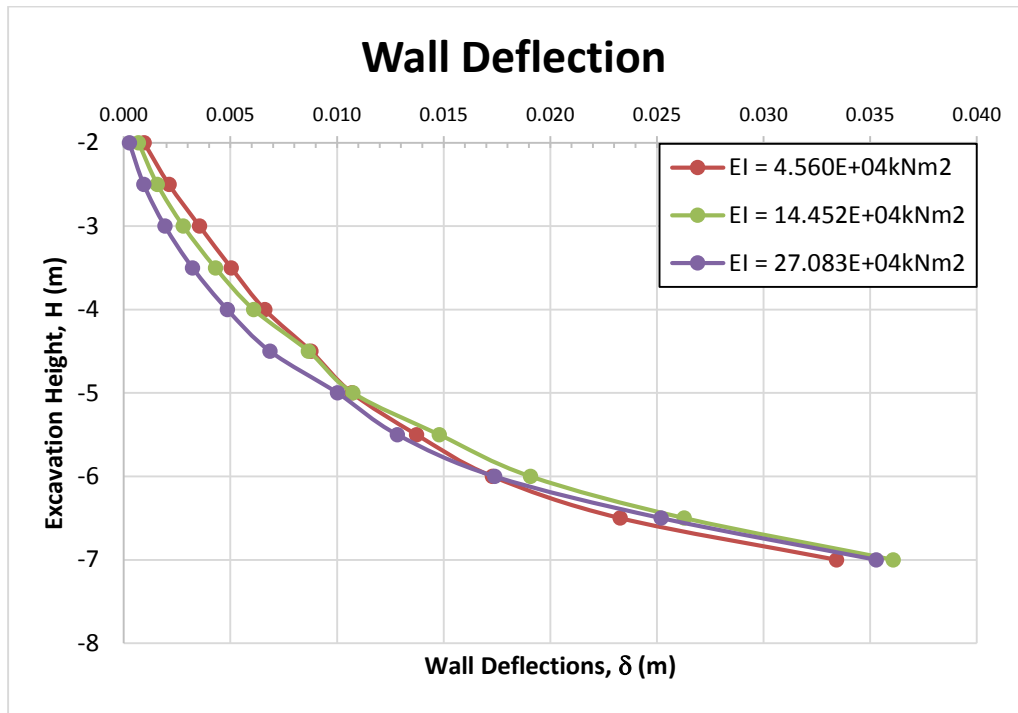


Figure 8.13: Effect of wall deflection ( $\delta$ ) on wall stiffness for  $L = 10\text{m}$ ,  $d = 2$  and  $s = 2$ .

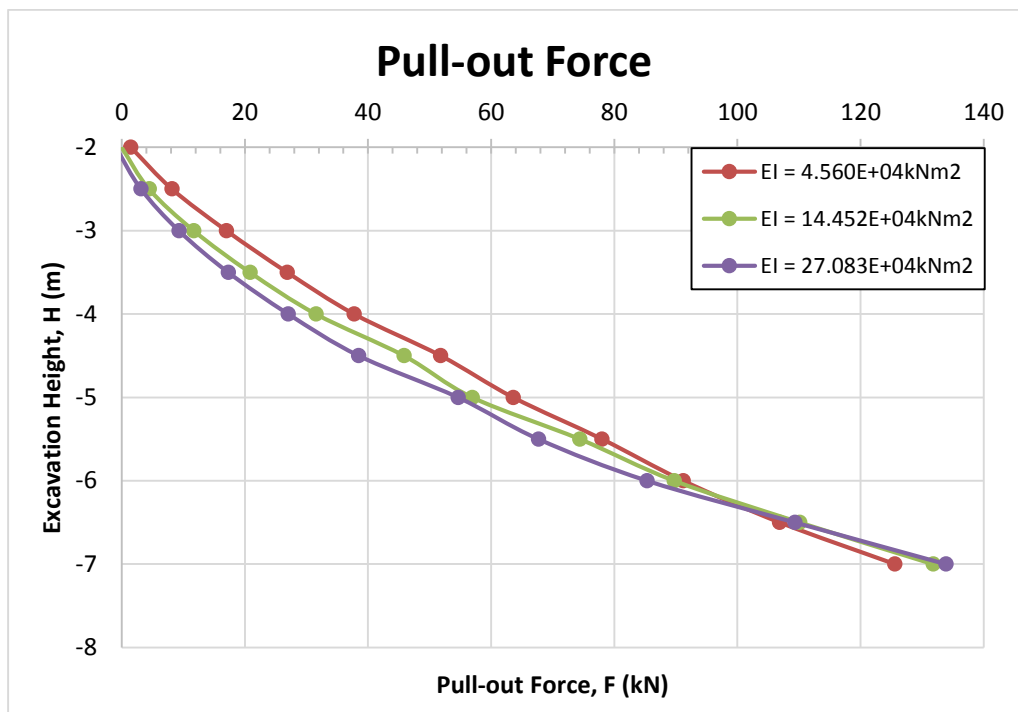


Figure 8.14: Effect of pull-out force ( $F$ ) on wall stiffness for  $L = 10\text{m}$ ,  $d = 2$  and  $s = 2$ .

### 8.3 Summary

This chapter examines the behaviour of discrete deadman anchorage system due to the effects of tie rod length, anchor embedment depth, anchor spacing, soil friction angle, wall depth, and wall stiffness on the response of anchored wall.

The effects of tie rod length, anchor embedment depth and wall depth show that there are optimal performance on the response of anchored wall. However, the study of soil friction angle shows that increasing soil friction angle increases the performance of anchored wall.

On the other hand, anchor spacing has significant impact on the response of anchored wall. The narrower the spacing of anchor, the minimal the deflection of anchored wall. Furthermore, the behaviour of deadman anchorage system for wall stiffness with FSP IIIA, PU32 and Diaphragm wall ( $T = 0.5\text{m}$ ) give similar results in terms of wall deflection and pull-out force.

Parametric study shows that there are relationships among these factors on the response of deadman anchorage system. However, the behaviour of discrete deadman anchor on the combination of these influence factors is very complicated in the understanding of the interaction between soil and structure.

By understanding the soil-structure interaction in the presence of these parameters, practicing geotechnical engineers are able to determine the

potential failure mechanisms and provide the best design solution in geotechnical practice.

# CHAPTER 9

---

## DESIGN CHARTS

### 9.1 Introduction

The previous chapter shows that anchored wall has an optimal response on the investigated effects of tie rod length, anchor embedment depth and wall depth. For soil friction angle, increasing soil friction angle improves the performance of anchored wall. In addition, the narrower the spacing of anchor, the minimal the deflection of anchored wall.

Thus, this chapter presents the relationships among these parameters on the response of anchored wall. Design charts are developed from these relationships in order to provide a better understanding on the behaviour of discrete deadman anchor and the soil-structure interaction.

## 9.2 Relationship among Tie Rod Length, Anchor Embedment Depth and Wall Depth

Investigation on the relationship among effects of tie rod length ( $L$ ), wall depth ( $D$ ) and maximum allowable excavation height ( $H$ ) for anchor embedment depth ( $d$ ) up to 3m was carried out.

Figure 9.1 to Figure 9.3 show the relationship among these effects for anchor embedment depth up to 3m with interval of 1m. The presented data was determined based on two design criteria:

1. The maximum excavation height is limited to the deflection of anchored wall that not more than 0.5% of excavation height ( $H$ );
2. The response of anchored wall which able to provide the minimum wall deflection after fulfilling design criteria (1).

In these figures, the BLUE plotted data represents the minimum response of anchor wall with respect to the length of tie rod ( $L$ ). The RED plotted data represents the maximum response of anchor wall with respect to  $L$ , whereas the GREEN plotted data represents the optimum response of anchor wall with respect to  $L$  for various excavation heights ( $H$ ).

A polynomial trend line (best fit line) is generated in order to fit the optimum plotted data that is considered good as the  $R^2$  value is beyond 0.9. The  $R^2$  value for anchor embedment depth of 1m to 3m with intervals of 1m are 0.9426, 0.9739 and 0.9565, respectively, as shown in Figure 9.1 to

Figure 9.3. The  $R^2$  value beyond 0.9 shows strong relationship between H and L/D.

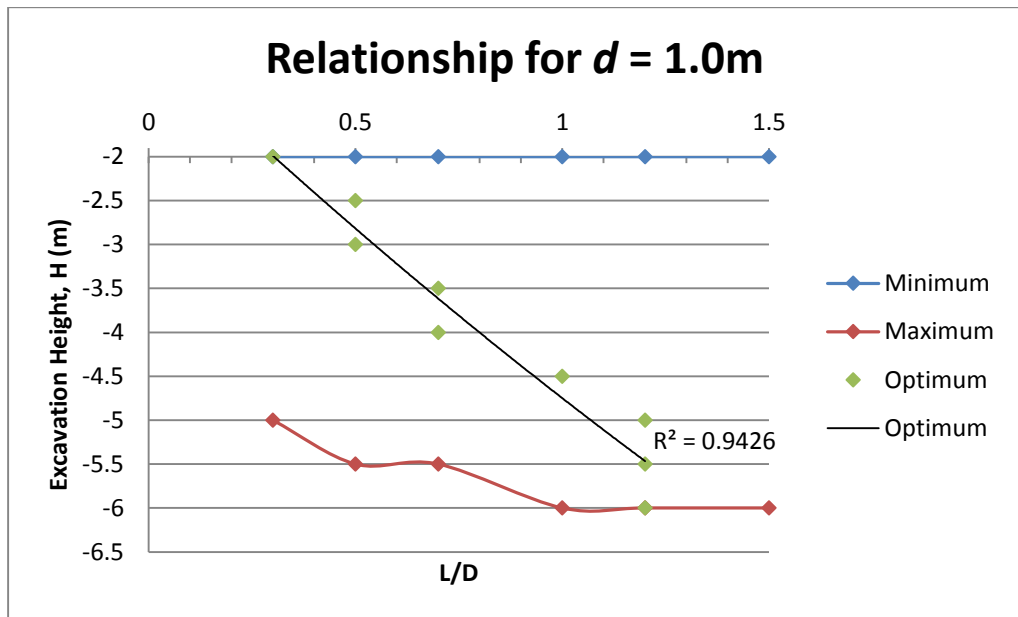


Figure 9.1: Relationship for  $D = 10.0\text{m}$  with anchor embedment depth of 1m.

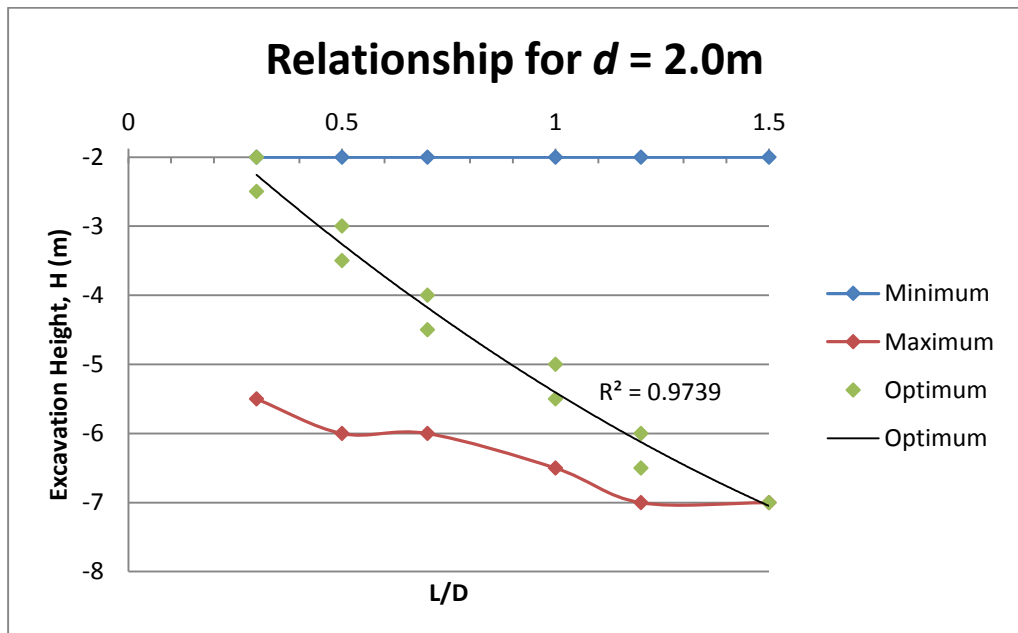


Figure 9.2: Relationship for  $D = 10.0\text{m}$  with anchor embedment depth of 2m.

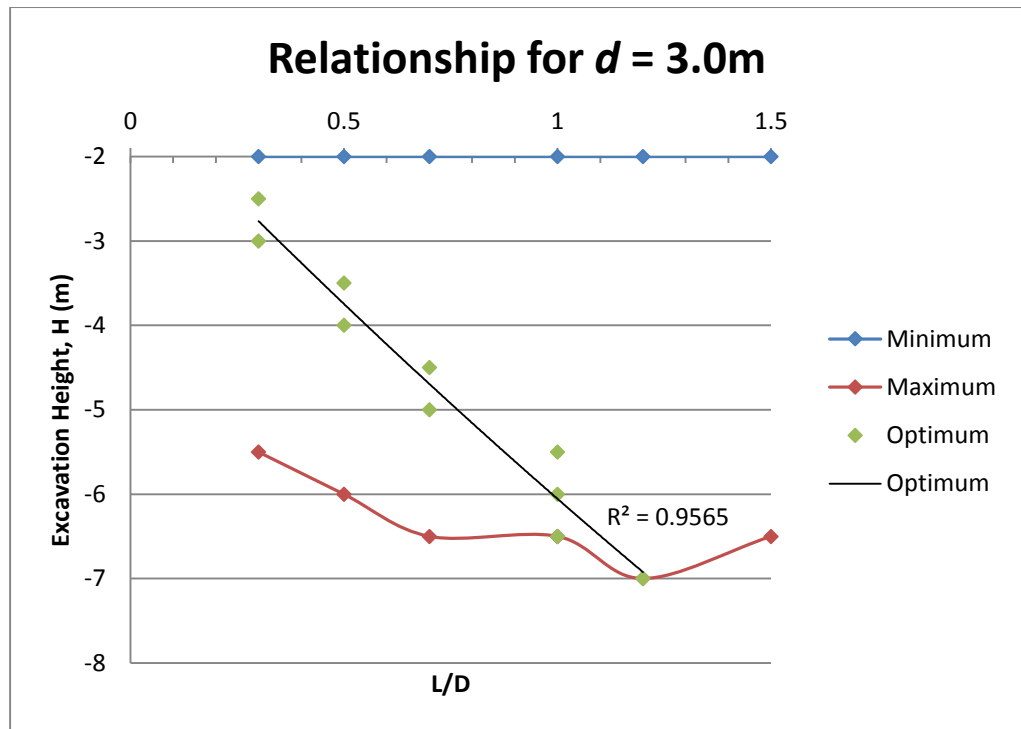


Figure 9.3: Relationship for  $D = 10.0\text{m}$  with anchor embedment depth of  $3\text{m}$ .

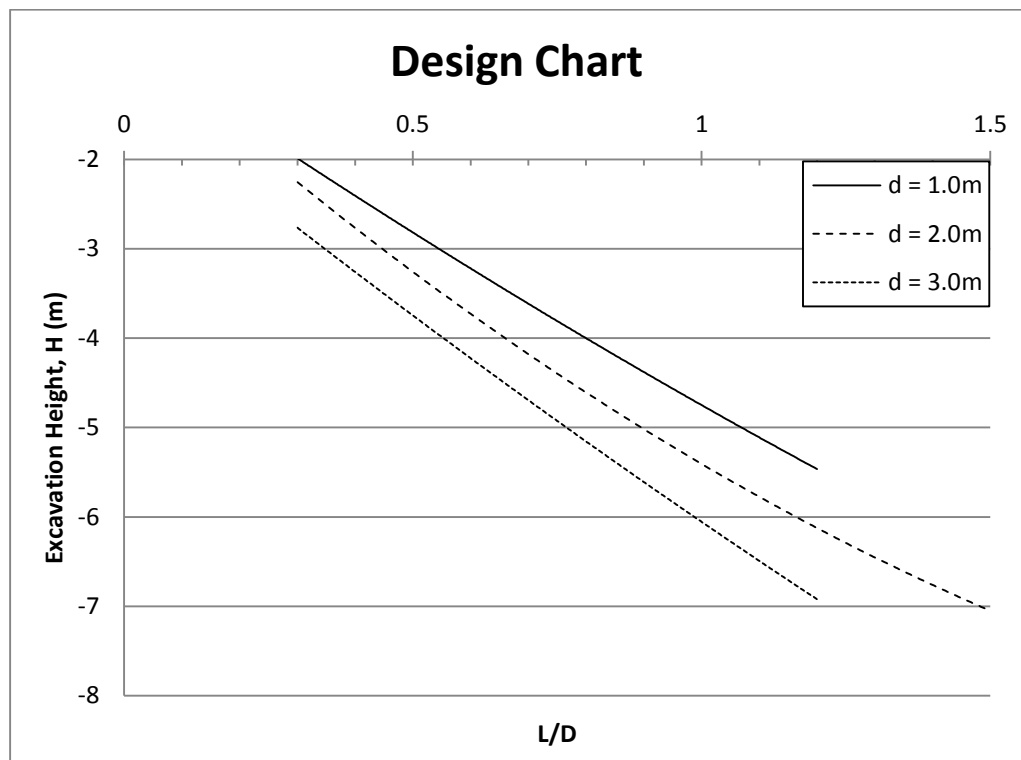


Figure 9.4: Design chart for case of  $D = 10.0\text{m}$ ,  $s = 2.0\text{m}$  and  $\phi = 30^\circ$ .

By conjoining the best fit lines from Figure 9.1 to Figure 9.3, the design chart for case of  $D = 10.0\text{m}$ ,  $S = 2.0\text{m}$  and  $\phi = 30^\circ$  is developed.

### **9.3 Relationship of the Load Corresponding to the Optimum Response of Anchored Wall**

The optimum response of anchored wall on the effects of tie rod length ( $L$ ), wall depth ( $D$ ) and maximum allowable excavation height ( $H$ ) for anchor embedment depth ( $d$ ) up to 3m have been determined. This section discusses the load corresponding to the optimum response of anchored wall.

The relationship of load corresponding to the optimum response of anchored wall for anchor embedment depth up to 3m is presented in Figure 9.5 to Figure 9.7. By conjoining these three charts, the corresponding load for Figure 9.4 is illustrated in Figure 9.8. The design chart and the corresponding load are determined based on several restrictions:

- 1) The diameter of tie rod is 25mm
- 2) The size of deadman anchor is 100mm x 100mm x 10mm

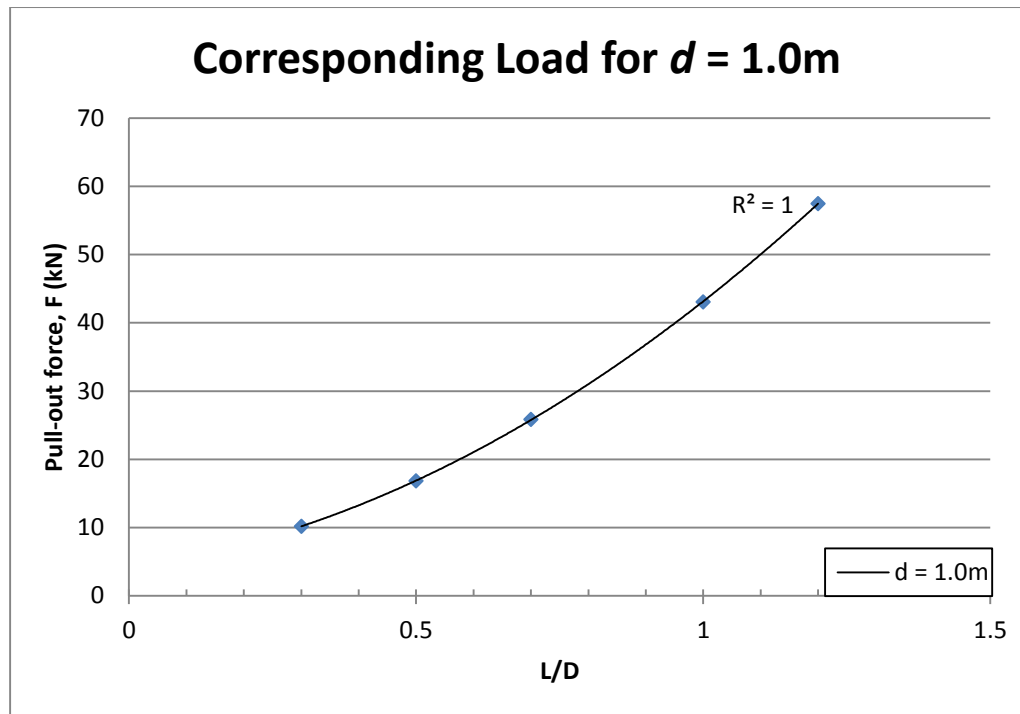


Figure 9.5: Relationship of corresponding load to the optimum response of anchored wall ( $D=10.0\text{m}$ ) for anchor embedment depth of 1.0m.

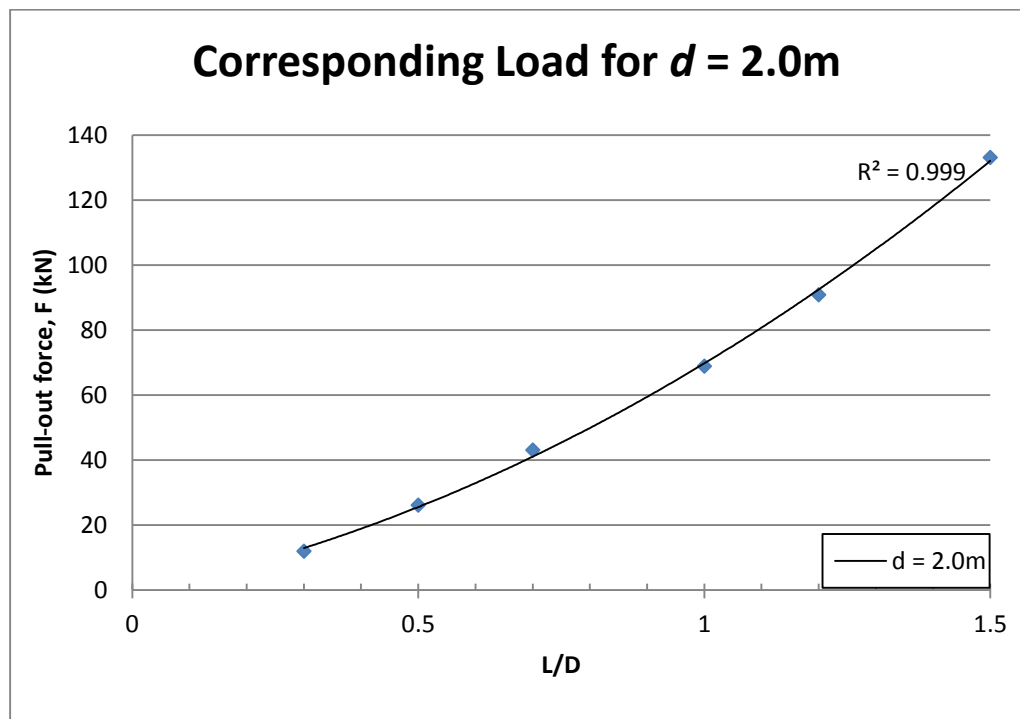


Figure 9.6: Relationship of corresponding load to the optimum response of anchored wall ( $D=10.0\text{m}$ ) for anchor embedment depth of 2.0m.

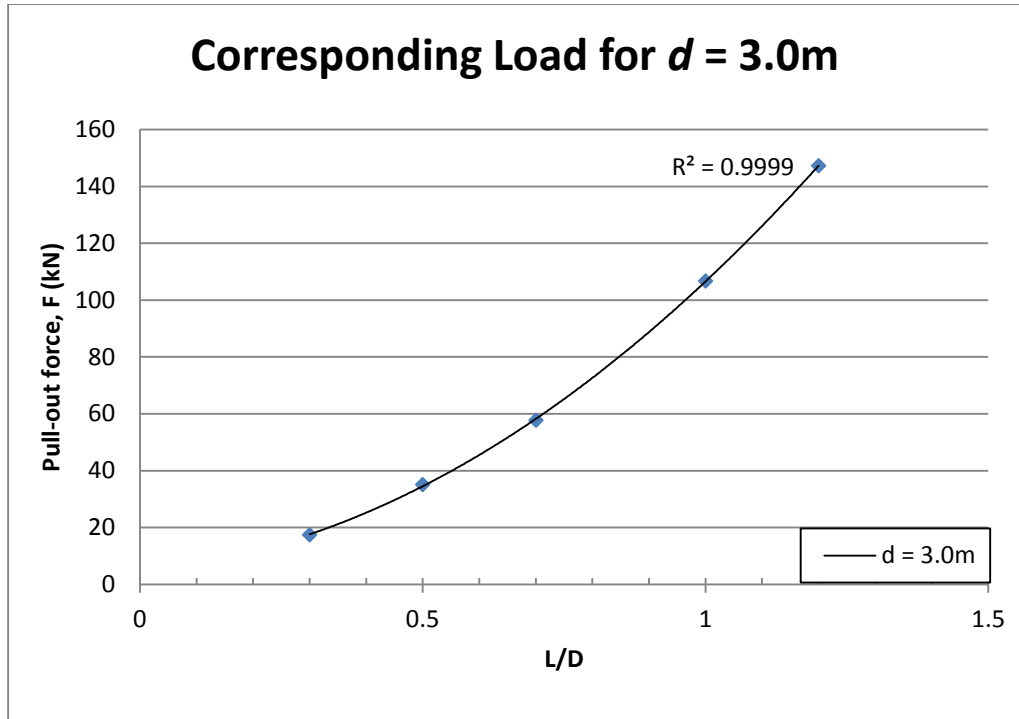


Figure 9.7: Relationship of corresponding load to the optimum response of anchored wall ( $D=10.0\text{m}$ ) for anchor embedment depth of  $3.0\text{m}$ .

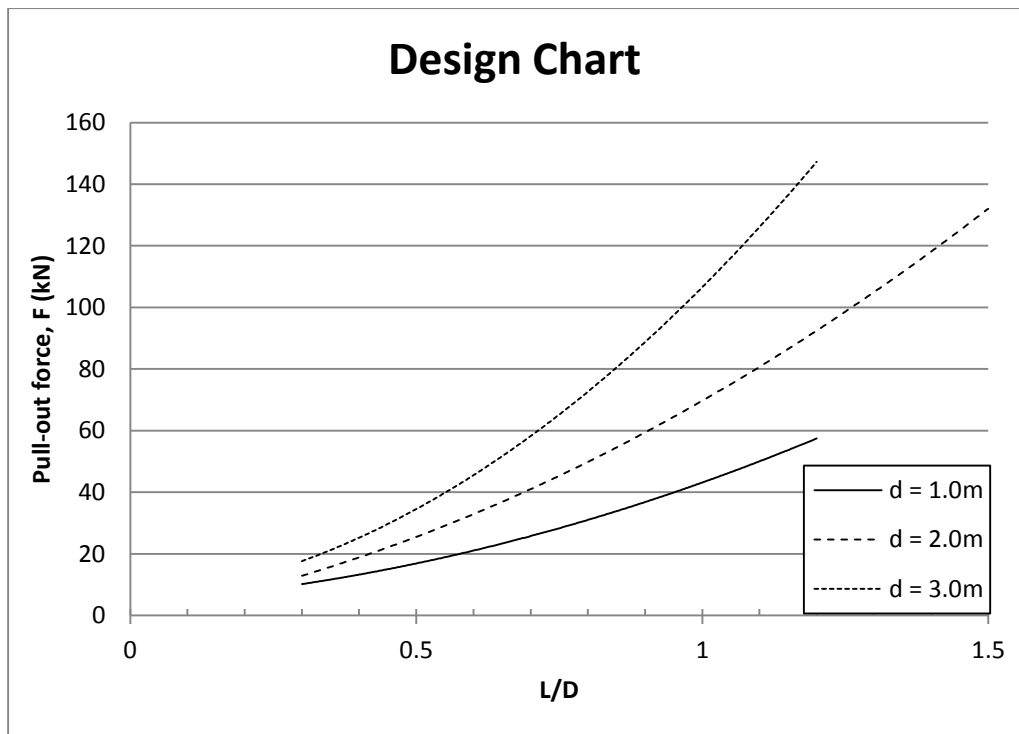


Figure 9.8: Design chart of corresponding load for case of  $D = 10.0\text{m}$ ,  $s = 2.0\text{m}$  and  $\phi = 30^\circ$ .

## 9.4 Design Charts

The design charts are developed for various cases of anchor spacing ( $s$ ) and friction angle of soil ( $\phi$ ) with various wall depth ( $D$ ). All of these design charts are subjected to anchor embedment depth ( $d$ ) up to 3.0m.

The design charts are categorised as in the following cases:

- 1) Case 1: Anchor spacing ( $s$ ) = 2.0m and friction angle of soil ( $\phi$ ) =  $30^\circ$  with wall depth ( $D$ ) of 10.0m, 15.0m and 20.0m.
- 2) Case 2: Anchor spacing ( $s$ ) = 2.0m and friction angle of soil ( $\phi$ ) =  $40^\circ$  with wall depth ( $D$ ) of 10.0m, 15.0m and 20.0m.
- 3) Case 3: Anchor spacing ( $s$ ) = 5.0m and friction angle of soil ( $\phi$ ) =  $30^\circ$  with wall depth ( $D$ ) of 10.0m, 15.0m and 20.0m.
- 4) Case 4: Anchor spacing ( $s$ ) = 5.0m and friction angle of soil ( $\phi$ ) =  $40^\circ$  with wall depth ( $D$ ) of 10.0m, 15.0m and 20.0m.

Nevertheless, some assumptions are made during the development of these design charts, which are as follows:

- 1) The Young's Modulus of soil is assumed to be 30MPa.
- 2) The soil is assumed to follow non-associate flow rules.
- 3) The soil is assumed to be in drained condition with absence of water table.
- 4) The tie rod diameter is assumed to be 25mm.
- 5) The deadman anchor is assumed to be 1.0m x 1.0m x 0.5m.
- 6) The thickness of wall is assumed to be 0.5m diaphragm wall.

### **9.4.1 Case 1: Anchor Spacing ( $s$ ) = 2.0m and Friction Angle of Soil ( $\phi$ ) = 30°**

Figure 9.4 and Figure 9.8 present, respectively, the design charts of the optimum response of anchored wall and the pull-out force corresponding to the tie rod length, for anchor spacing ( $s$ ) = 2.0m and friction angle of soil ( $\phi$ ) = 30° with wall depth ( $D$ ) of 10.0m.

#### **9.4.1.1 For Wall Depth ( $D$ ) of 15.0m**

Figure 9.9 and Figure 9.10 present, respectively, the design charts of the optimum response of anchored wall and the pull-out force corresponding to the tie rod length, for anchor spacing ( $s$ ) = 2.0m and friction angle of soil ( $\phi$ ) = 30° with wall depth ( $D$ ) of 15.0m.

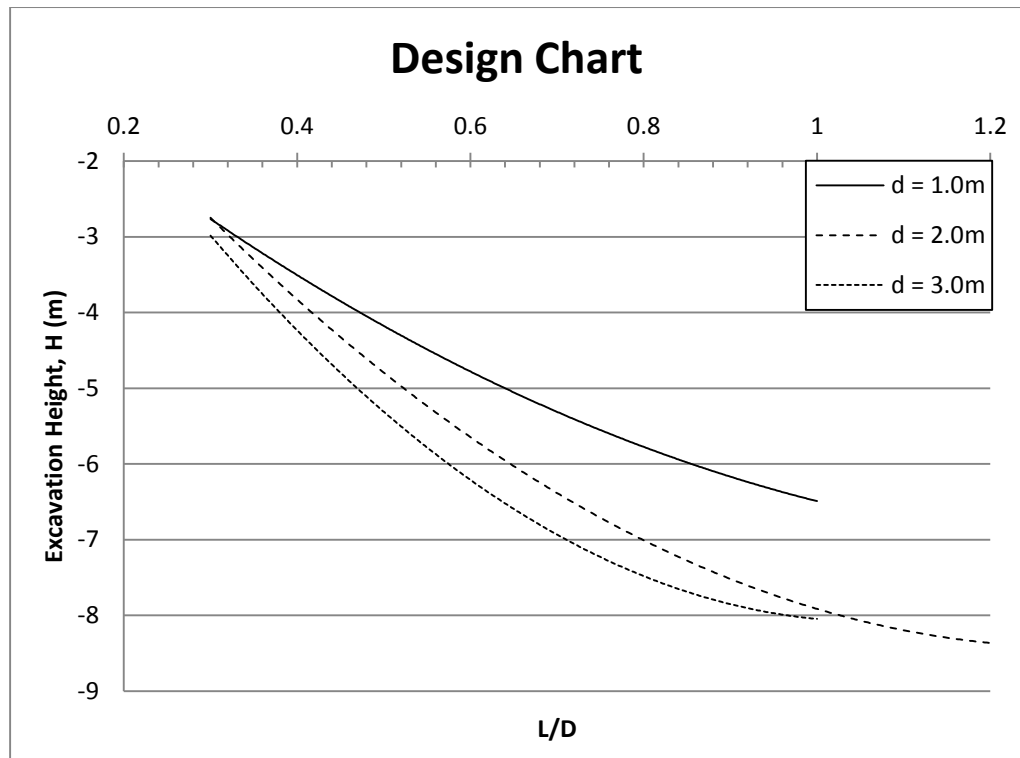


Figure 9.9: Design chart for case of  $D = 15.0\text{m}$ ,  $s = 2.0\text{m}$  and  $\phi = 30^\circ$ .

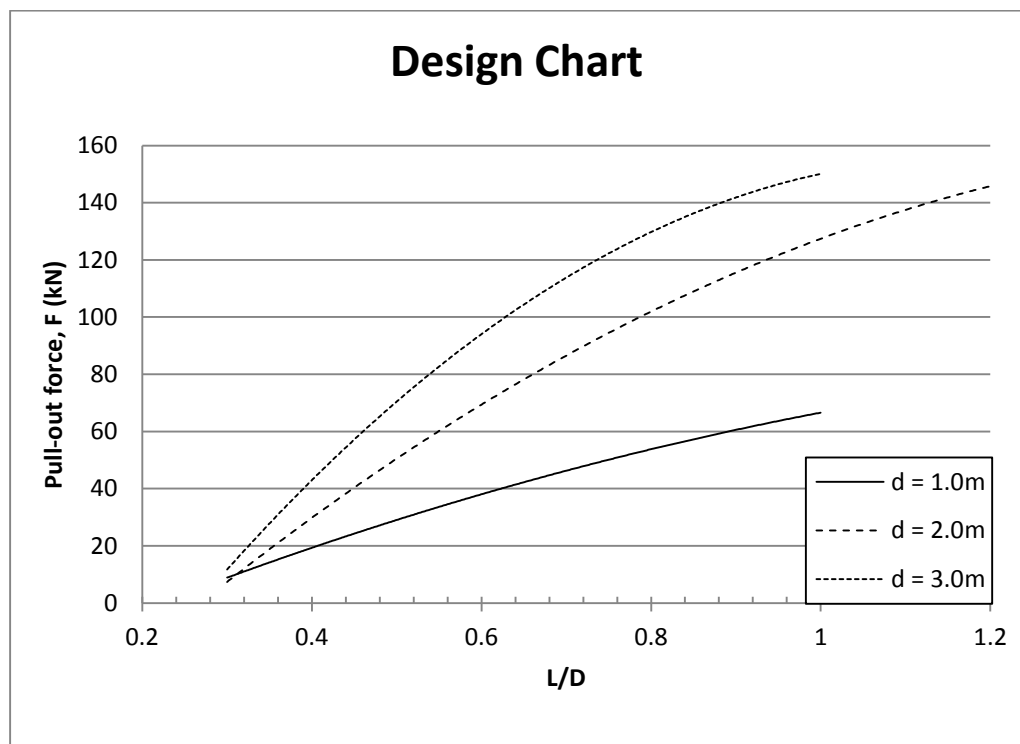


Figure 9.10: Design chart of corresponding load for case of  $D = 15.0\text{m}$ ,  $s = 2.0\text{m}$  and  $\phi = 30^\circ$ .

### 9.4.1.2 For Wall Depth ( $D$ ) of 20.0m

Figure 9.11 and Figure 9.12 present, respectively, the design charts of the optimum response of anchored wall and the pull-out force corresponding to the tie rod length, for anchor spacing ( $s$ ) = 2.0m and friction angle of soil ( $\phi$ ) =  $30^\circ$  with wall depth ( $D$ ) of 20.0m.

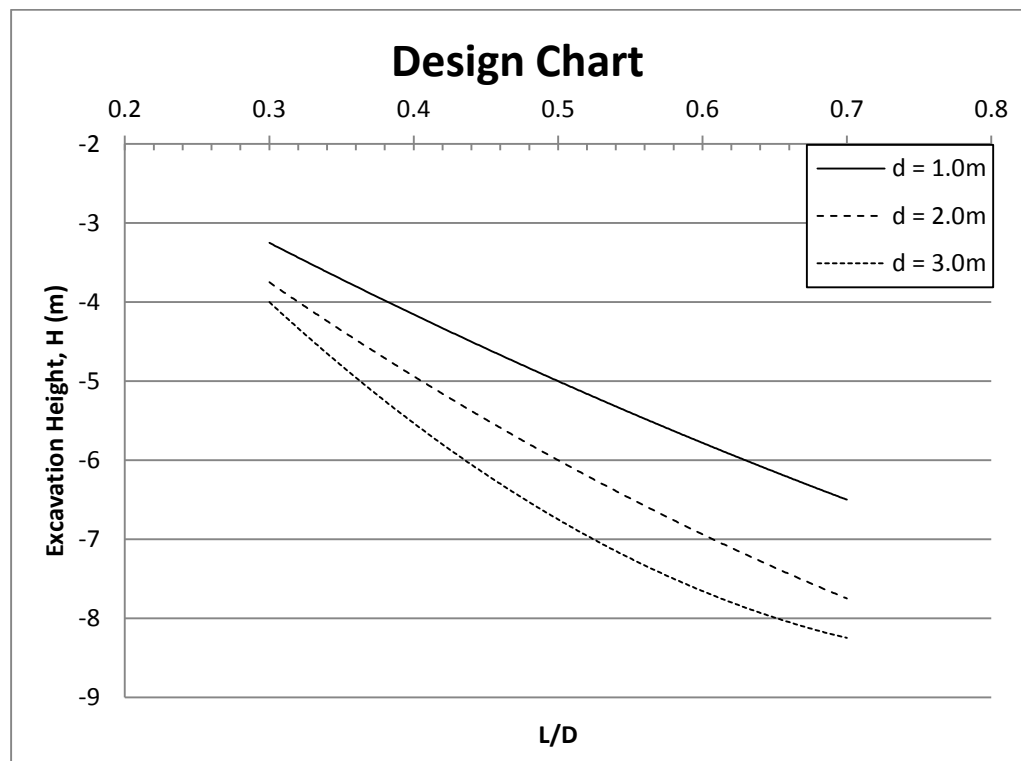


Figure 9.11: Design chart for case of  $D = 20.0\text{m}$ ,  $s = 2.0\text{m}$  and  $\phi = 30^\circ$ .

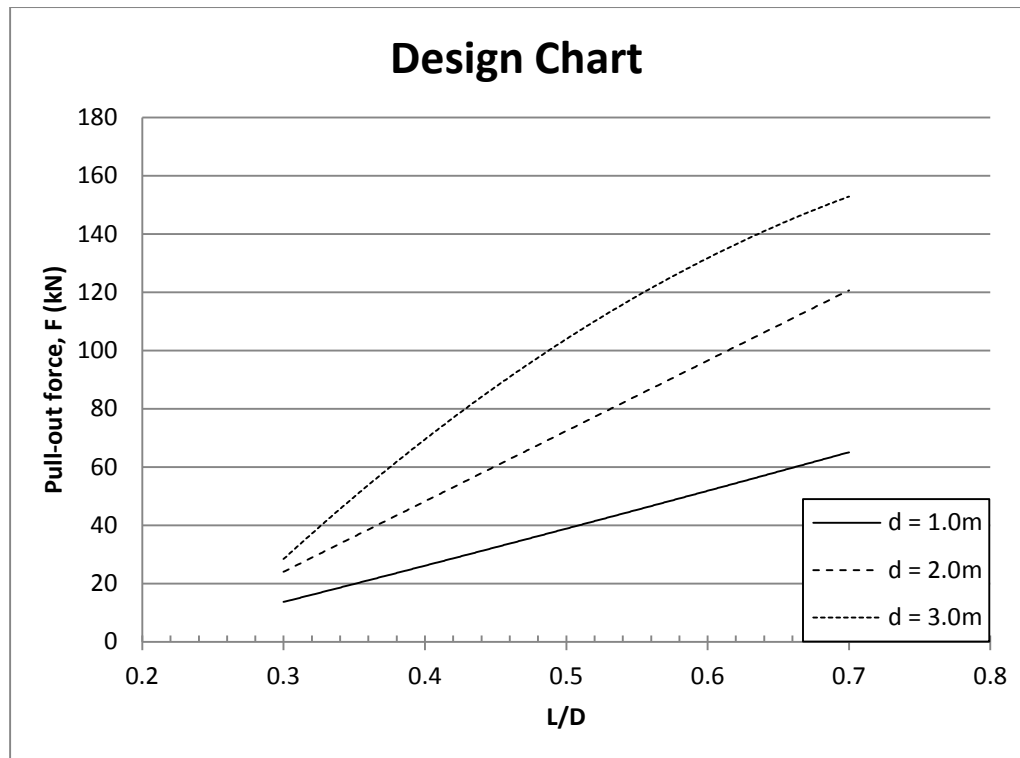


Figure 9.12: Design chart of corresponding load for case of  $D = 20.0\text{m}$ ,  $s = 2.0\text{m}$  and  $\phi = 30^\circ$ .

## 9.4.2 Case 2: Anchor Spacing ( $s$ ) = 2.0m and Friction Angle of Soil ( $\phi$ ) = $40^\circ$

### 9.4.2.1 For Wall Depth ( $D$ ) of 10.0m

Figure 9.13 and Figure 9.14 present, respectively, the design charts of the optimum response of anchored wall and the pull-out force corresponding to the tie rod length, for anchor spacing ( $s$ ) = 2.0m and friction angle of soil ( $\phi$ ) =  $40^\circ$  with wall depth ( $D$ ) of 10.0m.

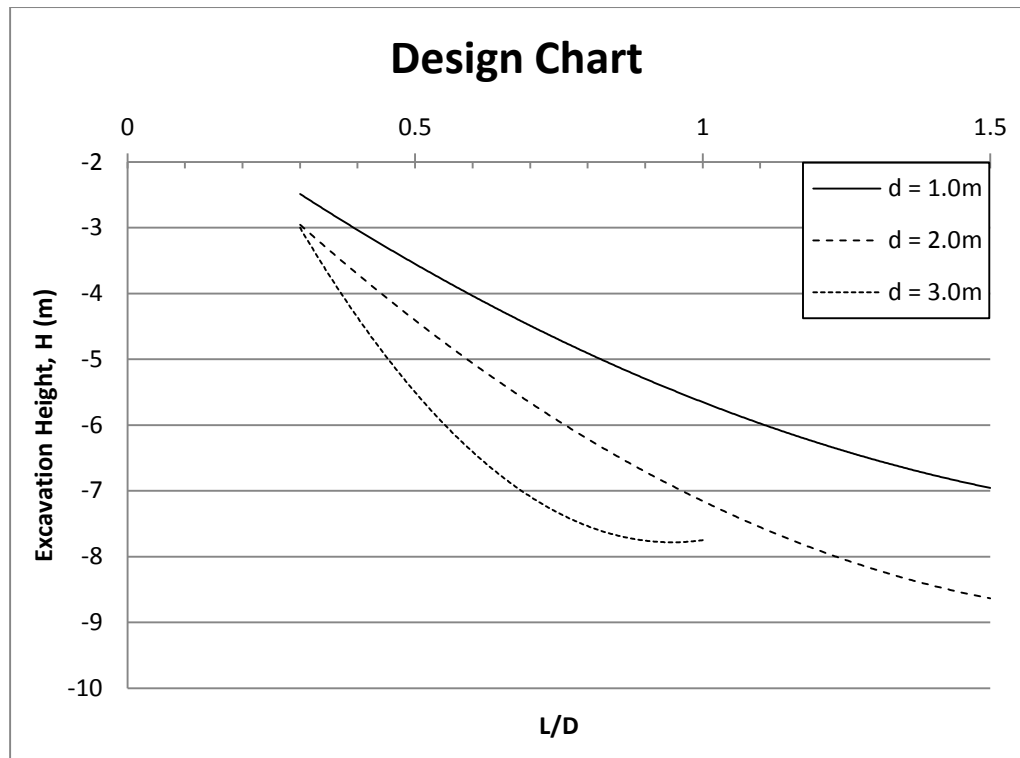


Figure 9.13: Design chart for case of  $D = 10.0\text{m}$ ,  $s = 2.0\text{m}$  and  $\phi = 40^\circ$ .

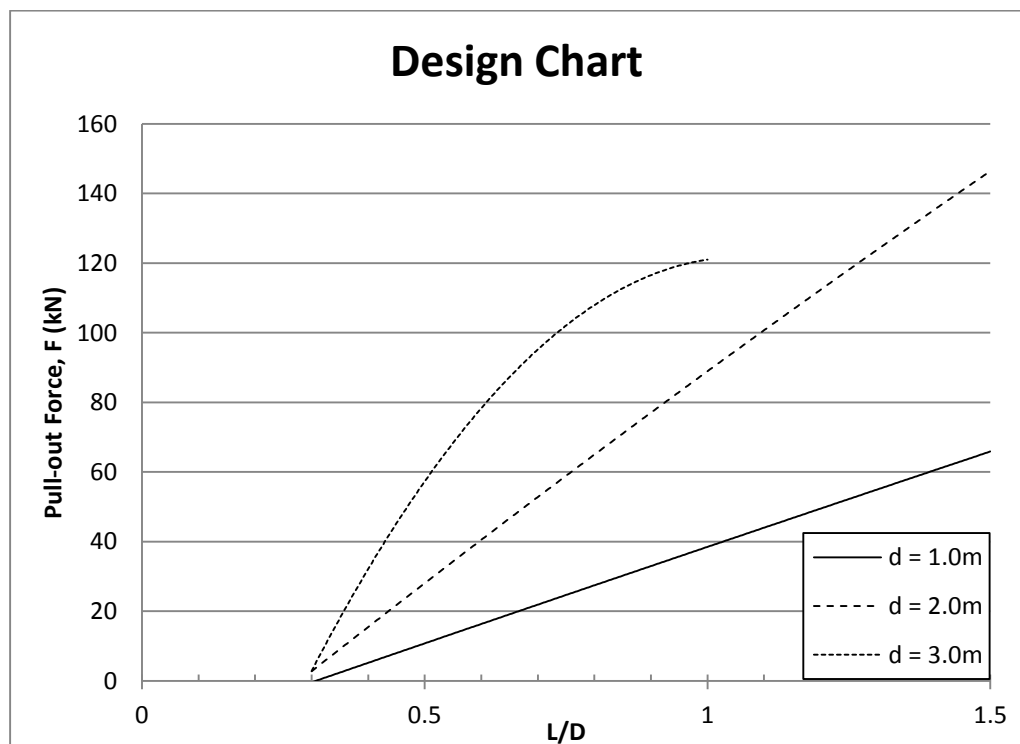


Figure 9.14: Design chart of corresponding load for case of  $D = 10.0\text{m}$ ,  $s = 2.0\text{m}$  and  $\phi = 40^\circ$ .

### 9.4.2.2 For Wall Depth ( $D$ ) of 15.0m

Figure 9.15 and Figure 9.16 present, respectively, the design charts of the optimum response of anchored wall and the pull-out force corresponding to the tie rod length, for anchor spacing ( $s$ ) = 2.0m and friction angle of soil ( $\phi$ ) =  $40^\circ$  with wall depth ( $D$ ) of 15.0m.

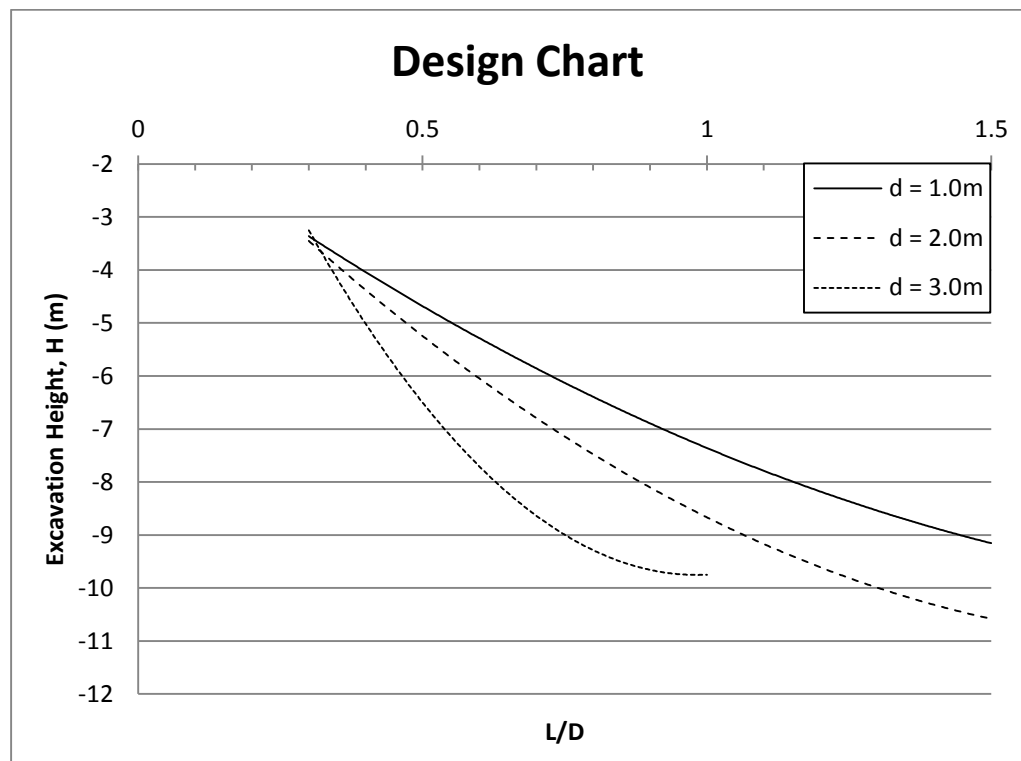


Figure 9.15: Design chart for case of  $D = 15.0\text{m}$ ,  $s = 2.0\text{m}$  and  $\phi = 40^\circ$ .

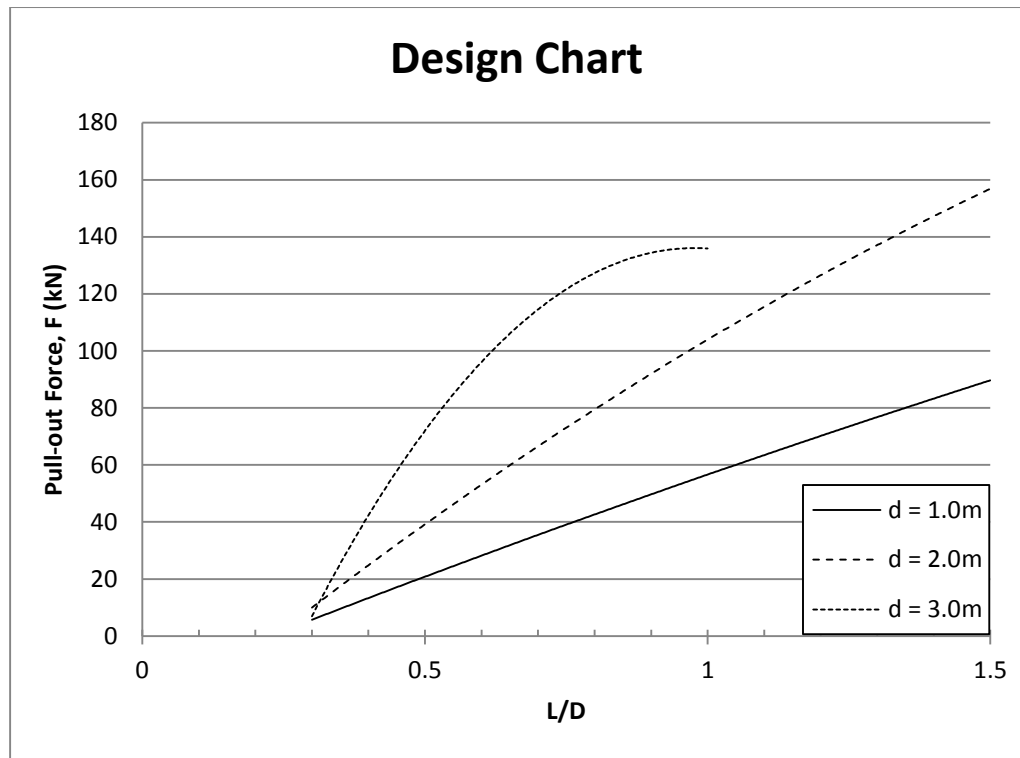


Figure 9.16: Design chart of corresponding load for case of  $D = 15.0\text{m}$ ,  $s = 2.0\text{m}$  and  $\phi = 40^\circ$ .

#### 9.4.2.3 For Wall Depth ( $D$ ) of 20.0m

Figure 9.17 and Figure 9.18 present, respectively, the design charts of the optimum response of anchored wall and the pull-out force corresponding to the tie rod length, for anchor spacing ( $s$ ) = 2.0m and friction angle of soil ( $\phi$ ) =  $40^\circ$  with wall depth ( $D$ ) of 20.0m.

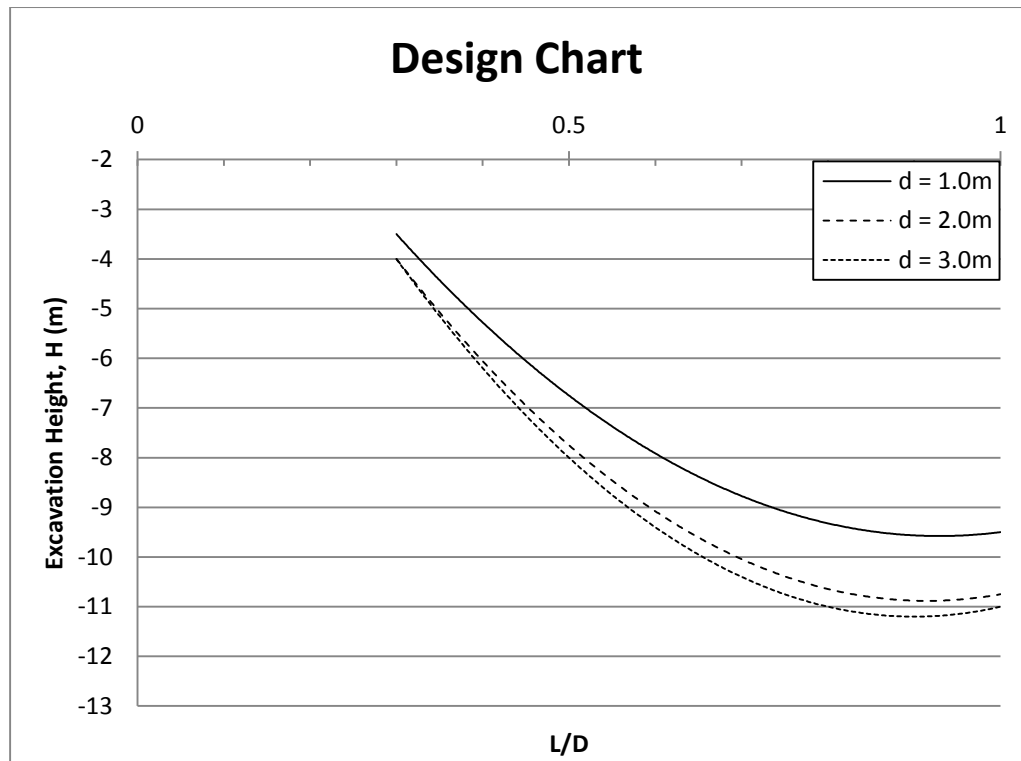


Figure 9.17: Design chart for case of  $D = 20.0\text{m}$ ,  $s = 2.0\text{m}$  and  $\phi = 40^\circ$ .

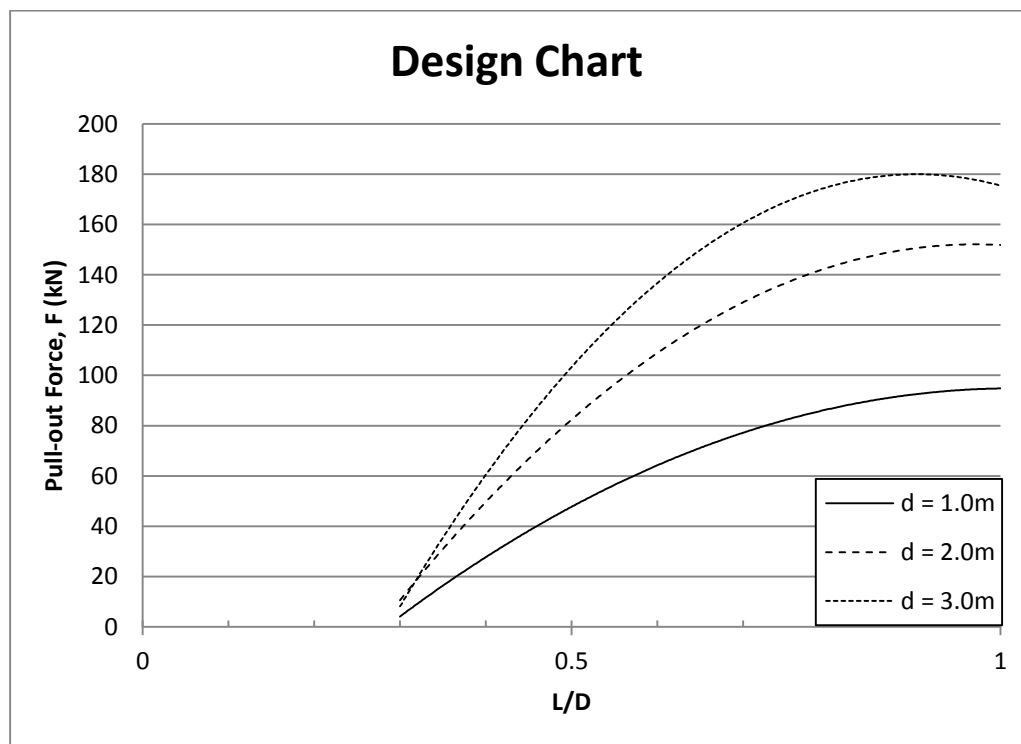


Figure 9.18: Design chart of corresponding load for case of  $D = 20.0\text{m}$ ,  $s = 2.0\text{m}$  and  $\phi = 40^\circ$ .

### 9.4.3 Case 3: Anchor Spacing ( $s$ ) = 5.0m and Friction Angle of Soil ( $\phi$ ) = 30°

#### 9.4.3.1 For Wall Depth ( $D$ ) of 10.0m

Figure 9.19 and Figure 9.20 present, respectively, the design charts of the optimum response of anchored wall and the pull-out force corresponding to the tie rod length, for anchor spacing ( $s$ ) = 5.0m and friction angle of soil ( $\phi$ ) = 30° with wall depth ( $D$ ) of 10.0m.

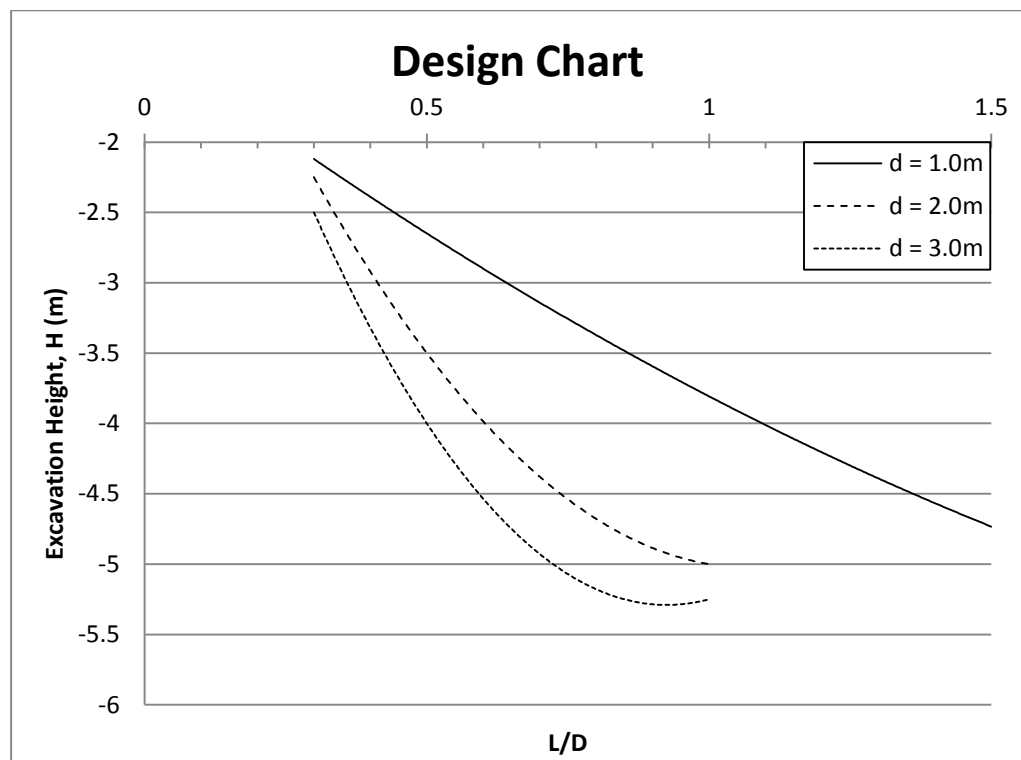


Figure 9.19: Design chart for case of  $D = 10.0\text{m}$ ,  $s = 5.0\text{m}$  and  $\phi = 30^\circ$ .

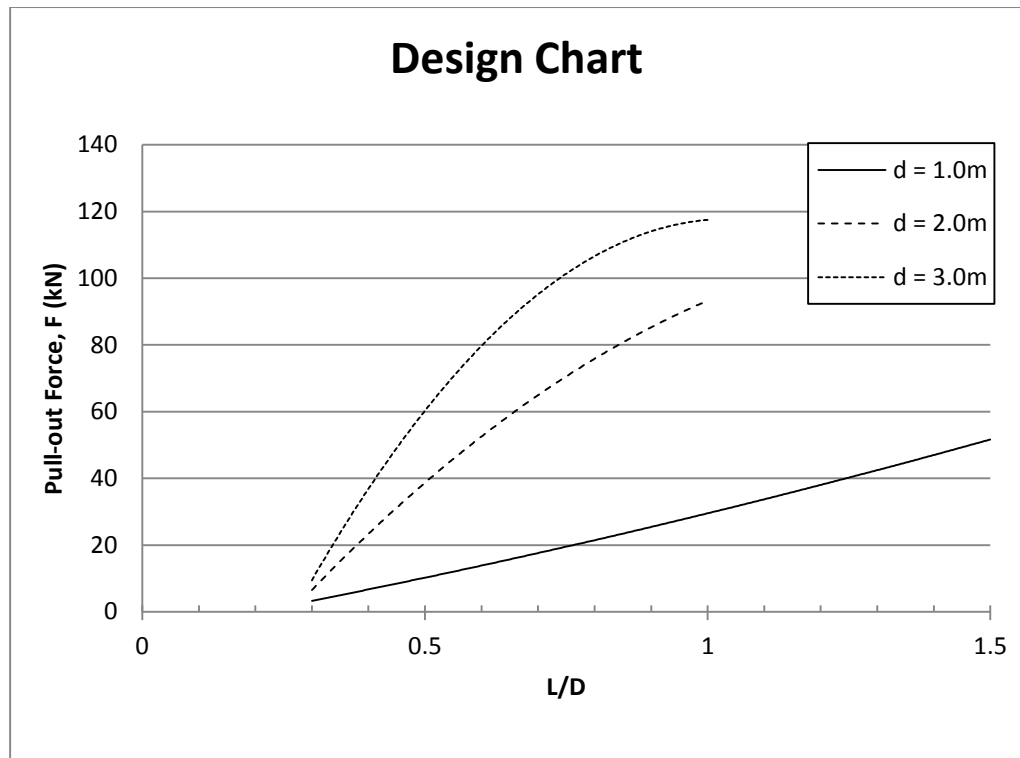


Figure 9.20: Design chart of corresponding load for case of  $D = 10.0\text{m}$ ,  $s = 5.0\text{m}$  and  $\phi = 30^\circ$ .

#### 9.4.3.2 For Wall Depth ( $D$ ) of 15.0m

Figure 9.21 and Figure 9.22 present, respectively, the design charts of the optimum response of anchored wall and the pull-out force corresponding to the tie rod length, for anchor spacing ( $s$ ) = 5.0m and friction angle of soil ( $\phi$ ) =  $30^\circ$  with wall depth ( $D$ ) of 15.0m.

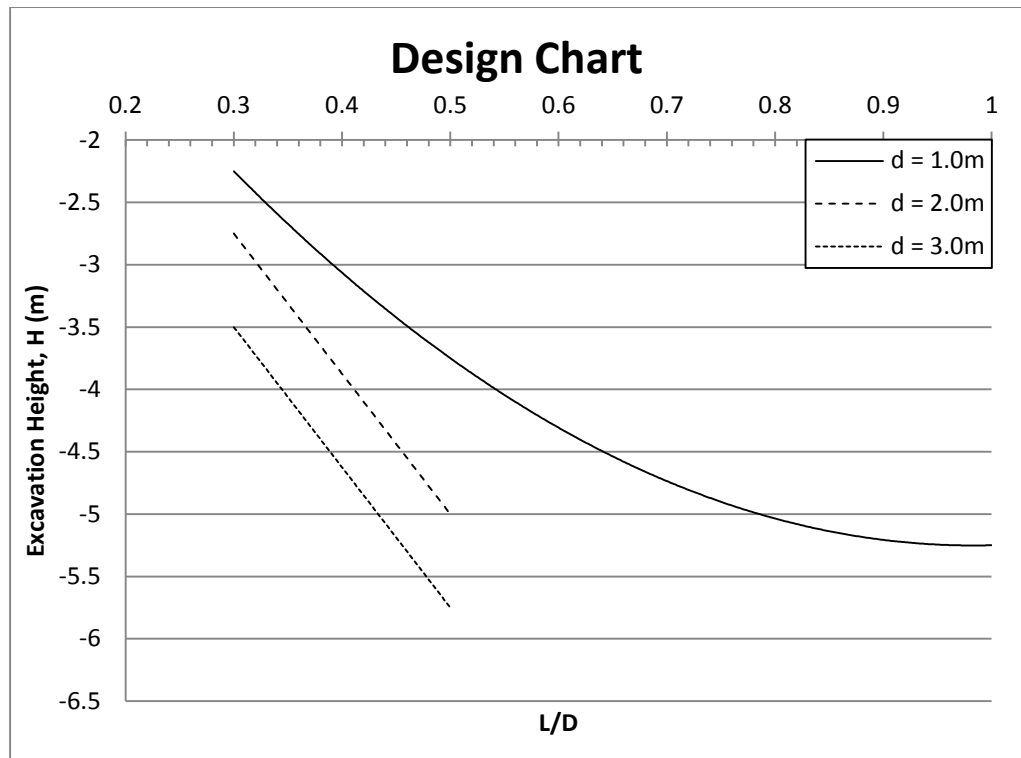


Figure 9.21: Design chart for case of  $D = 15.0\text{m}$ ,  $s = 5.0\text{m}$  and  $\phi = 30^\circ$ .

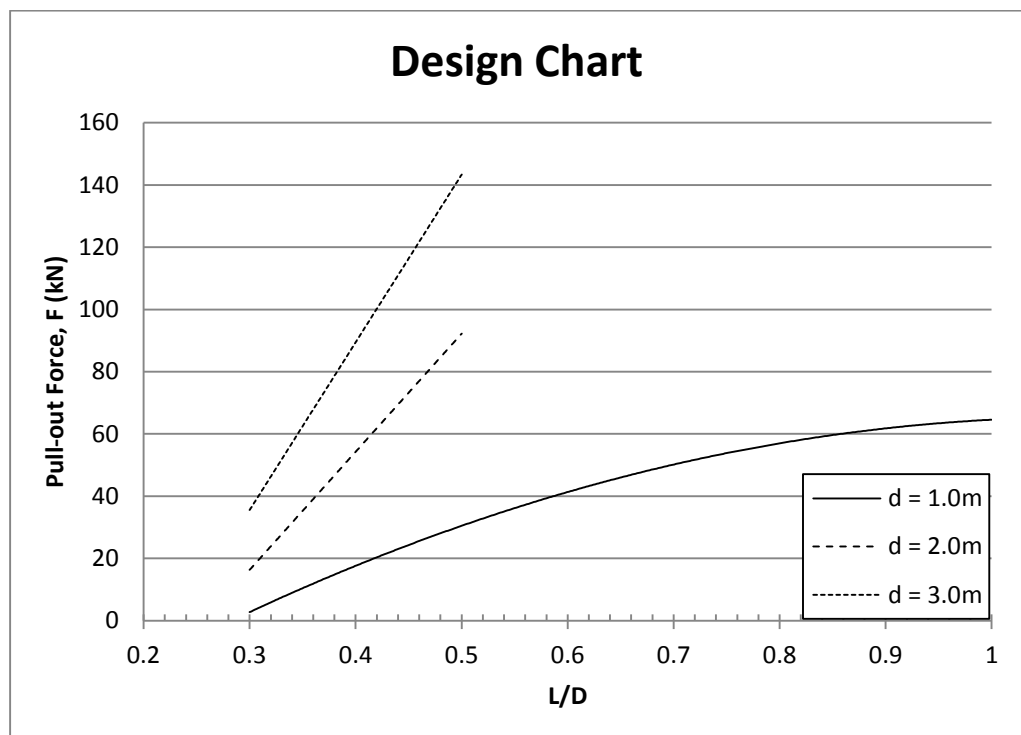


Figure 9.22: Design chart of corresponding load for case of  $D = 15.0\text{m}$ ,  $s = 5.0\text{m}$  and  $\phi = 30^\circ$ .

### 9.4.3.3 For Wall Depth ( $D$ ) of 20.0m

Figure 9.23 and Figure 9.24 present, respectively, the design charts of the optimum response of anchored wall and the pull-out force corresponding to the tie rod length, for anchor spacing ( $s$ ) = 5.0m and friction angle of soil ( $\phi$ ) =  $30^\circ$  with wall depth ( $D$ ) of 20.0m.

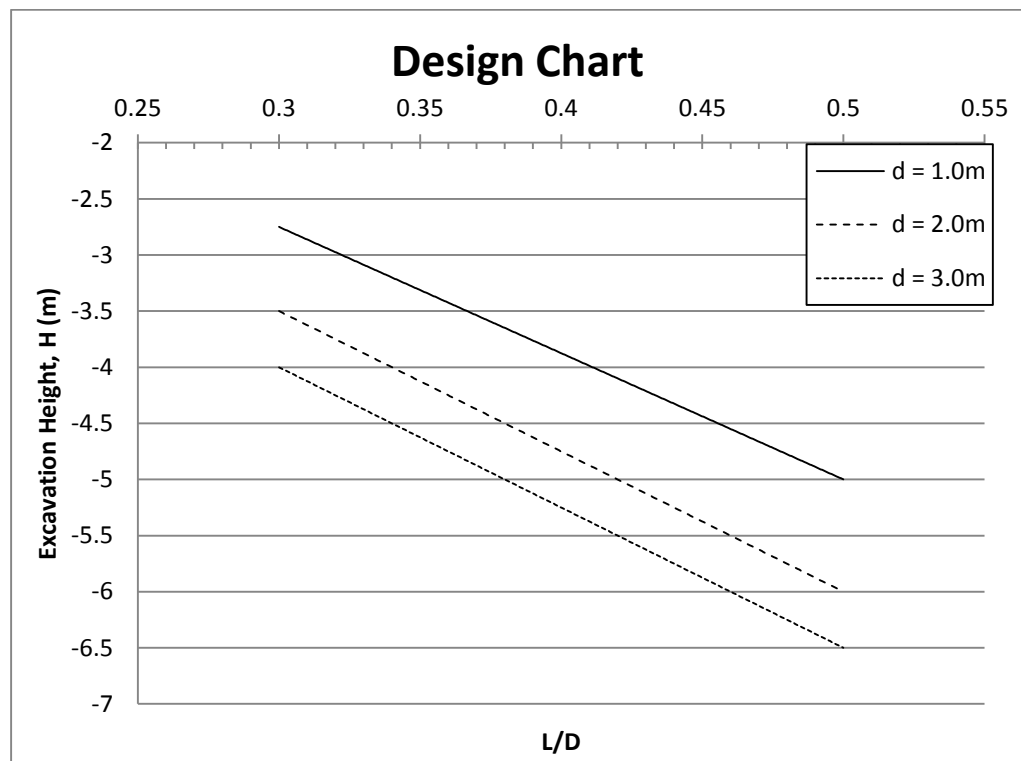


Figure 9.23: Design chart for case of  $D = 20.0\text{m}$ ,  $s = 5.0\text{m}$  and  $\phi = 30^\circ$ .

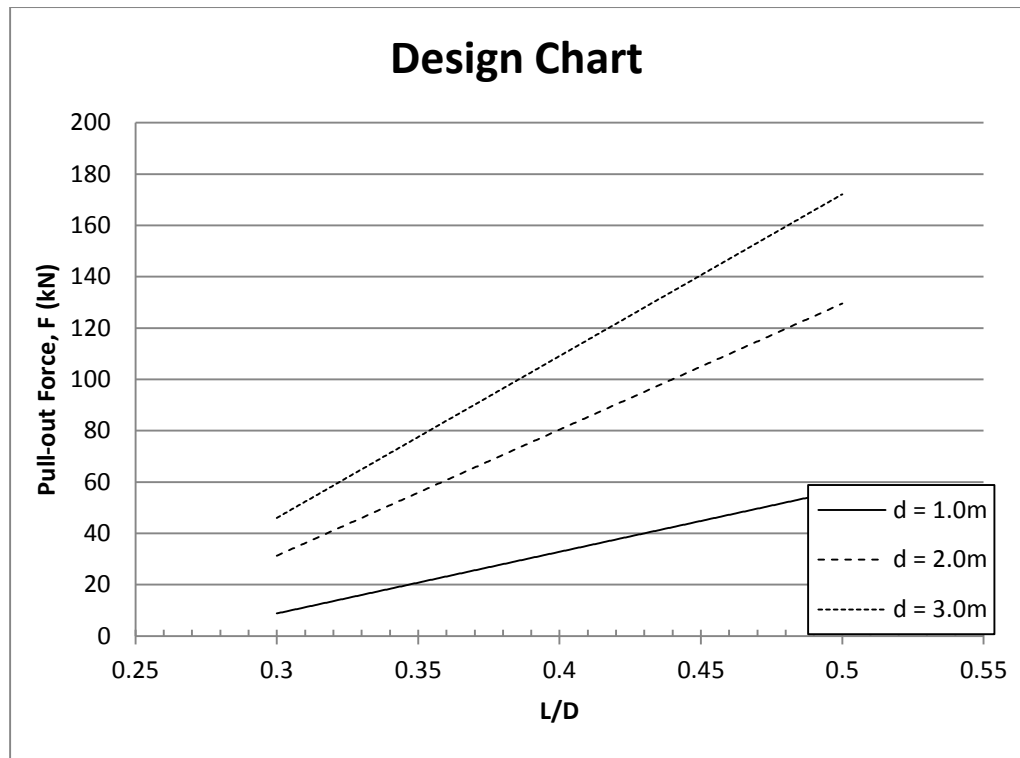


Figure 9.24: Design chart of corresponding load for case of  $D = 20.0\text{m}$ ,  $s = 5.0\text{m}$  and  $\phi = 30^\circ$ .

#### 9.4.4 Case 4: Anchor Spacing ( $s$ ) = 5.0m and Friction Angle of Soil ( $\phi$ ) = $40^\circ$

##### 9.4.4.1 For Wall Depth ( $D$ ) of 10.0m

Figure 9.25 and Figure 9.26 present, respectively, the design charts of the optimum response of anchored wall and the pull-out force corresponding to the tie rod length, for anchor spacing ( $s$ ) = 5.0m and friction angle of soil ( $\phi$ ) =  $40^\circ$  with wall depth ( $D$ ) of 10.0m.

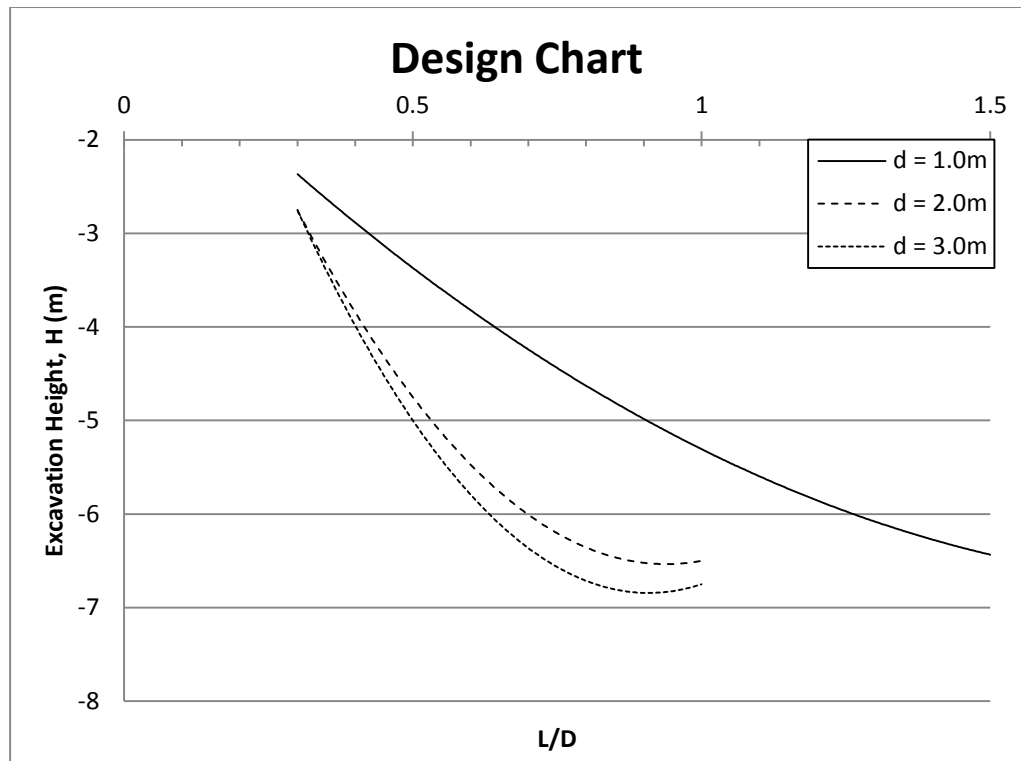


Figure 9.25: Design chart for case of  $D = 10.0\text{m}$ ,  $s = 5.0\text{m}$  and  $\phi = 40^\circ$ .

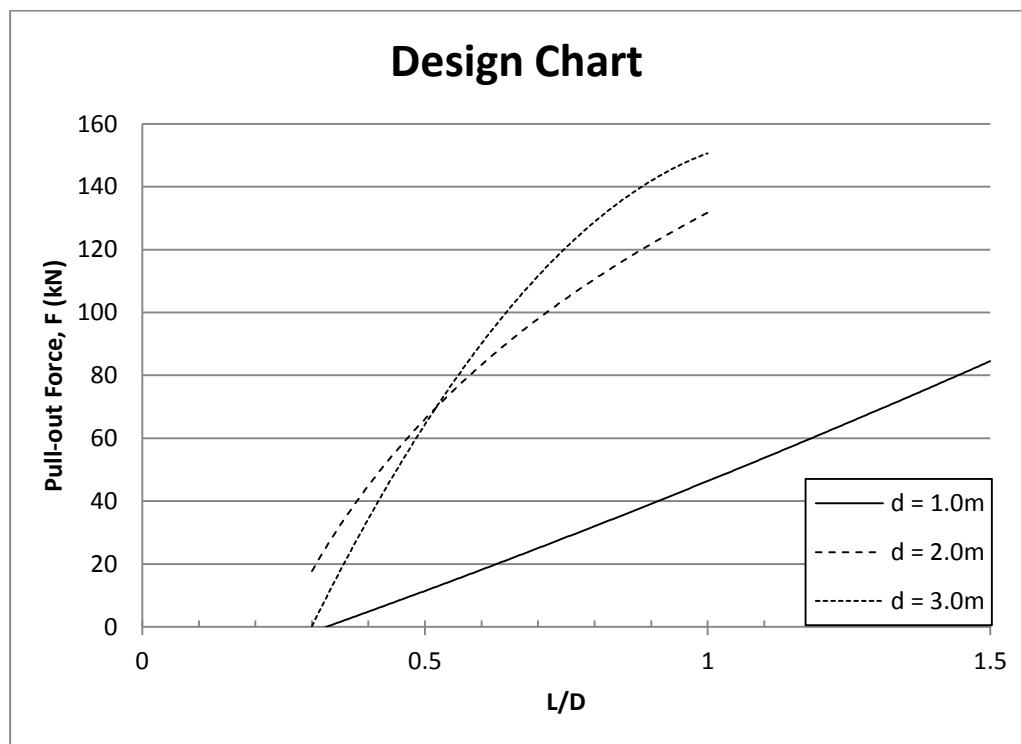


Figure 9.26: Design chart of corresponding load for case of  $D = 10.0\text{m}$ ,  $s = 5.0\text{m}$  and  $\phi = 40^\circ$ .

### 9.4.4.2 For Wall Depth ( $D$ ) of 15.0m

Figure 9.27 and Figure 9.28 present, respectively, the design charts of the optimum response of anchored wall and the pull-out force corresponding to the tie rod length, for anchor spacing ( $s$ ) = 5.0m and friction angle of soil ( $\phi$ ) =  $40^\circ$  with wall depth ( $D$ ) of 15.0m.

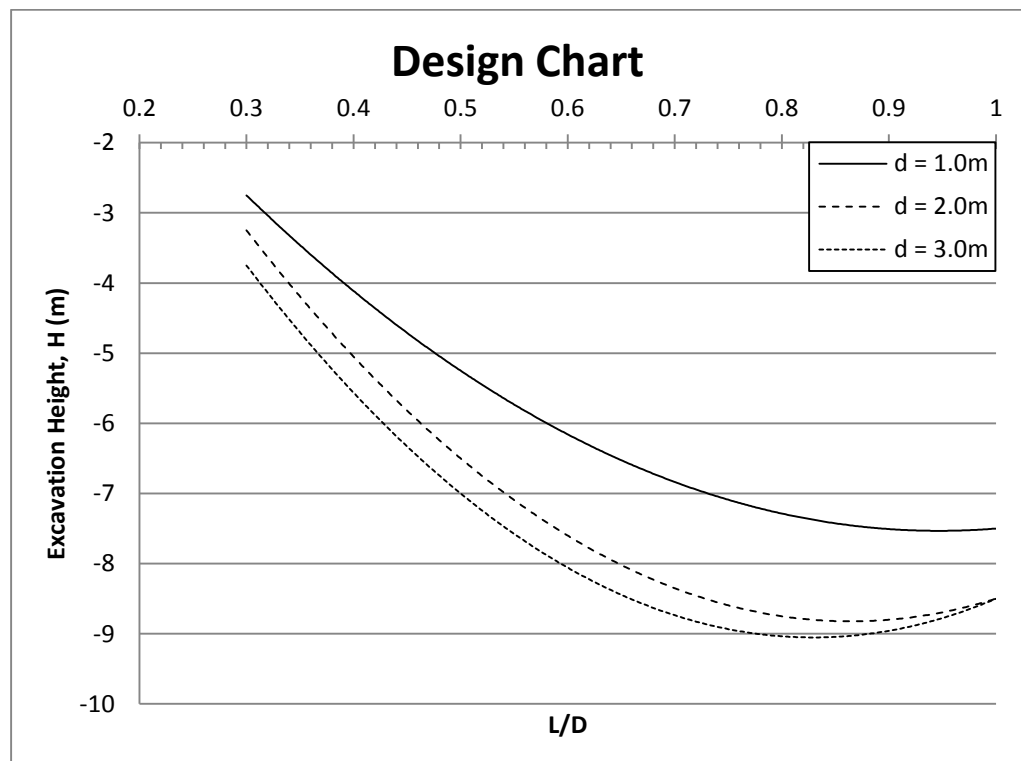


Figure 9.27: Design chart for case of  $D = 15.0\text{m}$ ,  $S = 5.0\text{m}$  and  $\phi = 40^\circ$ .

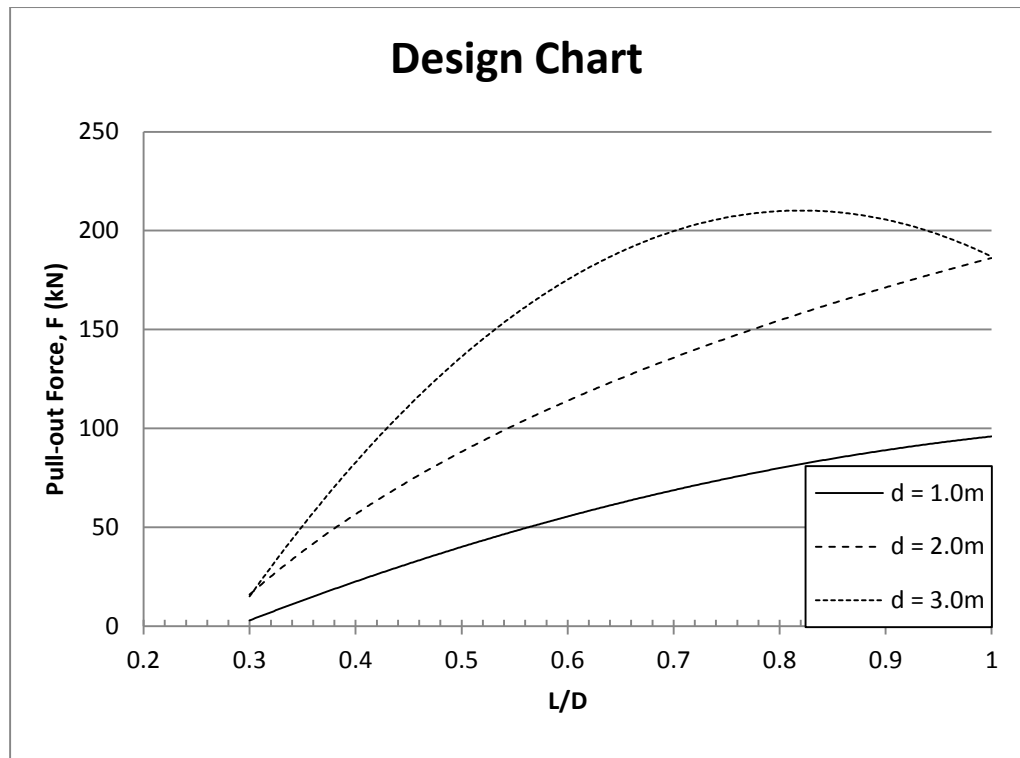


Figure 9.28: Design chart of corresponding load for case of  $D = 15.0\text{m}$ ,  $s = 5.0\text{m}$  and  $\phi = 40^\circ$ .

#### 9.4.4.3 For Wall Depth ( $D$ ) of 20.0m

Figure 9.29 and Figure 9.30 present, respectively, the design charts of the optimum response of anchored wall and the pull-out force corresponding to the tie rod length, for anchor spacing ( $s$ ) = 5.0m and friction angle of soil ( $\phi$ ) =  $40^\circ$  with wall depth ( $D$ ) of 20.0m.

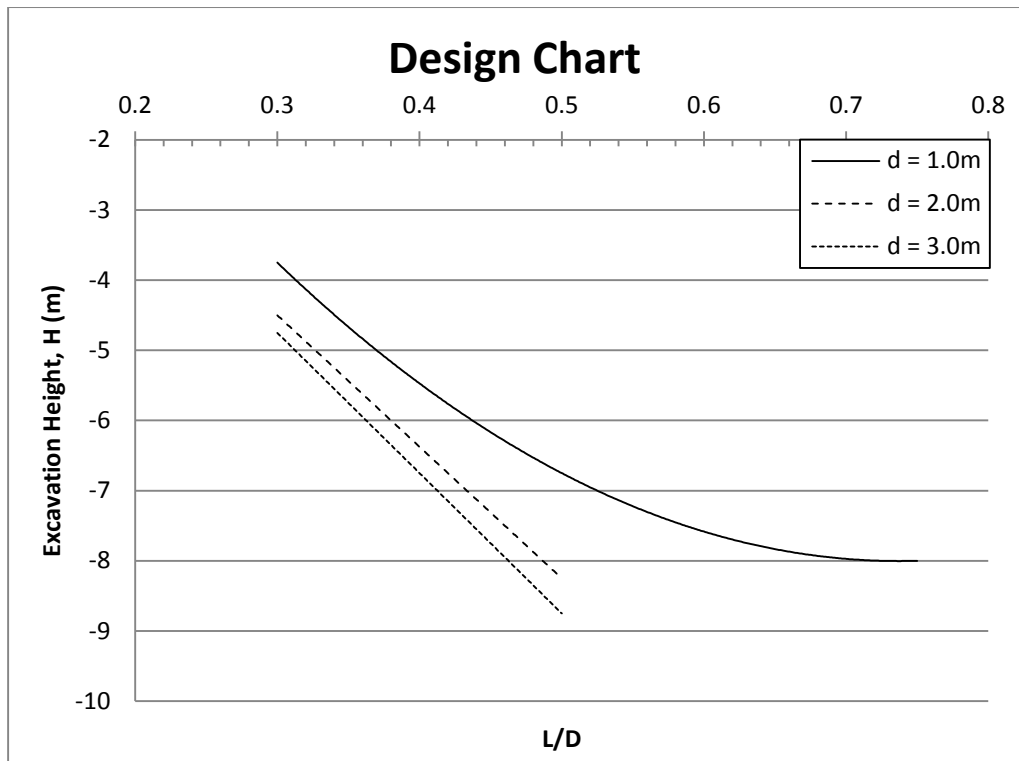


Figure 9.29: Design chart for case of  $D = 20.0\text{m}$ ,  $s = 5.0\text{m}$  and  $\phi = 40^\circ$ .

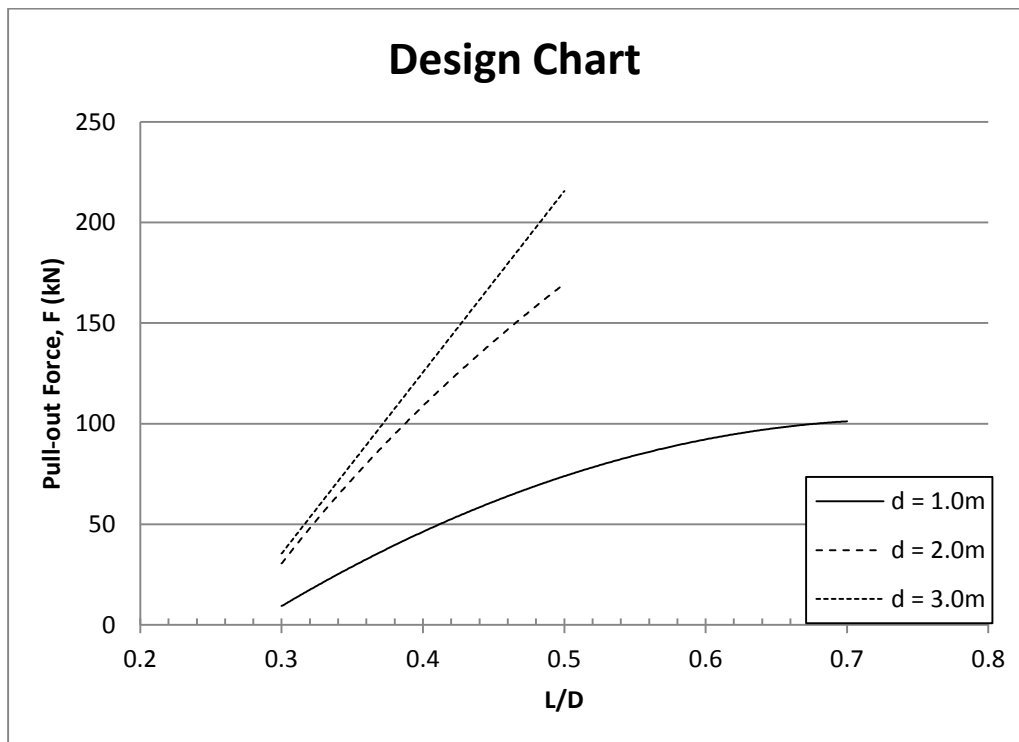


Figure 9.30: Design chart of corresponding load for case of  $D = 20.0\text{m}$ ,  $s = 5.0\text{m}$  and  $\phi = 40^\circ$ .

## 9.5 Application on the Design Charts

The developed design charts allow engineers to design anchored wall directly provided that the site conditions are similar to the soil strength and geometric variables that were used in this research.

The design procedures with the use of design chart are as follows:

- 1) Determine the height of excavation.
- 2) Determine the strength of soil.
- 3) Determine the spacing of deadman anchor.
- 4) Determine the depth of wall.
- 5) Select the length of tie rod and embedment depth of deadman anchor.
- 6) Revise the determination of the spacing of deadman anchor and/or depth of wall if the required length of tie rod exceeds the site boundary.

## 9.6 Summary

The developed design charts in this chapter can be implemented during preliminary or early design stages, such as earthwork planning, cost estimation, bill of quantity, etc. Furthermore, these design charts provide a benchmark during the design stage.

For variables, such as friction angle of soil, spacing of deadman anchor, and wall depth that lie within the range of design charts, the length of tie rod can be interpolated.

# CHAPTER 10

---

## CONCLUSIONS AND RECOMMENDATIONS

### 10.1 Conclusions

The current research developed design charts for the design of anchored wall with deadman anchorage system. The design charts were developed via finite element analysis utilising the finite element software, *PLAXIS*. This research also aims to provide better understanding on the interaction between soil, anchor and wall. Hence, this research is of practical importance to civil engineers in providing them with design charts for the design of anchored wall in geotechnical engineering.

The following conclusions can be drawn from the preceding discussion from Chapters 3 to 9:

1. The finite element prototype is developed for the numerical studies in this research. Several factors have been taken into consideration during the development of finite element prototype. These comprise the type of model, type of element, finite element discretisation, boundary conditions and the input material properties.
2. 1-g small-scale laboratory test is concluded for the verification of finite element prediction. The result of finite element analysis can predict the result of 1-g small-scale laboratory test reasonably well provided that the input material properties are appropriate. The input soil properties are determined from laboratory tests. The laboratory tests include sieve analysis test, direct shear box test, oedometer test and density test.
3. The finite element analysis is further verified by comparing the finite element analysis with the existing analytical solutions in literature. In contrast to 1-g small-scale laboratory test, the existing analytical solutions in literature predict the ultimate pull-out capacity of discrete deadman anchor in ultimate limit state with a factor of safety more than 2.5. However, the analytical solutions proposed by Terzaghi (1943) and Oversen (1964) predict the result of finite element analysis with factor of safety more than 1.0 but less than 2.5.

4. The variation between 2-D and 3-D finite element analyses has been assessed. Factors such as anchor spacing and wall stiffness cause significant variation between 2-D and 3-D finite element analyses. 3-D finite element analysis produces a more realistic result. However, 2-D finite element analysis only produces a limited set of plane-strain result, which may not be reliable for certain cases. In addition, the limitation of 2-D FEA with plane strain assumption has been acknowledged.
5. The model simplification technique is able to simply complex models with multiple discrete deadman anchors into simplified model with single discrete deadman anchor. The performances of simplified model are almost identical up to certain extent.
6. A model simplification chart is developed to distinguish the extent to which complex models with multiple discrete deadman anchors can be simplified to model with single discrete deadman anchor with the percentage of variation not more than 5%. The model simplification technique has an important advantage in studying the behaviour of discrete deadman anchorage system, which reduces the computational duration and eliminates the small variations occurred in the complex model.
7. One of the main contributions of this research is to study/understand the behaviour of discrete deadman anchorage system in anchored wall. Several factors influence the behaviour of discrete deadman anchorage system in anchored wall. These include the length of tie rod, embedment depth of anchor, spacing

of anchor, friction angle of soil, depth of anchored wall, and stiffness of anchored wall.

8. Design charts for earth retaining wall with discrete deadman anchorage system are developed based on several key factors. These factors include the length of tie rod, embedment depth of anchor, spacing of anchor, and friction angle of soil.
9. The design charts provide the most efficient solution for the design, in which the wall deflection is limited to 0.5% of excavation height. These design charts can be implemented during preliminary or early design stages, such as earthwork planning, cost estimation, bill of quantity, etc.

## **10.2 Recommendations for Future Research**

Future research work can be conducted on the following aspects:

1. Several factors are beyond the scope of work of the current research. These include the diameter of tie rod, size of deadman anchor, shape of deadman anchor, ground water conditions. Hence, future study can be conducted on these aspects. The behaviour of discrete deadman anchorage system in anchored wall and current design charts can be further improved by including the abovementioned factors.

2. Extend the current research to study the behaviour of multiple-plates deadman anchor in anchored wall in sand condition. This includes the effects of configurations of multi-plates deadman anchors, numbers of multiple-plates deadman anchor, spacing between multi-plates deadman anchor, and spacing between multi-plates deadman anchor.
3. Perform a more extensive numerical study on the behaviour of deadman anchor in anchored wall in clay condition.
4. Extend the current research to deal with dynamic problems. This is to be considered when anchored wall is to deal with berthing structure or to deal with earthquake.

# REFERENCES

---

---

- Abbo, A. J. (1997). *Finite Element Algorithms for Elastoplasticity and Consolidation*. University of Newcastle, Callghon, NSW, Australia.
- Abbo, A. J., & Sloan, S. W. (1998). *SNAC (Solid Non-linear Analysis Code), A Finite Element Program for the Analysis of Elasto-plasticity and Consolidation*. University of Newcastle, Callaghon, NSW, Australia, Department of Civil, Surveying and Environmental Engineering, University of Newcastle, Callaghon, NSW, Australia.
- Abdi, M. R., & Arjomand, M. A. (2011). Pullout Tests Conducted on Clay Reinforced with Geogrid Encapsulated in Thin Layers of Sand. *Geotextiles and Geomembranes*, 29(6), 588–595.  
doi:10.1016/j.geotexmem.2011.04.004
- Abdullahi, M. (2009). Evaluation of Causes of Retaining Wall Failure. *Leonardo Electronic Journal of Practices and Technologies*, (14), 11–18.
- Akinmusuru, J. O. (1978). Horizontally Loaded Vertical Plate Anchors in Sand. *Journal of Geotechnical Engineering, ASCE*, 104(2), 283–286.

- 
- Balla, A. (1961). The Resistance of Breaking-out of Mushroom Foundations for Pylons. In *Proceedings of the 5th International Conference on Soil Mechanics and Foundations Engineering* (pp. 569–576). Paris.
- Basudhar, P. K., & Singh, D. N. (1994). A Generalized Procedure for Predicting Optimal Lower Bound Break-out Factors of Strip Anchors. *Geotechnique*, 44(2), 307–318.
- Bhattacharya, P., & Kumar, J. (2012). Horizontal Pullout Capacity of A Group of Two Vertical Strip Anchors Plates Embedded in Sand. *Geotechnical and Geological Engineering*, 30(2), 513–521.  
doi:10.1007/s10706-011-9484-z
- Biarez, I., Boucraut, L. M., & Negre, R. (1965). Limiting Equilibrium of Vertical Barriers Subjected to Translation and Rotation Forces. In *Proceedings of the 6th International Conference on Soil Mechanics and Foundation Engineering, Vol II* (pp. 368–372). Montreal, Canada.
- Brinkgreve, R. B. J., Broere, W., & Waterman, D. (2006). *Plaxis 2D User Manual - Version 8*. Delft: PLAXIS.
- BS 1377-2. (1990). *Methods of Test for Soils for Civil Engineering Purposes — Part 2: Classification Tests*. London: British Standard Institution.
- BS 1377-5. (1990). *Methods of Test for Soils for Civil Engineering Purposes — Part 5: Compressibility, Permeability and Durability Tests*. London: British Standard Institution.

- BS 1377-7. (1990). *Methods of Test for Soils for Civil Engineering Purposes — Part 7 : Shear Strength Tests ( Total Stress )*. London: British Standard Institution.
- BS 8002. (1994). *Code of Practice for Earth Retaining Structures*. London: British Standard Institution.
- BS 8110-1. (1997). *Structural Use of Concrete — Part 1: Code of Practice for Design and Construction (Vol. 3)*. London: British Standard Institution.
- BS 8110-2. (1985). *Structural Use of Concrete - Code of Practice for Special Circumstances*. London: British Standard Institution.
- BS EN 1992-1-2. (2004). *Eurocode 2 : Design of Concrete Structures — Part 1-2: General Rules - Structural Fire Design (Vol. 3)*. London: British Standard Institution.
- Caquot, A., & Kerisel, F. (1948). *Tables for the Calculation of Passive Pressure, Active Pressure and Bearing Capacity of Foundations*. Gauthier-Villars, Paris.
- Carder, D. R. (1995). *Ground Movements Caused by Different Embedded Retaining Wall Construction Techniques (p. 172)*. Berkshire, U.K.
- Chan, S. H. (2002). *Iterative Solution for Large Indefinite Linear System from Biot's Finite Element Formulation*. National University of Singapore.

- Chandrasekaran, V. S., & King, G. J. W. (1974). Simulation of Excavation Using Finite Elements. *Journal of Geotechnical Engineering, ASCE, 100*, 1086–1089.
- Coduto, D. P. (2011). *Foundation Design: Principles and Practices* (second edi., pp. 735–823). London: Prentice-Hall International Limited.
- Coulomb, C. A. (1776). Essai sur une application des regles des maximis et minimis a quelques problemes de statique relatifs a l'architecture. *Memoires de l'Academie Royale Pres Divers Savants, 7*.
- Das, B. M. (1975). Pullout Resistance of Vertical Anchors. *Journal of Geotechnical Engineering, ASCE, 101*(9), 999–1003.
- Das, B. M. (1990). *Earth Anchors*. Amsterdam: Elsevier.
- Das, B. M., & Seeley, G. R. (1975). Load-displacement Relationship for Vertical Anchor Plates. *Journal of Geotechnical Engineering, ASCE, 101*(7), 711–715.
- David, M. P., & Lidija, Z. (2001). *Finite Element Analysis in Geotechnical Engineering Application*. Heron Quay, London: Thomas Telford Ltd.
- Dickin, E. A., & King, G. J. W. (1997). Numerical Modelling of the Load-displacement Behaviour of Anchor Walls. *Computers and Structures, 63*(4), 849–858.

- 
- Dickin, E. A., & Leung, C. F. (1983). Centrifugal Model Tests on Vertical Anchor Plates. *Journal of Geotechnical Engineering, ASCE*, 109(12), 1503–1525.
- Dickin, E. A., & Leung, C. F. (1985). Evaluation of Design Methods for Vertical Anchor Plates. *Journal of Geotechnical Engineering, ASCE*, 111(4), 500–520.
- Duncan, J. M., & Chang, C. Y. (1970). Non-linear Analysis of Stress and Strain in Soils. *Journal of Soil Mechanics and Foundations Division, ASCE*, 96, 1629–1653.
- El Sawwaf, M., & Nazir, A. (2006). The Effect of Soil Reinforcement on Pullout Resistance of an Existing Vertical Anchor Plate in Sand. *Computers and Geotechnics*, 33(3), 167–176.  
doi:10.1016/j.compgeo.2006.04.001
- Fernie, R., & Suckling, T. (1996). Simplified Approach for Estimating Lateral Movement of Embedded Walls in U.K. Ground. In *Proceeding International Symposium on Geotechnical Aspects of Underground Construction in Soft Ground* (pp. 131–136). City University, London.
- Geddes, J. D., & Murray, E. J. (1996). Plate Anchor Groups Pulled Vertically in Sand. *Journal of Geotechnical Engineering, ASCE*, 122(7), 509–516.
- Ghaly, A. M. (1997). Load-displacement Prediction for Horizontally Loaded Vertical Plates. *Journal of Geotechnical and Geoenvironmental Engineering, ASCE*, 123(1), 74–76.

- Gue, S. S., & Tan, Y. C. (1998). *Design and Construction Considerations for Deep Excavation* (pp. 1–69).
- Hanna, A. M., Das, B. M., & Foriero, A. (1988). Behaviour of Shallow Inclined Plate Anchors in Sand. *Special Topics in Foundations, Geotechnical Special Technical Publication No. 16, ASCE*, 54–72.
- Hansen, J. B. (1953). *Earth Pressure Calculations*. Danish Technical Press. Copenhagen, Denmark.
- Hoshiya, M., & Mandal, J. N. (1984). Some Studies on Anchor Plates in Sand. *Soils and Foundations*, 24(1), 9–16.
- Hueckel, S. (1957). Model Tests on Anchoring Capacity of Vertical and Inclined Plates. In *Proceedings of the 4th International Conference of Soil Mechanics and Foundation Engineering* (pp. 2, 203–206). London: Butterworth Scientific Publications.
- Kame, G. S., Dewaikar, D. M., & Choudhury, D. (2012). Pullout Capacity of a Vertical Plate Anchor Embedded in Cohesion-less Soil. *Earth Science Research*, 1(1), 27–56. doi:10.5539/esr.v1n1p27
- Kok, S. T. (2010). *Analysis and Design of Passive Pile in Open Excavation*. University Putra Malaysia.
- Kumar, J., & Sahoo, J. P. (2012). Upper Bound Solution for Pullout Capacity of Vertical Anchors in Sand Using Finite Elements and Limit Analysis.

---

*International Journal of Geomechanics*, ASCE, 12(June), 333–337.

doi:10.1061/(ASCE)GM.1943-5622.0000160.

Lade, P. V, & Duncan, J. M. (1975). Elasto-plastic Stress-strain Theory for Cohesionless Soil. *Journal of Geotechnical Engineering, ASCE*, 101, 1037–1060.

Leung, H., Gani, C., Okada, W., & Terzaghi, S. (2011). Comparison of the Effectiveness of Deep Soil Mix Columns Using 2-D and 3-D Plaxis. *Plaxis Bulletin*, 20–22.

Long, M. (2001). Database for Retaining Wall and Ground Movements due to Deep Excavations. *Journal of Geotechnical and Geoenvironmental Engineering*, 127(March), 203–224.

Merifield, R. S. (2002). *Numerical Modelling of Soil Anchors*. University of Newcastle.

Merifield, R. S., & Sloan, S. W. (2006). The Ultimate Pullout Capacity of Anchors in Frictional Soils. *Canadian Geotechnical Journal*, 43, 852–868. doi:10.1139/T06-052

Meyerhof, G. G. (1951). The Ultimate Bearing Capacity of Foundations. *Geotechnique*, 2(4), 301–332.

Meyerhof, G. G. (1973). Uplift Resistance of Inclined Anchors and Piles. In *Proceedings of the 8th International Conference on Soil Mechanics and Foundation Engineering* (pp. 167–172). Moscow.

- 
- Meyerhof, G. G., & Adams, J. I. (1968). The Ultimate Uplift Capacity of Foundations. *Canadian Geotechnical Journal*, 5(4), 225–244.
- Muntohar, A. S., & Liao, H.-J. (2013). Finite Element Analysis of the Movement of the Tie-Back Wall in Alluvial-Silty Soils. *Procedia Engineering*, 54, 176–187. doi:10.1016/j.proeng.2013.03.017
- Murray, E. J., & Geddes, J. D. (1987). Uplift of Anchor Plates in Sand. *Journal of Geotechnical Engineering, ASCE*, 113(3), 202–215.
- Murray, E. J., & Geddes, J. D. (1989). Resistance of Passive Inclined Anchors in Cohesionless Medium. *Geotechnique*, 39(3), 417–431.
- Naser, A.-S. (2006). Pullout Capacity of Block Anchor in Unsaturated Sand. *ASCE*, (May 2009), 403–414. Retrieved from [www.ascelibrary.org](http://www.ascelibrary.org)
- Neely, W. J., Stuart, J. G., & Graham, J. (1973). Failure Loads of Vertical Anchor Plates in Sand. *Journal of Soil Mechanics and Foundations Division, ASCE*, 99(9), 669–685.
- Ou, C. Y., Hsien, P. G., & Chiou, D. C. (1993). Characteristics of Ground Surface Settlement During Excavation. *Canadian Geotechnical Journal*, 30, 758–767.
- Ovesen, N. K. (1964). Passive Anchor Slabs, Calculation Methods and Model Tests. *Danish Geotechnical Institute, Bull. no. ,* 5–39.

Ovesen, N. K. (1981). Centrifuge Tests on the Uplift Capacity of Anchors. In *Proceedings of the 10th International Conference on Soil Mechanics and Foundations Engineering*.

Ovesen, N. K., & Stromann, H. (1972). Design Method for Vertical Anchor Slabs in Sand. In *Proceeding of Speciality Conference on Performance of Earth and Earth Supported Structures* (pp. Vol 1–2, 1418–1500).

Peck, R. B., Hanson, W. E., & Thornburn, T. H. (1974). *Foundation Engineering* (2nd Editio.). John Wiley and Sons.

*Plaxis 3D User Manual*. (2012). Delft: PLAXIS.

Premalatha, P. V. (2009). Analysing the Optimum Length of Tierod Anchors for a Berthing Structure. *Indian Geotechnical Society Chennai Chapter*, 61–67.

Rankine, W. (1857). On the Stability of Loose Earth. *Philosophical Transactions of the Royal Society of London*, 147.

Rosato, D. V., Schott, N. R., & Rosato, M. G. (Eds.). (2001). *Plastic Institute of America Plastics Engineering, Manufacturing and Data Handbook* (pp. 1301–1307). AH Dordrecht: Kluwer Academic Publisherse.

Rowe, R. K. (1978). *Soil Structure Interaction Analysis and Its Application to The Prediction of Anchor Behaviour*. University of Sydney, Australia.

- Rowe, R. K., Booker, J. R., & Balaam, N. P. (1978). Application of the Initial Stress Method to Soil-Structure Interaction. *International Journal of Numerical Methods in Engineering*, 12(5), 879–880.
- Rowe, R. K., & Davis, E. H. (1982a). The Behaviour of Anchor Plates in Clay. *Geotechnique*, 32(1), 9–23.
- Rowe, R. K., & Davis, E. H. (1982b). The Behaviour of Anchor Plates in Sand. *Geotechnique*, 32(1), 25–41.
- Sloan, S. W. (1988). Lower Bound Limit Analysis Using Finite Elements and Linear Programming. *International Journal of Numerical and Analytical Methods in Geomechanics*, 12, 61–67.
- Smith, J. E. (1962). *Deadman Anchorages in Sand* (p. R 199). Port Hueneme, California.
- Sokolovskii, V. V. (1965). Static of Granular Media. In *Pergamon Press* (p. 232). New York.
- Standard practice for classification of soils for engineering purpose (Unified Soil Classification System). (2006) (pp. 1–12). West Conshohocken, United State: ASTM International.
- Sum Hup Sheet Piling Sdn Bhd (589051-M). (n.d.). Retrieved from [www.sumhup.com.my](http://www.sumhup.com.my)
- Terzaghi, K. (1943). *Theoretical Soil Mechanics*. New York: John Willey and Sons, Inc.

Visone, C. (2008). *Performance-based Approach in Seismic Design of Embedded Retaining Walls*. University of Napoli Federico II.

Weissenbach, A., Hettler, A., & Simpson, B. (2002). 3.4 Stability of excavations (pp. 273–407). John Wiley and Sons. Retrieved from [www.knovel.com](http://www.knovel.com)

Wong, I. H., Poh, T. Y., & Chuah, H. L. (1997). Performance of Excavations for Depressed Expressway in Singapore. *Journal of Geotechnical and Geoenvironmental Engineering, ASCE*, 123(7), 617–625.

# APPENDIX A

## MATERIAL PROPERTIES

### A.1 Soil Properties

Soil Classification Chart				Soil Classification	
Criteria for Assigning Group Symbols and Group Names Using Laboratory Tests <sup>A</sup>				Group Symbol	Group Name <sup>B</sup>
COARSE-GRAINED SOILS More than 50% retained on No. 200 sieve	Gravels	Clean Gravels	$C_u \geq 4$ and $1 \leq C_c \leq 3^E$	GW	Well-graded gravel <sup>F</sup>
	More than 50% of coarse fraction retained on No. 4 sieve	Less than 5% fines <sup>C</sup>	$C_u < 4$ and/or $1 > C_c > 3^E$	GP	Poorly graded gravel <sup>F</sup>
		Gravels with Fines	Fines classify as ML or MH	GM	Silty gravel <sup>G,H</sup>
	Sands	More than 12% fines <sup>C</sup>	Fines classify as CL or CH	GC	Clayey gravel <sup>G,H</sup>
		Clean Sands	$C_u \geq 6$ and $1 \leq C_c \leq 3^E$	SW	Well-graded sand <sup>I</sup>
	50% or more of coarse fraction passes No. 4 sieve	Less than 5% fines <sup>D</sup>	$C_u < 6$ and/or $1 > C_c > 3^E$	SP	Poorly graded sand <sup>I</sup>
FINE-GRAINED SOILS 50% or more pass the No. 200 sieve	Sands with Fines	Fines classify as ML or MH	SM	Silty sand <sup>G,H</sup>	
		Fines classify as CL or CH	SC	Clayey sand <sup>G,H</sup>	
	Sils and Clays Liquid limit less than 50	inorganic	PI > 7 and plots on or above "A" line <sup>J</sup>	CL	Lean clay <sup>K,L,M</sup>
		organic	PI < 4 or plots below "A" line <sup>J</sup>	ML	Silt <sup>K,L,M</sup>
	Sils and Clays Liquid limit 50 or more	inorganic	Liquid limit - oven dried < 0.75	OL	Organic clay <sup>K,L,M,N</sup>
		organic	Liquid limit - not dried < 0.75	OH	Organic silt <sup>K,L,M,Q</sup>
	Sils and Clays Liquid limit 50 or more	inorganic	PI plots on or above "A" line	CH	Fat clay <sup>K,L,M</sup>
		organic	PI plots below "A" line	MH	Elastic silt <sup>K,L,M</sup>
HIGHLY ORGANIC SOILS	Primarily organic matter, dark in color, and organic odor	Liquid limit - oven dried < 0.75	PT	Peat	
		Liquid limit - not dried < 0.75			

Figure A.1: Unified Soil Classification System (ASTM Designation D-2487). ("Standard practice for classification of soils for engineering purpose (Unified Soil Classification System)," 2006)

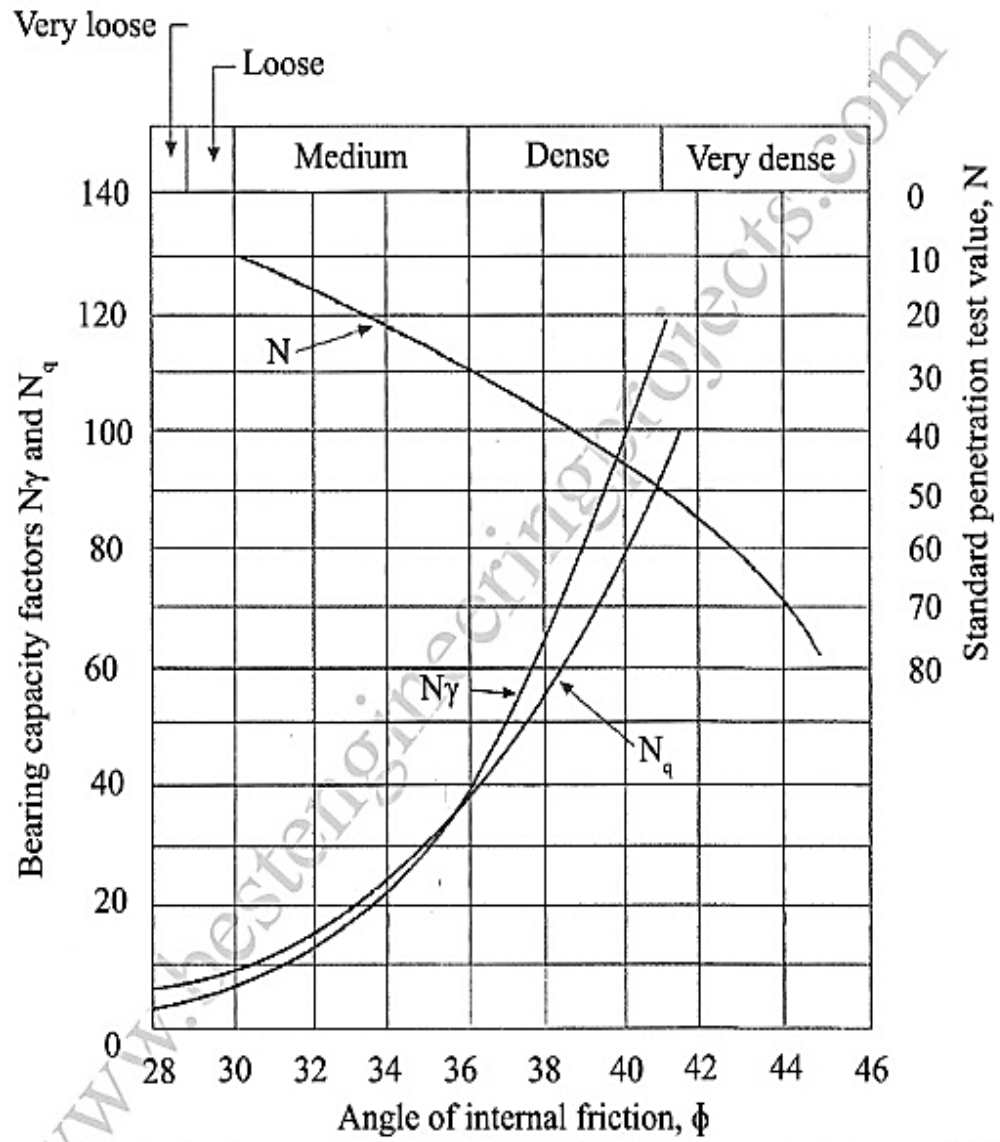


Figure A.2: Relationship between SPT 'N' value and  $\phi$ ,  $N_q$  and  $N_\gamma$ . (Peck, Hanson, & Thornburn, 1974)

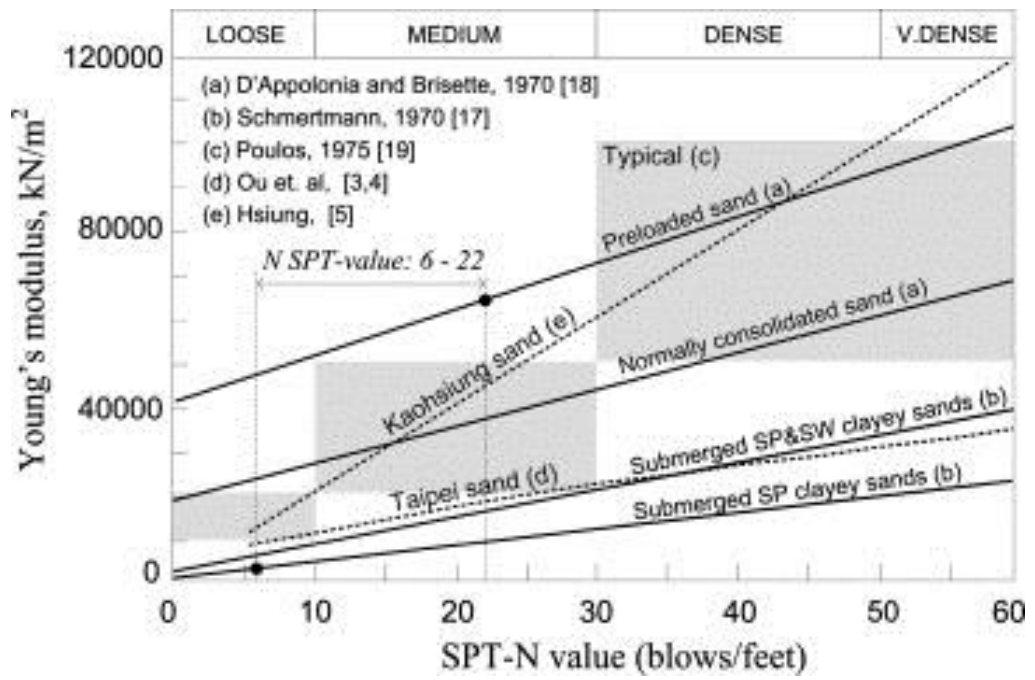


Figure A.3: Relationship between SPT 'N' value and Young's Modulus.

(Source: unknown)

## A.2 Concrete Properties

Table A.1: Typical range for the static modulus of elasticity at 28 days of normal-weight concrete. (BS 8110-2, 1985)

$f_{cu,28}$	$E_{c,28}$	
	Mean value	Typical range
N/mm <sup>2</sup>	kN/mm <sup>2</sup>	kN/mm <sup>2</sup>
20	24	18 to 30
25	25	19 to 31
30	26	20 to 32
40	28	22 to 34
50	30	24 to 36
60	32	26 to 38

### A.3 Steel Properties

Generic material type	Shear modulus, MPa	Shear stress, MPa	At	Poisson's ratio
ABS	960	51.0	Ultimate	0.35
	810	37.9	Ultimate	0.35
	810	32.9	Ultimate	0.35
	660	30.0	Ultimate	0.36
Acetal copolymer	1000	53	Ultimate	0.35
Acetal homopolymer	1330	65.5	Ultimate	0.35
	1330	68.9	Ultimate	0.35
Acrylic		44.6		
Nylon (DAM) (0.2% moisture)		66.2	Ultimate	0.34–0.43
		57.9	Ultimate	0.34–0.43
		59.3	Ultimate	0.34–0.43
		62.7	Ultimate	0.34–0.43
Nylon (50% RH) (2.5% moisture)				0.35–0.50
				0.35–0.50
		55.8	Ultimate	0.35–0.50
				0.35–0.50
Phenolic		82.7	Ultimate	
Polycarbonate	785	41.3	Yield	0.37
		68.9	Ultimate	
Phenylene ether copolymer		62.6	Ultimate	
		66.2	Ultimate	
Polysulfone	917	41.4	Yield	0.37
		62.1	Ultimate	
Steel, structural ASTM A7-61T	79200	120	Yield	0.27
Brass, naval	38000	280–310	Ultimate	
Aluminum, wrought 2014-T6	30000	240	Yield	0.33
		270	Ultimate	
Pine (southern long-leaf) (with grain)		10		
Oak (white) (with grain)		13.0		

Figure A.4: Examples of specific room temperature shear stress-strain data and Poisson's ratio for several plastics and other materials. (Rosato et al., 2001)

Generic material type	Modulus, MPa	Yield stress, MPa	Elongation at yield, %	Elongation at break, %
ABS	2,600	52	2.5	25–75
	2,200	43	2.5	25–75
	2,200	40	2.5	25–75
	1,800	34	3.3	25–75
Acetal copolymer	2,800	61	12	75
	2,800	61	12	60
Acetal homopolymer	3,100	68.9	12	75
	3,100	68.9	12	40
	3,100	68.9	12	25
Acrylic	2,960	72		5.4
	2,239	48		
	1,720	38	5.0	35
Nylon (DAM) (0.2% moisture)		82.7	5	60
				60
		60.7	7	150
		51.0	20	290
Nylon (50% RH) (2.5% moisture)		58.6	25	>300
				210
		51.0	40	>300
		40.7	30	285
Phenolic	19,310	55.2		0.29
	10,340	58.6		0.57
	7,590	48 <sup>b</sup>		0.63
Polycarbonate	2,380	62	6–8	110
	2,240	62	6–8	90
Polyethylene		30		900
		29		900
		24		900
		14		500
Phenylene ether copolymer	2,500	58	4–6	50–100
	2,500	55	4–6	50–100
Polypropylene	1,400	35.5	12	
	1,200	27.3	13	<300
	830	20.0	6.3	
Polystyrene	3,100	52		2.5
	2,070	31		30
	2,070	25		60
	1,930	25		50
Polysulfone	2,482	70.3	5–6	50–100
	2,482	70.3	5–6	50–100
	2,482	68.9	5–6	50–100
Steel, structural ASTM A7-61T	200,000	230		
Brass, naval	100,000	170–340		
Aluminum, wrought 2014-T6	73,000	410		
Pine (southern long-leaf)	13,700			
Oak (white)	11,200			

Figure A.5: Examples of room temperature tensile stress-strain data for several plastics and other materials. (Rosato et al., 2001)

## A.4 Sheet Pile Wall Properties

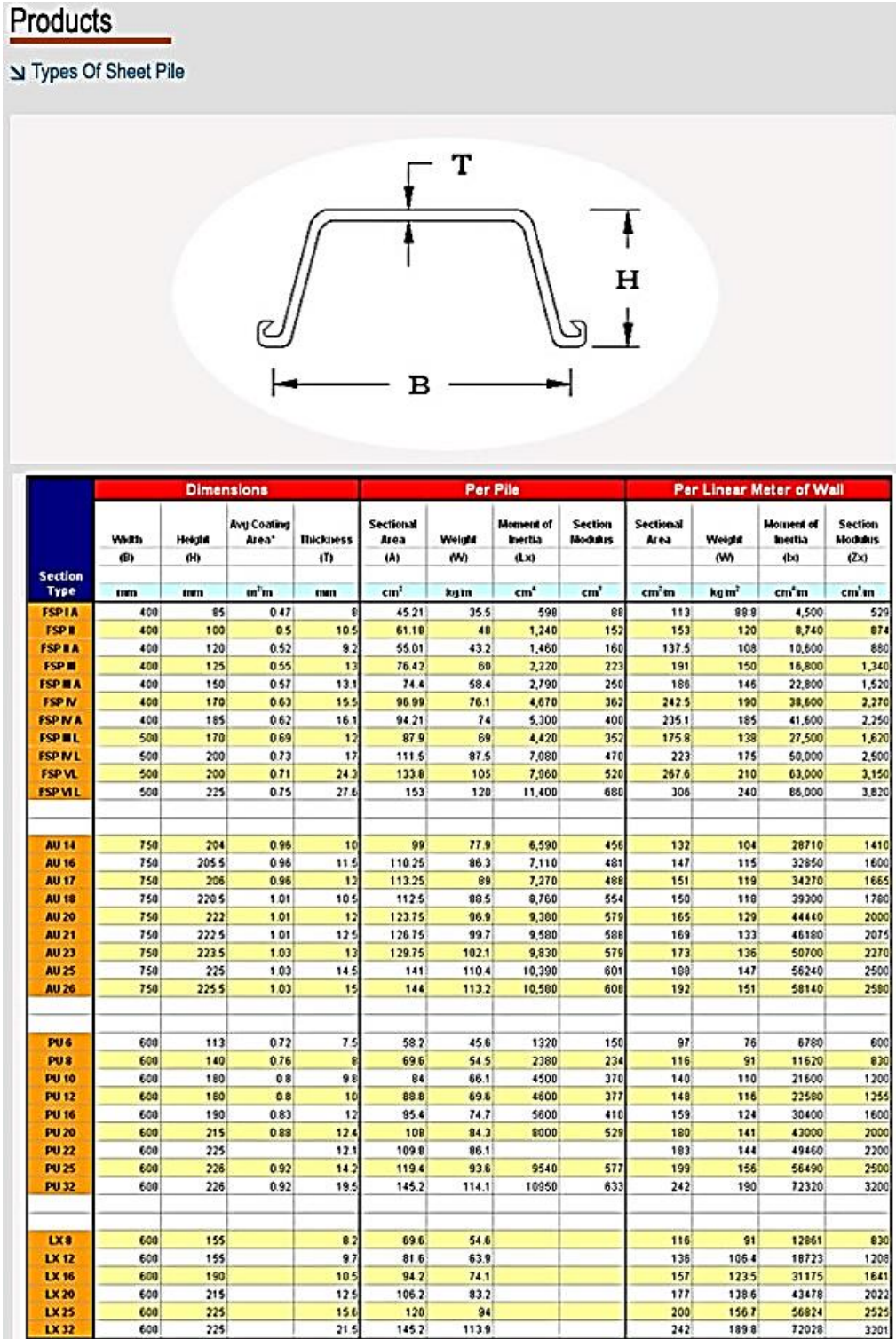


Figure A.6: Examples of sheet pile properties (Sum Hup Sheet Piling Sdn Bhd)

# APPENDIX B

---

---

## RESULTS OF SOIL TEST

### B.1 Direct Shear Box Test

One of three set of direct shear box test results are presented in this section. There are as follows:

Table B.1: Summary of the results for direct shear box test.

Mass (kg)	$\rho$	$\sigma'_n$	$\tau_{\max}$	$\tau_{\text{ult}}$
0	1.534	47.222	0.000	0.000
2	1.548	100.000	46.125	46.125
4	1.539	155.556	93.375	86.625
6	1.511	208.333	133.875	133.875

Table B.2: Measurement input table for direct shear box test.

<b>Data (Units converted by multipliers in equations)</b>			<b>0 kg</b>	<b>2 kg</b>	<b>4 kg</b>	<b>6 kg</b>
Mass of box+ bottom plate & grid + screws	<b>M<sub>1</sub></b>	g	1210.8	1210.8	1210.8	1210.8
Mass of top half box + top plate + grid + screws + bearing	<b>M<sub>2</sub></b>	g	1255.4	1255.4	1255.4	1255.4
Mass of box+ bottom plate & grid + screws + sample	<b>M<sub>3</sub></b>	g	1360.4	1366.2	1364.8	1354.4
Mass of specimen = (M <sub>3</sub> - M <sub>1</sub> )	<b>M<sub>s</sub></b>	g	149.6	155.4	154.0	143.6
Mass of hanger	<b>M<sub>4</sub></b>	kg	0.3536	0.3536	0.3536	0.3536
Mass added to hanger	<b>M<sub>5</sub></b>	kg	0	2	4	6
Plan area of failure = width x breadth	<b>A</b>	mm <sup>2</sup>	3600	3600	3600	3600
Effective thickness of bottom grid	<b>t<sub>b</sub></b>	mm	3	3	3	3
Effective thickness of top grid	<b>t<sub>t</sub></b>	mm	3	3	3	3
Depth to bottom of lower grid	<b>d<sub>1</sub></b>	mm	36.4	36.4	36.4	36.4
Depth to top of upper grid	<b>d<sub>2</sub></b>	mm	3.3	2.5	2.6	4.0
Thickness of specimen = (d <sub>1</sub> -d <sub>2</sub> -t <sub>t</sub> -t <sub>b</sub> )	<b>t<sub>s</sub></b>	mm	27.1	27.9	27.8	26.4
Volume of specimen = t <sub>s</sub> A	<b>V<sub>s</sub></b>	mm <sup>3</sup>	97560	100400	100080	95040
Density of Speciment = (M <sub>s</sub> /V <sub>s</sub> ) x10 <sup>3</sup>	<b>ρ<sub>s</sub></b>	T/m <sup>3</sup>	1.534	1.548	1.539	1.511
Total force acting on shear surface = 9.8 x [(M <sub>5</sub> +M <sub>4</sub> ) + (M <sub>2</sub> +M <sub>s</sub> /2)x10 <sup>-3</sup> ]	<b>N</b>	N	17	36	56	75

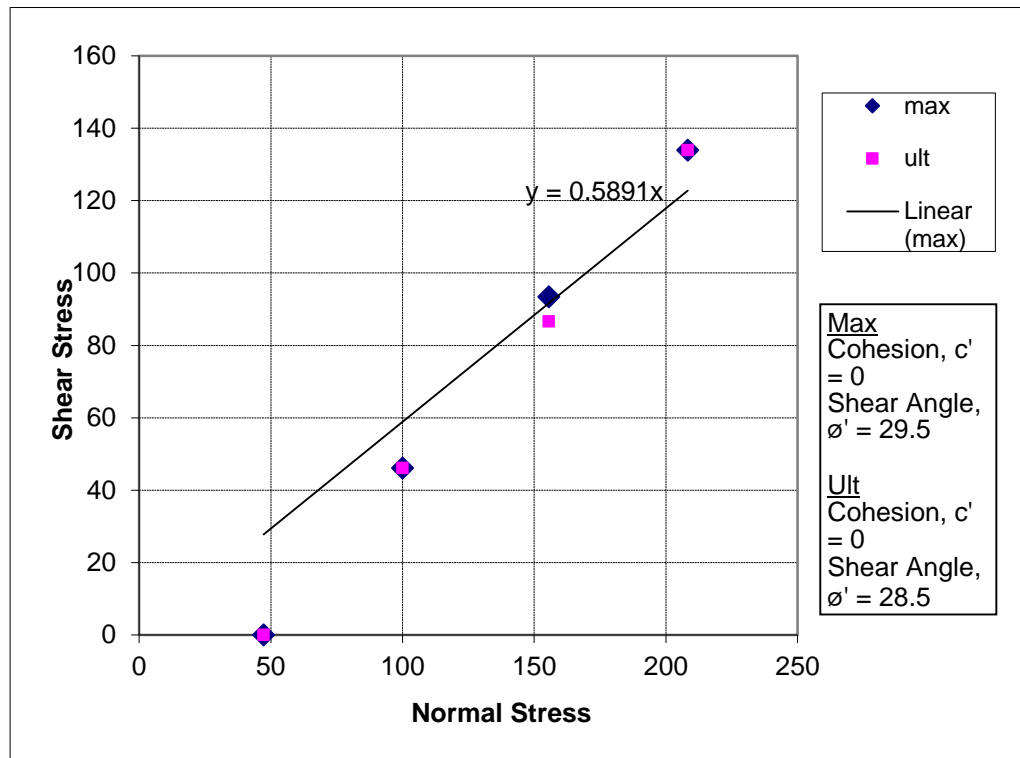


Figure B.1: Shear stress against normal stress plot for direct shear box test.

## B.2 Oedometer Test

One of three set of oedometer test results are presented in this section.

There are as follows:

Table B.3: Measurement of the consolidation ring for oedometer test.

Measurement of the consolidation ring			
Diameter, mm	<b>D</b>	=	50.10
Height (Original height of the sample), mm	<b>H<sub>0</sub></b>	=	19.50
Area, mm <sup>2</sup>	<b>A</b>	=	1971.36
Initial volume, mm <sup>3</sup>	<b>V<sub>0</sub></b>	=	38441.47

Table B.4: Summary of the results for oedometer test.

	Pressure stage (kPa)				
	25	50	75	100	125
Vertical displacement $\Delta h_i$ (mm)	0.58	0.77	0.932	1.056	1.19
Strain	0.029744	0.039487	0.047795	0.054154	0.061026

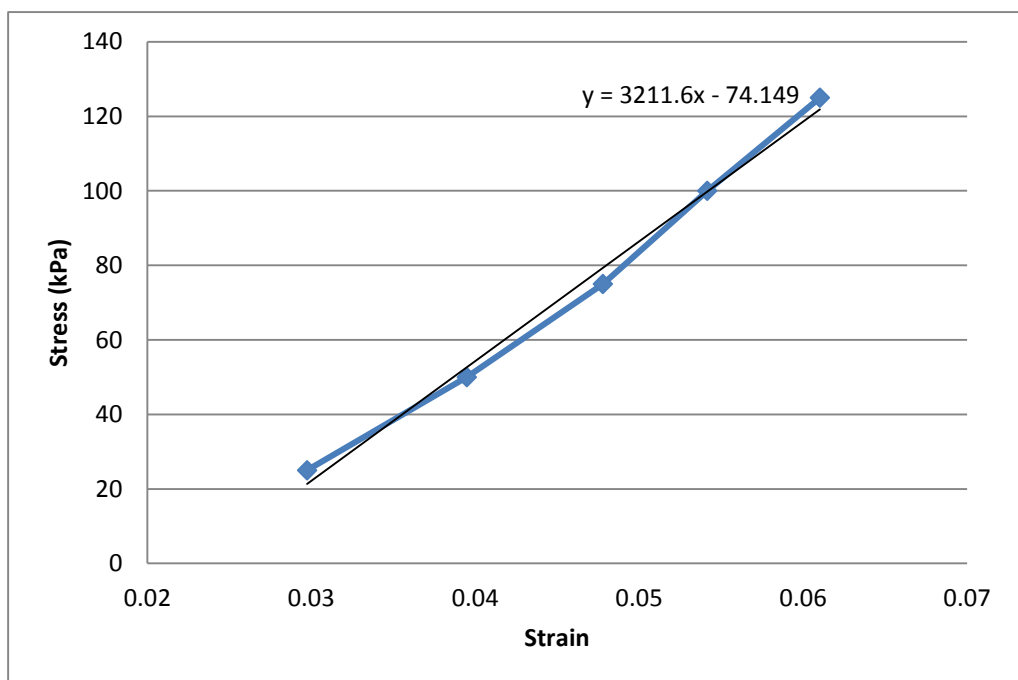


Figure B.2: Stress strain plot for oedometer test.